To the Graduate Council:

I am submitting herewith a dissertation written by Charles Stuart Daw entitled, "Solids Segregation in Gas-Fluidized Beds of Large Particles." I have examined the final copy of this dissertation for form and content and recommend that it be accepted in partial fulfillment of the requirements for the degree of Doctor of Philosophy, with a major in Chemical Engineering.

George C. Frazier

George C. Frazier, Major Professor

We have read this dissertation and recommend its acceptance:

Donald C. Bogue

Joseph J. Perona

L. Lee Wilkerson

Accepted for the Council:

Lew Minkel

Vice Provost
and Dean of The Graduate School

SOLIDS SEGREGATION IN GAS-FLUIDIZED BEDS OF LARGE PARTICLES

A Dissertation

Presented for the

Doctor of Philosophy

Degree

The University of Tennessee, Knoxville

Charles Stuart Daw

June 1985

ACKNOWLEDGMENTS

I wish to express my sincere appreciation to Dr. George Frazier for his patience, guidance, and continuing support throughout my Ph.D. program. I am also grateful to the other members of my advisory committee, Drs. Joe Wilkerson, Don Bogue, and Joe Perona for their advice and help.

I owe a special thanks to my supervisors at Oak Ridge National Laboratory, John Jones, Don Burton, and Ted Fox, for their understanding and assistance in helping me complete my graduate work.

Finally, I am very grateful for those many friends and family who have been so accommodating to my strange schedules and lack of spare time. Their support has been essential.

ABSTRACT

A series of experiments was performed to develop an improved understanding of the fundamental nature of solids segregation in gas-fluidized beds of relatively large particles. Large particles were selected because they are becoming increasingly important in industrial fluidized beds but have not been very thoroughly investigated.

Segregation experiments were conducted with binary systems of large particles in a 10.2 cm (4 in.) diameter bed fluidized with air at ambient temperature and pressure. The particles studied ranged from 1750 μm (0.069 in.) to 6270 μm (0.247 in.) mean diameter and from 0.905 g/cm^3 (56.5 lb/ft^3) to 7.50 g/cm^3 (468 lb/ft^3) absolute density. Air velocity, particle properties, bed height, relative amounts of jetsam and flotsam, and bed internals were varied to determine their influence on the steady-state segregation pattern. Transient segregation and steady-state bed expansion were also measured.

A mixing index was developed which proved to be extremely useful in quantifying the variation of segregation with bed parameter changes. In correlating this index with air flow, it was discovered that abrupt changes sometimes occurred in the segregation pattern when small changes were made in the air flow. These abrupt changes appeared to be associated with changes in the fluidization mode. Such abrupt changes have not been previously reported.

The steady-state segregation profiles were found to be in good agreement with a modified form of the Gibilaro-Rowe model developed

originally for small particle beds. The parameter representing large-scale circulation effects was found to have a similar range as previously reported for small-particle beds. The parameter representing bulk-phase dispersion was found to be appreciably larger than previously reported. The transient segregation phenomena appeared to be simulated reasonably well by a transient form of the Gibilaro-Rowe model. A special limiting case of the Gibilaro-Rowe model was also found to be useful in describing the solids and void distribution in an expanded bed. The Gibilaro-Rowe model was combined with differential mass balances to illustrate the expected performance of fluidized bed reactors which exhibit this type of segregation.

TABLE OF CONTENTS

LIST OF TABLES

LIST OF FIGURES

NOTATION*

a	parameter in Eq. 6.7 defined after Eq. 6.7, [-]
A	parameter in Eq. 5.13 defined after Eq. 5.13, [-]
A_b	cross section of bulk solids phase, [L^2]
A_c	cross section of fluidized bed, [L^2]
A_s	projected bubble cross section in Burgess et al.'s model, [L^2]
A_w	cross section of wake solids phase, [L^2]
b	parameter in Eq. 5.26 defined after Eq. 5.26, [-]; also parameter in Eq. 6.7 defined after Eq. 6.7, [-]
B_i	parameter in Eq. 5.14 defined after Eq. 5.14, [1/L]
B_2	term in Gibilaro-Rowe model defined after Eq. 2.13, [-]
C	parameter in Eq. 5.15 defined after Eq. 5.15, [-]
C_B	parameter in Eq. 5.16 defined after Eq. 5.16, [-]
C_J	volume of jetsam per unit volume of space in expanded bed, [-]
C_{b1}	active gas species concentration in the bubble phase at the top of the reactor, [moles/L^3]
C_H	active gas species concentration in the gas exiting the reactor, [moles/L^3]
C_o	active gas species concentration in the gas entering the reactor, [moles/L^3]

*F = force, L = length, M = mass, T = time, - = dimensionless

C_p in Chap. 5, number concentration of particles, [No. of particles/L^3]

C_{po} in Chap. 5, number concentration of particles at the datum, [No. of particles/L^3]

C_{p_1} active gas species concentration in the emulsion phase at the top of the reactor, [moles/L^3]

C_s segregation index proposed by Geldart and defined in Sect. 2.4.11, [-]

d_F flotsam particle diameter, [L]

$\overline{d}_F$ mean flotsam particle diameter, [L]

d_J jetsam particle diameter, [L]

$\overline{d}_J$ mean jetsam particle diameter, [L]

d_p particle diameter, [L]

$\overline{d}_p$ mean particle diameter, [L]

D bed diameter, [L]

D' ratio of particle diameters used in Eq. 2.6, [-]

D_B bubble diameter, [L]

D'_ϕ shape corrected particle diameter ratio defined after Eq. 2.18, [-]

D bulk phase dispersion coefficient expressed in expanded bed coordinates, [L^2/T]

D_s bulk phase dispersion coefficient expressed in static bed coordinates, [L^2/T]

E parameter in Eq. 5.18 defined after Eq. 5.18, [-]

f_m the fraction of the bubble wake which is assumed completely mixed in the Burgess et al. model, Sect. 2.4.8, [-]

$f(u_o-u_{mf})$ unspecified function in Eq. 2.6 and described after Eq. 2.6

g acceleration due to gravity, $[L/T^2]$

H expanded bed height, [L]

H_{mf} bed height at minimum fluidization, [L]

H_s static bed height, [L]

H^* reduced bed aspect ratio defined after Eq. 2.18, [-]

i_u demixing index proposed by Goosens et al.

I mixing index defined by Eq. 4.1, [-]

I_{exp} the experimentally determined value for I, [-]

I_{mod} the value of I predicted by the modified Gibilaro-Rowe model using the "best-fit" parameters, [-]

J_J rate of jetsam dispersion in the bulk solids phase, [L/T]

k original Gibilaro-Rowe segregation rate coefficient, $[L^3/T]$

k' modified Gibilaro-Rowe segregation rate coefficient, [L/T]

k_a first order reaction rate constant, [1/t]

k_a' sorption reaction rate constant, [1/T]

$\tilde{k}_a$ dimensionless sorption reaction rate constant defined after Eq. 6.1, [-]

$\tilde{k}'_a$ dimensionless sorption reaction rate constant defined by Eq. 6.2, [-]

$\tilde{k}_g$ active species generation rate constant, [moles/(L^3T)]

$\tilde{k}'_g$ modified active species generation rate constant, [moles/L^3]

k_s segregation rate coefficient expressed in static bed coordinates, [L/T]

K_E solids interchange coefficient defined by Eq. 2.21, [1/T]

K_1, K_2 empirical constants in Eq. 2.4, [1/T]

ℓ location of boundary between well-mixed and segregated regions in Fan and Chang model, Sect. 2.4.9

L demixing criterion defined by Eq. 2.6, [-]

L_1, L_2, L_3, L_4 characteristic lengths involved in transport coefficients, [L]

L_s characteristic particle descent distance in Burgess et al. model, [L]

L_w characteristic vertical wake length in Burgess et al. model, [L]

m_f mass of fluid particles in Eq. 5.18, [M]

m_1, m_2 terms in Eq. 6.3, defined after Eq. 6.3, [-]

M mixing index defined after Eq. 2.6 and in Sect. 2.4.11, [-]

M' Fan and Chang mixing index defined by Eq. 2.20, [-]

n number of samples

n_{po} number fraction of particles at datum defined after Eq. 5.18, [-]

N_o Avogadro's number

p_i partial pressure of component i, $[F/L^2]$

p_{io} partial pressure of component i at datum $[F/L^2]$

P term in Gibilaro-Rowe model in Chaps. 2 and 5 defined after Eq. 2.13, [-]; also pressure in Chaps. 4 and 5, $[F/L^2]$

P_r reduced pressure defined after Eq. 5.26, [-]

q parameter in Eq. 6.7 defined after Eq. 6.7, [-]; also bulk/wake exchange coefficient in original Gibilaro-Rowe model, $[L^2/T]$

Q the effective gas flow through the bubbles in Chap. 6, $[L^3/T]$; also term in Eq. 2.17 defined after Eq. 2.17, [-]

r axial dispersion parameter in the original Gibilaro-Rowe model, Sect. 2.4.6, $[L^4/T]$; also parameter in Eq. 6.7 defined after Eq. 6.7, [-]

R ratio of particle densities used in Eqs. 2.6 and 2.18, [-]; also ideal gas constant, [FL/(mole K)]

R_c radius of bubble cloud, [L]

R_b bubble radius, [L]

R_{ij} segregation index proposed by Cooke et al. and defined in Sect. 2.4.12, [-]

R_s segregation factor proposed by Yoshida et al. and defined in Eq. 2.22, [-]

s	sample standard deviation in units of measured quantity
S_J	rate of jetsam segregation in bulk solids phase, [L/T]
SSD	sum of squared deviations, defined by Eq. 5.20, [-]
SST_{max}	the quantity $(1-\bar{v}_J)\bar{v}_J$, representing the maximum possible SSD, [-]
t	time, [T]
T	absolute temperature, [K]
u_b	rise velocity of bubble swarm, [L/T]
u_{bf}	minimum superficial gas velocity at which bubbling occurs, [L/T]
u_{br}	single bubble rise velocity [L/T]
u_e	emulsion phase gas velocity, [L/T]
u_{mf}	minimum fluidizing velocity, [L/T]
u_{mfF}	flotsam minimum fluidizing velocity, [L/T]
u_{mfJ}	jetsam minimum fluidizing velocity, [L/T]
u_o	superficial gas velocity, [L/T]
$\bar{u}_R$	average flotsam rise velocity defined after Eq. 2.15, [cm/s]
u_s	solids velocity in emulsion phase, [L/T]
u_{tF}	flotsam terminal velocity, [L/T]
v_J	average volume fraction of jetsam in the solids at a given axial position, [-]
v_J^B	volume fraction of jetsam in the bulk solids phase, [-]

v_J^w volume fraction of jetsam in the wake solids phase, [-]

v_{Ji} jetsam volume fraction in solids sample i, [-]

v_{Jo} volume fraction of jetsam in the solids at the bottom of the bed, [-]

v_{Jl} volume fraction of jetsam in the solids at the top of the bed, [-]

v_p volume fraction of emulsion phase in a horizontal slice of the bed, [-]

v_{si} volume fraction of bed solids in sample [-]

v_w volume fraction of bed solids in the wake solids phase, [-]

v_1, v_2 volume fraction of components 1 and 2, respectively, [-]

V_b average volume of an individual bubble, [L^3]

V_w fraction of bubble assumed to be wake solids in Burgess et al model, [L]

w, w_s solids circulation rate in Gibilaro-Rowe model (same in modified and unmodified models, expanded and static coordinates), [L^3/T]

x_1, x_2 mass function of components 1 and 2, respectively, [-]

x_F mass fraction of flotsam in solids, [-]

$\bar{x}_F$ mean flotsam mass fraction, [-]

x_J mass fraction of jetsam in solids, [-]

$\bar{x}_J$ mean jetsam mass fraction, [-]

x_{Fo} mass fraction of smaller component at time zero in Sutherland and Wang model, defined after Eq. 2.4, [-]

x_{Jl} jetsam mass fraction in solids at the top of the bed, [-]

X average depth of penetration used in Eq. 2.16, [cm]; also phase interchange coefficient defined after Eq. 6.1, [-]

y axial position in expanded bed, [L]

y_s axial position in static bed, [L]

Y_i number concentration of key component in solids sample: per the Fan and Chang model, Sect. 2.4.9, [number/L^3]

$\overline{Y}$ average Y in the bed, [number/L^3]

z normalized axial position, for static coordinates defined as y_s/H_s, for expanded coordinates defined as y/H, [-]

z_c the location of the beginning of the distinct upper layer in terms of static bed coordinates, [-]

z* location of the interface predicted by Gibilaro-Rowe model, defined after Eq. 2.8, [-]

α parameter in Fan and Chang model defined in Sect. 2.4.9, [1/T]; also parameter in Eq. 6.7 defined after Eq. 6.7, [-]

β parameter in Fan and Chang model defined in Sect. 2.4.9, [1/T]; also the fraction of gas passing through the bed as bubbles, defined after Eq. 6.1, [-]

γ parameter representing ratio of phase exchange tendency to segregation tendency in the Gibilaro-Rowe model, defined in Sect. 2.4.6

δ bubble volume fraction in the bed, Chap. 2, [-]; also parameter in Eq. 6.7 defined after Eq. 6.7, [-]

ε void fraction, [-]

ε_{mf} void fraction at minimum fluidization, [-]

ε_s void fraction in the static bed, [-]

ζ parameter in Eq. 6.7 defined after Eq. 6.7, [-]

ρ_1, ρ_2 density of components 1 and 2, respectively, [M/L^3]

ρ_f fluid density in Eqs. 5.17 and 5.18, [M/L^3]

ρ_F flotsam particle density, [M/L^3]

ρ_J jetsam particle density, [M/L^3]

ρ_p particle density in Eq. 5.18, [M/L^3]

σ variance about mean composition, [units of composition]

σ_e standard deviation of error in units of measured quantity

θ dimensionless time, defined after Eq. 5.21, [-]

λ_B dispersion/segregation parameter for solids in Brownian motion defined after Eq. 5.18, [-]

λ_D dispersion/segregation parameter in the original Gibilaro-Rowe model, $\gamma/(kH)$, [-]

λ_{Ds} dispersion/segregation parameter in the modified Gibilaro-Rowe model, $D_s/(k_s H_s)$, [-]

λ'_{Ds} the value of λ_D above z_c, [-]

λ_G dispersion/segregation parameter for ideal gases defined after Eq. 5.16, [-]

λ_p dispersion/segregation parameter for solids expansion, defined after Eq. 5.24, [-]

λ_p' the value of λ_p above H_{mf}, [-]

λ_w circulation/segregation parameter in the original Gibilaro-Rowe model, w/k, [-]

λ_{ws} circulation/segregation parameter in the modified Gibilaro-Rowe model, $w/[A_b\ k_s\ (1-\varepsilon_s)]$, [-]

μ parameter in Eq. 6.7 defined after Eq. 6.7, [-]

μ_1 mole fraction of component 1, [-]

$\overline{\mu}_1$ mean mole fraction of component 1, [-]

μ_{10} mole fraction of component 1 at datum, [-]

ϕ_b bubble-phase gas composition defined after Eq. 6.11, [-]

ϕ_F sphericity of flotsam particles, [-]

ϕ_J sphericity of jetsam particles, [-]

ϕ_s particle sphericity, [-]

ϕ_p emulsion-phase gas composition defined after Eq. 6.11, [-]

ϕ_t gas composition at the reactor exit (the average ϕ), representing the net elution of the reactive species, $(1-\beta)\ \phi_p + \beta\ \phi_b$, [-]

Ω_f term in Eq. 5.18, defined after Eq. 5.18 [1/L]

Ω_p term in Eqs. 5.17 and 5.18, defined after Eq. 5.17, [1/L],

$\langle\ \rangle$ Singularity function, equal to 0 for argument <0, equal to 1 for argument ≥ 0, [-]

1. INTRODUCTION

Gas-fluidized beds are key components in many chemical and energy conversion processes, including coal gasification, coal combustion, oil refining, and minerals beneficiation. When the fluidized particles have more than one size or density, there is a tendency for the lighter and smaller particles to go to the top of the bed; i.e., to segregate. Depending on the particular process, segregation can enhance or reduce the overall efficiency.

Fluidized bed combustion of high sulfur coal is an example of how segregation can be deleterious. In this case, the goal is to burn coal in a fluidized bed of calcined limestone so that the sulfur dioxide by-product can be "captured" by reacting it with the calcium oxide. It is desirable to have the coal and calcium oxide well-mixed so that the sulfur dioxide coming from the coal has good exposure to the sorbent.* Segregation reduces this exposure because the coal particles, being less dense, tend to migrate to the top of the bed.

Minerals beneficiation is a case in which segregation can be helpful. It is often desirable to separate as much of the inert materials as possible before processing ores in expensive or energy intensive operations. Fluidized bed segregation offers a means of accomplishing this separation when other methods are unsuitable or too expensive.

---

*In fact the optimum condition would be to have the coal at the bottom of the bed, but this is not practically realizable since the coal is typically much less dense and similar in size to the limestone. In practice, the best possible condition is well-mixed.

Solids segregation is known to occur in both gas and liquid fluidized beds. Gas-fluidized beds are unique from liquid-fluidized beds because of the formation of gas voids or bubbles. Bubbles are produced by turbulent interactions between the gas and solids, and they usually form when the superficial gas velocity slightly exceeds that required to support the weight of the bed (i.e., the minimum fluidizing velocity). The nature of the bubbles and the circulation patterns created by them can vary widely depending on the bed design and the properties of the fluidized particles. The variation in flow behavior with particle size is particularly important, and it has become common practice to classify fluidized beds into two general types, large-particle and small-particle. As is discussed in Section 2, the boundary between large and small-particle beds depends on particle density and bed geometry as well as particle size. For purposes of general discussion, however, it is often useful to define large-particle beds as those with particles larger than 1 mm.

Previous segregation studies have focused almost exclusively on small-particle beds. This investigation has been directed specifically at segregation in large-particle beds. My objectives have been: (1) to develop a qualitative, phenomenological description of the axial segregation patterns which can occur in large-particle beds, (2) to interpret these phenomena in terms of specific hydrodynamic processes, (3) to compare the large-particle segregation phenomena with those observed in small-particle beds, (4) to develop a mathematical model which can be

used as a basis for interpreting, organizing, and correlating segregation data, and (5) to draw conclusions about the implications of segregation for fluidized bed reactor performance.

To accomplish these objectives, I have drawn on three primary sources of information: the substantial literature on small-particle fluidized beds, the less extensive literature on large-particle beds, and my own small-scale experiments with selected systems of large particles. My strategy has been to summarize the key points of general agreement in the literature regarding flow behavior and segregation patterns, and then to fill in some of the gaps with experiments. I have also attempted to evaluate the basic assumptions of previous segregation models. This has led me to select and refine one specific model as being the most useful description of segregation in binary, large-particle systems. I then combined this model with the generally accepted methods for modeling bubbling fluidized bed reactors to explore the implications for reactor performance.

Chapter 2 reviews the current state of knowledge regarding flow behavior and segregation in gas-fluidized beds. Chapters 3 and 4 describe my experimental methods, apparatus, and results for large particles. Chapters 5 and 6 contain additional discussions regarding segregation modeling and the implications for chemical reactors. Chapter 7 contains my final conclusions and recommendations. My raw experimental data and the results of parameter fitting are tabulated in the Appendix.

2. LITERATURE REVIEW

2.1 Flow Behavior in Fluidized Beds

Although the detailed hydrodynamics of gas-fluidized beds is extremely complex, it is still possible to separate the observed flow patterns into a few basic categories. Figure 2.1 illustrates the categories which are commonly referred to in the literature. When gas is passed slowly upward through a bed of solids, it percolates through the interstitial voids and causes the bed to expand slightly. As the flow increases,* a point is reached where the drag on the particles just balances their weight, and then the bed is said to be at the minimum fluidizing condition. Particles at this condition may vibrate somewhat, but they are still trapped by the surrounding solids and remain essentially fixed in one location.

The minimum fluidizing condition in practical situations often occurs over a range of gas velocities due to variations in particle size and density. Nevertheless, it is usually possible to identify an effective minimum fluidizing gas velocity, denoted here by u_{mf}, which is experimentally reproducible. This is determined by observing the gas velocity above which there is little or no change in the overall pressure drop. The minimum fluidizing velocity can also be estimated from the particle and gas properties by using the equation developed by Ergun (1952) or a modified equation developed by Wen and Yu (1966).

*Gas flow is usually expressed in terms of u_o, the superficial linear velocity. This is determined by dividing the volumetric flow at the average temperature and pressure in the bed by the open cross section; i.e., the cross section when there are no solids present.

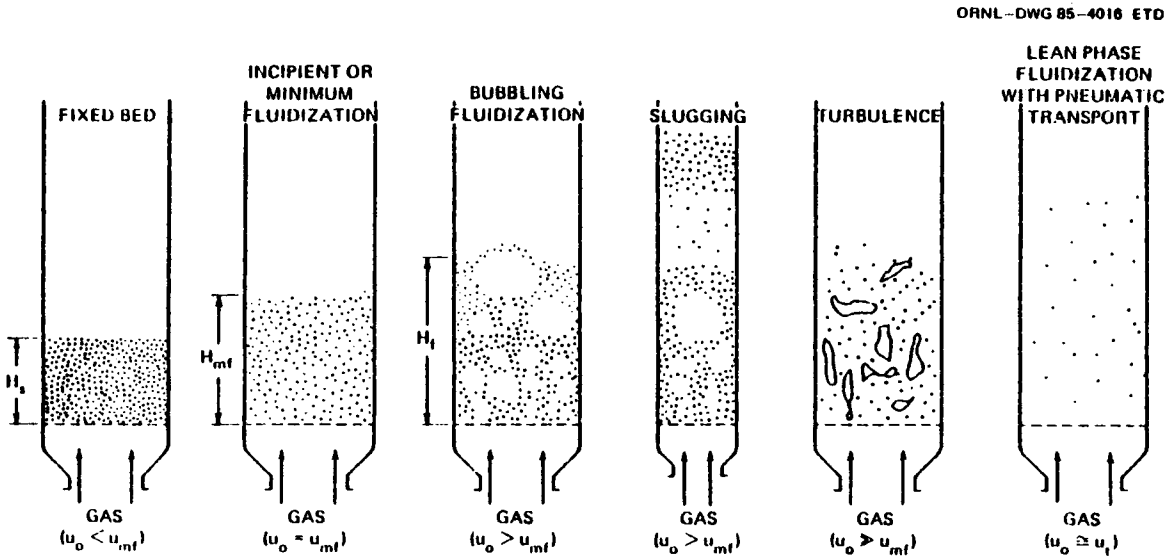

Figure 2.1. The basic flow patterns which occur in gas-fluidized beds (adapted with modification from Kunii and Levenspiel (1969)).

Increasing the gas flow above the minimum fluidizing velocity results in the formation of turbulent instabilities which take the form gas voids or bubbles. These move up through the solids and induce a net circulation; particles moving upwards in association with the bubbles and then downwards in other areas. Still higher flow rates cause more solids agitation, and sometimes "slugging" begins to occur. Slugging is a severe form of bubbling in which the bubbles fill the entire bed cross-section and force slugs of solids upwards. Slugging is usually accompanied by violent pressure and flow oscillations.

Beyond slugging is the "turbulent" regime. In this condition, the oscillations become less than those produced by bubbling or slugging, and the bed takes on a more homogeneous appearance. The voids become smaller and transient; the circulation patterns break up into smaller, more localized eddies. Continuing to increase the gas flow ultimately leads to solids elutriation when the particle terminal velocities are exceeded. This is the pneumatic conveying limit.

For all flow regimes above u_{mf}, local properties such as solids density, gas velocity, and solids velocity can fluctuate widely with respect to both space and time. Thus it is essentially impossible to precisely describe the state of any particular location in the bed at any particular instant. The usual convention is, instead, to use the time-averaged characteristics, such as the average bubble size, gas velocity, or solids composition. These time-averaged characteristics can be further averaged with respect to spatial location. It is common to find references to the average properties for the bed as a whole, such as the overall average bubble size, the mean superficial velocity, and the

overall bed solids composition. It is important to remember, however, that average properties alone are not sufficient to describe some aspects of fluidized bed behavior. Some phenomena, such as segregation and mixing, are greatly affected by temporal and spatial variations.

Bubble size and velocity are generally good indicators of the fluctuation intensity or degree of turbulence. Sometimes bubble characteristics are grossly described by the "state of fluidization." Beds having few bubbles and little solids circulation are said to be exhibiting particulate behavior. Liquid-fluidized beds usually behave this way. Beds with large bubbles and vigorous circulation are said to be exhibiting aggregative fluidization.

Bubbles are also classified by how fast they move relative to the gas percolating through the interstitial voids. When the average bubble velocity exceeds the average interstitial gas velocity, the resulting hydrodynamics are said to follow the "fast-bubble" regime. When the average interstitial gas velocity is greater, the hydrodynamics are said to follow the "slow-bubble" regime.

2.2 Bubble Dynamics and the Two-Phase Theory

The most important concept to arise in the development of fluidized-bed hydrodynamic models has been the so-called two-phase theory. Originally proposed by Toomey and Johnstone (1952), the two-phase theory assumes that the bed can be separated into two regions; an emulsion phase* containing the bulk of the solids and the interstitial gas, and a bubble phase which consists of the bubbles themselves and their associated solids (i.e., wake). It is further assumed that the emulsion phase

*Also called bulk phase or particulate phase.

remains at the minimum fluidizing conditions. Figure 2.2 illustrates these basic features. Note that when the solids circulation is sufficiently high, the emulsion-phase gas velocity can actually be negative relative to the distributor plate, even though it is still at minimum fluidizing conditions relative to the solids themselves.

When the two-phase approach is adopted, the next step is to understand the motion of the bubbles and their interaction with the surrounding solids and interstitial gas. A detailed analysis of fluid and particle motion near rising bubbles was first made by Davidson (1961). He assumed that the emulsion phase follows potential flow and that the interstitial gas flow relative to the particles follows Darcy's Law. Modifications to Davidson's original analysis have been suggested by other investigators, such as Murray (1965) and Partridge and Rowe (1966), but Davidson's model continues to be the most popular.

One of Davidson's most important results was that the rise velocity of a single bubble depends only on the square root of the bubble diameter; that is,

$$u_{br} = 0.711\ (g\ D_B)^{1/2} \tag{2.1}$$

where u_{br} is the bubble rise velocity, g is the acceleration due to gravity, and D_b is the bubble diameter. Davidson and Harrison (1963) subsequently showed that the rise velocity of a swarm of bubbles is given by

$$u_b = u_o - u_{mf} + u_{br} \cdot \tag{2.2}$$

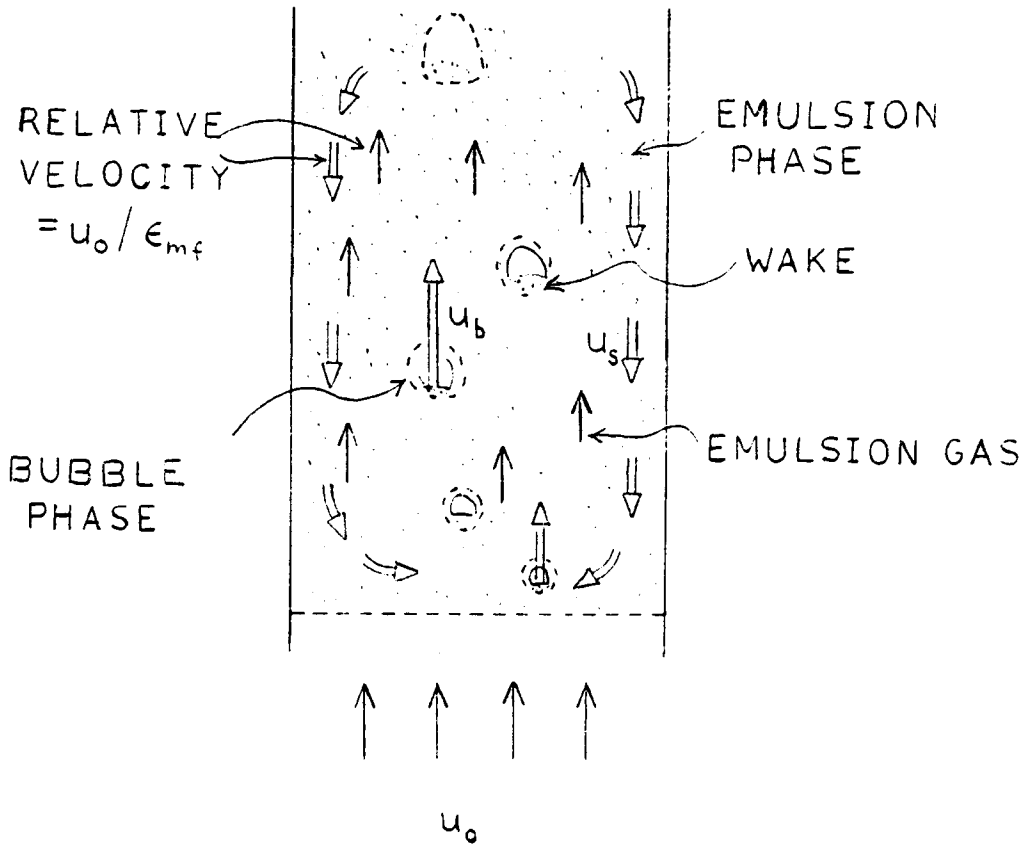

Figure 2.2. The basic features of the two-phase theory for gas-fluidized beds.

Note that u_{br} is still the relative velocity between the bubble and emulsion phases. For any given gas velocity, these results make it possible to essentially characterize the bed with two parameters, the bubble diameter and the minimum fluidizing velocity.

Davidson's work was extended by Pyle and Rose (1965) who developed a theory describing flow within the rising bubble. For the most part these theories have been able to explain bubble behavior quite well, in particular the observations related to "fast" and "slow" bubbles. These are illustrated in Figure 2.3. The bubbles depicted in the lower part of the figure represent fast bubbles, where the bubble rise velocity is greater than the interstitial gas velocity. In this case, gas enters the bottom of the bubble, flows upward through it, and exits at the top into a circulating stream which returns to the bottom. The effect is to create a captive gas cloud which moves up through the bed "attached" to the bubble. Various fluidized-bed reactor models have been developed for bubbles of this type, most notably those of Rowe (1964), Partridge and Rowe (1966), Latham et al. (1968), Kunii and Levenspiel (1969), Kato and Wen (1969), and Fryer and Potter (1972). The recirculating gas cloud is a key assumption of these models, and mass transfer coefficients between the bubble and emulsion gas are defined accordingly. In general, the recirculating gas cloud tends to reduce the interphase mass transfer.

Slow bubbles, depicted in the upper part of the figure, occur when the bubble rise velocity is less than the interstitial gas velocity. Here the gas uses the bubbles as a shortcut on its way through the bed, and there is no recirculated gas cloud. Slow bubbles are expected to

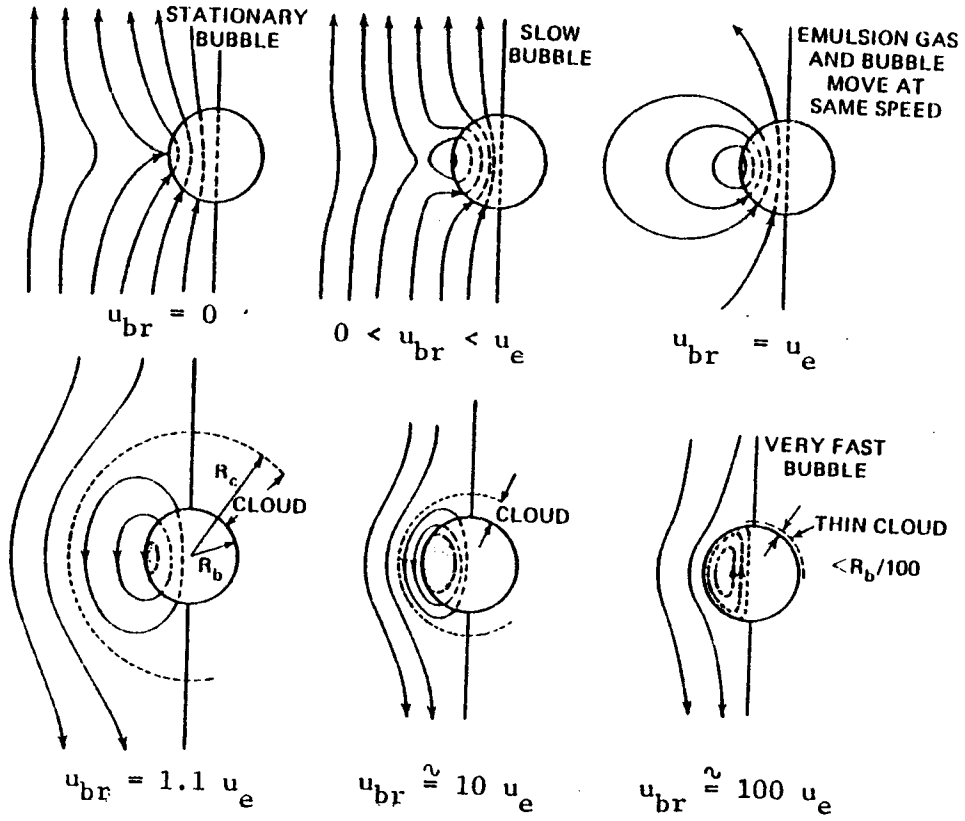

Figure 2.3. The gas flow patterns around bubbles as described by the theories of Davidson (1961) and Pyle and Rose (1965) (adapted with modification from Kunii and Levenspiel (1969)).

occur when the bubble diameter is small or when u_{mf} is large. Investigators such as Cranfield (1978), McGrath and Streatfield (1971), Canada et al. (1978), and Jovanovic (1979) have studied and confirmed the behavior of such bubbles.

A distinctive form of slow bubbles occurs when the bubble growth rate is of the same magnitude as the bubble rise velocity; i.e.,

$$\frac{d(D_B)}{dt} \simeq u_b \cdot \tag{2.3}$$

This regime has characteristically large pressure oscillations similar to slugging and is even sometimes referred to as "apparent" slugging or the "exploding-bubble" regime. Its occurrence has been reported for shallow beds of large particles by investigators such as Cranfield and Geldart (1974), Canada et al. (1978), McGaw (1977), and Jovanovic (1979). True slugging develops in deeper beds where the bubbles can grow to the bed diameter before reaching the surface.

As applications for fluidized beds have expanded, it has become necessary to develop correlations for a wider range of particle sizes. Guidelines for separating the different types of particle behavior have therefore become increasingly important. Geldart (1973) made a significant contribution in this area by developing a general classification scheme based on size and density. Figure 2.4 illustrates Geldart's system.

In terms of Geldart's classification system, most studies before 1975 concentrated on class A and B particles, which typically exhibit fast bubble behavior. More recent studies, such as those by Catapovic

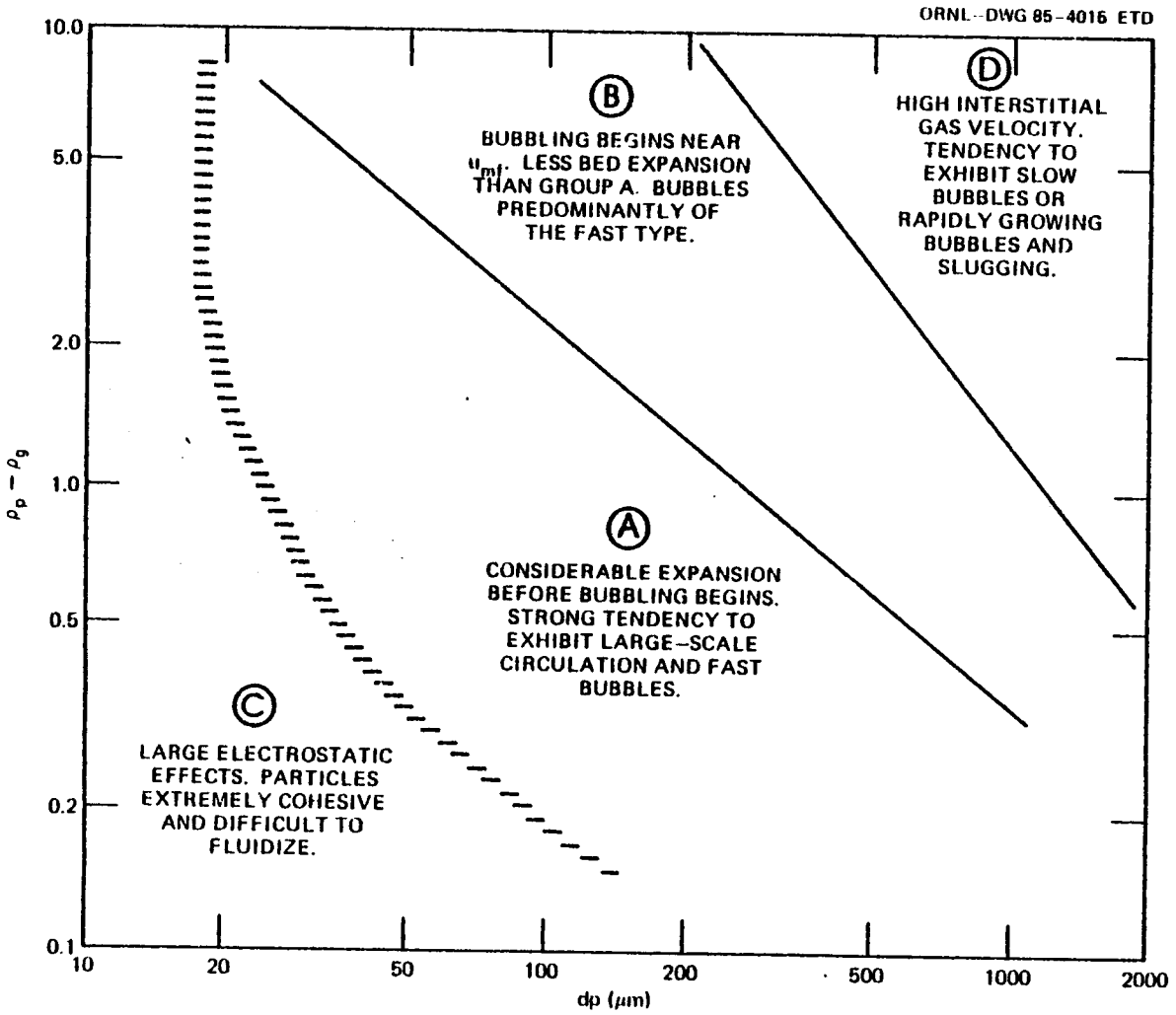

Figure 2.4. The fluidization classification scheme proposed by Geldart (1973) based on particle size and density (adapted with modification from Geldart (1973)).

et al. (1978), Jovanovic (1979), Cranfield (1978), and Canada et al. (1978), have looked at Geldart's class D particles, which tend to have slow bubbles and a strong tendency toward slugging.

Geldart's classification system has been supplemented by the general flow map of Catapovic et al. (1978). An example map for limestone and dolomite is shown in Figure 2.5. The flow regime is shown as a function of the superficial gas velocity, the minimum fluidizing velocity, and the particle diameter. For a given particle size, the bed can be seen to follow two possible transition paths as gas velocity is increased: (1) slow bubbles to fast bubbles to turbulence or (2) slow bubbles to rapidly growing bubbles to turbulence. Van Deemter (1980) has further combined the schemes of Catapovic et al. and Geldart into a single map.

The turbulent regime noted in the upper part of Catapovic et al's. map is a relatively unexplored phenomenon, first described by Yerushalmi et al. (1976). This condition can occur in both large and small-particle beds, but apparently occurs at lower excess gas velocities (i.e., at lower ratios of u_o/u_{mf}) for large particles. As described previously, bubbles are replaced by transient voids and intense eddies which enhance mixing. The appearance is similar to a dense fluid in turbulent flow. Pressure oscillations appear damped over what they are in bubbling or slugging flow. Also as one might expect, the assumptions inherent in the two-phase model do not appear adequate for describing the turbulent regime [see for example Avidan and Yerushalmi (1981) and Staub and Canada (1978)].

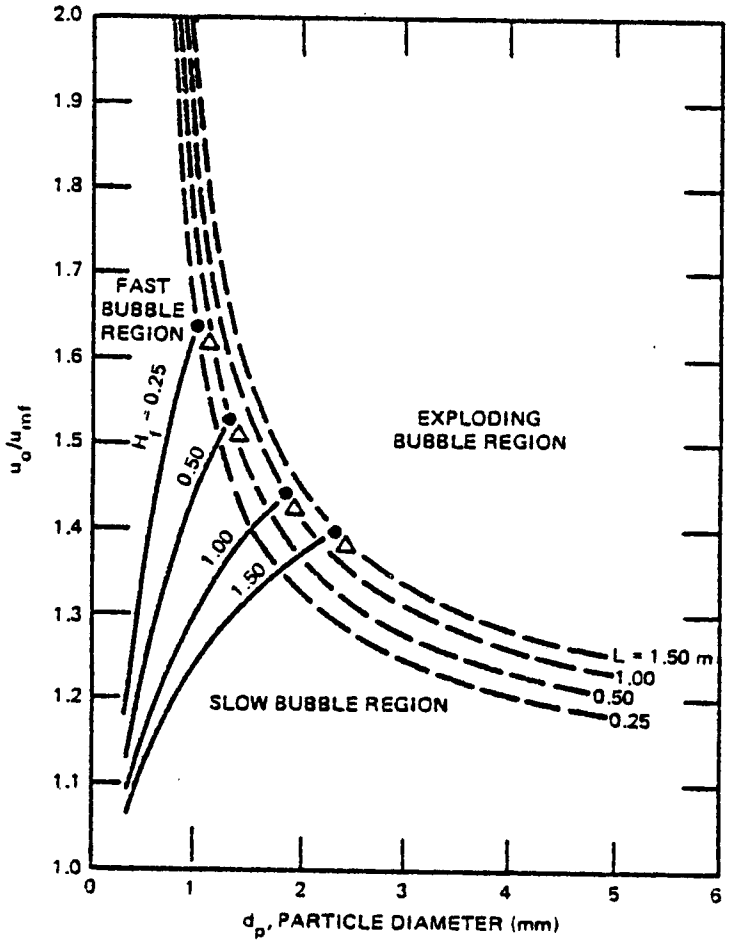

Figure 2.5. The general flow map of Catapovic et al.(]978) which relates the flow regime in limestone and dolomite to superficial gas velocity, the minimum fluidizing velocity, and the particle diameter (adapted with modification from Catapovic et al.(1978)).

2.3 Solids Motion

As discussed in the following section, solids motion is a key concern in gas-fluidized-bed segregation. It is controlled by bubble motion, and can be sluggish or rapid depending on the bubble size and frequency. Solids motion in large-particle beds is of particular interest in this investigation.

With gas velocities just above minimum fluidization, solids motion is sluggish. At higher gas velocities, definite large-scale circulation occurs. Perhaps the most common pattern is that in which the bubbles and their associated solids tend to move up near the center of the bed, the solids spread over the top of the bed, and then they flow down near the walls to the bottom where the cycle repeats. Cranfield (1978) and Sitnai (1981) report this type of pattern. In another pattern the circulation is reversed and gas and solids flow upwards near the walls and downwards near the center. This pattern does not appear to have been clearly documented in the literature, but it has been observed independently by myself and Lackey (1984) at Oak Ridge National Laboratory. Asymmetric circulation can occur when gas flow is accidently or intentionally unevenly distributed [e.g., see Piccinini (1980) and Rios et al. (1980)].

The detailed behavior of solids near a single rising bubble has been described by Rowe et al. (1965) for small particles and Cranfield (1978) for large particles. Rowe et al. reported two distinct mixing mechanisms, only one of which is important for gas-fluidized beds of particles greater than 100 μm. In this mechanism, solids are drawn up in a finger behind each bubble and, in addition, solids move in a wake

with the bubble to the surface, spilling periodically on the way. Rowe has recently indicated [Rowe (1984)] that the amount of solids spilled from the wake is probably a small fraction of the total solids in the wake. Cranfield (1978) reported that in large particle beds the finger is drawn up behind the bubble also, but that captive wake formation and shedding did not occur. His results also indicated that the solids finger stopped somewhat short of the bed surface.

The effect of internal tubes and baffles on solids motion is, in general, known only qualitatively. Harrison and Grace (1971), Chen and Chao (1982), and Avidan et al. (1981) illustrate considerable data for different designs of bed internals and flow environments. In general it appears that horizontal tubes have a significant damping effect on the solids velocities although the shapes of the circulation profiles appear to be relatively unaffected. Vertical and inclined tubes can provide channeling paths for bubbles and particles and actually enhance circulation. Thus tube configuration can have a profound effect on the solids flow behavior. The erosion and temperature gradient problems encountered at the Grimethorpe pressurized-fluidized-bed-combustion facility [McKendrick (1982)] illustrate the need for a fundamental understanding of the relation between tube configuration and solids circulation.

2.4 Previous Studies of Solids Segregation

In the past thirty years there have been at least twenty-three studies related to solids segregation in gas-fluidized beds. Table A-1 in the Appendix summarizes the scope and results of these studies. Only five studies, those by Fan and Chang (1979), Yoshida et al. (1980), Geldart et al. (1981 a&b), and Cooke et al., have looked at beds

composed at least partly of large particles. These studies and those of Katz (1957), Shannon (1959), Sutherland and Wong (1964), Goosens et al. (1971), Capes and McIlhinney (1972), Rowe et al. (1972 a&b, 1974) and Nienow (1978 a&b), Chen and Keairns (1975, 1978), and Burgess et al. (1977) are the most directly relevant to the present investigation. This subset of 18 studies forms the nucleus of the following discussion.

2.4.1 Katz (1957)

Katz investigated the segregation of binary mixtures of different sized particles of glass, magnesium, and graphite. He focused specifically on the effects of differing particle size (two-density systems were not studied), and he measured both pressure drop and axial particle distribution as a function of gas velocity and particle size difference. Because of the small particle sizes used (74 to 840 μm diameter), the flow regimes he encountered would be expected to be typical of small-particle behavior.

Katz observed that in multi-particle-size beds, the transition from the fixed to fluidized states occurred over a range of gas flows. As the difference between the particle sizes increased, the transition region became wider, but it was always smaller than the range between the minimum fluidizing velocities of the components. Within this transition region, the beds consisted of two sections separated by an interface. The lower, static phase, had an excess of coarse particles, the upper, fluidized phase an excess of fine particles. The relative proportions of the two phases also changed with gas flow rate, the upper phase increasing in size and in coarse content with gas flow. The compositions of the two phases appeared to be independent of the overall bed composition for bed compositions between 20 and 80 weight % coarse particles.

Katz represented this behavior in terms of phase-composition versus gas-flow diagrams.

Katz reported considerable difficulty with static electricity and humidity in running his experiments. He went to great lengths to eliminate the effects of these variables, but still attributed some unexpected behavior to them, even when he used a metal column, conducting solids, and dry air. Subsequent investigators have not reported this degree of difficulty. One of the unexpected phenomena reported by Katz is perhaps worthy of specific mention. This is his observation that the composition of the upper phase exhibited maxima and minima as gas flow was increased. He appeared to consider this behavior as resulting from experimental error or static effects and did not pursue it further. The significance of this observation will be made clear in subsequent discussions of my experimental results. It may be that Katz observed a true hydrodynamic phenomenon without realizing it.

2.4.2 Shannon (1959)

Shannon studied segregation in mixtures of two and three sizes of small glass beads (<0.6 mm diameter). He also observed the fluidization behavior of several other materials, including sand, cracking catalyst, and iron ore. He concluded that the extent of segregation is determined by the minimum fluidizing velocity of each component and the overall gas velocity; higher gas velocities and smaller differences in the minimum fluidizing velocities tending to enhance mixing and reduce segregation. His data indicated that segregation was not significant unless the ratio of minimum fluidizing velocities for consecutively size components was greater than 2.

Shannon pictured segregated beds as having essentially two parts: (1) a lower layer consisting of expanded but fixed solids, and (2) an upper layer consisting of fully fluidized solids. In keeping with this picture, he described an idealized model of segregation in which the upper layer is composed entirely of the solids which have a minimum fluidizing velocity below the actual superficial gas velocity, and the lower layer is composed entirely of solids which have a minimum fluidizing velocity above the actual superficial gas velocity. He explained deviations from this ideal behavior by noting that: (1) localized voidage variations produce velocities higher and lower than the average, (2) very small particles (e.g. <100 μm diameter) are affected by static electricity and humidity, (3) once heavier particles move into a fluidized layer of lighter particles, the collisions of the lighter particles tend to counteract resettling of the heavier particles, and (4) lighter particles in the defluidized layer can become "trapped" by the heavier particles and may not move even if the gas velocity is higher than the light particles' minimum fluidizing velocity. Shannon developed a qualitative description of how the particle distribution is altered by these non-idealities, and he demonstrated that his experimental data are consistent with the expected trends. Shannon also noted that when the superficial air velocity was above the minimum fluidizing velocity of the large component, mixing was almost uniform over the bed except for a slightly higher concentration of the larger solids at the bottom of the column.

2.4.3 Sutherland and Wong (1964)

Sutherland and Wong (1964) studied segregation of sand particles (<.35 mm diameter) in gas-fluidized beds containing screen packing. The screen packing inhibited bubble growth and coalescence, producing pseudo-particulate flow, similar to the flow in liquid-fluidized beds. They found that the packing enhanced segregation by reducing the large-scale solids circulation which is induced by bubble flow. They point out that at steady-state, the segregation profile represents a dynamic equilibrium between segregation and circulation.

In order to quantify their results, Sutherland and Wong used two segregation indices: (1) an overall segregation efficiency defined as

$$\left(\overline{d}_{p\ \text{bottom}}/\overline{d}_{p\ \text{top}}\right)_{\text{experimental}} \Big/ \left(\overline{d}_{p\ \text{bottom}}/\overline{d}_{p\ \text{top}}\right)_{\substack{\text{maximum possible}\\ \text{segregation}}} \times 100\% ,$$

where bottom and top refer to the bottom and top sampling points, and (2) an incremental segregation efficiency defined in an analogous way for smaller sections of the column. Perhaps one of the most interesting trends they observed was that the overall segregation efficiency reached a minimum at some gas velocity between the minimum fluidizing velocity of the largest component and the terminal velocity of the smallest component. At velocities above or below this optimum value, segregation increased.

Sutherland and Wong also proposed a model for the rate of segregation development in the lower part of the bed. They assumed that the bed can be divided into two well-mixed regions, a small one near the bottom where concentration changed with time, and a larger upper region

where concentration changes were not significant. Then they postulated an equation for the time rate of change of the smaller component

$$\frac{dx_F}{dt} = -K_1 x_F + K_2 (x_{Fo} - x_F) , \qquad (2.4a)$$

where

x_F = mass fraction of the smaller component at time t,

x_{Fo} = mass fraction of the smaller component at time zero,

K_1 = empirical segregation rate constant, and

K_2 = empirical mixing rate constant.

The first term is supposed to represent the segregation effect, and the second term the mixing effect. K_1 and K_2 were assumed to be independent of time and composition, thus allowing the rate equation to be integrated to give

$$\ln \frac{(K_2 + K_1) x_F - K_2 x_{Fo}}{K_1 x_{Fo}} = (K_1 + K_2)t . \qquad (2.4b)$$

This result agreed fairly well with Sutherland and Wong's data, but it did not explain concentration changes at the top of the column or the shape of the axial concentration profiles.

2.4.4 Goosens, Dumont, and Spaepen (1971)

Goosens, et al. investigated the segregation behavior of binary mixtures of fine uranium dioxide and alumina (Geldart's groups A and C) near the minimum fluidizing conditions for both components. They did not measure solids concentration profiles, but instead they quantified segregation tendency with a demixing index, i_u defined by

$$i_u = \frac{u_{move}}{u_{mf}} ,$$

where u_{move} is the superficial gas velocity at which all particles of a mixture begin to move and umf is the minimum fluidizing velocity of the mixture. Their qualitative observations indicated that this index correlated well with segregation; high values representing segregated conditions. They further proposed a "demixing criterion" for predicting the tendency of solids to segregate. This criterion is given by

$$L = 1 + \frac{(1 - \bar{x}_J)\, \bar{x}_J\, R\, (D' - 1)^2}{[\bar{x}_J + (1 - \bar{x}_J)\, RD']^2} , \qquad (2.5)$$

where

L = relative demixing criterion,

$\bar{x}_J$ = overall weight fraction of the heavy (jetsam) component,

$R = \rho_J/\rho_F$ = ratio of particle densities of the two components (jetsam/flotsam), and

$D' = \bar{d}_J/\bar{d}_F$ = ratio of harmonic mean diameters of the two components (jetsam/flotsam).

Goosens, et al. derived this relationship using the assumption that the segregation tendency for two solids near minimum fluidizing conditions is related to the ratio of the flow resistance of a completely segregated bed to the flow resistance of a well-mixed bed. For non-segregating systems L is just equal to 1. The more L deviates from 1 (it is always greater than 1), the greater the segregation tendency.

2.4.5 Capes and McIlhinney (1972)

Like Sutherland and Wong (1964), Capes and McIlhinney (1972) also investigated small particles in gas-fluidized beds containing screen packing. Their objectives were to measure the expansion and segregation characteristics of mixtures of glass, sand, polyvinylactate, nickel, and lead particles less than 1.55 mm in diameter. They did not use a quantitative segregation index or measure the solids concentration profiles, but they did note qualitative trends. In particular, they observed a strong correlation between segregation and the bulk density differences between the components; segregation was increased by increasing the bulk density difference between the components and decreased as the average particle density increased. Bulk density here is defined as the overall density a component would have if it were by itself in a bed at the conditions of interest. When two components had different bulk densities, the component with the higher density acted as jetsam, the other as flotsam.

Capes and McIlhinney observed that the expansion in screen-packed bed is equivalent to the sum of the expansions of the individual components, regardless of the degree of mixing. They further noted that the bulk densities of different components can vary at different rates with gas velocity, and thus the bulk densities can become equal and then reverse in magnitude as gas velocity is increased. Under some circumstances, a reduction in segregation or even an inversion in flotsam-jetsam roles could be expected. Capes and McIlhinney did not observe such an inversion, but they pointed to studies of liquid-fluidized beds

in which this did happen. They concluded that the circulation in gas-fluidized beds may inhibit this effect.

2.4.6 Rowe, Nienow and Agbim (1972 a&b); Gibilaro and Rowe (1974); Nienow, Rowe, and Cheung (1978); and Nienow, Rowe, and Chiba (1978)

P. N. Rowe and coworkers at University College, London, have probably been the most prolific investigators of solids segregation in gas-fluidized beds. Most of their experiments have been carried out with solids having mean sizes up to about 700 μm, densities up to 8.86 g/cm^3, and gas velocities up to 0.85 m/s (2.8 ft/s). Cylindrical beds up to 22 cm (8.7 in.) in diameter as well as two-dimensional beds were used.

Rowe et al. (1972 a&b) made extensive measurements of segregation in open,* gas-fluidized beds of small particles. Binary systems of particles, differing in either size or density, were fluidized with air in beds of varying depth and diameter. The investigators consistently observed a uniform composition over a wide middle region of the fluidized bed height, even when appreciable segregation occurred elsewhere. They concluded that the degree of mixing depends very strongly on the gas velocity, and even strongly segregating systems can be either separated or well mixed by controlling this parameter. In segregating conditions, only the bottom region approached a pure composition of jetsam, while at the top the flotsam was always contaminated with jetsam. Typical illustrations of these patterns are shown in Figure 2.6. The horizontal axis

*That is, beds without internals such as tubes, baffles, or screen packing.

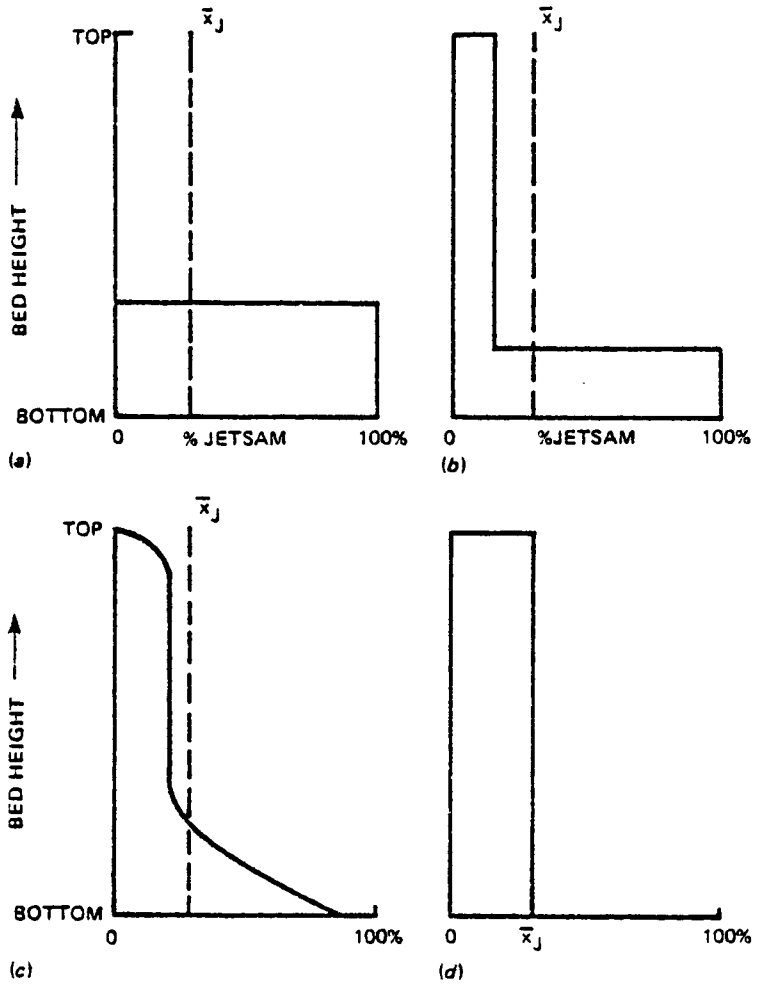

Figure 2.6. Typical segregation patterns observed by Rowe et al. (1972 a & b) in open, gas-fluidized beds of small particles (adapted with modification from Rowe et al.(]972b)).

represents the weight fraction of jetsam present in the solids, the vertical axis represents the axial position in the bed.

Segregation was found to vary as $(\rho_J/\rho_F)^{-5/2}$ and decreased as velocity increased (ρ_J = particle density of jetsam, ρ_F = particle density of flotsam). Segregation was also found to vary weakly with particle size by the relationship $(d_J/d_F)^{-1/5}$. These relationships indicate that segregation depends much more strongly on density differences than size differences. For systems containing an excess of jetsam, the composition of the upper region was given by the relationship

$$x_{J1} = f(u_o - u_{mf})(\rho_J/\rho_F)^{-5/2}\ (d_J/d_F)^{-1/5}\ , \qquad (2.6)$$

where

x_{J1} = mass fraction of jetsam near the top of the bed (measured as fraction of the solid phase), and

$f(u_o - u_{mf})$ = function of unspecified form; approximately linear in $u_o - u_{mf}$ at low values of $u_o - u_{mf}$.

The composition at the top of the bed was also used to define an overall mixing index, $M = x_{J1}/\bar{x}_J$. When $M = 0$, the bed is perfectly segregated; when $M = 1$, the bed is perfectly mixed.

Rowe et al. also concluded that there are three distinct mechanisms which influence the extent of segregation:

(1) the lifting of particles in rising bubble wakes,

(2) the falling of particles through bubbles, and

(3) the falling of particles through voids induced by the passage of bubbles.

The first mechanism tends to reduce segregation and favor mixing. It is the only way particles can move to the top of the bed. In the second and third mechanisms, large, heavy particles fall faster than small, light ones.

Based on their observations, Rowe et al. concluded that the first two mechanisms are the most important and that the third mechanism only occurs occasionally. They also noted a fourth mechanism which was never seen to cause segregation but appeared to preserve it. This is the quasi-hydrostatic effect which causes low density particles to "float" on a bed of denser particles. This effect only appeared to prevent low density particles from moving down; it did not appear to cause them to move up.

In 1974, Gibilaro and Rowe proposed a model to describe steady-state segregation in small particle beds. This model addresses the mechanisms of solids mixing and segregation observed by Rowe et al. (1972), and it appears to do a good job of simulating the typical concentration profiles when parameters are properly adjusted. Four basic processes are accounted for:

(1) Solids are picked up from the bottom of the bed in bubble wakes and carried to the top. Here they leave the wake phase and join the downward moving bulk phase. The volumetric solids circulation rate is assumed to be approximately constant across any horizontal plane.

(2) There can be an exchange of solids between the bulk and wake phases. The rate of exchange is defined in terms of the total volumetric rate (of solids) per unit height of bed. This is assumed to be constant over the length of the bed.

(3) Apart from wake circulation, bubbles cause some axial displacement of solids by a "drift" mechanism. It is assumed that this can be approximated as a pseudo-diffusion (Fickian) process with a constant dispersion coefficient.

(4) Jetsam overtakes flotsam by falling more rapidly through bubbles or disturbed regions of the bed. At each point the downflow of segregating jetsam is compensated by an equal upflow of flotsam from below. The rate of this transition at any level is proportional to the product of the jetsam concentration at that level and the flotsam concentration in the level immediately below.

Figure 2.7 summarizes the physical picture represented by these assumptions. The resulting differential equations describing the jetsam transport in the bulk and wake phases, respectively, are

$$\frac{r}{H}\frac{d^2v_J^B}{dz^2} + (w + k - 2kv_J^B)\frac{dv_J^B}{dz} + qH\,(v_J^W - v_J^B) = 0 \qquad (2.7a)$$

and

$$w\frac{dv_J^W}{dz} - qH\,(v_J^B - v_J^W) = 0\ , \qquad (2.7b)$$

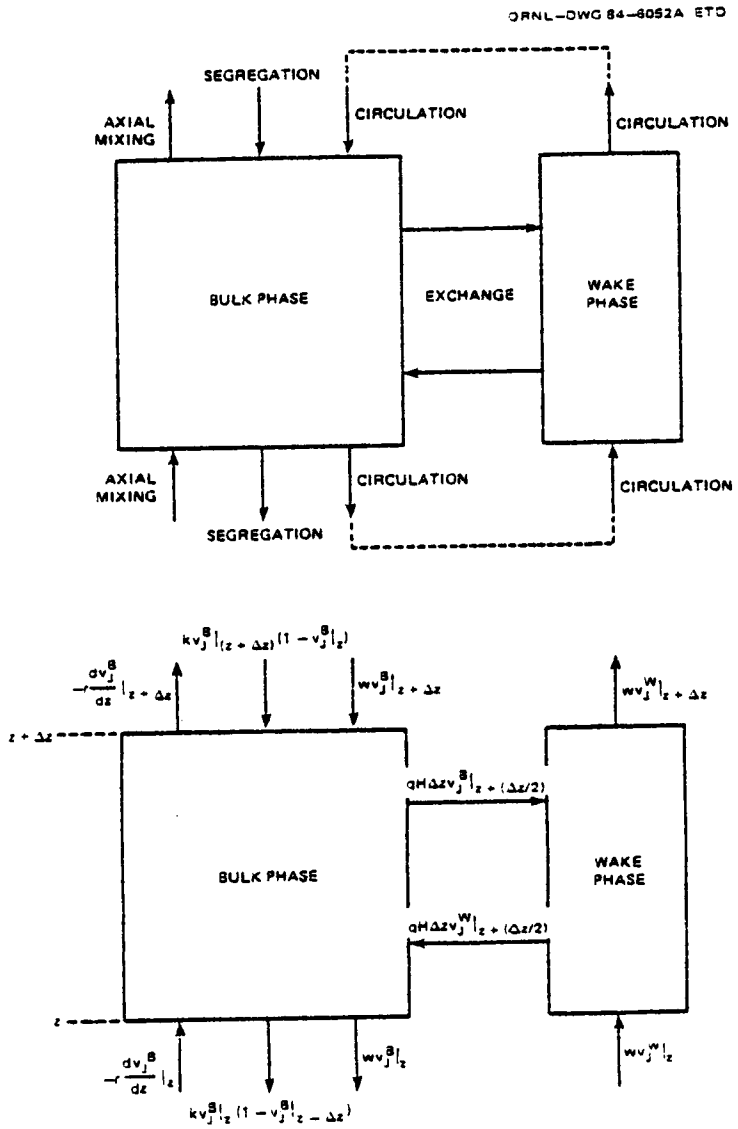

Figure 2.7. Illustration of the assumptions made by Gibilaro and Rowe (1974) in their steady-state segregation model.

where

r = an axial mixing coefficient [L^4/t],

H = total bed height [L],

z = normalized axial position = y/H [-],

v_J^B = volume fraction of solids in bulk phase which are jetsam [-],

v_J^w = volume fraction of solids in wake phase which are jetsam[-],

w = solids circulation rate [L^3/T],

k = segregation coefficient [L^3/T], and

q = bulk/wake exchange rate coefficient [L^2/T].

To simplify matters, Gibilaro and Rowe assumed that the transport parameters r, w, k, and q were constant over the bed height.

Rather than attempting to integrate the coupled equations directly, Gibilaro and Rowe considered three special cases where some of the parameters could be neglected and simplifications made. The special cases analyzed were: (1) strongly segregating systems where axial mixing and phase exchange are negligible, (2) systems with exchange between the wake and bulk phases but no axial mixing, and (3) systems with axial mixing and wake circulation but no exchange between phases.

For Case 1, the solution is

for $0 \leq z < z^*$, $v_J^B = 1$, (2.8a)

for $z = z^*$, $v_J^B = (\lambda_w + 1)/2$, (2.8b)

for $z^* < z \leq 1$, $v_J^B = \lambda_w$, (2.8c)

for $0 \leq z \leq 1$, $v_J^w = 1$, and (2.8d)

for $0 \leq z \leq 1$, $v_J = v_w v_J^w + (1 - v_w)\, v_J^B$, (2.8e)

where

λ_w = dimensionless ratio of circulation to segregation parameters = w/k,

v_J = average of wake phase and bulk phase jetsam fractions,

z^* = interface location = $\dfrac{(\bar{v}_J - v_w) - \lambda_w(1 - v_w)}{(1 - v_w)(1 - \lambda_w)}$,

$\bar{v}_J$ = average overall volume fraction of solids which are jetsam, and

v_w = volume fraction of solids in the bed which are in the wake phase.

Figure 2.8 illustrates the appearance of the bulk phase concentration profile. When v_w is small, as it is in many cases, this profile would represent the actual overall bed profile.

An interesting limit for Case 1 occurs when there is insufficient jetsam present to form the bottom layer. The condition for this is

$$\bar{v}_J < v_w + (1 - v_w)\lambda_w \ .$$

In this case the profiles become

$$v_J^B = \frac{1}{2}\left\{1 + \frac{\lambda_w}{v_w} + \left[\left(1 + \frac{\lambda_w}{v_w}\right)^2 - \frac{4\,\bar{v}_J\,\lambda_w}{v_w}\right]^{1/2}\right\} \ , \qquad (2.9a)$$

$$v_J^w = v_J^B + (v_J^B/\lambda_w)\,(1 - v_j^B) \ , \qquad (2.9b)$$

and

$$v_J = \bar{v}_J \ . \qquad (2.9c)$$

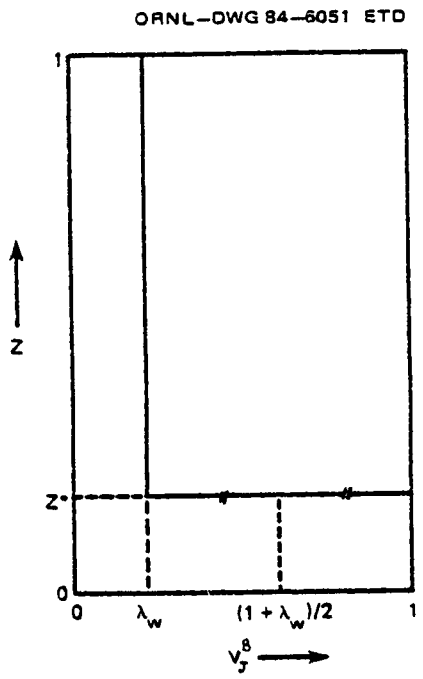

Figure 2.8. The bulk-phase profile predicted by the Gibilaro and Rowe model for Case 1 - strongly segregating systems where axial mixing and phase exchange are negligible (adapted with modification from Gibilaro and Rowe (1974)).

Thus from the standpoint of the average concentration profile, the bed appears well-mixed, although the wake and bulk phases differ widely in composition. On a small scale, the bed can be quite heterogeneous.

For Case 2, the solution becomes

$$\text{for } 0 \leq z < z^*,\ v_J^B = 1 \ , \tag{2.10a}$$

$$\text{for } z = z^*,\ v_J^B = (1 + \lambda_w)/2 \ , \tag{2.10b}$$

$$\text{for } z^* < z \leq 1,\ \left(\frac{v_J^B}{\lambda_w}\right)^{1+\lambda_w} \left(\frac{1 - v_J^B}{1 - \lambda_w}\right)^{1-\lambda_w} = e^{-\gamma(z - z^*)} \ , \tag{2.10c}$$

$$\text{for } 0 \leq z < z^*,\ v_J^W = 1 \ , \tag{2.10d}$$

$$\text{for } z^* \leq z \leq 1,\ v_J^W = v_J^B + \frac{v_J^B}{\lambda_w}(1 - v_J^B), \text{ and} \tag{2.10e}$$

$$\text{for } 0 \leq z \leq 1,\ v_J = v_J^W v_w + (1 - v_w)\, v_J^B \ , \tag{2.10f}$$

where

γ = dimensionless ratio of phase exchange to segregation parameters = Hq/w, and

z^* = interface location, determined as in Case 1.

Figure 2.9 illustrates the average composition profile. This appears very similar to Case 1, except that above the interface the profile slopes to the left due to the loss of jetsam from the upward moving wake phase. Also as in Case 1, an interesting limit occurs when there is insufficient jetsam present to form a bottom layer. This time the bulk phase composition is given by

$$\left(\frac{v_J^B}{v_{Jo}^B}\right)^{1+\lambda_w} \left(\frac{1 - v_J^B}{1 - v_{Jo}^B}\right)^{1-\lambda_w} = e^{-\gamma z} \ , \tag{2.11}$$

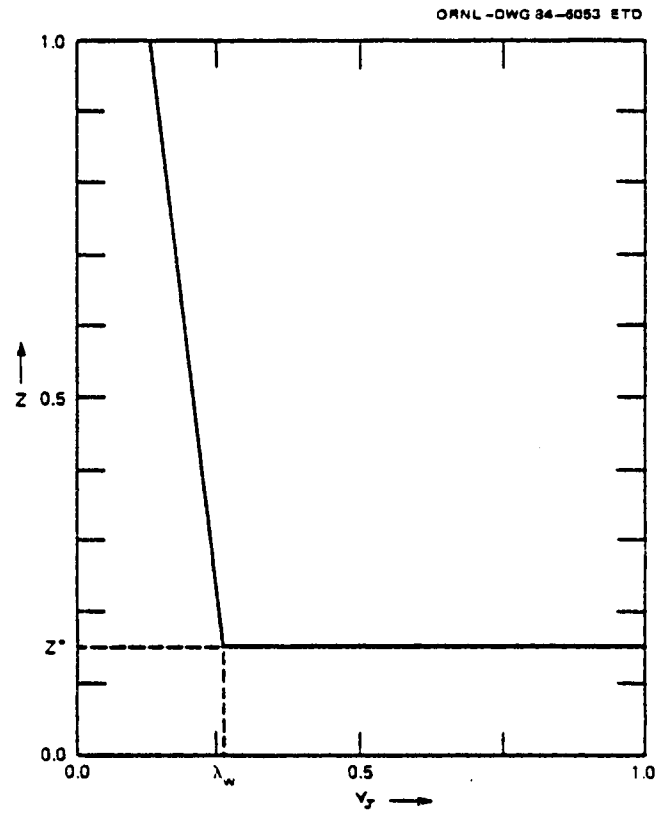

Figure 2.9. The average composition profile predicted by the Gibilaro-Rowe model for Case 2 - systems with exchange between the wake and bulk phases but no axial dispersion (adapted from Gibilaro and Rowe (1974)).

where v_{Jo}^{B} is the bulk phase composition at the bottom of the bed, which must lie between 0 and λ_w. It is found iteratively by satisfying the overall integral condition (conservation of jetsam),

$$\bar{v}_J = (1 - v_w) \int_0^1 v_J^B \, dz + v_w \int_0^1 v_J^W \, dz \, . \tag{2.12}$$

Gibilaro and Rowe's solution to Case 3 accounts for the effects of circulation, segregation, and axial dispersion without any phase exchange. The resulting expressions for the profiles are

$$\text{for } 0 \leq z \leq 1, \; v_J^B = \frac{1}{2} \left[\lambda_w + 1 + P\left(\frac{1 + B_2 e^{zP/\lambda_D}}{1 - B_2 e^{zP/\lambda_D}} \right) \right], \tag{2.13a}$$

$$\text{for } 0 \leq z \leq 1, \; v_J^W = v_{Jo}^B, \text{ and} \tag{2.13b}$$

$$\text{for } 0 \leq z \leq 1, \; v_J = v_w v_J^W + (1 - v_w) v_J^B \, , \tag{2.13c}$$

where λ_D = dimensionless ratio of axial dispersion to segregation parameters = r/kH ,

$$P = [\lambda_w + 1)^2 - 4\lambda_w v_{Jo}^B]^{1/2} \, , \text{ and}$$

$$B_2 = \frac{\left(\lambda_w + 1 - 2 v_{Jo}^B + P\right)}{\left(\lambda_w + 1 - 2 v_{Jo}^B - P\right)} \, .$$

As before, v_{Jo}^B is evaluated iteratively from the integral boundary condition, Eq. 2.12. In this case the result is

$$\bar{v}_J = (1 - v_w)\left[\frac{(\lambda_w + 1 + P)}{2} - \lambda_D \ln\left(\frac{1 - B_2 e^{P/\lambda_D}}{1 - B_2}\right)\right] + v_w v_{Jo}^B \quad . \tag{2.14}$$

Figures 2.10 through 2.12 illustrate the effects of the value of λ_w, λ_D, and the overall jetsam fraction on the shape of the concentration profile. Equations 2.13 collapse to Case 1 when $\lambda_D \to 0$.

From comparison with Rowe et al's. (1972 a and b) earlier experiments, Gibilaro and Rowe concluded that the observed profiles were matched closely by the solutions for Case 1 and Case 3. They further concluded that phase interchange is usually a very small effect and can generally be neglected. Axial spreading was seen to be important only at high gas velocities or in weakly segregating systems. The value of λ_D was rarely found to be > 0.1.

Nienow, Rowe, and Chiba (1978) studied the segregation of a small proportion of large particles in gas-fluidized beds of small particles. They conducted experiments with jetsam particles varying in diameter from 240 μm to 880 um and varying in density from 1.49 g/cm^3 to 1.80 g/cm^3. The flotsam ranged from 0.50 cm to 1.63 cm diameter and 0.97 g/cm^3 to 1.64 g/cm^3 density. They found that large particles behave as flotsam when their density is less than the bulk density of the small particle bed. Otherwise, mixing and segregation appear to be insensitive to density and particle shape over a wide range.

In their analysis, Nienow et al. point out that beds with large excesses of jetsam (e.g. < 10% flotsam) have qualitatively different concentration profiles than those beds studied earlier by Rowe et al. (1972 a and b). In the flotsam-lean case, they saw bubbles form in and rise through jetsam. These produced pure jetsam wakes which pushed up

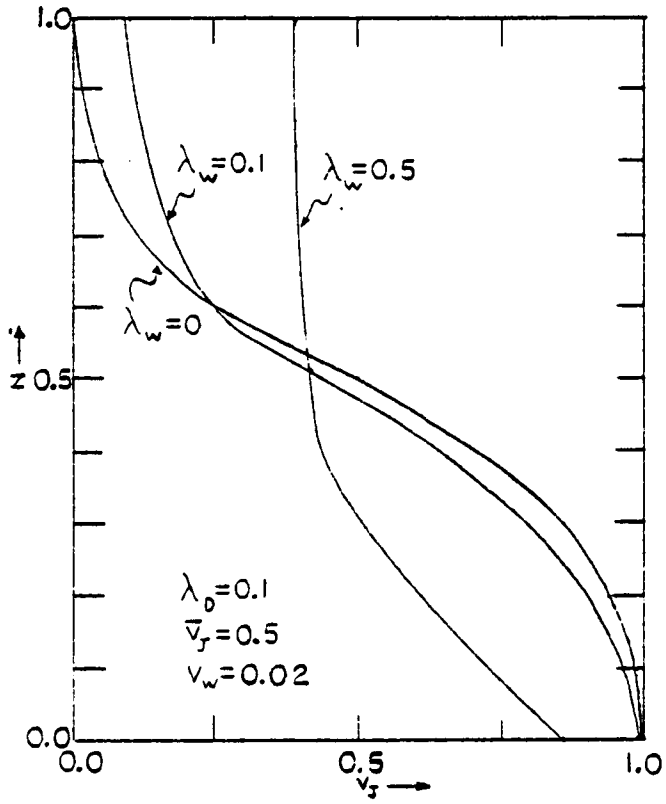

Figure 2.10. Typical average profiles predicted by the Gibilaro-Rowe model for various values of the parameter λ_w in Case 3 - systems with axial mixing and wake circulation but no interphase exchange.

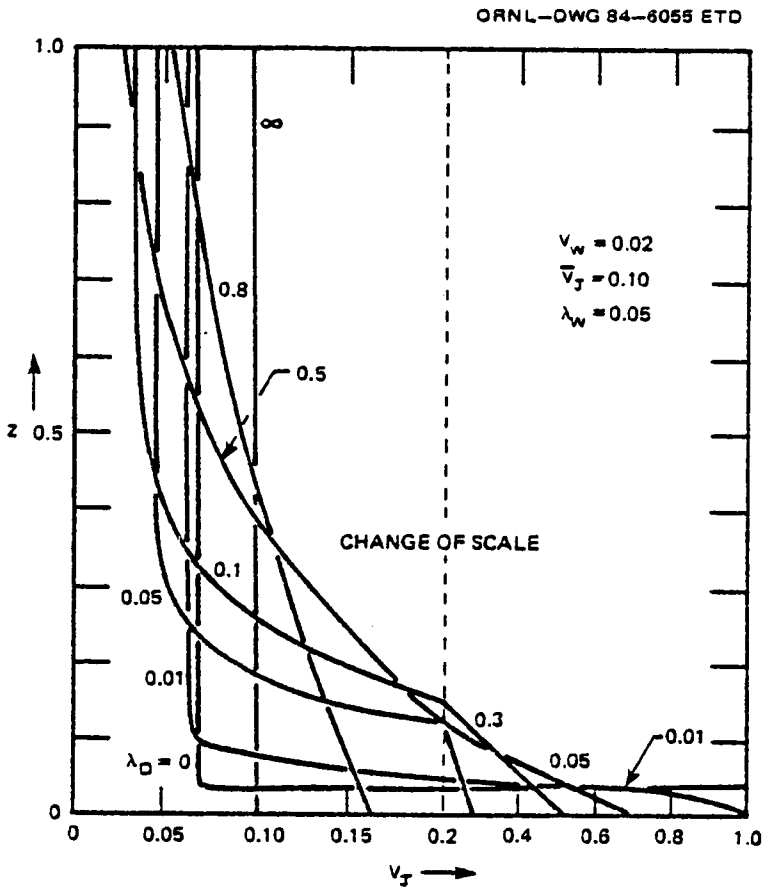

Figure 2.11. Typical average profiles predicted by the Gibilaro-Rowe model for various valves of the parameter λ_D in Case 3 - systems with axial mixing and wake circulation but no interphase exchange (adapted with modification from Gibilaro and Rowe (1974)).

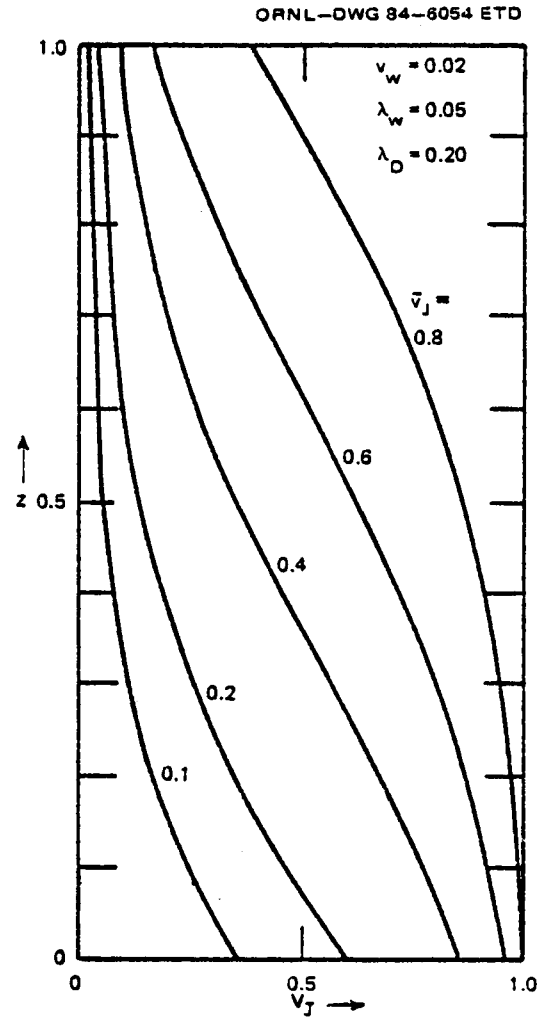

Figure 2.12. Typical average profiles predicted by the Gibilaro-Rowe model for various values of the overall jetsam fraction in Case 3 - systems with axial mixing and wake circulation but no interphase exchange (adapted with modification from Gibilaro and Rowe (1974)).

into and through the top flotsam layer to fall back on it. Thus flotsam was buried and began to sink in the bulk phase. Bubbles passing near flotsam particles caused them to move back upwards in short, rapid jerks. In this way a layer of pure flotsam was never achieved and the concentration of flotsam diminished more or less continuously with increasing depth.

Nienow et al. were able to correlate the behavior of beds in which the large particles acted as flotsam. Two separate correlations related the average rise velocity and average depth of penetration of flotsam particles as functions of gas velocity. These relationships were

$$\overline{u}_R = 1.9\ (u_o - u_{mfJ})^{1/2} \tag{2.15}$$

and

$$X/H = 0.12\ (u_o - u_{mfJ})^{1/2}\ , \tag{2.16}$$

where

$\overline{u}_R$ = average rise velocity of a large flotsam particle (cm/s),

u_o = superficial gas velocity (cm/s),

u_{mfJ} = minimum fluidizing velocity of the main bed material, which was jetsam (cm/s),

X = average depth of penetration of large particles (cm), and

H = bed height (cm).

In general, the velocities of the rising flotsam particles were an order of magnitude less than the bubble rise velocities. The relations for rise velocity and penetration depth did not appear to depend on the size and density of the flotsam. Thus if two kinds of flotsam were present, they were likely to remain in constant proportion over the bed.

Nienow, Rowe, and Cheung (1978) investigated axial concentration profiles for beds of small particles with less than 50% volume fraction of jetsam. They conducted experiments with a variety of solids ranging in size from 928 μm to 70 μm and ranging in density from 8.86 to 1.05 g/cm^3. Using these data and the data of other investigators, they developed two correlations which can be used to predict the mixing index; i.e., $M = x_{J_1}/\bar{x}_J$. The mixing index itself was correlated in a relationship of the form:

$$M = \frac{1}{1 + e^{-Q}} , \tag{2.17}$$

where

$$Q = \left(\frac{u_o - u_{to}}{u_o - u_{mfF}}\right) \exp\,(u_o/u_{to}) .$$

The term u_{to} is called the "takeover velocity" and is the velocity at which M = 0.5. The minimum fluidizing velocity used, u_{mfF}, is the minimum fluidizing velocity of the flotsam. Another empirical correlation was developed for the takeover velocity:

$$\frac{u_{to}}{u_{mfF}} = \left(\frac{u_{mfJ}}{u_{mfF}}\right)^{1.2} + 0.9\,(R - 1)^{1.1}\,(D_\phi')^{0.7} - 2.2\,\bar{x}_J^{\,0.5}\,(H^*)^{1.4} , \tag{2.18}$$

where

R = particle density ratio = ρ_J/ρ_F,

D_ϕ' = shape corrected particle diameter ratio = $\phi_J d_{PJ}/\phi_F d_{PF}$,

H^* = reduced aspect ratio = 1 - exp (-H/D), and

D = bed diameter.

This correlation fit their experimental data with a standard deviation of ±10%. They recommended great caution in using the correlation for conditions outside the study ranges, for jetsam rich systems, or for equal density systems.

2.4.7 Chen and Keairns (1975, 1978)

Chen and Keairns (1975) measured the segregation of small particles of different size and density at low gas velocities near the minimum fluidizing velocity of the mixture. Char and dolomite, varying in size from 150 μm to 2800 μm diameter and from 0.72 to 2.8 g/cm^3 in density, were fluidized at different velocities in a 100 mm diameter bed operating at up to 660 kPa and a 114 mm diameter bed operating at atmospheric pressure. The principal objective was to obtain basic data regarding the two-stage fluidized bed coal gasifier being developed by Westinghouse Electric Corporation. Solids mixtures were made to be representative of two-component, three-component, and multi-component systems.

Chen and Keairns' method of characterizing the segregation was based on the phase diagram approach of Katz (1957), Kondukov and Sosna (1967) and Gelperin and Einstein (1971). This approach assumes that fluidized beds are analogous to physical substances undergoing phase changes; i.e., transition from an unfluidized state to a fluidized state is considered to be very similar to a solid melting. In this sense, minimum fluidizing velocity can be thought of as a psuedo-melting temperature. The velocity at which the lightest particles start to fluidize is called the velocity for beginning fluidization, and the velocity at

which the heaviest particles fluidize is the velocity for total fluidization. Between these velocities the bed is viewed as an equilibrium system having an upper and lower phase, each with a characteristic, uniform composition.

Chen and Keairns' major conclusions were:

- All mixtures tested, except for a two-size mixture of dolomite with a u_{mf} ratio less than 2, became segregated as the gas velocity dropped below the total fluidization velocity of the mixture. Coarse or heavy particles settled to the bottom, fine or light particles went to the top.
- Phase diagrams are useful for depicting the segregation of two-component systems at velocities between beginning and total fluidization. These can be used analogously to temperature-composition diagrams for liquid-solid systems.
- Segregation occurred for fully fluidized beds with mixtures of different size dolomite at pressures up to 372 kPa and with mixtures of char and dolomite at pressures up to 609 kPa.
- Segregation of overlapping wide-size mixtures of char and dolomite may be treated as if they are two-component mixtures of different densities, with the u_{mf} for each component determined by the mean particle size of each mixture.
- Greater than 95% separation of the agglomerated ash particles can be achieved for a fluidized bed combustor/gasifier if the gas velocity is close to the minimum fluidizing velocity of the ash particles.

The most significant shortcoming of Chen and Keairns' approach is that phase diagrams do not predict concentration profiles. As Rowe et al. have shown, the assumption of two constant composition layers is an oversimplification in many cases. The concept of using gas velocity as a kind of pseudo-temperature seems promising, however. This illustrates a fundamental similarity between particles in fluidized beds and atoms or molecules. Just as temperature is a measure of the average kinetic energy on an atomic scale, gas velocity (or a function of it) represents the average kinetic energy of the fluid bed particles. In the same way that corresponding states theory allows physical property correlations to be generalized for different substances, generalized fluidized-bed correlations may be possible by using non-dimensional psuedo-temperatures (e.g., u_o/u_{mf}).

The study by Chen and Keairns in 1978 is primarily a practical demonstration of continuous particle separation using a pressurized cold model simulating the Westinghouse combustor/gasifier. It is a follow-up of the experiments reported in 1975, and compares separation of char and dolomite at low velocity (near the mixture u_{mf}) and at high velocity (near the char terminal velocity). The maximum separation at low velocity occurred at a gas velocity near 1.5 times the mean u_{mf} of the dolomite at low pressure (atmospheric) and near the mean u_{mf} of the dolomite at high pressure (660 kPa). The degree of separation appeared to increase with pressure. The distinctive flow patterns in the models makes direct extrapolation to other fluidized beds difficult.

2.4.8 Burgess, Fane, and Fell (1977)

Burgess, Fane, and Fell experimentally investigated segregation in gas-fluidized beds containing binary mixtures of sand (143-512 μm), ballotini (143-900 μm), iron powder (143-215 μm), and steel shot (340 μm). The densities of these materials varied from 2.7 (sand) to 7.5 g/cm^3 (steel shot). Burgess et al. found that for initially segregated beds having components of equal density but different size, mixing commenced at gas velocities just above the minimum fluidizing velocity for the flotsam. In this case, particles of the unfluidized jetsam were gathered in the bubble wakes forming at the interface between the layers. Mixtures of particles having different size and density, however, did not begin mixing until the gas velocity exceeded the minimum fluidizing velocity of the jetsam. For such systems the jetsam was the denser component, even if it had a similar or lower minimum fluidizing velocity than the other component.

Burgess et al. ran both steady-state and transient experiments. In some cases, the steady-state concentration profile was found to depend on the initial conditions. This occurred when gas velocities were less than the jetsam minimum fluidizing velocity and portions of the bed defluidized as the flotsam moved upwards. At higher gas velocities, the bed always reached the same steady-state segregation profile, regardless of the initial condition.

Based on these observations and Rowe et al's. earlier work, Burgess et al. proposed a numerical segregation/mixing model capable of predicting concentration profiles under both transient and steady state conditions. The basic assumptions are:

(1) The bed is divided into finite sized increments in the axial direction. Each slice is assumed to be composed of bulk phase and wake phase, as in the Gibilaro and Rowe (1974) model.

(2) For simulation of mixing, the bubble wakes are assumed to be composed of a well-mixed region and a stagnant region. As the wake phase moves vertically from level to level, particles are exchanged with the bulk.

(3) Segregation is simulated by allowing jetsam to fall down through the bubbles as they pass upwards. Each time a bubble moves from one slice to another, jetsam particles fall an average distance L_s.

(4) The rate of bubbling is assumed to be given by the two phase theory (i.e., all gas in excess of minimum fluidization becomes bubbles). The minimum fluidization velocity is calculated at each level based on the local composition.

(5) A transient mass balance on each slice of the bed gives the concentration profile at any time. The mass balances are left in finite difference form, and results are obtained numerically via computer.

In order to evaluate the various effects of wake mixing, segregation, and phase exchange, the following parameters are required:

- V_w, the fraction of the bubble which is wake,
- L_w, the wake length, represents a characteristic vertical wake mixing length,
- L_s, the segregation distance, represents the distance a jetsam particle falls during passage of a bubble,
- A_s, the projected bubble area as the bubble moves upward, and
- f_m, the fraction of the wake which is completely mixed.

Burgess et al. use the following assumptions to get these parameters:

- Bubble size is estimated by the correlation of Mori and Wen (1975) using the local u_{mf} and the center height of the bubbling zone;
- V_w is assumed to be 30%, $L_w = 0.575\ D_B$, and $A_s = \frac{\pi D_B^2}{4}$;
- The local mixture u_{mf} is calculated from the Ergun equation and an expansion correlation developed by Burgess et al.;
- Bubble velocities are calculated from Nicklin's (1962) correlation;
- f_m is assumed to be 0.5;
- L_s is an adjustable parameter.

This model has apparently been used successfully to simulate concentration profiles, but there are three principal shortcomings:

- The complex, numerical nature of the bubble wake calculations make it very difficult to follow the effects of changes in the various parameters. Burgess et al. do not explain the variety of experimental profiles seen in terms of these parameters.
- It is not clear that the assumption of a well-mixed region and a stagnant region in the bubble wake are supported by experimental evidence.
- The typical values used for V_w, L_w, and f_m may or may not be applicable to other systems (e.g. large particles). These quantities would be expected to change with the fluidization regime.

2.4.9 Fan and Chang (1979)

Fan and Chang were the first to study segregation in beds composed only of large particles. The "particles" were table tennis balls weighing 2.42 and 2.50 g. Fan and Chang report that this slight weight difference, created by putting sand in some of the balls, increased the minimum fluidizing velocity from 2.0483 m/s to 2.0726 m/s. Remarkably, this tiny difference produced noticeable segregation at air velocities up to 3.4 m/s.

In two-dimensional beds they observed that bubble or slug-induced drift and gross circulation were the predominant solids mixing mechanisms. Segregation seemed to result from preferential upward drift of lighter balls in the vicinity of rising bubbles and preferential downward movement of heavier balls in the disturbed regions behind bubbles. As has been observed elsewhere, Fan and Chang noted that large particles tend to make a rapid transition from a bubbling-bed to a slugging-bed condition as gas velocity increased above the bubbling point.

Transient experiments revealed that axial mixing was more rapid when the initial condition was "inverted" (i.e., the flotsam was placed on the bottom and the jetsam on top) than when flotsam and jetsam were placed on the top and bottom, respectively. However, both initial conditions lead to a unique equilibrium concentration distribution, with the lighter balls always on top. The equilibrium concentration was generally characterized as being nearly uniform in the top part of the bed with a much steeper gradient in the lower part of the bed.

Fan and Chang developed a non-stationary numerical random walk model to represent the axial concentration distribution as a function of the operating time. This model predicts the concentration profile as a

function of time and ultimately predicts the steady state profile as $t \to \infty$. The basic features are:

(1) The bed is divided into vertical sections, each of which is internally homogenous and represents a discrete state.

(2) The motion of particles can be described by a random walk process, represented as a Markow chain, in which transitions from one state to an adjacent state occur with specific probabilities.

(3) The bed consists of two mixing regions, a segregated region at the bottom and a completely mixed region in the upper part of the bed. The proportions of these regions is dependent on particle properties, bed geometry, and operating conditions. The location of the boundary between these two regions is specified by an empirical constant, ℓ.

(4) The random walk process in the mixed (upper) region is a stationary process; i.e., the transition rate between adjacent levels is time invariant.

(5) The random walk process in the segregated (lower) region is a nonstationary process; i.e., the transition rate between adjacent levels varies with time.

(6) In the completely mixed region, the transition rate from one state to an adjacent state occurs by interchange of particles. The rate of any such transition is spatially invariant and equal to a positive real constant, α.

(7) In the segregated region, an equivalent transition (i.e., a transition not resulting in an increase or decrease of segregation) occurs with rate α. The rate of segregating transitions is $\alpha + \beta$. The rate of unsegregating transitions is $\alpha - \beta$.

This model appears to fit Fan and Chang's experimental results reasonably well and also gives concentration profiles of the same form as those reported in the results of Rowe et al. In some ways it is more readily amenable to physical interpretation than Burgess et al's. model. Fan and Chang show that the parameters α and β can be correlated with the excess air rate (i.e., $u_o - u_{bf}$), but the parameter ℓ remains strictly empirical.

Fan and Chang also introduce a more general and potentially more useful mixing index for describing the state of a segregating system. They note that for any mixed system, a variance may be defined by

$$\sigma^2(t) = \frac{1}{n-1} \sum_{i=1}^{n} [Y_i(t)-\bar{Y}]^2 , \qquad (2.19)$$

where n is the number of samples taken and $Y_i(t)$ and $\bar{Y}$ are the number concentration of some key component (e.g., jetsam) in the ith sample and the number average key component concentration, respectively.* The degree of mixing is then defined as

$$M'(t) = 1 - \frac{\sigma^2(t)}{\sigma_o^2} , \qquad (2.20)$$

where σ_o^2 is the variance of the completely segregated state, $\bar{Y}(1 - \bar{Y})$. Such an index is more useful than the previously defined indices (e.g., $M = x_{J_1}/\bar{x}$) because it is sensitive to changes throughout the bed rather than in just one part. It also lends itself to more direct statistical interpretation.

---

*Note that the quantity n - 1 should be replaced by n if $\bar{Y}$ is known exactly, rather than estimated from the samples. See the discussion in Miller and Freund (1977), pp. 70 and 151.

2.4.10 Yoshida, Kameyama, and Shimizu (1980)

Yoshida, Kameyama, and Shimizu derived a numerical model for binary segregation of particles and tested the adequacy of the model with experimental results obtained for binary mixtures of different sized glass beads. Of the five particle sizes studied, only two (2.61 mm and 1.84 mm diameter) fit into the size range which could be clearly classified as large-particle. Interestingly, the results for all particle sizes appear to agree qualitatively with the patterns produced in the earlier studies by Rowe et al. (1972 a&b, 1974, 1978, 1978).

The Yoshida et al. model assumes a physical picture similar to that proposed by Gibilaro and Rowe (1974), except that it is numerical and is constructed to predict transient concentration profiles as well as steady state behavior. Wake and bulk phases are assumed to flow up and down the bed respectively, while solids are continually exchanged between them. The bed is represented by a number of compartments with height equal to D_B, the average bubble diameter, and mass balances are made between the phases in each compartment.

Solids are only allowed to move axially by convection in the wake and bulk phases; there is no explicit allowance for axial transport via drift dispersion. Exchange between the phases is estimated from the solids interchange coefficient proposed by Yoshida and Kunii (1968):

$$K_E = 3\ (1 - \varepsilon_{mf})\ u_{mf}/[(1 - \delta)\ \varepsilon_{mf} D_B]\ , \qquad (2.21)$$

where

K_E = solids interchange coefficient [1/t],

ε_{mf} = void fraction at minimum fluidizing condition [-],

δ = bubble volume fraction [-], and

D_B = average bubble diameter [L].

The actual rate of jetsam exchange is given by

$$Ex(i) = K_E \delta/(1 - \delta) \quad [1 - (1 - R_s)\, D_B]\, v_J^W - R_s\, v_J^B \ , \qquad (2.22)$$

where

$Ex(i)$ = rate of jetsam exchange between wake and emulsion phase in compartment i $[L^3/t]$,

R_s = segregation factor [-],

v_J^B = volume fraction of solids in emulsion phase which are jetsam [-], and

v_J^W = volume fraction of solids in bubble phase which are jetsam [-].

The resulting jetsam balance for the i^{th} compartment is

$$\frac{dv_J^B(i)}{dt} = \frac{u_b}{D_B} v_J^W (i - 1) - \frac{u_b}{D_B} v_J^W (i) - Ex(i) \ , \qquad (2.23a)$$

and

$$\frac{dv_J^B(i)}{dt} = \frac{u_s}{D_B} v_J^B (i + 1) - \frac{u_s}{D_B} v_J^B (i) + Ex(i) \ , \qquad (2.23b)$$

where

$v_J^W (i)$ = volume fraction of wake phase in the i^{th} compartment which is jetsam,

$v_J^B (i)$ = volume fraction of bulk phase in the i^{th} compartment which is jetsam,

u_b = bubble velocity, and

u_s = emulsion solids velocity.

Applying the boundary conditions at the top and bottom of the bed, Yoshida et al. numerically integrated these equations for various values

of D_B, δ, and R_s. These parameters had to be varied arbitrarily to "fit" the experimental data. In most cases there was a noticeable discrepancy between the calculated and experimental results, even with the "fitted" values of the parameters. This discrepancy was particularly noticeable in the upper part of the bed, where the model predicted continually decreasing jetsam concentration with increasing height, rather than the observed constant composition. To correct this, Yoshida et al. proposed using a variable segregation factor. They tried using $R_s = 1 - v_J^B$, which gives a somewhat better result.

Yoshida et al. conclude that their model does a good job of simulating the transient concentration profiles, but they point out that more understanding of the segregation factor is needed. On the surface at least, it appears that the arbitrary use of this term makes it little more than a "fudge" factor for making the model appear to simulate reality. It appears that the most serious problems with the predicted profiles actually center around the wake-bulk phase exchange terms, which are specified rather arbitrarily for this system.

Another important criticism of Yoshida et al's study is that all data used to test the model were generated at gas velocities between the minimum fluidizing velocities of the components. It would be expected that such conditions would result in a partially defluidized bed with regions having no bubbles at all. This does not seem to have been accounted for in the model.

2.4.11 Geldart (1981) and Geldart, Baeyens, Pope, and Van de Wijer (1981)

Geldart (1981 a) reports the results of experiments with mixtures of large and small particles of sand, metal shot, and alumina sized between 45 and 5000 μm and fluidized in three beds; a 0.29 m diameter × 5 m high aluminum and glass column, a 0.076 m diameter × 7.3 m high glass column, and a 0.01 m thick × 0.3 m wide × 1.5 m high two-dimensional bed made of Perspex (i.e., plexiglass). Most of the experiments were made using the first bed at gas velocities up to 5 m/s with and without internal tubes. Geldart's primary objectives were to characterize the elutriation of fine particles from beds of coarse solids, and to determine particle residence times in both the bed and freeboard at gas velocities typical of fluidized bed combustion. In pursuit of this, however, he also made some useful observations which pertain to segregation of the large and small particles. Those most important to this investigation are:

- Bed density decreased with increasing distance above the distributor when the bed is fluidized. This result clearly demonstrates that assumptions of constant voidage in high-velocity-large-particle beds are incorrect.
- The bed internals (tubes) had a profound effect on the density distribution. In some cases, three separate zones are produced; a high density section below the internals, a low density zone surrounding the internals, and another low density section above the internals.

- Segregation by size difference appeared to be an intrinsic feature of large-particle beds. Two indices were found to be useful; a coefficient of segregation, C_s, and a mixing index M. These were defined as

$$C_s = 100 \left(\frac{x_{Fl} - x_{Fo}}{x_{Fl} + x_{Fo}} \right) ,$$

where x_{Fl} and x_{Fo} are the fines weight fractions at the top and bottom of the bed, respectively, and

$$M = x_{Fz} / \bar{x}_F$$

where x_{Fz} is the fines weight fraction at some level z in the bed and $\bar{x}_F$ is the overall average fines weight fraction in the bed.

- If the gas velocity is well above the incipient fluidization velocity (e.g., $u_o - u_{mf} > 1$ m/s) segregation is relatively insensitive to gas velocity up to 5 m/s.
- In runs with in-bed tubes, the fines were re-injected below the tubes and no significant affect due to the tubes was seen. Segregation increased as the fines size decreased, as the large-particle size increased, and as the gas velocity approached u_{mf}.
- Although fines clearly had a tendency to move to the top of the bed, they could still be found to some degree everywhere, even at 5 m/s. This certainly indicates a strong tendency for mixing.
- The existence of segregation could have a profound impact on development of fluidized bed correlations. In particular, use of

mean concentrations for correlating elutriation data may be considerably in error.

In a related study of large-particle beds, Geldart et al. (1981 b) report additional observations using the 0.29 m diameter bed with solids mixtures of different size (onyx sand, grit, limestone, and sand fines) and different density (cubical polyvinyl chloride, polyethylene, and limestone). Their conclusions reinforce those of Geldart (1981 a) and include, in addition:

- The mixing index, M, defined for the top of the bed can be correlated quite well with the expressions developed by Nienow, Rowe, and Cheung (1978) for u_{to}, M, and Q.
- In beds of particles with different densities, the region near the distributor is particularly rich in jetsam and the remainder of the bed has a fairly uniform composition. When only size differences are present, the concentration gradient is less steep.

2.4.12 Cooke, Napier, Parkinson, and Rogers (1982)

Cooke et al. also looked at beds containing large particles, but they focused on the behavior of the large particles rather than the fines. Their major concern was to address the problem of accumulation of large ash particles at the bottom of fluidized bed combustors burning washery rejects. To accomplish this, they measured segregation in an ambient-temperature, 1m × 0.25 m fluidized bed containing ash particles (of essentially constant density) sized 0.5 to 25 mm at superficial gas velocities up to 5 m/s. These experiments were followed up with test runs of a 0.6 m × 0.6 m fluidized bed combustor burning two sizes of

washery discard (sized 3 mm × 0 and 6 mm × 0) and run-of-mine coal (sized 13 mm × 0).

Cooke et al. obtained composition versus axial position profiles in the ambient temperature bed similar to those seen by Rowe et al. for small particles, except that all of Cooke et al's. data are for multi-component (i.e., multiple-size-cut) systems rather than binary systems. An interesting feature of these curves is that some of the components appear to act as flotsam near the bottom of the bed and then become jetsam at higher levels. This makes intuitive sense, as one could expect mid-size particles to be lighter than average when many large particles are present, but heavier than average when many fines are present.

In addition to measuring the axial composition profiles in the ambient-temperature bed, Cooke et al. quantified segregation by a segregation index R_{ij} where

$$R_{ij} = \frac{\text{Percentage of weight in layer i of a given size fraction}}{\text{Percentage of weight in layer j of a given size fraction}} .$$

The layer numbers referred to specific axial sampling cuts of the bed, with 0 defined as the bottom layer and 5 defined as the top layer. This index was determined for five size intervals and trends were noted as gas velocity and tube internals were changed. Based on the results of this analysis, they concluded that:

- Segregation of large particles is probably an inherent feature of the fluidization of wide-size-range particles when they are fluidized at velocities less than the minimum fluidizing velocity of the large components.

- Washery discard particles larger than 6 to 10 mm clearly migrated to the bottom of the bed at fluidizing velocities of 1.5 to 3.5 m/s. The degree of segregation decreased with increasing velocity, but even at 3.5 m/s, R_{15} for 10 mm particles was greater than 2.
- Internal tube surfaces clearly increased segregation.
- Some segregation may be acceptable provided the large particles have sufficient mobility to migrate to the ash discharge pipes.

In tests of the 0.6 m × 0.6 m combustor, Cooke et al. noted that no defluidized layer formed when burning 3 mm × 0 and 6 mm × 0 washery discard at velocities as low as 1.3 m/s and 1.5 m/s, respectively, as long as there was bottom discharge from the bed. While running with 13 mm × 0 coal, defluidization occurred near 1.8 m/s. Cooke et al. were able to demonstrate that this could be reduced to a manageable degree by three techniques; increased discharge from the bottom of the bed, fines recycle, and modifying the air distributor to include a high velocity spout.

2.4.13 Summary of previous segregation studies

Based on the studies described in the preceding sections, the following conclusions appear to be generally supported:

- Segregation can be an important factor in gas-fluidized beds, especially when there is a wide range of particle sizes or of densities. Other factors being equal, particles with higher density or larger size tend to sink. Particles tending to sink are termed jetsam, and particles tending to rise are termed flotsam.

- Bubbles tend to act against segregation by causing large-scale solids circulation. The more vigorous and unrestrained the bubbling, the better the solids are mixed and the less they segregate.
- Bed internals, such as tubes, baffles, or screen packing, tend to reduce the amount of solids circulation and thereby enhance segregation. In the limit, as more internals are added, gas-fluidized beds appear to exhibit particulate fluidization behavior similar to liquid-fluidized beds.
- Particle density differences appear to be more important than particle size differences in causing segregation.
- Segregation can occur even in fully fluidized beds. For fully fluidized beds, segregation appears to be a maximum when the gas velocity is near the minimum fluidization velocity of the jetsam or when the gas velocity approaches the terminal velocity of the flotsam.
- When the gas velocity exceeds the minimum fluidizing velocity of the jetsam, the steady-state distribution of solids is always the same, regardless of the initial conditions.
- When the gas velocity is between the minimum fluidizing velocities of the components, the segregation patterns can exhibit hysteresis; that is, the steady-state composition profile may depend on the initial conditions.
- Segregation patterns can often be approximated by picturing the bed as consisting of two zones, an upper zone which is well-mixed and a lower zone which contains most of the jetsam.

- Qualitatively, the general segregation patterns observed in beds of small and large particles appear similar.
- Numerical indices have been developed to quantify segregation and mixing. The variety of indices reported makes direct comparisons between data sets difficult.
- The most useful mixing (or segregation) indices appear to be those based on some type of overall variation about the mean bed composition. Indices based on a composition at one position (e.g., the top of the bed) do not reflect profile changes occurring elsewhere.

3. EXPERIMENTAL EQUIPMENT AND METHODS

3.1 The Fluidized Bed

I carried out my experiments in the 10.2 cm (4 in.) diameter bed illustrated in Figure 3.1. Dry air* at essentially room temperature and pressure was the fluidizing medium. The air was metered with rotometers to give superficial air velocities up to 7.6 m/s (25 ft/s). It could be shut off in less than one second with a gate valve at the rotometers. Air distribution was accomplished with the grounded metal tuyere plate shown in Figure 3.2, which was designed to have a pressure drop at least 20% of the total bed pressure drop at the lowest velocities studied. In most cases, the tuyere plate pressure drop was more than 10 times the bed pressure drop. This practically eliminated pressure fluctuations in the air metering system caused by bed pressure fluctuations. Except for high velocity conditions (e.g., u_o >4.6 m/s), number 5 lead shot were usually added in sufficient quantity to cover the tuyeres by 5 cm. This further aided air distribution and prevented bed particles from settling below the air inlet holes.

The vessel itself was constructed of clear schedule 40 polyvinyl chloride (PVC) pipe. Water manometers were connected with pressure taps at various axial positions below and above the air distributor. In addition, the adjustable pressure probe shown in Figure 3.3 was used to measure pressures at arbitrary levels in the bed. The probe was held in place with an adjustable clamp above the bed. The opening size on both the fixed and adjustable pressure taps was 0.32 cm (1/8 in.), and a roll

*Dew point at approximately -70°C.

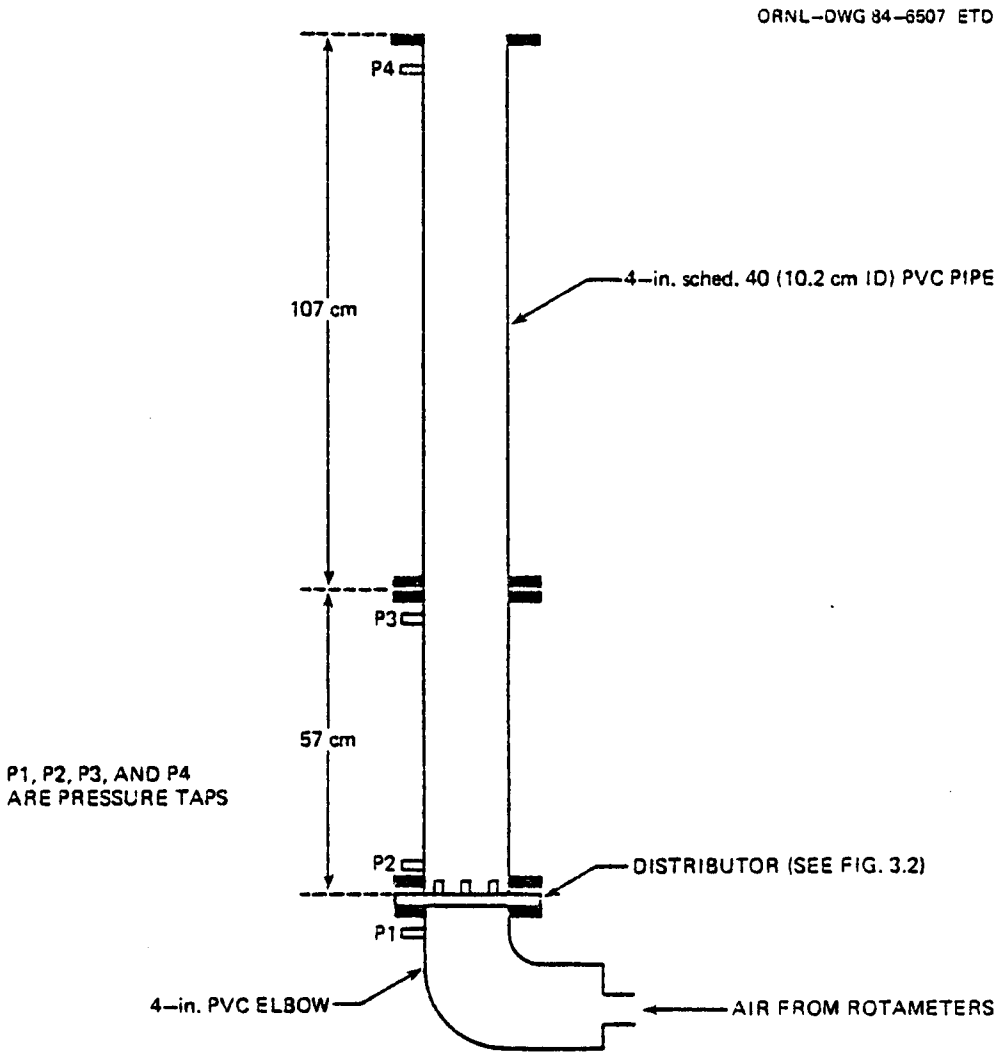

Figure 3.1. The 10.2 cm (4 in.) diameter fluidized bed used in these experiments.

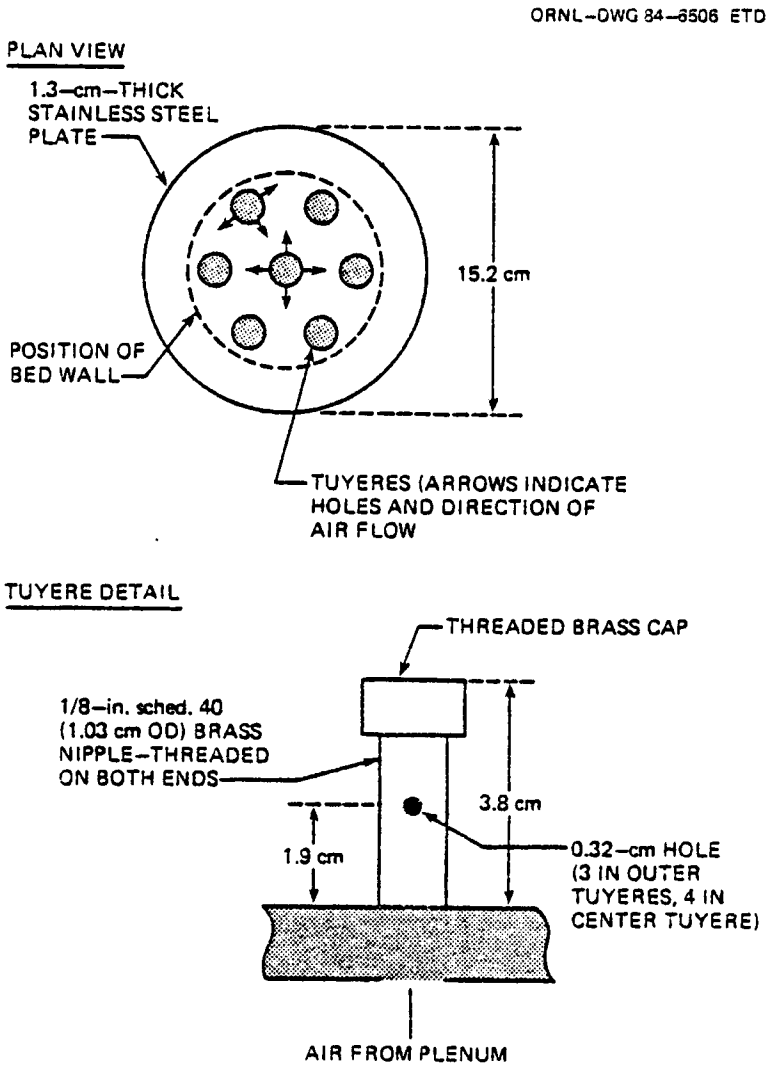

Figure 3.2. Tuyere plate used for distributing air at the bottom of the fluidized bed.

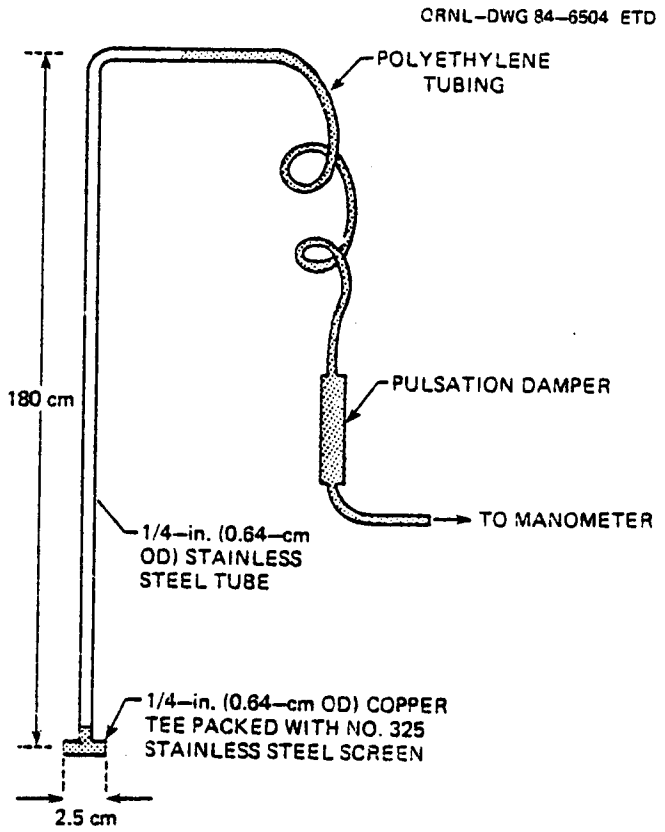

Figure 3.3. Adjustable pressure probe for measuring pressure at arbitrary levels in the fluidized bed.

of 325 mesh stainless steel screen was inserted in each of these to prevent plugging.

Experiments were conducted both with and without internal surfaces. Surfaces were created by inserting 10.2 cm (4 in.) diameter × 7.6 cm (3 in.) tall cylinders of 2.5 cm (1 in.) × 3.8 cm (1.5 in.) hexagonal "chicken" wire (0.813 mm or 0.032 in. diameter) into the PVC cylinder. The cylinders lay flat against the walls, and provided a surface "roughening" effect as well as anchor points for horizontal tubes. When horizontal tubes were installed, they consisted of 0.8 cm (5/16 in.) diameter brass tubes anchored on both ends at the midpoints of the wire cylinders. Usually only one tube was installed per cylinder. In a few experiments cylinders were installed with two tubes each. Due to a slight overlapping of the cylinders, the single-tube per cylinder arrangement had a tube spacing of approximately 6.4 cm (2.5 in.) apart. Experiments were run with alternating tubes parallel or perpendicular to one another.

3.2 The Solids

The physical properties of the solids studied are summarized in Table 3.1. Mean particle size ranged from approximately (1750 μm to 6350 μm and density ranged from 0.905 g/cm^3 to 7.50 g/cm^3. All the particles were well within Geldart's class D (see Section 2.2). In the segregation experiments, the size ratio ranged from 1.06 to 2.10 and the density ratio ranged from 1.30 to 3.33.

Using the properties of the spherical particles, I estimated the minimum fluidizing velocities with the Ergun equation and compared the

Table 3.1. Physical properties of the experimental solids

Solid	Particle size (μm)	Particle density (g/cm^3)	Minimum fluidizing velocity† (m/s)	Terminal velocity† (m/s)
Crushed Kentucky No. 9 Coal	#1 range - 1840 × 3360 Mean* - 1890	1.38	0.860 (2.82 ft/s)	8.02 (26.3 ft/s)
	#2 range - 1680 × 2380 Mean* - 1750	1.38	0.808 (2.65 ft/s)	7.71 (25.3 ft/s)
Crushed Three Rivers Limestone	#1 range - 1840 × 3360 Mean* - 2000	2.69	1.31 (4.30 ft/s)	11.5 (37.8 ft/s)
	#2 range - 2380 × 3360 Mean* - 2720	2.69	1.60 (5.25 ft/s)	13.4 (44.1 ft/s)
Clear acrylic spheres	6090 (essentially monosize)	1.175	1.69 (5.55 ft/s)	13.6 (44.5 ft/s)
Black acrylic spheres	6270 (essentially monosize)	1.175	1.72 (5.64 ft/s)	13.8 (45.2 ft/s)
Polypropylene spheres	3175 (essentially monosize)	0.905	0.991 (3.25 ft/s)	8.41 (27.6 ft/s)
Glass beads	#1 range - 2380 × 3360 Mean* - 3020	2.25	1.54 (5.05 ft/s)	13.0 (42.5 ft/s)
	#2 range - 4760 × 6350 Mean* - 4530	2.25	1.95 (6.40 ft/s)	15.9 (52.1 ft/s)
Steel shot	4346 (essentially monosize)	7.50	3.51 (11.5 ft/s)	28.4 (93.1 ft/s)

*Effective mean determined from minimum fluidizing velocity using Ergun equation (i.e., $\overline{\phi_s d_p}$).

†Experimentally determined at atmospheric conditions.

‡Estimated from density and mean particle size at atmospheric conditions.

results with the experimentally measured values. The calculated velocities for the clear acrylic, polypropylene, and steel spheres were 1.67 m/s (5.49 ft/s), 1.01 m/s (3.32 ft/s), and 3.69 m/s (12.1 ft/s), respectively. These compare quite well with the observed velocities, and confirm the accuracy of the air metering system.

3.3 Electrostatic Effects

It was expected that the PVC pipe and the insulating solids would readily retain electrostatic charges. Preliminary experiments indicated that the particles did become charged, most noticeably at moderate to high velocities [e.g., velocities greater than 2.5—3 m/s (8—10 ft/s)]. The main evidence for charge buildup was that the particles would adhere to the walls or group into clusters.

The first solution considered was to humidify the inlet air by spraying a small stream of water into the inlet lines. This reduced the static charging, but it was extremely difficult to control and frequently resulted in a film of water forming on the particles. The water film in turn altered particle behavior due to surface tension effects.

I next tried using anti-static agents, most notably Scotchguard® spray and Bounce® anti-static cloths made for use in clothes dryers. The spray was applied to both the particles and the fluidized-bed wall. The clothes were wiped only on the bed walls. Both of these proved extremely effective in eliminating static. At higher flow rates the anti-statics were usually depleted after 15—20 minutes. This proved to be no problem, however, since experiments at these flows never took more than 5 minutes to reach steady state.

When experiments with metal internals were made, it was clear that these prevented any observable static buildup. Even when the bed walls were simply lined with wire mesh, no charging was observed.

3.4 The Procedure for Segregation Experiments

As is described in the next section, most of the segregation data were collected for steady-state conditions. Steady-state experiments for binary systems were always preceded by exploratory runs to determine the rapidity at which steady-state was reached. These usually consisted of repeated measurements of the top composition of the bed as a function of time, while fluidizing the bed at a relatively low gas velocity. In general, I found that as long as the gas velocity was above u_{mfJ}, the time required to reach steady state was usually significantly less than 5 minutes. At velocities near u_{mfJ}, the run times were extended to 10 minutes, especially when bed internals were present.

Steady-state experiments involving gas velocities between u_{mfJ} and u_{mfF} required much longer times. Runs up to 1 hour in length were made to insure that the final profiles had been reached. Preliminary experiments were again used to determine how long these runs needed to be.

Almost all steady-state experiments were run with one of two initial conditions, segregated or well-mixed. In the former case, the solids were carefully added in layers, the jetsam on the bottom. In the latter cases, a well-mixed bed was created by dividing the solids into eight equal, well-mixed portions and adding them one at a time to the bed. After the initial solids condition was established, the fluidizing air was brought up to the desired condition, and the system allowed to reach steady-state. Then the bed was slumped.

Transient experiments were carried out by: (1) starting with one component already fluidized and then adding the other component rapidly to the top of the bed; or (2) turning on the air flow after both solids had been added to the bed. After the specified time had elapsed, the fluidizing air was shut off.

3.5 The Sampling Procedure

After the fashion of Rowe et al. (1972), Geldart (1981), and Cooke et al. (1982), I determined the axial solids composition profiles by removing sequential layers from the slumped bed. I used two methods to accomplish this, vacuuming and hand scooping. In both cases I found that maintaining arbitrarily constant sample sizes could lead to confusion in the data analysis, particularly where there were rapidly changing gradients and the number of samples is rather limited. Thus I tried to take smaller samples in sections of the bed which obviously had high concentration gradients. Usually 5 to 8 samples were collected from each bed.

The vacuum sampler is illustrated in Figure 3.4. This device consisted of an air eductor at the top of a 2.5 cm (1 in.) brass pipe, and a "catch" bag on the eductor vent for collecting the solids. The brass pipe was kept grounded to prevent static buildup. Hand scooping was done with a 5.1 cm (2 in.) diameter, 2.5 cm (1 in.) deep plastic dish. The vacuum sampler was by far the most convenient sampling method when bed internals were present. As the solids were removed, internals above the current level were pulled out of the bed to facilitate access to the solids below. Use of the wire mesh cylinders for supporting the horizontal tubes greatly reduced the time and effort.

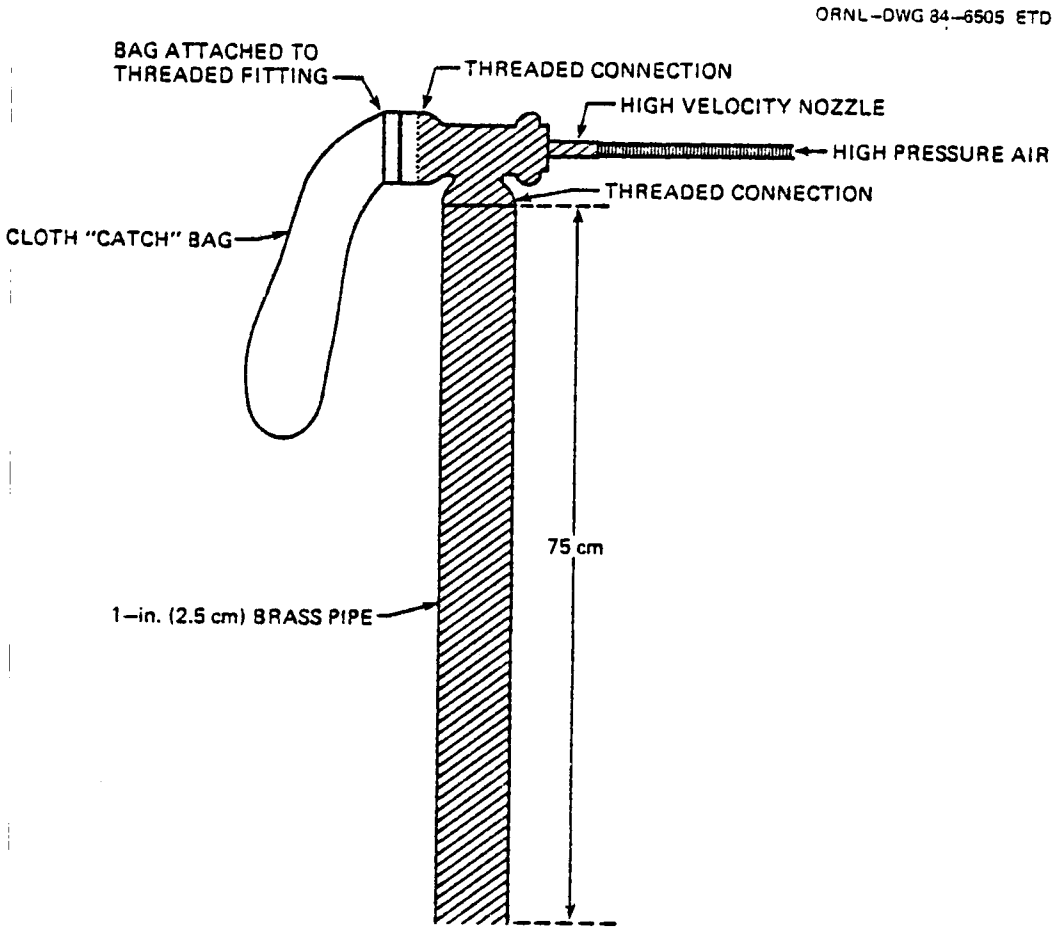

Figure 3.4. Vacuum device used to remove samples from the slumped bed.

Perhaps the greatest concern in sampling the bed was to minimize sample bias. Both vacuum and hand scooping methods were subject to possible bias associated with sampling the bed in a slumped rather than fluidized condition. Under some circumstances it may be possible that the slumping action itself produces a separation or mixing of particles. This is certainly a valid criticism, but the data of Sutherland and Wong (1964), which were taken using active-bed sampling, show the same type of patterns seen by investigators using slumped-bed samples, such as Rowe et al. (1972), Geldart (1981), and Cooke et al. (1982). In addition, since most of the segregation data available for small-particle beds has been based on slumped-bed samples, I concluded that large-particle vs small-particle comparisons would best be made on a consistent sampling basis.

Slumped-bed sampling also introduces another complication which must be taken into account. This is the problem of non-uniform bed expansion. One would expect that a section of the bed rich in flotsam would tend to expand more than a section rich in jetsam at the same fluidizing velocity. When the bed collapses, this expansion pattern and the relative axial positions of the solids are "compressed." As is discussed later in Chapter 5, this problem appears amenable to analysis. The main point here is that slumped-bed sampling produces a transformed axial profile which is different from the actual profile. Determining what the profile was actually like in the expanded bed requires information about the expansion characteristics. A few experiments were run with the portable pressure probe to get an indication of the trends in the expansion profile.

A potential bias which is associated specifically with vacuum sampling is the separation of particles as they are entrained and pulled up into the sampling tube. This would be expected to be a maximum when air velocity in the tube is greater than the terminal velocity of one component but less than the terminal velocity of the other. To be sure that this was not a significant factor, the air velocity was always adjusted to be much greater than the terminal velocity of both components, and experiments were run designed to reveal the presence of such biasing. These experiments consisted of creating beds by hand with known composition profiles, vacuum sampling them, and then comparing the measured profiles with those known to have originally existed. Table 3.2 illustrates results for a system containing glass beads and steel shot. Note that the average results for ten trials are very close to the makeup compositions and strongly suggest that the sampling method had very little, if any, bias. Most of the error is probably associated with positioning the vacuum probe at the desired levels.

Similar experiments were made to test for bias associated with the hand scooping method which might result from the "scooping" disturbances. As shown in Table 3.3, such an effect did not appear to occur. The variance here was even less than with the vacuum method, probably because it was easier to control the sampling level.

3.6 Sample Analysis

I analyzed the bed samples by one of two basic methods, separation of the components or measurement of the average sample density. Most of the analyses were carried out using the former technique based on screening, magnetic separation, or hand separation.

Table 3.2. Evaluation of bias associated with vacuum sampling
System - 2380 × 3360 μm glass beads and 4346 μm steel shot

Height above bottom (cm)	Number of shot originally added	Number of shot found (Run #)										Average
		1	2	3	4	5	6	7	8	9	10	
10.2-15.2	12	11	14	12	11	9	12	14	13	11	12	11.9
5.1-10.2	25	27	20	31	24	27	28	23	27	24	25	25.6
0-5.1	50	49	53	44	52	51	47	50	47	52	50	49.5

Estimated variances: s^2 for (10.2-15.2 cm) = 2.33, s = 1.53
s^2 for (5.1-10.2 cm) = 9.78, s = 3.13
s^2 for (0-5.1 cm) = 8.11, s = 2.85

Table 3.3. Evaluation of bias associated with hand scooping
System - 2380 × 3360 μm glass beads and 4346 μm steel shot

Height above bottom (cm)	Number of shot originally added	Number of shot found (Run #)										Average
		1	2	3	4	5	6	7	8	9	10	
10.2-15.2	12	12	14	12	13	14	12	13	11	13	12	12.6
5.1-10.2	25	29	25	25	25	21	23	25	25	26	25	24.9
0-5.1	50	46	48	50	49	52	52	49	51	48	50	49.5

Estimated variances: s^2 for (10.2-15.2 cm) = 1.33, s = 1.13
s^2 for (5.1-10.2 cm) = 4.11, s = 2.03
s^2 for (0-5.1 cm) = 3.89, s = 1.97

Screening could only be used when there was a size difference between the components. Magnetic separation could only be used when steel shot was one of the components. In cases where size and magnetic differences did not exist, hand separation was carried out on small "sub-samples." These "sub-samples" were representative portions of the actual samples which were obtained by splitting the sample with a riffle box. After separation, each component was weighed and the composition based on weight fraction and volume fraction was calculated. Weight and volume fractions are related by the relationship

$$v_1 = (x_1/\rho_1)/(x_1/\rho_1 + x_2/\rho_2) \ ,$$

where the subscripts denote components 1 and 2, respectively.

I also analyzed some mixed coal and limestone samples by immersing them in water and measuring their average density. It was then possible to determine the sample composition, since each component had a different density and only one possible combination could give the observed average valve. This technique was found to work reasonably well, although the wetting and drying problems made the hand separation technique more efficient and less cumbersome.

3.7 Bed Pressure Profiles

Early in the segregation experiments, I observed that the assumption of uniform bed expansion was not valid in many cases, particularly at relatively high air velocities when the bed was slugging or exhibiting turbulent fluidization. This was not surprising since I have personally observed similar behavior in large industrial fluidized beds such as the 20 MW(e) atmospheric fluidized bed combustor operated by the

Tennessee Valley Authority at Shawnee, Kentucky.* In order to quantify this non-uniformity, I used the adjustable pressure probe described in Section 3.1 to develop axial pressure profiles for some typical fluidized conditions.

The pressure profiles were used to develop "expanded" segregation profiles as opposed to static profiles for some cases. The principal assumption required to do this is that the pressure drop over a given section of bed is proportional to the mass of solids within that section. This assumption should be reasonably good as long as the bed is completely fluidized. Knowing the mass of a sample and the masses of the samples above it allows it to be located on the pressure-versus-position profile. This in turn locates the bottom of the sample in terms of the expanded position coordinate.

The primary experimental uncertainty in developing the pressure profile was due to the significant pressure fluctuations characteristic of fluidized beds. These were reduced by inserting a Taylor model 585104 pulsation damping unit in the line between the pressure probe and the manometer. The final recorded pressure was the estimated mean manometer level. Thus the pressure profiles should reflect the time-average axial solids distributions.

3.8 The Experimental Strategy

Six parameters were initially chosen as the central focus for the segregation experiments. These were particle density ratio, particle size ratio, superficial gas velocity, internal surfaces, static bed

*For a description of this facility see High and Bass (1983).

height, and overall bed composition. It was not feasible to set up a detailed experimental design, such as a factorial or Box-Behnken design, because of the relatively large number of variables, because of the considerable time involved in running a single experiment and analyzing the samples (usually about 2 hours), and because of the uncertainty as to the appropriate parameter levels to use in the design. For this reason, my approach was more subjective and empirical in nature, and my intent was to look instead for general patterns of behavior rather than detailed correlations. I tried to guide the direction of each experiment by the results obtained in previous experiments.

As is discussed in Section 4, this subjective approach appears to have been justified by the results. Some rather complex and unexpected phenomena were observed, especially with regard to gas velocity. Direct correlation of these phenomena with particle properties and flow conditions will likely prove to be extremely difficult. As these patterns became apparent, I tried to confirm and describe them in more detail and to see if the variety of segregation patterns produced could be explained by specific physical processes. To do this I focused on three rather different particle systems: a two-size glass system, a glass-polypropylene system, and an acrylic-polypropylene system. The bulk of the data were gathered for these systems.

I also conducted a few preliminary transient experiments. These were designed to be a brief exploration of the suitability of a modified version of the Gibilaro-Rowe steady-state model for simulating the transient behavior patterns.

4. EXPERIMENTAL RESULTS

4.1 Steady-State Results

Two clearly different types of fluidization behavior were observed for all of the binary systems studied. When the superficial gas velocity was between the minimum fluidizing velocity of the two components, the bed usually separated into distinct layers; a fluidized, flotsam-rich upper layer and an unfluidized, jetsam-rich lower layer.* When the superficial gas velocity was above the minimum fluidizing velocity of the jetsam, there was never any formation of an unfluidized layer. Because the behavior in these two cases was so clearly different, each of them is treated separately in the following discussions. They are referred to as Region 1 segregation, where $u_{mfF} < u_o < u_{mfJ}$, and Region 2 segregation, where $u_o > u_{mfJ}$.

The following subsections, 4.1.1 through 4.1.7, describe the general segregation trends observed in the steady-state experiments. These have been organized according to the specific binary systems studied. The results are described in terms of the general shape of the concentration profiles and the magnitude of the mixing index, I. The definition of I is

$$I = \frac{\sum_{i=1}^{n} v_{si}(v_{Ji} - \bar{v}_J)^2}{\bar{v}_J(1 - \bar{v}_J)} \qquad (4.1)$$

*Defluidization sometimes did not occur when the overall jetsam fraction was low, e.g., <10 volume %, or the air velocity was near u_{mfJ}.

where

i = index referring to each sample

n = total number of samples taken,

v_{si} = the volume fraction of the total bed contained in sample i, and

v_{Ji} = the volume fraction of jetsam in sample i.

This definition has a similar basis to those proposed by Fan and Chang (1979) and McCabe and Smith (1967). All of these indices are based on an estimate of the variance of the solids composition. If a bed is completely mixed, all of the samples will have the same composition, and the variance will be zero. When the bed is completely segregated, the variance reaches its maximum value. The numerator in Eq. 4.1 is a variance estimate in terms of the sample volume fraction compositions. The denominator, $\overline{v}_J(1 - \overline{v}_J)$, is the maximum variance which occurs when the bed is completely segregated. Thus, I is essentially a "normalized" estimate of variance and can vary from zero to one.

Subsection 4.1.8 summarizes general observations which apply to most or all of the systems studied. These general observations are expanded further in Section 5 in terms of the parameters in the modified Gibilaro-Rowe model. Detailed experimental conditions and results are given in Table A.2 in the Appendix.

4.1.1 The limestone-coal system

In these experiments the static bed height ranged from approximately 23 cm to 28 cm and the overall jetsam volume fraction from approximately 0.64 to 0.94. The superficial gas velocity ranged from 0.72 m/s to 3.22 m/s. All runs were made without internals in the bed. Two

different size mixtures of coal and limestone were studied: (1) a mixture containing 1890 μm mean size coal (#1 coal in Table 3.1) and 2000 μm mean size limestone (#1 limestone in Table 3.1) and (2) a mixture containing 1750 μm mean size coal (#2 coal in Table 3.1) and 2720 μm mean size limestone (#2 limestone in Table 3.1). Most of the experimental runs were made with the second mixture.

Figure 4.1 illustrates the segregation profiles of the three runs made in Region 1. Note that the mixing indexes are given in the figure legend, and the general trend is that I increases with decreasing velocity; i.e., segregation increases with decreasing velocity. Also in the legend is the initial condition of the bed from which it was allowed to approach steady state. Note that run LC-9 started well-mixed, i.e., the bed solids were initially well-mixed and the air flow was increased slowly to its final value and then held constant. Runs LC-10 and LC-16 started differently. In these cases, the bed was completely fluidized with a u_o slightly greater than u_{mfJ}, and then the velocity was decreased to its final value and then held constant. The air velocity was reduced more rapidly in LC-10 than in LC-16.

As indicated by the mixing indices, LC-9 was the best-mixed case. The penetration of the jetsam into the upper, fluidized layer and the penetration of the flotsam into the lower, defluidized layer was greater than in both LC-10 and LC-16. Run LC-10 illustrates an interesting pattern seen in other systems under Region 1 conditions. In the bottom layer, the profile slopes to the right; i.e., the concentration of jetsam actually increases with height above the distributor. Careful observation confirmed that this pattern occurred when the air velocity

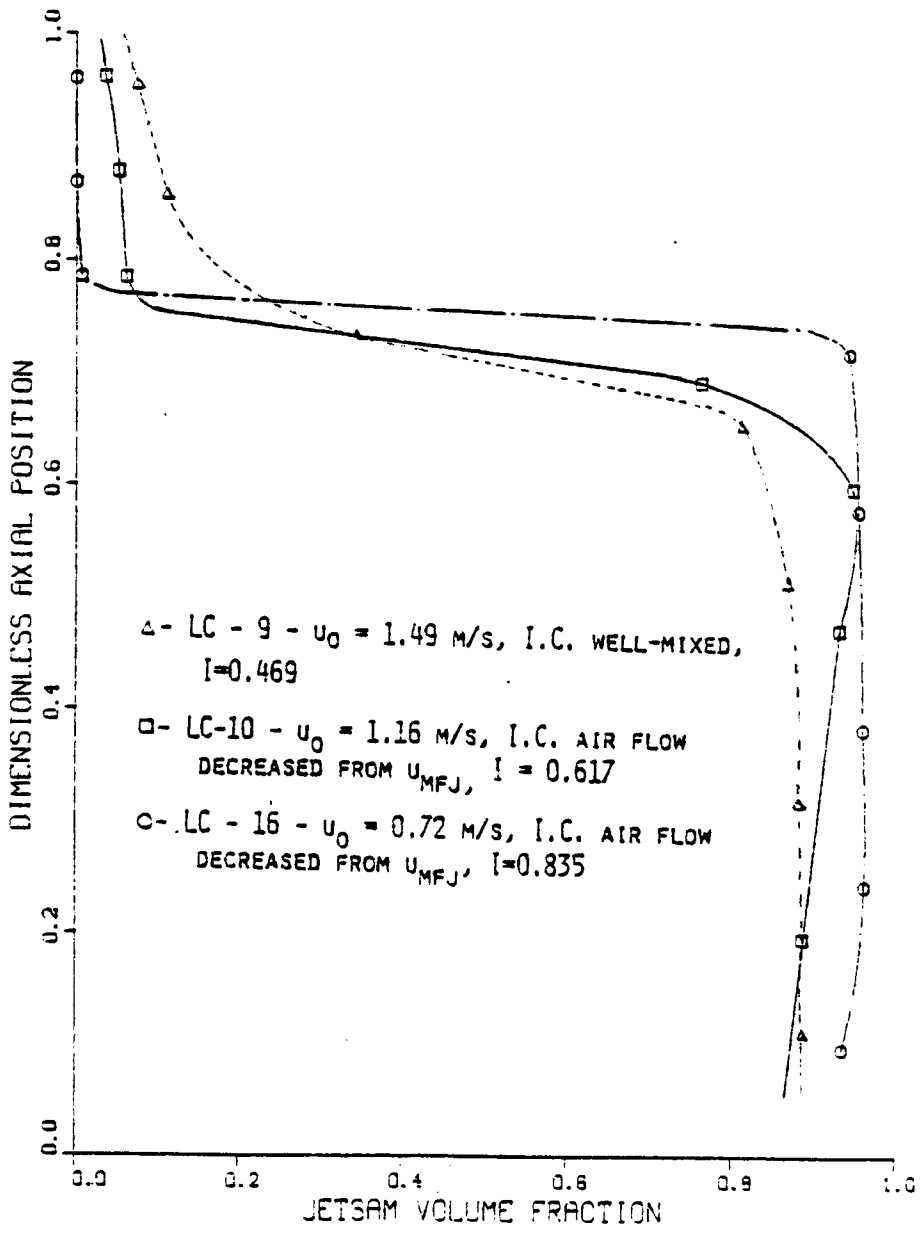

Figure 4.1. Effect of air velocity and initial condition on the segregation pattern for the limestone-coal system, Region 1.

was reduced relatively rapidly, and the jetsam defluidized faster than the flotsam could migrate upwards. The fluidized/defluidized interface tended to move upwards as velocity decreased as well, and at each higher position the concentration of flotsam was lower than before. The flotsam below the interface was completely trapped and thus the profile below the interface was effectively "frozen" in place. This created the inverted profile. The air velocity in run LC-16 was reduced at a slower rate, and the flotsam had time to migrate upwards as each successive level of the lower layer defluidized. Thus the profile in the lower section was nearly vertical.

For all three Region 1 cases, the upper portion of the bed exhibited patterns which had a modified sigmoid shape. The significance of this shape is discussed in more detail in Section 5, but it is sufficient to note here that this same shape tends to occur for many systems in Region 2 when u_o is relatively close to u_{mfJ}.

Figures 4.2, 4.3, and 4.4 illustrate some typical Region 2 patterns observed for coal and limestone. Note that again higher air velocity tended to enhance mixing. The pattern exhibited in LC-8 is qualitatively different from those in LC-4, 5, 6, and LC-7. A comparison between LC-8 and LC-4 is particularly interesting because both of these runs were made at essentially the same air velocity. The only difference is that the overall flotsam fraction is much reduced in LC-4. Thus the shape of the segregation profile can be significantly altered by the overall relative amounts of jetsam and flotsam. This observation has been made by others such as Rowe et al. (1978) and will be discussed in

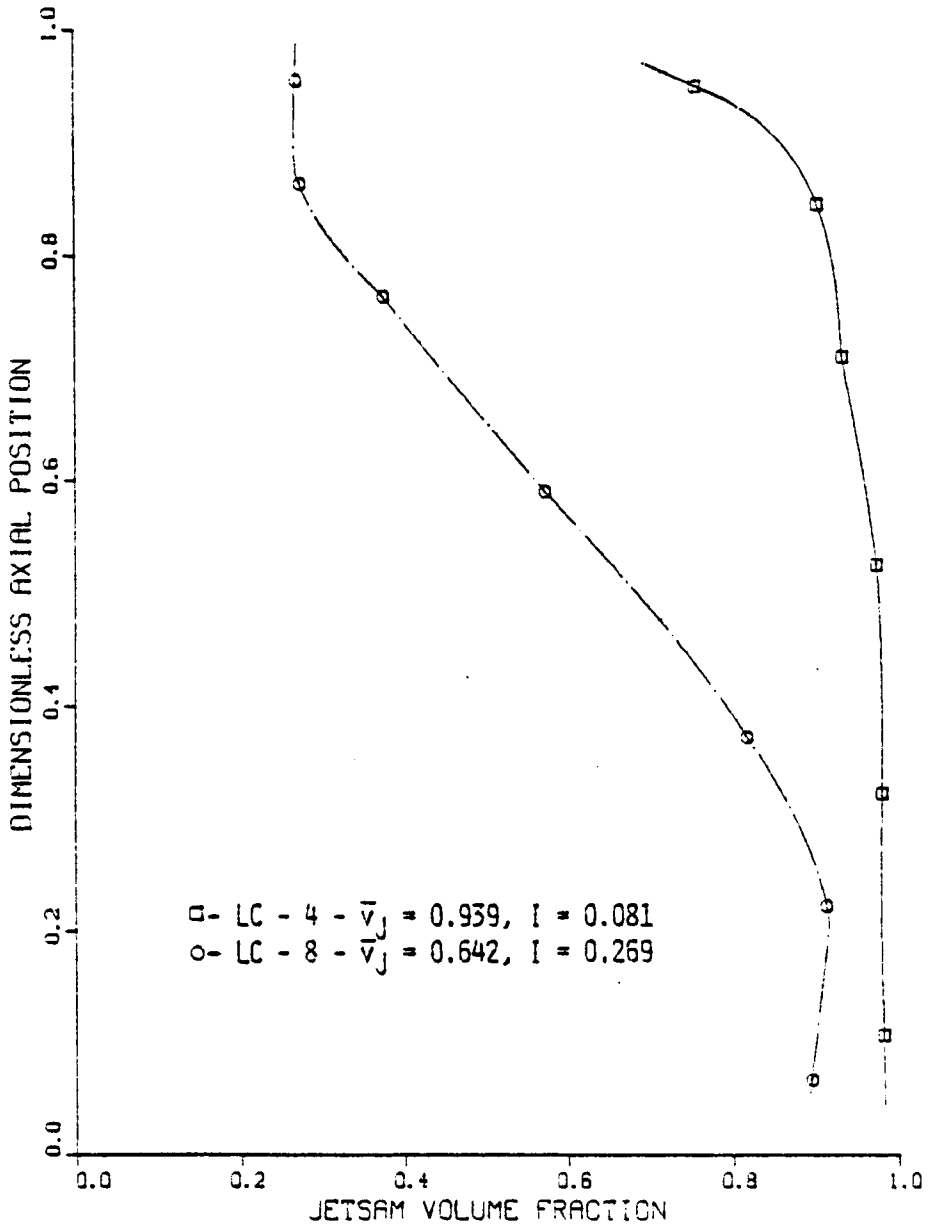

Figure 4.2. Effect of overall bed composition on the limestone-coal segregation profile, Region 2.

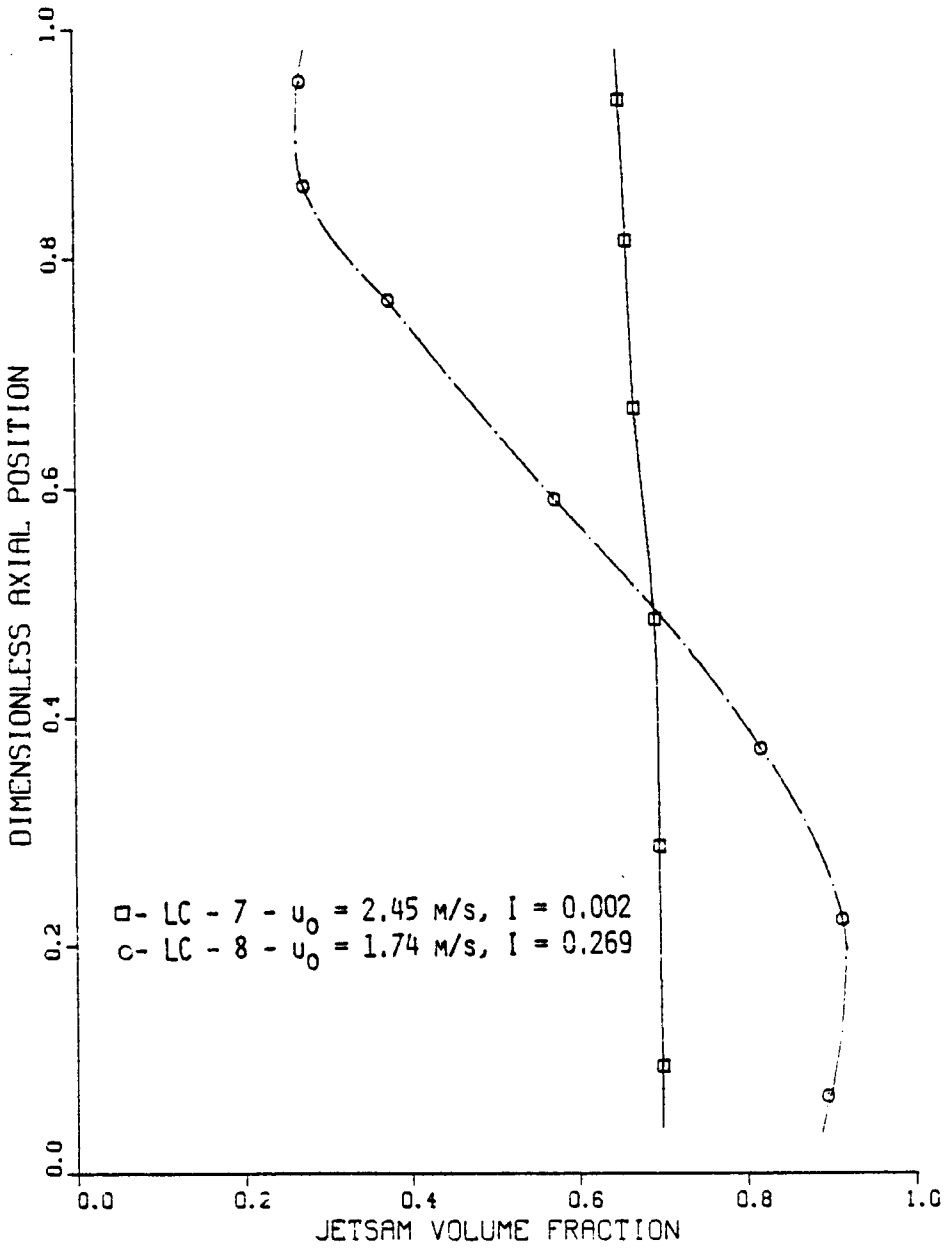

Figure 4.3. Effect of air velocity on the limestone-coal segregation profile at relatively large coal fraction, Region 2.

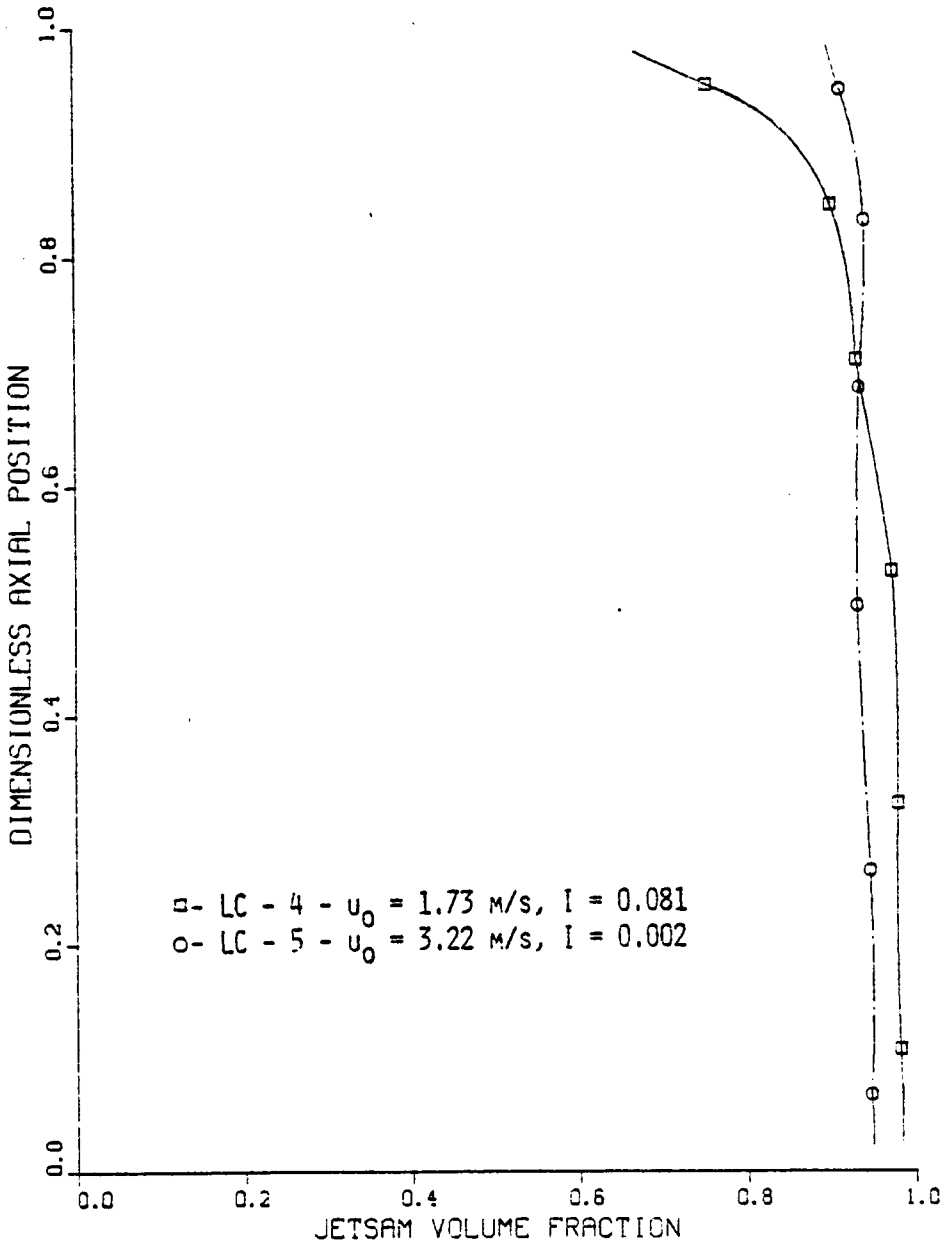

Figure 4.4. Effect of air velocity on the limestone-coal segregation profile at relatively low coal fraction, Region 2.

more detail in Section 5. Runs LC-6 and LC-7 are clearly close to complete mixing. In both cases, the air velocity is almost 60% greater than u_{mfJ}.

4.1.2 The steel-glass system

This system was distinctly different from the coal-limestone system because of the large difference in specific gravities of the components (#1 glass — 2.25 g/cm^3, steel — 7.50 g/cm^3). The static bed height in these experiments ranged from approximately 23 cm to 31 cm, the overall jetsam volume fraction ranged from 0.026 to 0.291, and the superficial air velocity ranged from approximately 2.6 m/s to 5.2 m/s. No bed internals were used in any of the experiments.

Figure 4.5 illustrates some typical segregation profiles for Region 1. Note that runs SG-1 and SG-3 were made with beds containing only a very small amount of steel shot, while run SG-6 had a higher fraction of steel shot. Both SG-1 and SG-3 were also started from a well-mixed condition, while SG-6 was started from a segregated condition. As in the Region 2 coal-limestone experiments, the overall bed composition had a large effect on the resulting segregation patterns. There was enough flotsam present in SG-1 and SG-3 to keep the bed completely fluidized, even though u_o was significantly less than u_{mfJ}. In SG-6, on the other hand, the bed remained totally segregated with the flotsam fluidized on top and the jetsam defluidized on bottom.

The patterns in SG-1 and SG-3 appear to indicate three distinct regions in the bed; a lower region with a steep composition gradient, a middle region with a nearly uniform composition, and an upper region

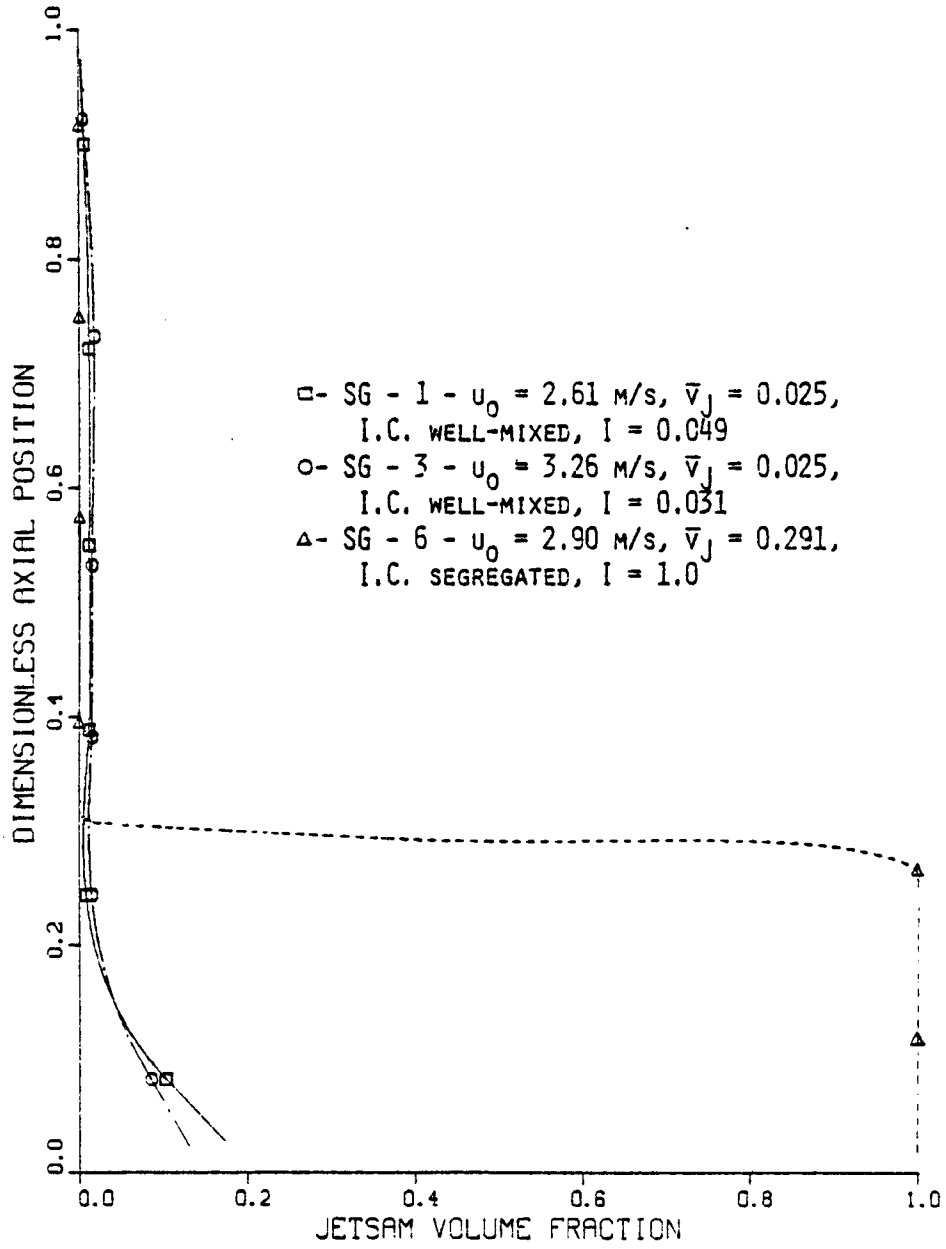

Figure 4.5. Typical steel-glass segregation profiles, Region 1.

with a relatively moderate composition gradient (the upper region is difficult to see in Figure 4.5 due to the scale). The well-mixed middle region seems somewhat surprising considering the strong tendency for the steel to settle. Close observation during the experiment revealed that the shot were lifted from the lower region by the bubbles. As the bubbles crossed into the flotsam-rich region, they tended to grow considerably in size and velocity, and this seemed to enhance the lifting effect. The agitation in the jetsam-rich region also appeared to help the bubbles entrain the shot. Even though the glass was vigorously bubbling in SG-6, the lack of agitation in the defluidized zone appeared to essentially eliminate shot entrainment. When the shot were entrained, many appeared to be carried nearly to the surface of the bed. The number of shot appeared to drop off significantly in the last 20% or so of the bed height (the upper region) as the bubbles collapsed near the surface.

Figure 4.6 shows some typical Region 2 segregation profiles. Run SG-8 was made with a superficial air velocity (3.86 m/s) approximately 10% greater than u_{mfJ}. Even though all solids were completely fluidized, there was essentially no mixing because of the large difference in particle densities. Run SG-9 illustrates the improved mixing which resulted at u_o = 4.65 m/s. Note that SG-9 profile exhibits the sigmoid shape seen in some of the limestone-coal experiments.

Run SG-10 illustrates an interesting phenomenon which was also seen in other experiments; the reduction in mixing with increased air flow. It is intuitive that more air flow results in more bubbling and more

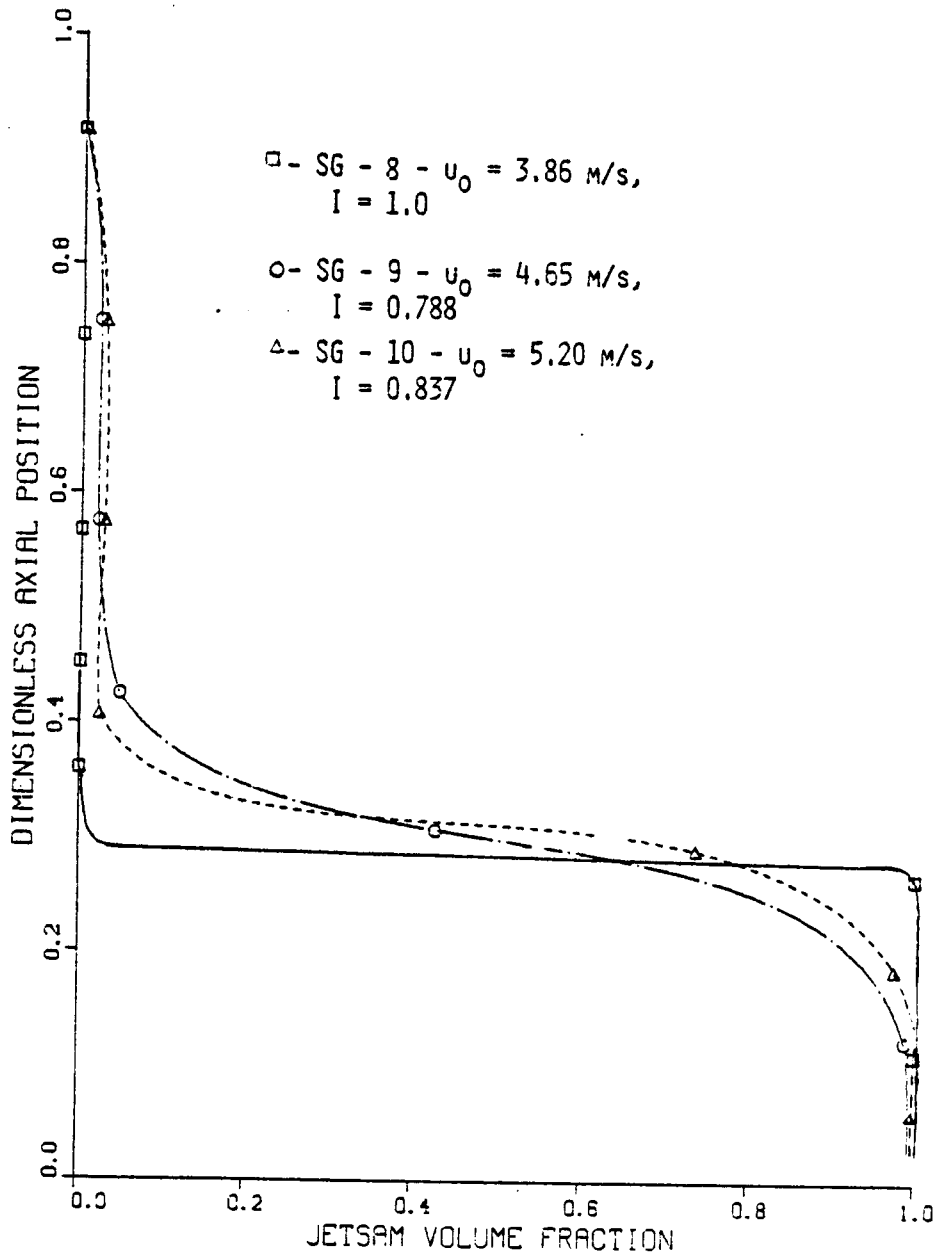

Figure 4.6. Typical steel-glass segregation profiles, Region 2.

bubbling should enhance mixing. In many cases, especially near u_{mfJ}, this behavior is, in fact, borne out. However, it would also be expected that as the terminal velocity of the lighter component is approached, the segregation should become more pronounced. Thus, somewhere between u_{mfJ} and u_{tF} there should be a segregation minimum. Air velocities above this minimum should produce increasingly greater segregation. The change between the profiles in SG-9 and SG-10 seems to indicate that the minimum was passed. As is illustrated in the results for other systems, there apparently can be more than one segregation minimum. Whether the steel-glass system would have continued to segregate more for velocities above 5.20 m/s is not known.

It should be pointed out that in Region 2 the gas velocity was anywhere from 2.3 to 3.4 times the minimum fluidizing velocity of the glass bends. As would be expected for a bed with such a high aspect ratio and no tubes, the glass tended to slug violently or exhibit turbulent flow. The visual appearance was thus highly chaotic, with frequently high oscillations in the bed height and pressure drop. In spite of this, the profiles measured in the slumped bed were relatively uniform, reproducible, and still followed the same basic patterns seen by Rowe et al. (1972). The implications of this observation for modeling are discussed in detail in Section 5.

4.1.3 The acrylic-glass system

This system was unusual in that the jetsam particles (#1 glass) were smaller than the flotsam particles (clear acrylic) and had a lower minimum fluidizing velocity (glass — 1.54 m/s, clear acrylic — 1.69 m/s). The static bed height varied from approximately 12.4 to 14 cm,

the superficial air velocity from 1.55 to 4.92 m/s, and the overall jetsam fraction from 0.333 to 0.900. Six Region 2 experiments were made with bed internals and one Region 1 experiment was made without bed internals.

As shown in Figures 4.7 and 4.8, Region 2 segregation decreased with increasing air velocity and overall jetsam fraction. The low velocity segregation profile (AG-1) is reminiscent of the sigmoid profiles seen in LC-9 and 10 and SG-9 and 10. As air velocity increased, the AG profile became more like the SG-1 and 3 profiles, except the top region was less distinct or non-existent. The air velocity in AG-4 was sufficient to give essentially complete mixing. Increasing the overall jetsam fraction appeared to produce results similar to those seen in LC-4 and 6.

Figure 4.9 illustrates the results for the Region 1 experiment (AG-5) and an unusual Region 2 profile (AG-3). The Region 1 behavior was especially unique for this system because the jetsam (glass) was well fluidized while the flotsam (acrylic) was slumped (although it was slightly agitated by the motion of the jetsam below). The agitation of the glass was sufficient to cause a few glass particles to migrate upwards into the acrylic layer. Some of the acrylic also penetrated down into the glass layer. This produced a sigmoid-shaped curve similar to those described previously.

Run AG-3 is unusual because of the inverted slope (increasing acrylic concentration) in the upper part of the bed. A possible explanation for this result is that conditions in the upper portion of the bed were sufficiently different from the conditions in the middle and

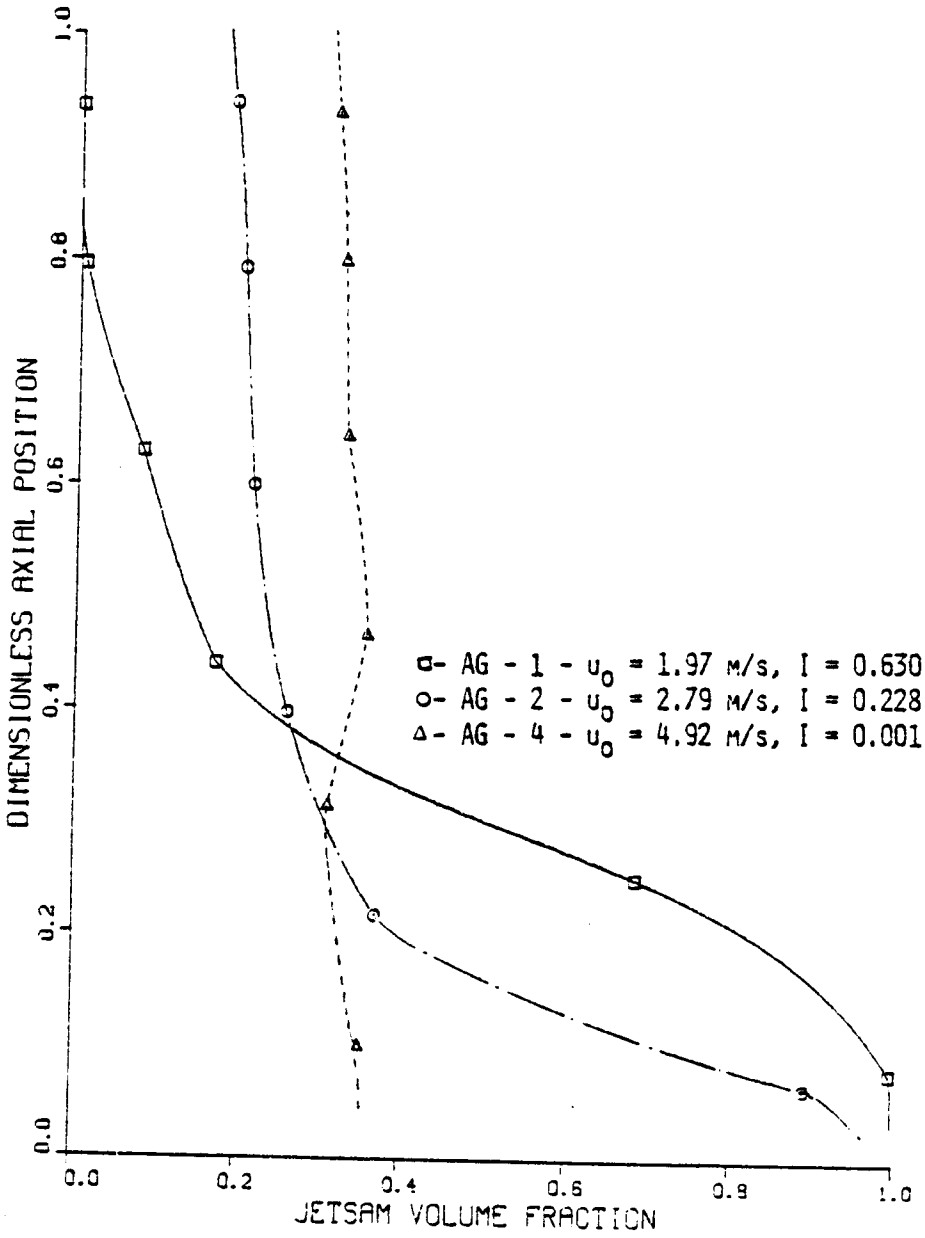

Figure 4.7. Effect of air velocity on the acrylic-glass segregation profile, Region 2.

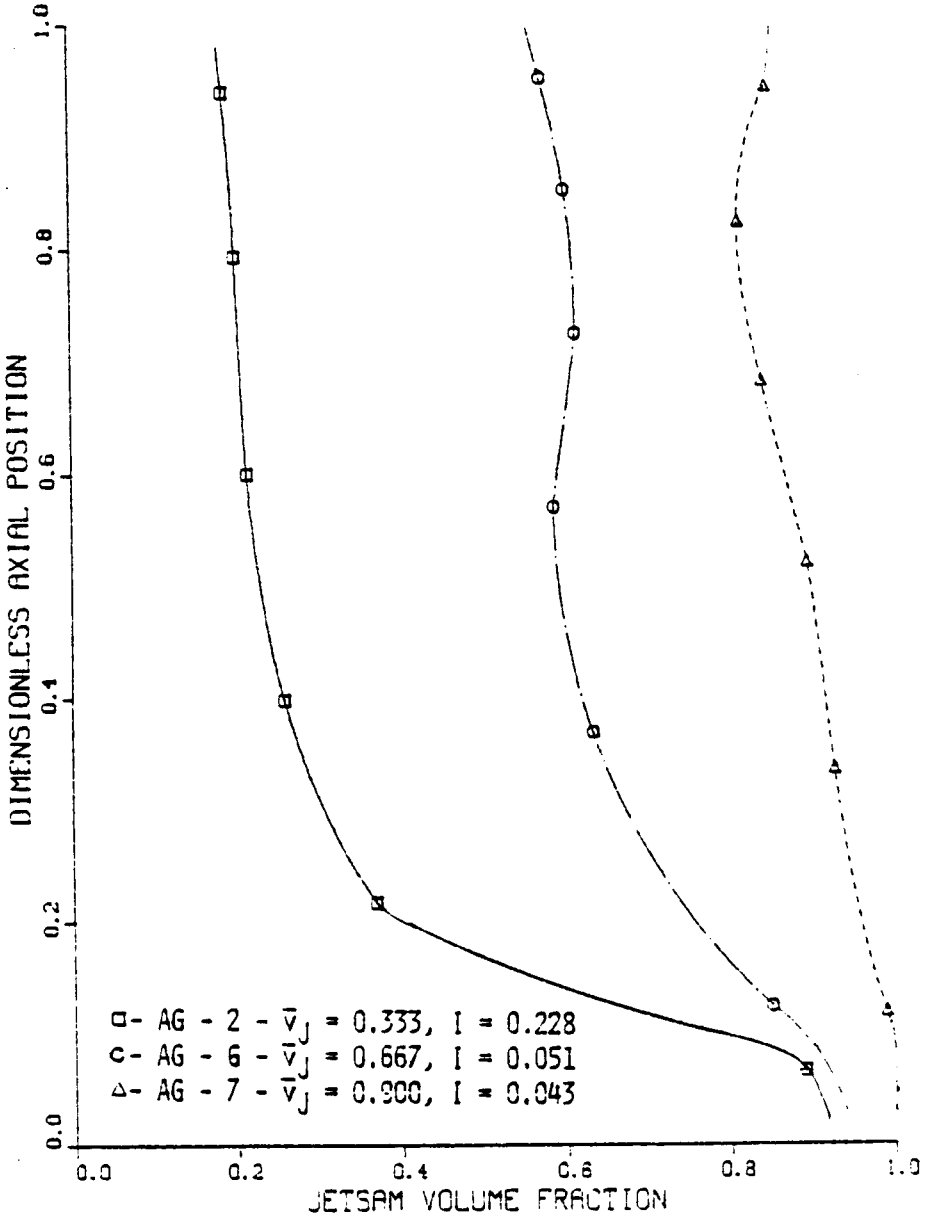

Figure 4.8. Effect of overall jetsam volume fraction on the acrylic-glass segregation profile, Region 2.

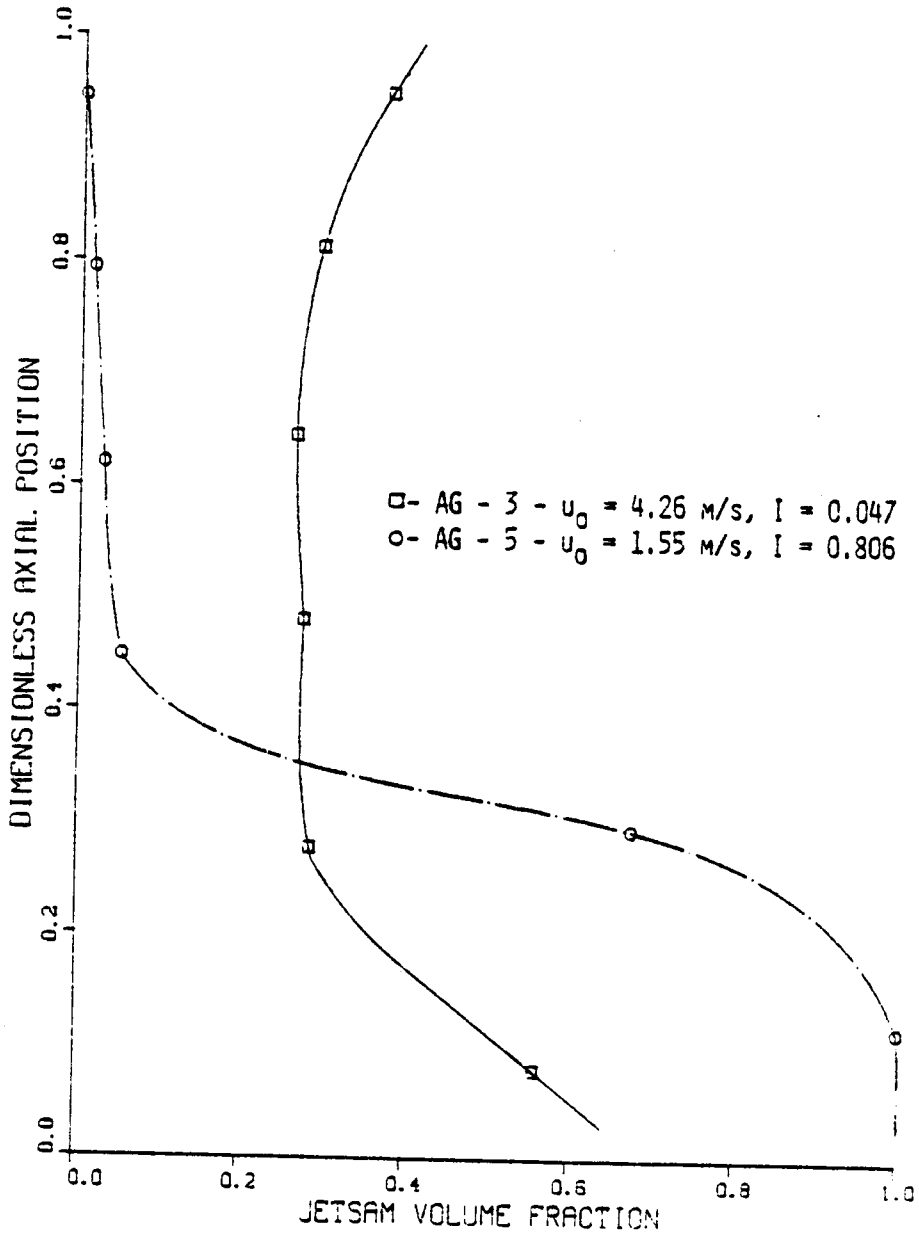

Figure 4.9. Region 1 segregation profile and unusual Region 2 profile for the acrylic-glass system.

lower portions to cause a reversal in the flotsam and jetsam roles of the glass and acrylic. This explanation is based on the observation that the upper zone usually did not contain bubbles but instead consisted of solids which were thrown out of the bed by the erupting bubbles (i.e., the splash zone). Thus, a different mixing-segregation mechanism would apply in this zone. The lower terminal velocity of glass would also make it seem reasonable that it could be entrained more easily under some circumstances. Note that this "inversion" phenomenon did not appear in AG-2 or 4 which were made at lower and higher air velocities respectively. Thus the phenomenon, if it is real, is not monotonic with air velocity.

4.1.4 The acrylic-acrylic system

Only one steady-state experiment was run with this system. The primary purpose of this experiment was to serve as a basis for some of the transient experiments discussed in Section 4.2 and to illustrate the degree of segregation which can be found in systems of very similar particles. Note in Table 3.1 (pg. 67) that there was only a slight difference in size between the black and clear acrylic, resulting in a difference of only about 0.03 m/s in their minimum fluidizing velocities. Even with this small difference, Figure 4.10 shows that significant segregation occurred at an air velocity approximately 18% greater than u_{mfJ}. This appears to support the observations of Fan and Chang (1979) who studied a system with components of the same size which were only slightly different in density.

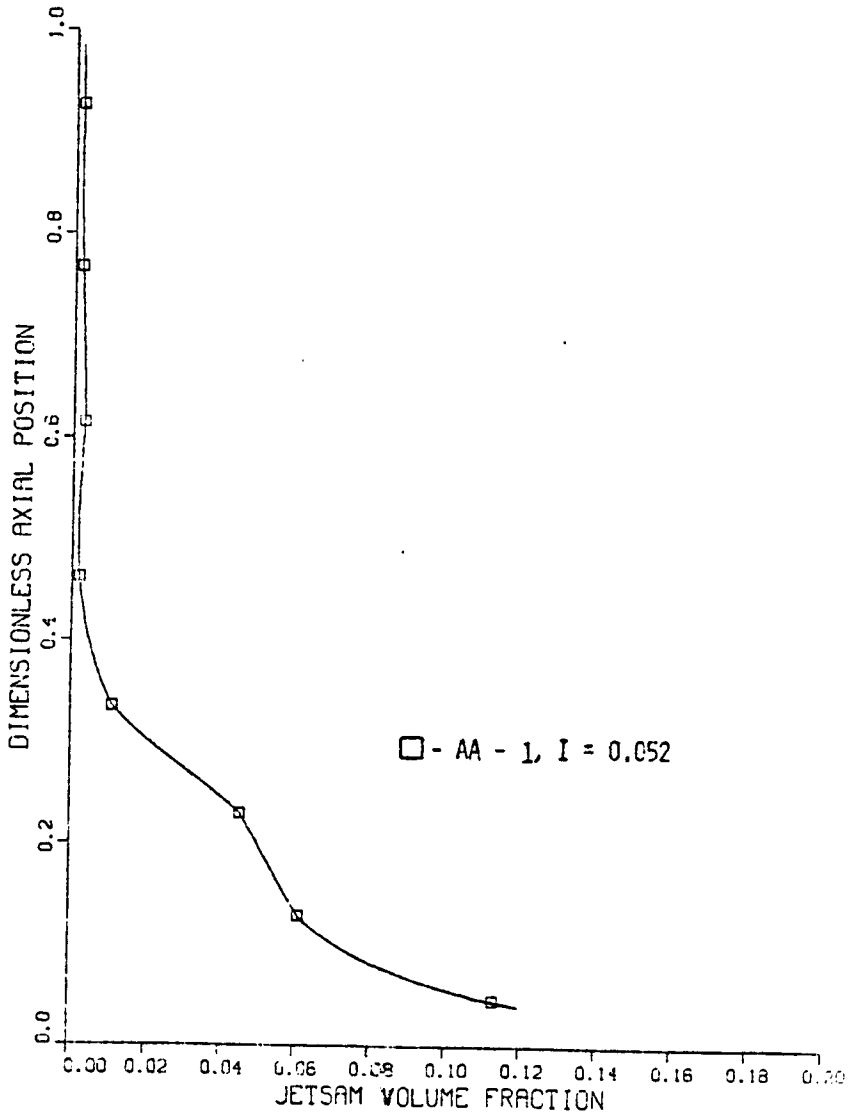

Figure 4.10. Region 2 segregation profile for the acrylic-acrylic system with slight size difference.

4.1.5 The glass-glass system

This system was composed of the glass beads designated #1 glass and #2 glass in Table 3.1. The static bed height ranged from approximately 7 cm to 21 cm, the overall jetsam volume fraction from approximately 0.13 to 0.93, and the superficial gas velocity from 1.6 m/s to 6 m/s. Runs were made both with and without internals in the bed.

A detailed study of the effects of gas velocity on this system revealed some unexpected behavior. Abrupt transitions occurred in the mixing index, I, as gas velocity changed in both Regions 1 and 2. These transitions were especially noticeable in Region 2, as depicted in Figures 4.11 and 4.12 for beds with and without tubes, respectively.

Since these localized maxima and minima (also referred to as "mixing/segregation resonances" in this report) have not been reported by previous investigators [except perhaps Katz (1957)], special efforts were made to confirm that these phenomena were real and not just variations due to experimental error. Replicate runs indicated that they were indeed real and that the patterns repeated themselves even when the bed was changed somewhat. Note, for instance, that the air velocities at which the "resonances" occurred were very much the same in Figures 4.11 and 4.12.

When tubes were present, increasing gas velocity just above u_{mfJ} resulted in decreased segregation. At approximately 2.3 m/s the mixing trend suddenly reversed, and segregation increased to a level even greater than that seen at u_{mfJ}. This maximum occurred at approximately 2.4 m/s. Further increases in glass velocity resulted in a rapid decrease in segregation. A slight "step" occurred at about 3.2 m/s, but

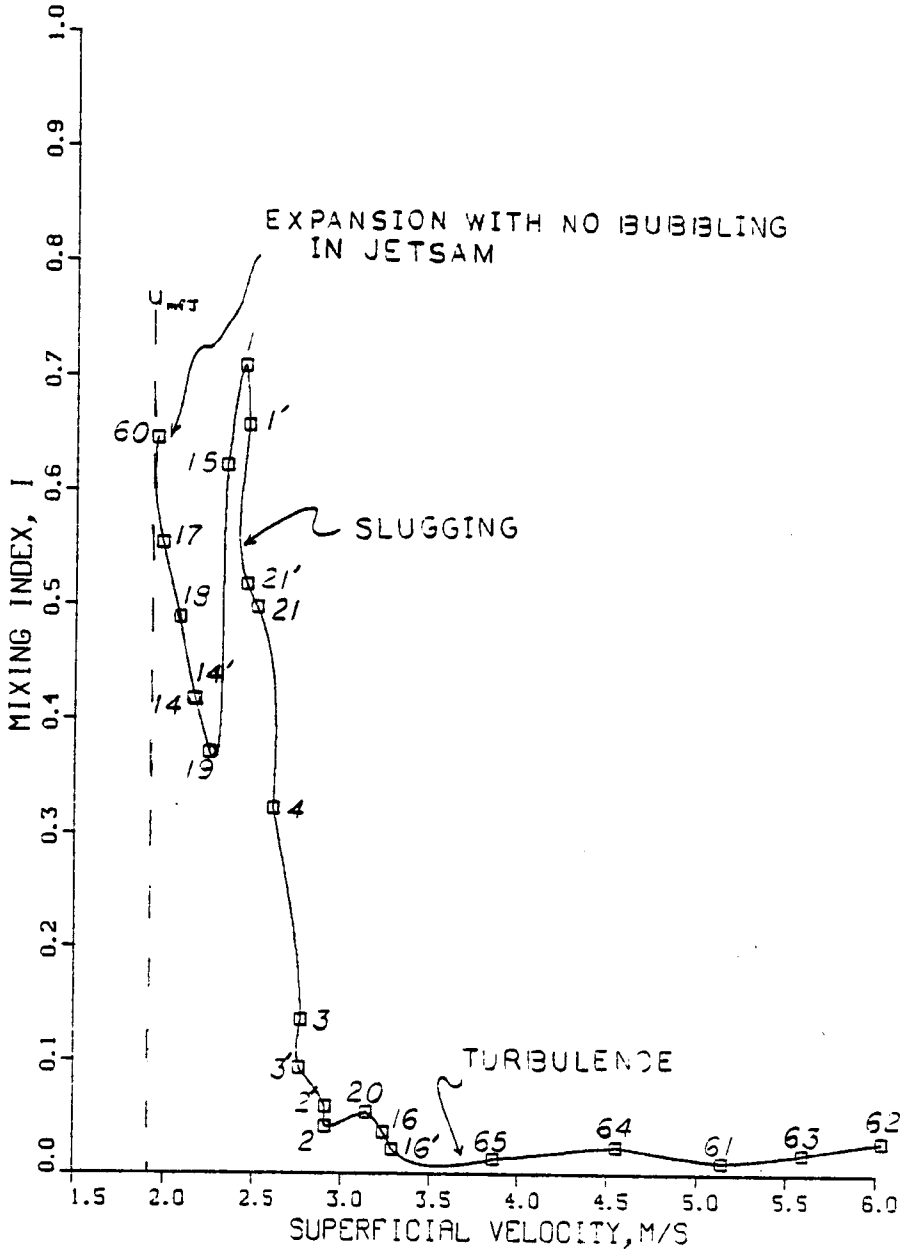

Figure 4.11. Variations in the glass-glass mixing index as a function of the air velocity when horizontal tubes were present, Region 2.

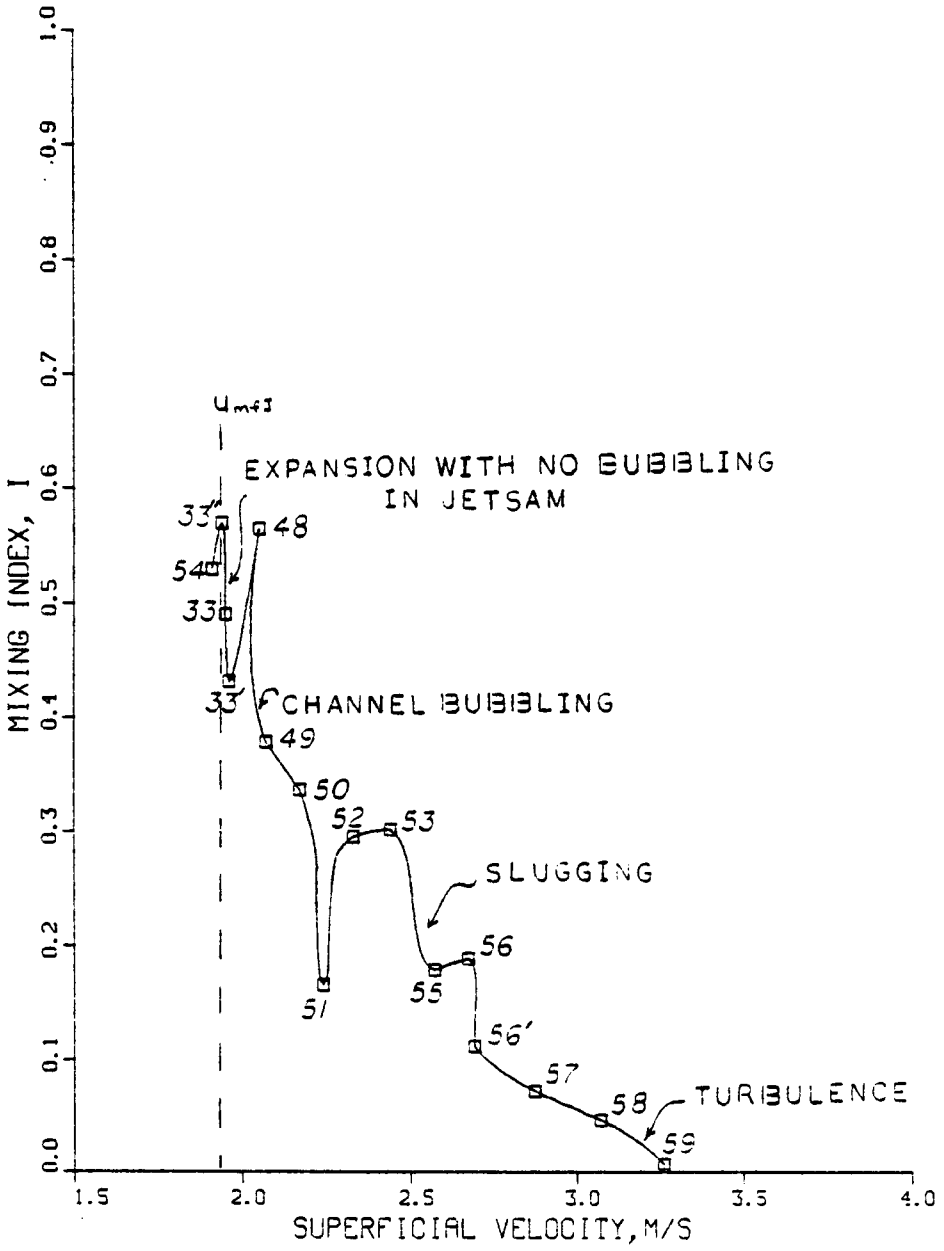

Figure 4.12. Variations in the glass-glass mixing index as a function of the air velocity when no tubes were present, Region 2.

beyond this the bed remained essentially well-mixed up to 6 m/s. When there were no tubes, segregation initially decreased with increasing gas velocity near u_{mfJ}, but then abruptly increased near 2.06 m/s. Still higher velocities produced a gradual downward trend in segregation until a minimum was reached near 2.25 m/s. Another peak occurred near 2.4 m/s as it did with tubes present.

Careful observations revealed that the abrupt mixing index transitions corresponded with clear changes in the bubbling mode of the jetsam. In general, the bubbling modes occurred in the following progression with increasing glass flow: (1) slight expansion with no bubbling, (2) streams of bubbles moving up through localized channels (channel bubbling), (3) large bubbles and large oscillations (slugging or pseudo-slugging), and (4) turbulence. These modes are indicated on Figures 4.11 and 4.12. Note that the tubes appeared to inhibit the effect of the transition from pre-bubble expansion to channel bubbling.

Figures 4.13, 4.14, and 4.15 illustrate typical examples of the segregation profiles which occurred when the gas velocity was increased above u_{mfJ}. Note that the sigmoid-type profiles at lower velocities give way to more well-mixed patterns at the higher flows. Profiles occurring in or near the turbulent region characteristically exhibit a nearly constant composition throughout most of the bed, except for a region near the top of the bed, where the jetsam concentration falls off rapidly. In most cases, the transition between these two regions appeared to occur at $z \simeq 0.8$.

The glass-glass system also exhibited abrupt mixing index changes in Region 1, although the size of the transitions appeared to be less

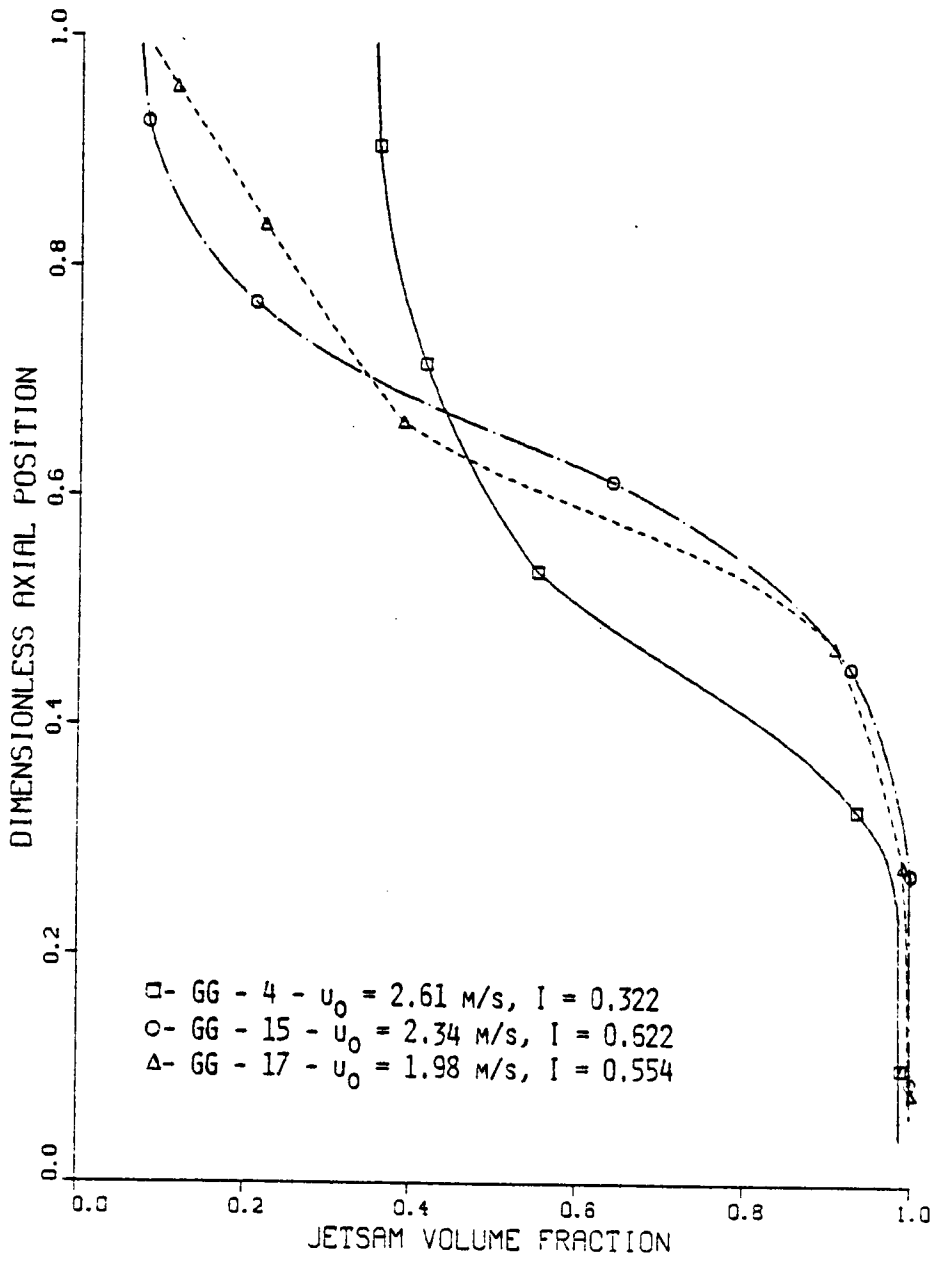

Figure 4.13. Effect of air velocity on the glass-glass segregation profile with horizontal tube internals, Region 2.

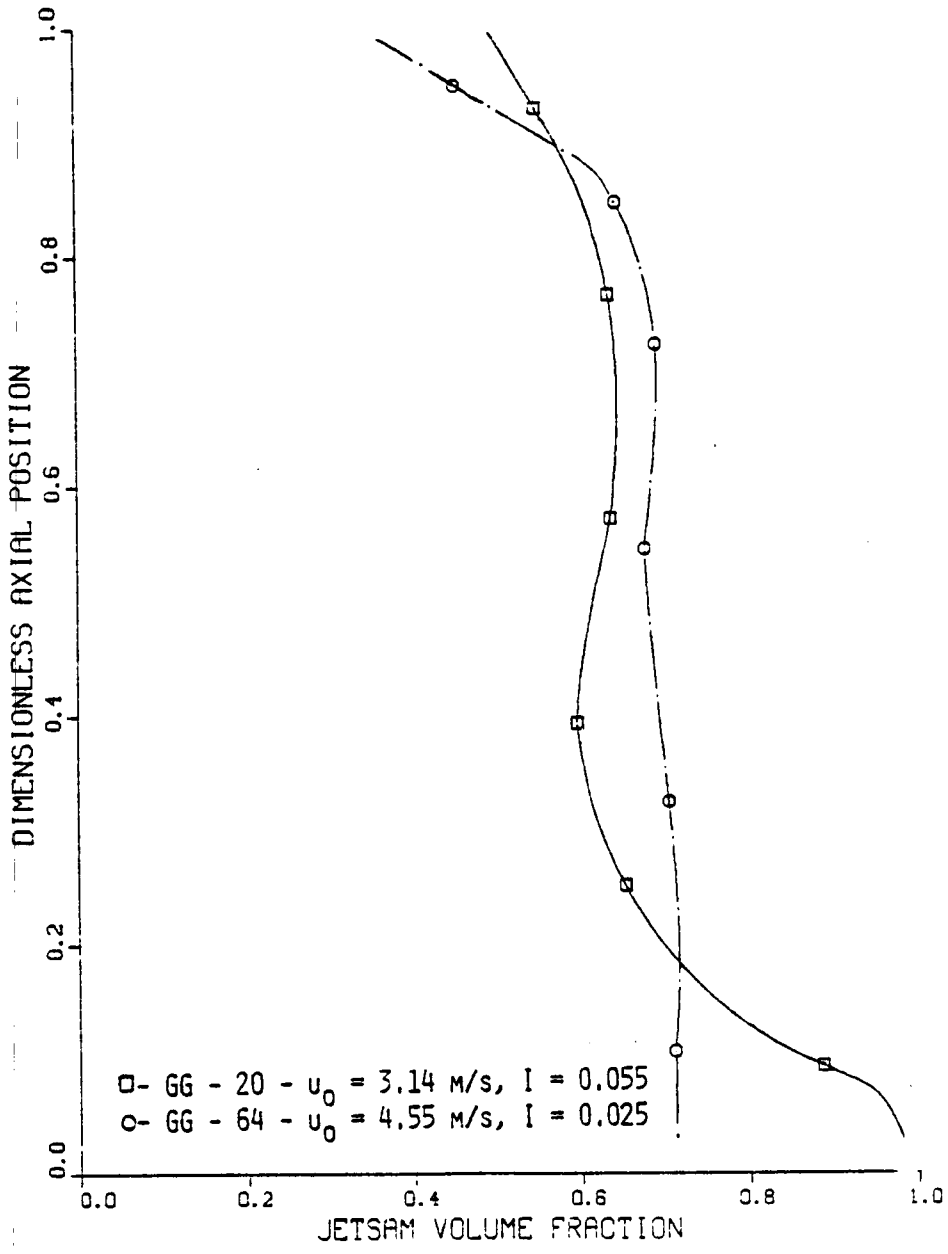

Figure 4.14. Effect of air velocity on the glass-glass segregation profile with horizontal tube internals, Region 2.

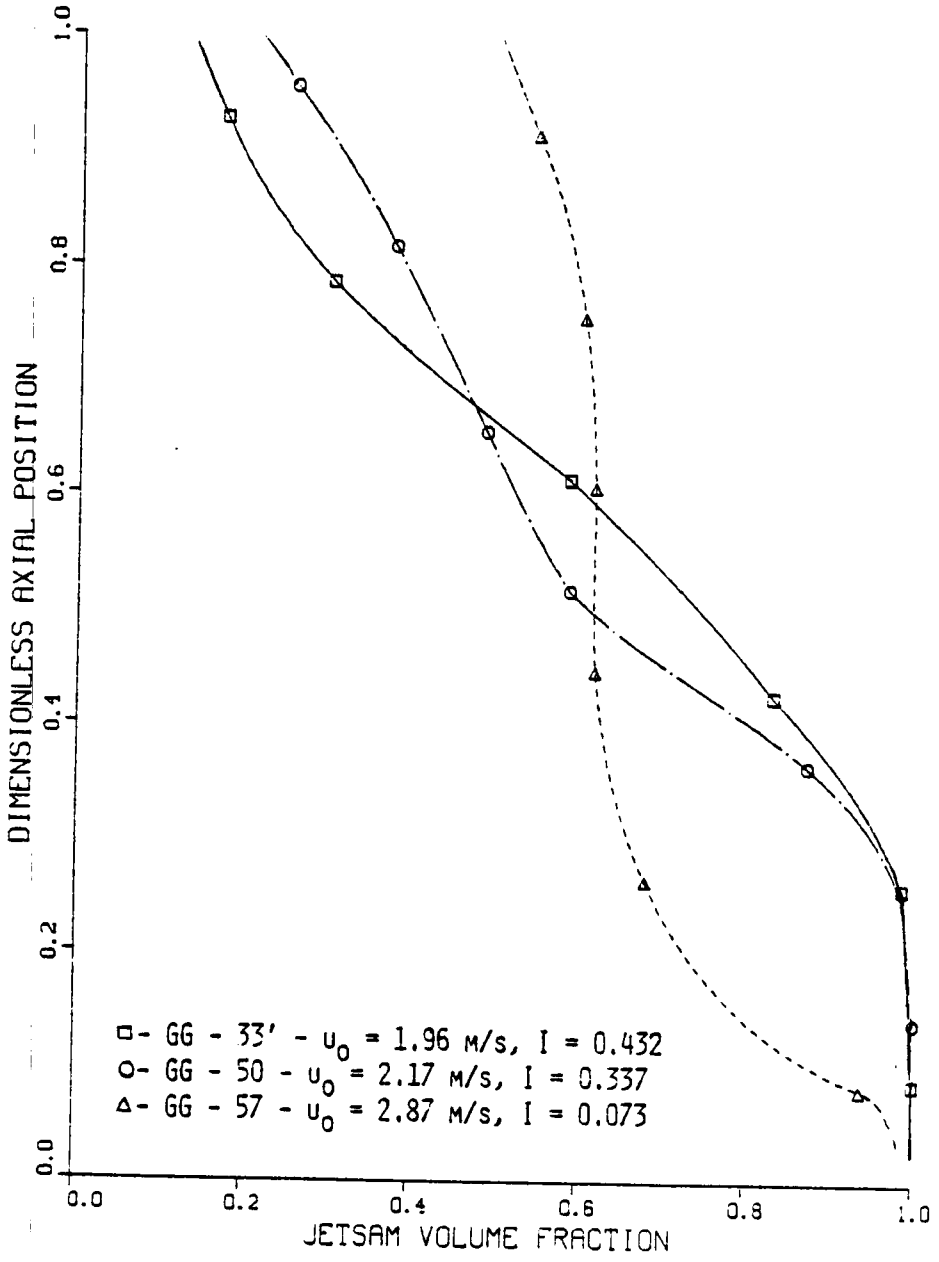

Figure 4.15. Effect of air velocity on the glass-glass segregation profile with no internals, Region 2.

than in Region 2. The behavior was also complicated by the hysteresis associated with defluidization. Figure 4.16 illustrates the mixing index as a function of the gas velocity and the initial condition of the bed. The arrows indicated on the curves represent the direction that the final point was reached from the initial condition, i.e., right-pointing arrows indicate the velocity was increased; left-pointing arrows indicate a reduction in velocity. Double arrows indicate the condition could be reached from both directions. The two straight lines with left-pointing arrows represent the results for initial conditions in which the bed was completely fluidized. Changes in the bubbling mode of the flotsam are also indicated.

Beginning at u_{mfF}, the gas velocity was increased for segregated and well-mixed initial conditions. Up to a velocity of about 1.79 m/s, the final conditions for these two initial conditions were noticeably different. When the bed was initially segregated, it tended to stabilize with a sigmoid-type profile, as typified by run GG-26 in Figure 4.17. The interface between the fluidized and unfluidized sections moved further downward with increasing velocity. Jetsam was pulled up into the fluidized region by small bubbles moving up through localized channels.

When the bed was initially segregated, the flotsam in the lower sections tended to move upward in a kind of collective "front." Motion continued in the lower section until the amount of flotsam present became insufficient to overcome the resistance of the surrounding jetsam. Defluidization in the lower section trapped the remaining flotsam, producing profiles with a characteristic "hump." Plots for runs GG-40 and

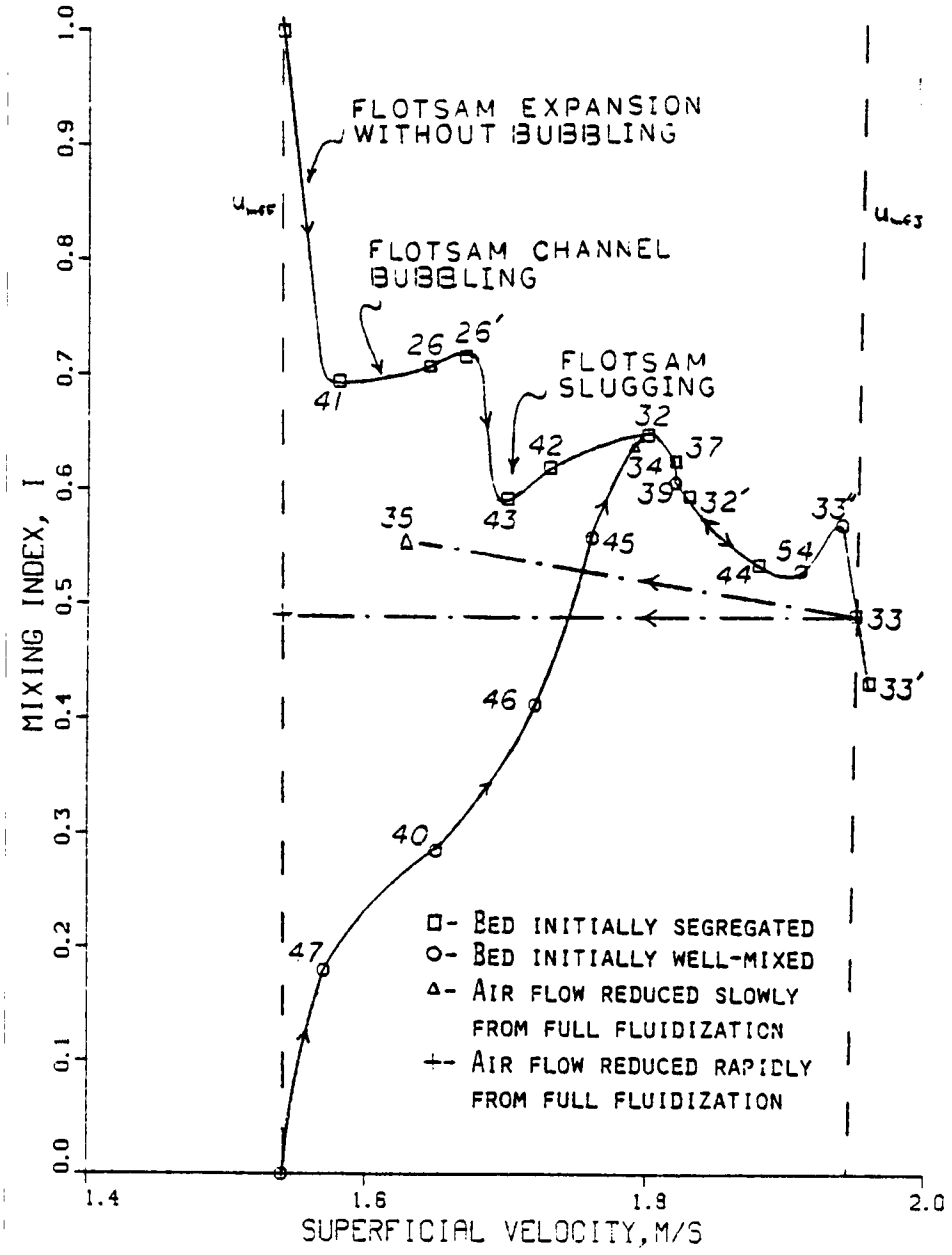

Figure 4.16. Variation in the glass-glass mixing index as a function of the air velocity and initial condition when no tubes were present, Region 1.

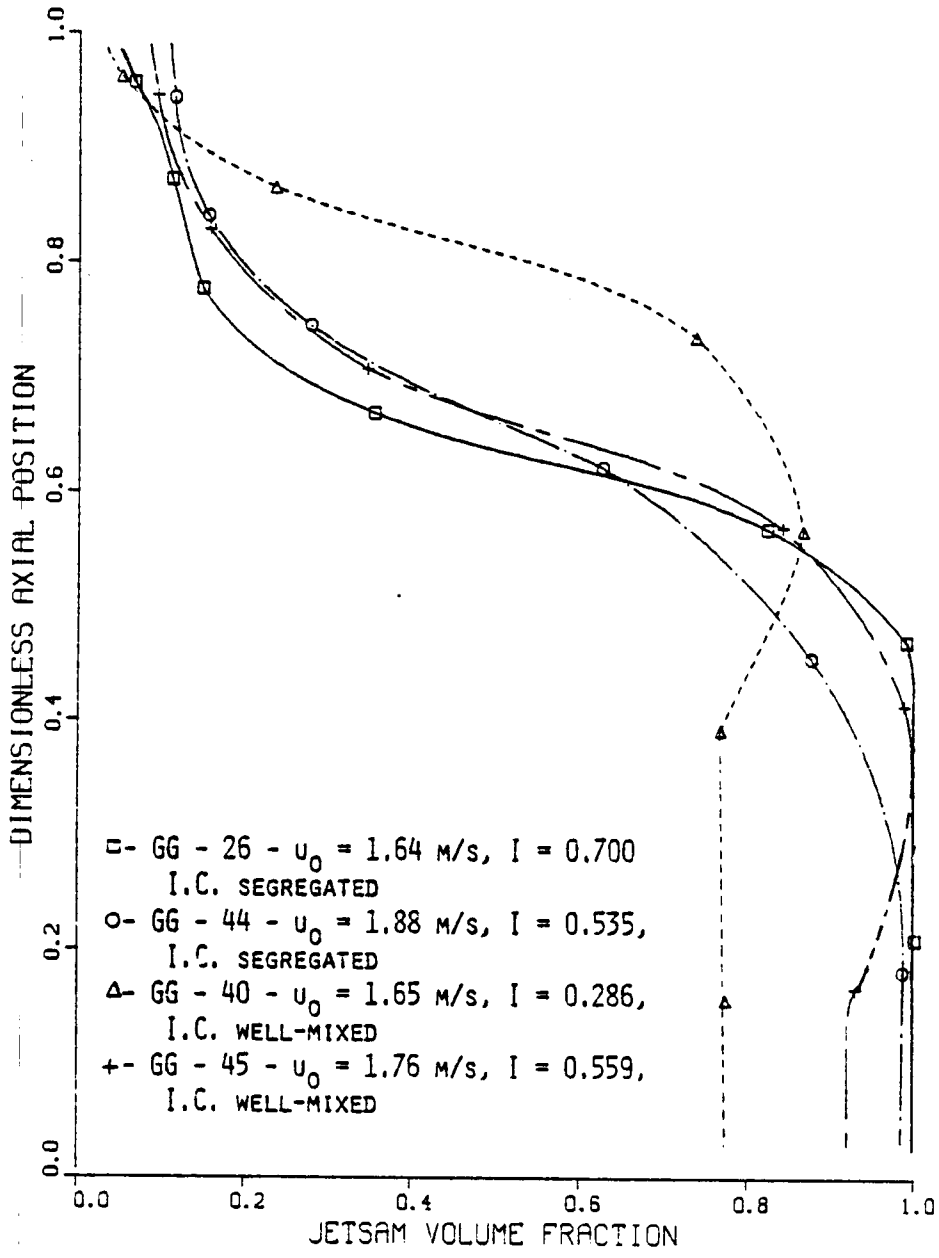

Figure 4.17. Typical Region 1 segregation profiles seen in the glass-glass system.

45 illustrate this type of profile in Figure 4.17. The "hump" appeared to be the remnants of a flotsam-poor zone left by the upward moving "front."

Above 1.79 m/s, both initial conditions yielded a sigmoid-type final profile. The gas velocity was sufficient to prevent entrapment of flotsam in the lower section of the bed, thus allowing a true dynamic equilibrium to be reached. This type of behavior appeared to resolve fairly smoothly into the Region 2 behavior just above u_{mfJ}, although there was apparently a small dip in the mixing index curve at u_{mfJ}. The plot for GG-44 is typical of the profiles in the region above 1.79 m/s and below u_{mfJ}.

Figures 4.18 and 4.19 illustrate the effects of bed internals on glass-glass segregation. At least at the velocity represented here, approximately 2.75 m/s, bed internals appeared to have only a minor effect. The profile for the condition with wire mesh lining the bed walls was virtually identical to the profile for the unlined bed. Installation of horizontal tubes appeared to increase the segregation slightly, the largest effect being in the mean composition of the middle well-mixed zone and in the steepness of the gradient in the bottom zone. Perhaps the largest effect was observed when the tube density was increased. This modification produced a profile essentially composed of two parts: a well-mixed upper zone and a steep gradient near the bottom. The upper gradient which had been present in the other cases was completely eliminated. This absence of an upper gradient corresponded with an observed change in the nature of the bed surface while

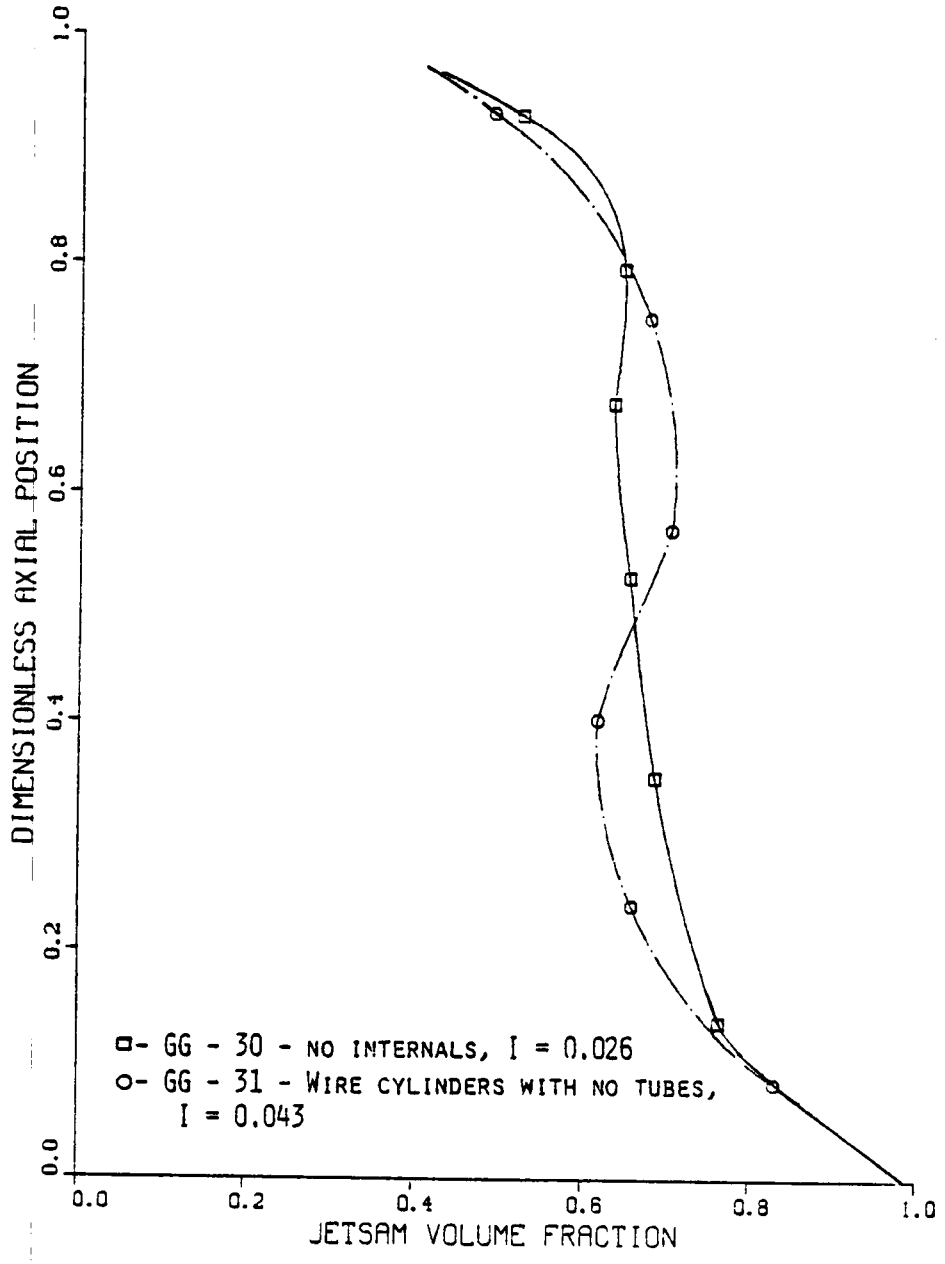

Figure 4.18 Effect of bed internals on the Region 2 glass-glass segregation profile.

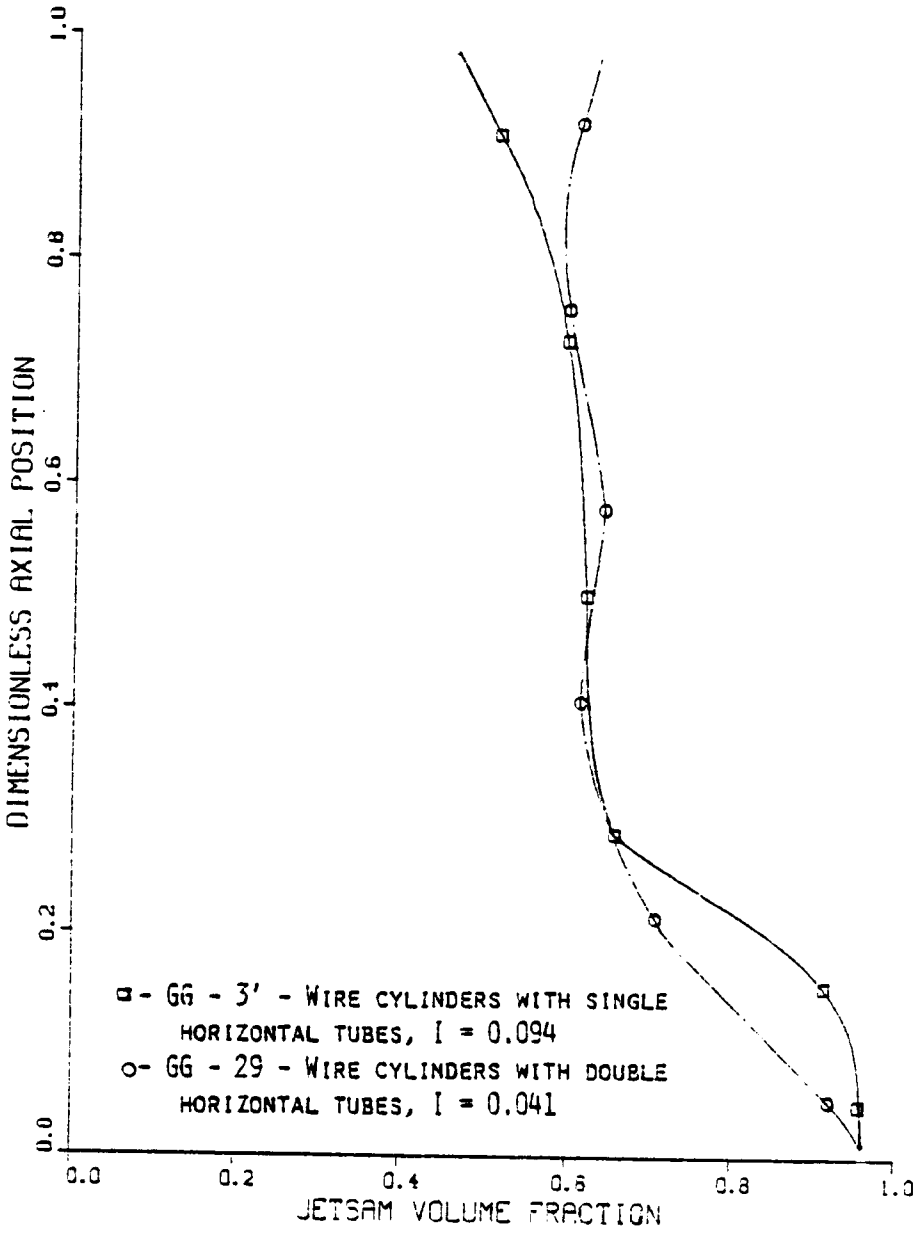

Figure 4.19. Effect of bed internals on the Region 2 glass-glass segregation profile.

it was fluidized; there appeared to be little or no "splash zone" present.

The effects of changes in overall bed composition are shown in Figure 4.20. For these conditions (u_o = 2.7-2.8 m/s and horizontal tube internals) the shapes at jetsam-lean, equal-ratio, and jetsam-rich compositions were markedly different. Low overall jetsam composition produced a profile very much like those seen in the steel-glass system (i.e., an almost uniform composition over the upper and middle portions of the bed with a steep gradient near the bottom), even though one would expect the segregation tendencies of these systems to be drastically different. High overall jetsam composition, on the other hand, produced profiles like those seen in the limestone-coal system (i.e., a gradually decreasing flotsam concentration with depth). The equal-ratio bed showed the three zones which were typical of the other glass-glass runs: an upper steep-gradient zone, a middle well-mixed zone, and a lower steep-gradient zone.

The relationship of bed height to the segregation profile at u_o = 2.7-2.8 m/s with tubes is illustrated in Figure 4.21. Interestingly, the very shallow bed had a very pronounced sigmoid shape. Beds approximately two and three times the depth of the shallow bed had similar profiles which were typical of the three-zone pattern.

4.1.6 The glass-polypropylene system

This system was composed of the #2 glass beads and the polypropylene spheres in Table 3.1. The static bed height ranged from about 7 cm to 29 cm, the overall jetsam volume fraction from approximately 0.50 to 0.95, and the superficial gas velocity from about 1.0 m/s to 5.9 m/s.

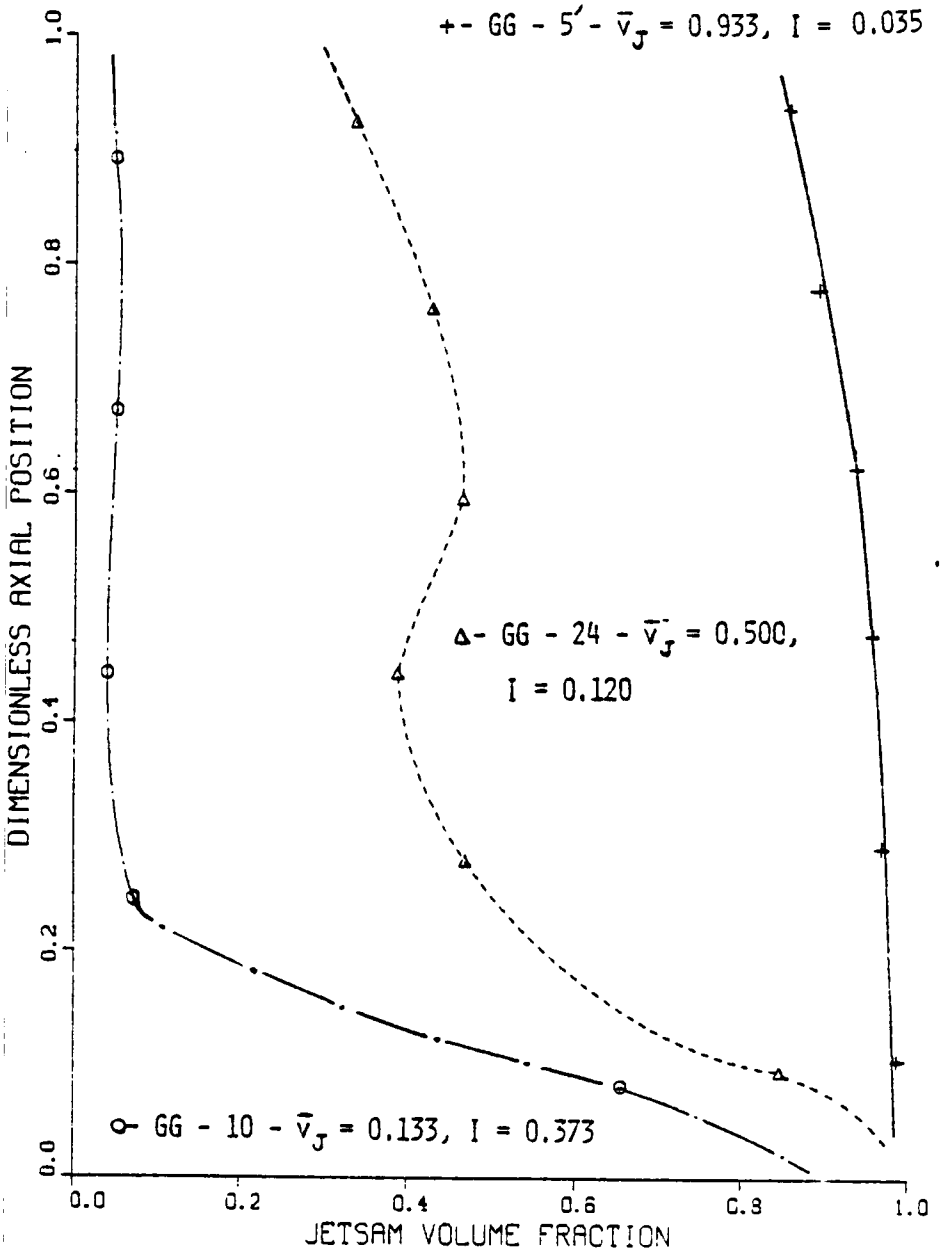

Figure 4.20. Effect of overall bed composition on the Region 2 glass-glass segregation profile.

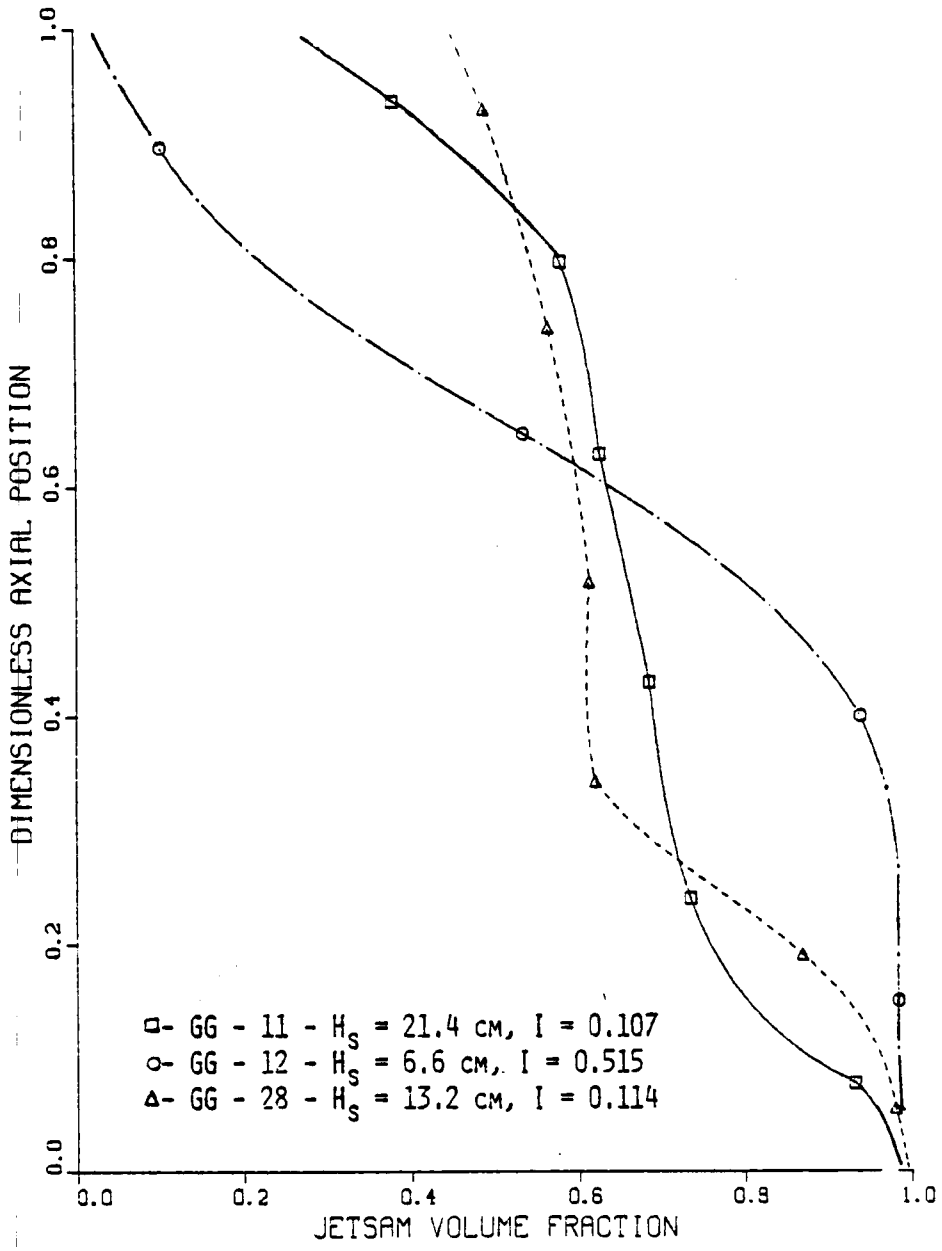

Figure 4.21. Effect of bed height on the Region 2 glass-glass segregation profile.

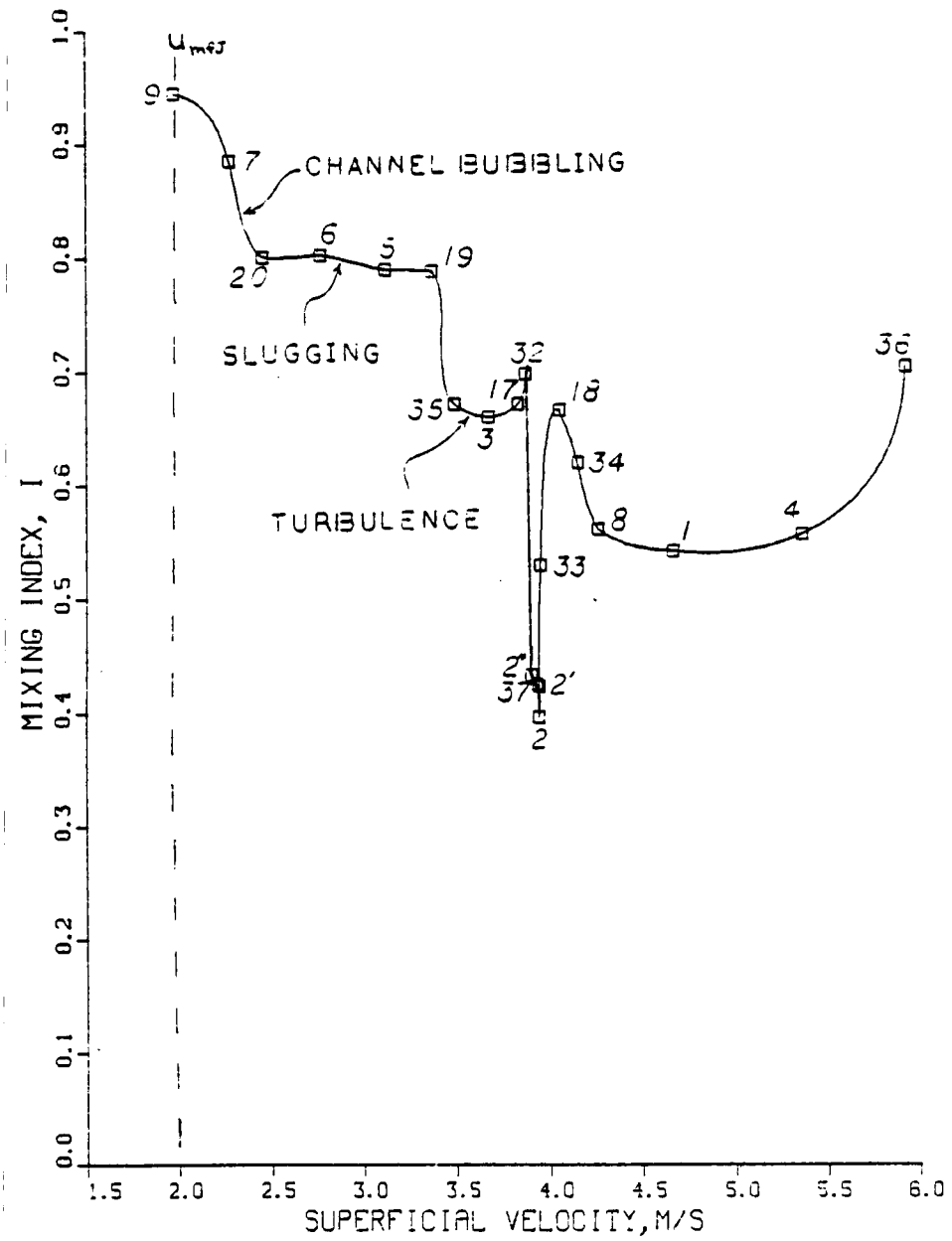

Figure 4.22. Variation of the glass-polypropylene mixing index as a function of the air velocity when horizontal tubes were present, Region 2.

All runs made in Region 2 were made with internals; all runs in Region 1 were made without internals.

Detailed observations of this system's velocity response revealed abrupt transitions in segregation similar to the glass-glass system. In general, the mixing index transitions seemed to correspond with changes in the bubbling mode of the flotsam (Region 1) or jetsam (Region 2). For instance, Figure 4.22 shows a change in the slope of the mixing index curve at 2.4 m/s, which is also the velocity at which slugging began in the jetsam. Another mixing index transition occurred at approximately 3.3 m/s where turbulent fluidization began. There was one transition, however, in Region 2 of the G-P system which did not show in the glass-glass system. This is the very strong "dip" at approximately 3.9 m/s. This transition did not appear to correspond to any clearly identifiable fluidization phenomena of the individual components. Note that the presence of this point was confirmed by four replicate runs.

Typical Region 2 segregation profiles for the G-P system are depicted in Figures 4.23 and 4.24. Run GP-2, which is one of those depicting the anomalous transition at 3.9 m/s, shows an unusually high penetration of flotsam into the lower portion of the bed and a shape unlike the others.

The Region 1 behavior of the G-P system was much less varied than that of the glass-glass system, primarily because of the greater differences between the components. For initially segregated runs, the bed tended to remain completely segregated until the air velocity exceeded about 1.6 m/s. Even then, the degree of segregation was nearly complete. The bed remained completely defluidized for initially well-mixed

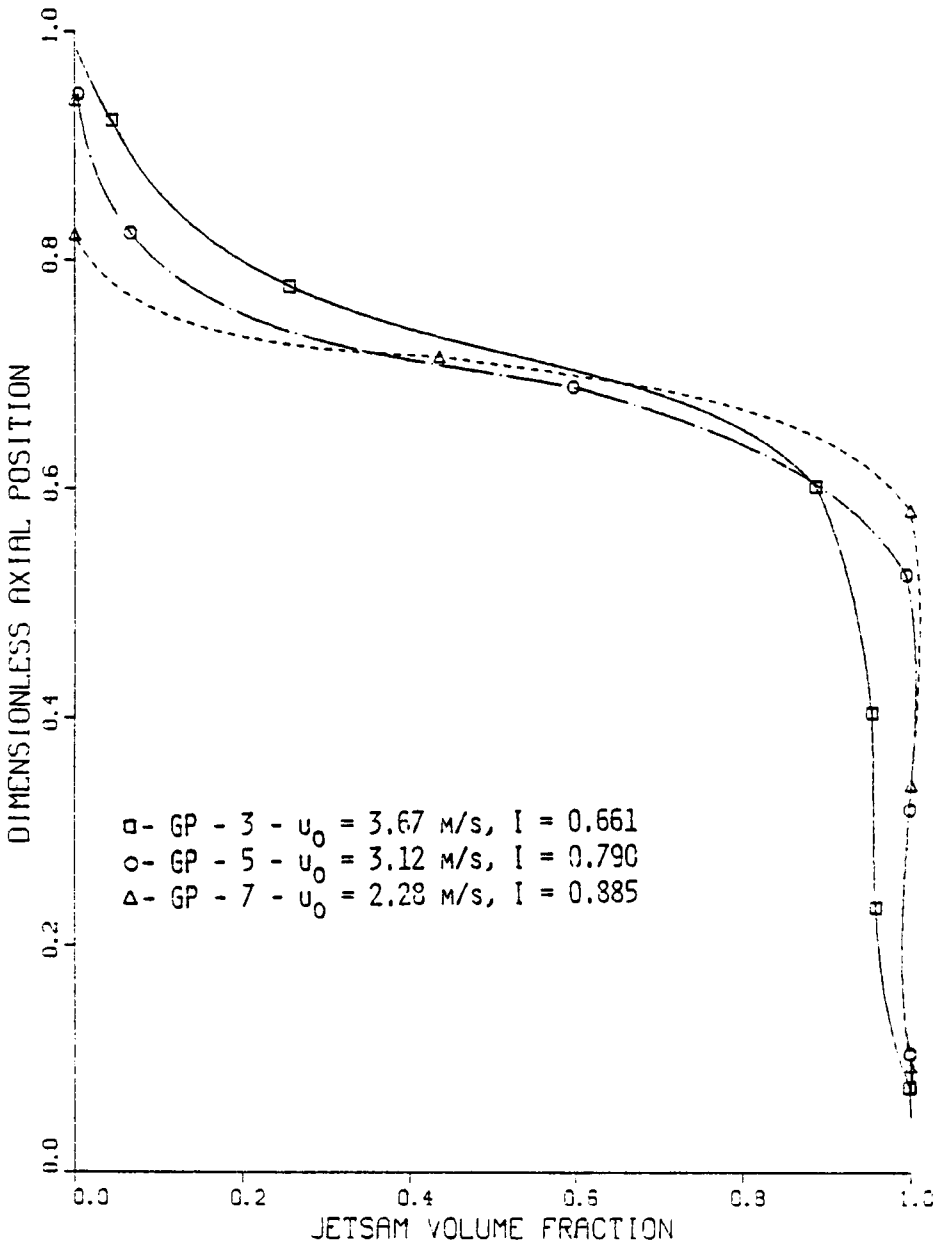

Figure 4.23. Effect of air velocity on the Region 2 glass-polypropylene segregation profile.

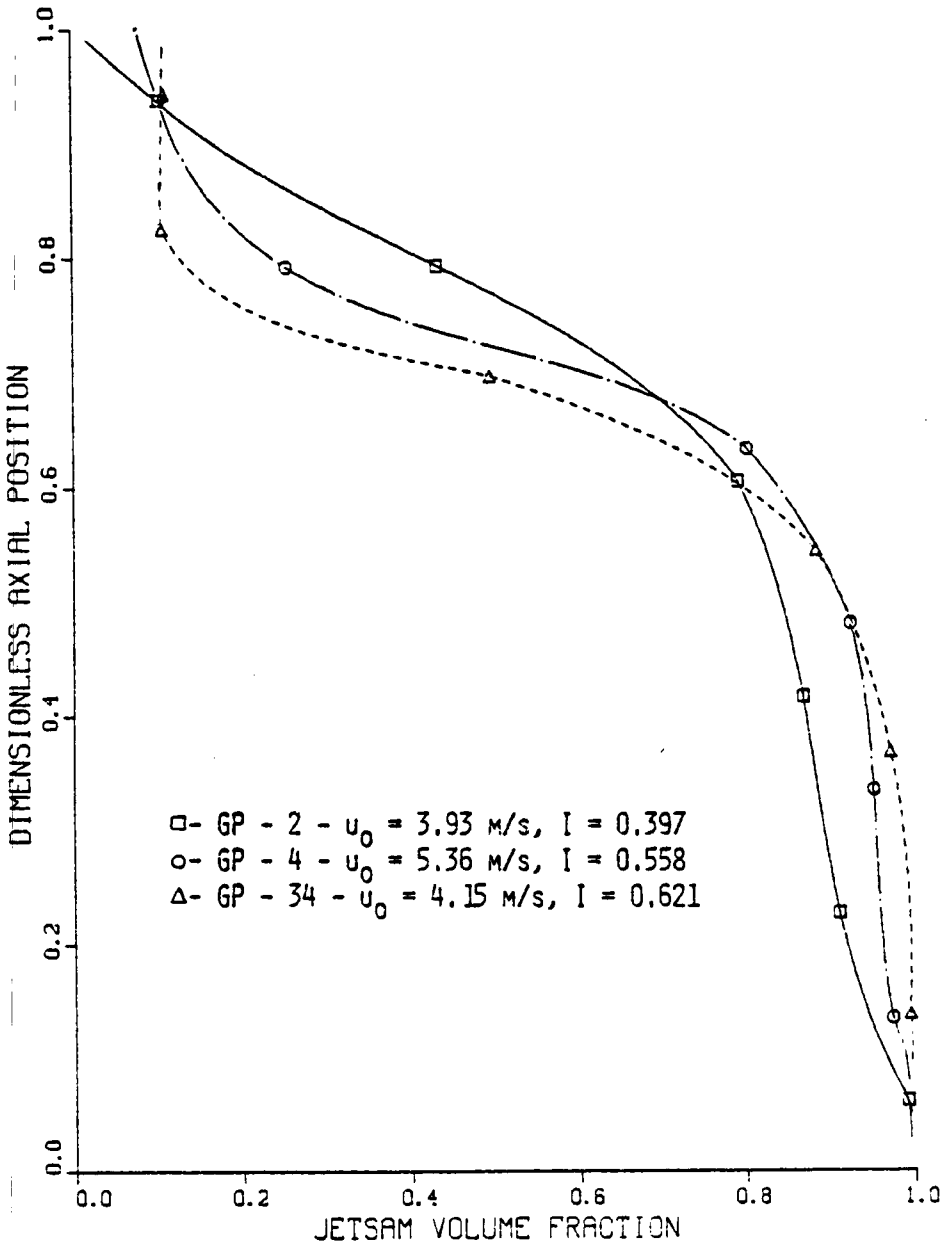

Figure 4.24. Effect of air velocity on the Region 2 glass-polypropylene segregation profile.

conditions until the air velocity exceeded 1.4 m/s. Above that velocity, the strong tendency toward segregation caused a rapid separation of the component. Figure 4.25 depicts these results in terms of the mixing index.

Typical Region 1 segregation profiles are given in Figure 4.26. Note the sigmoid shapes of the initially segregated run and the run at u_{mfJ}. Note also the characteristic "hump" in the profile for the lower velocity run with a well-mixed initial condition. These profiles were similar to the patterns observed for the glass-glass system.

Figures 4.27 and 4.28 illustrate the effects of variations in bed height and overall bed composition on the G-P profiles, respectively. All of these runs were made with $u_o \simeq 2.9$-3.0 m/s. There appears to be little difference in the sigmoid patterns which resulted, although the composition changes caused a shift in the location of the inflection.

4.1.7 The acrylic-polypropylene system

This system was composed of the clear acrylic and polypropylene spheres. The static bed height ranged from approximately 13 cm to 31 cm, the overall jetsam volume fraction from 0.667 to 0.857, and the superficial gas velocity from 1.0 m/s to 4.8 m/s. All runs except for AP-4 and 5 were in Region 2. Most runs were made with bed internals.

The variation of the Region 2 mixing index with velocity is depicted in Figure 4.29. Note that horizontal internal tubes were present in all of these runs. As in the glass-jetsam systems, the abrupt changes in mixing index appeared to correspond with transitions to bubbling, slugging/pseudo-slugging, and turbulence. Near u_{mfJ} the acrylic appeared more mobile than the glass, and channel bubbling was already

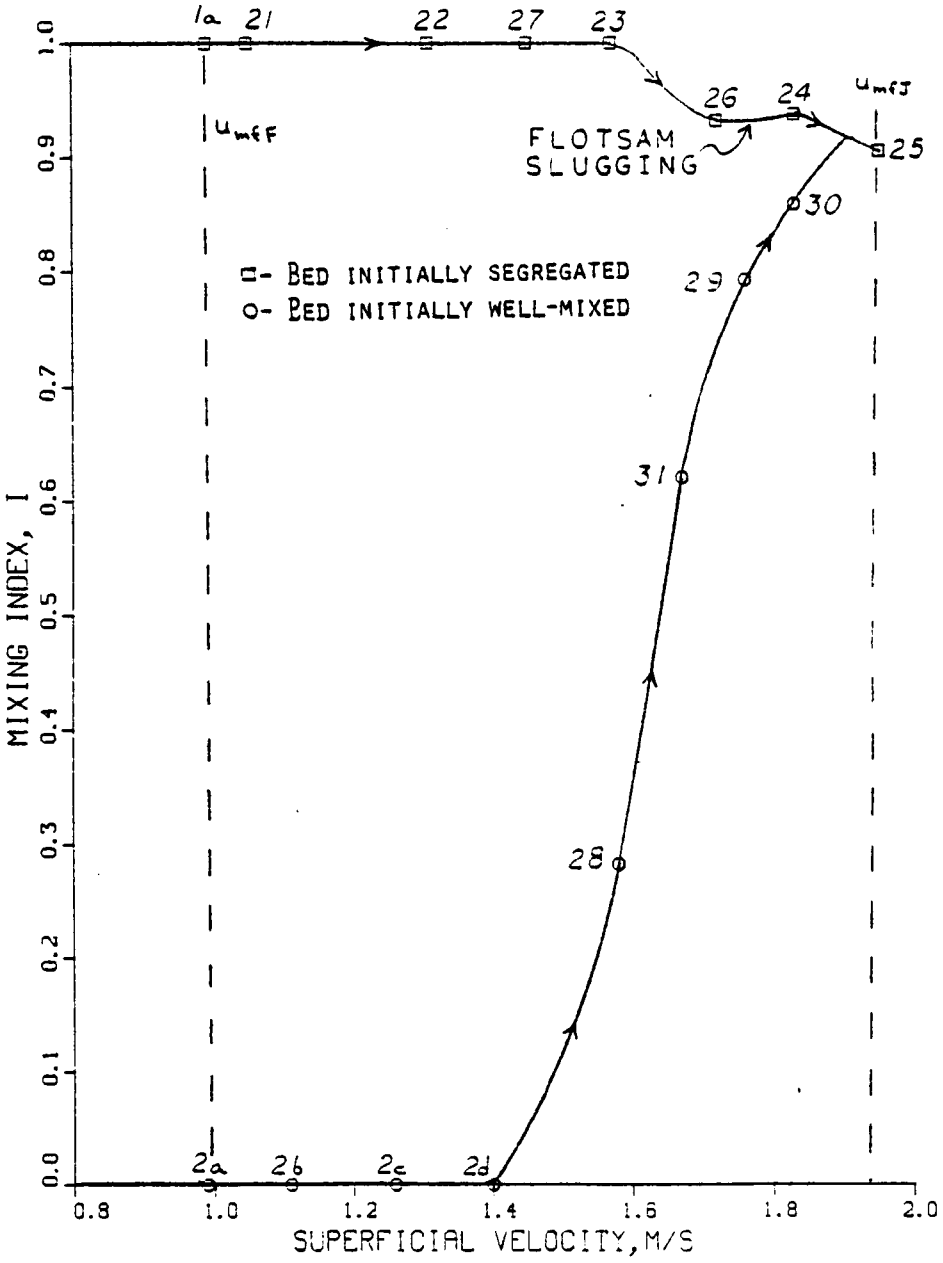

Figure 4.25. Variation of the Region 1 glass-polypropylene mixing index as a function of air velocity and initial condition.

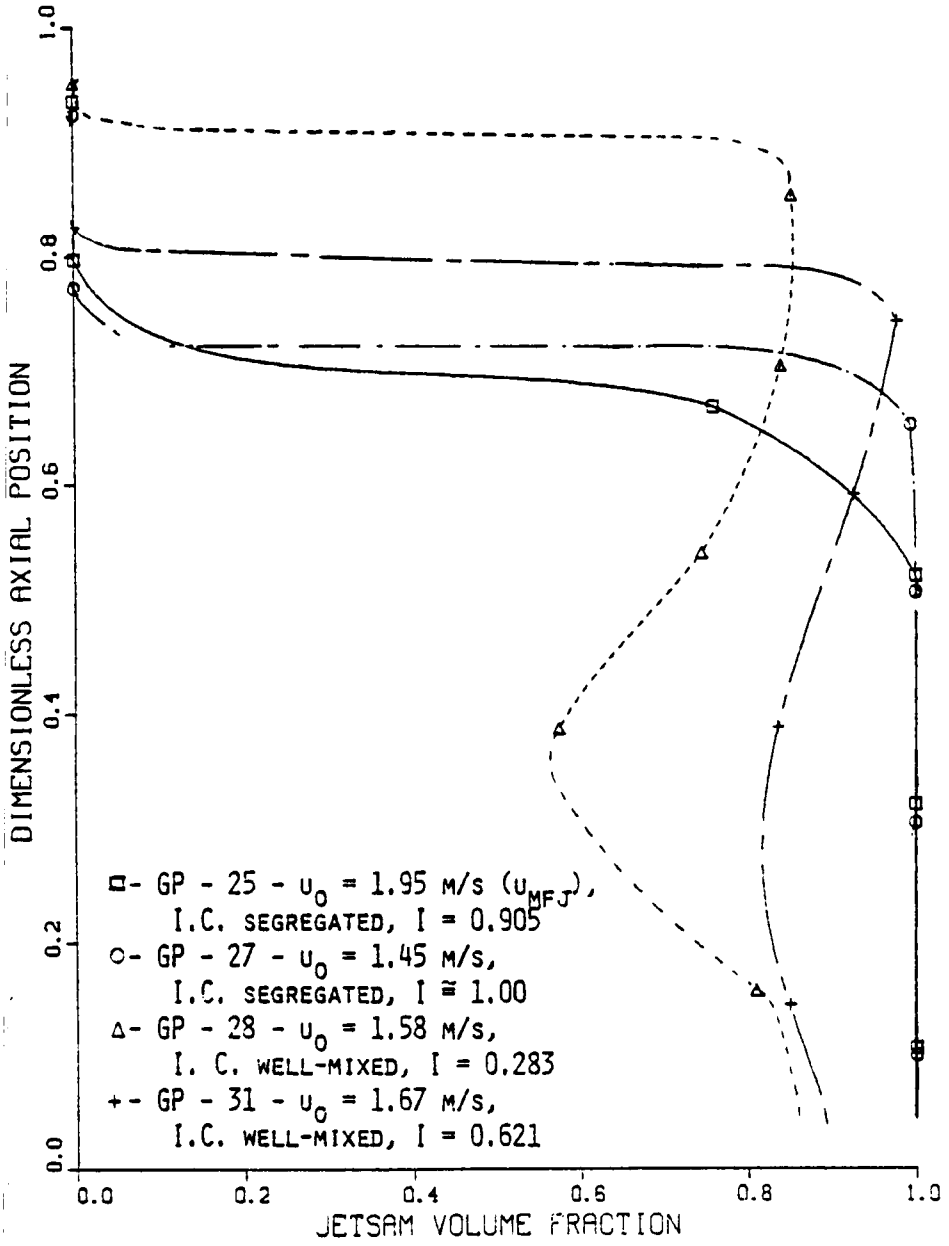

Figure 4.26. Typical Region 1 glass-polypropylene segregation profiles.

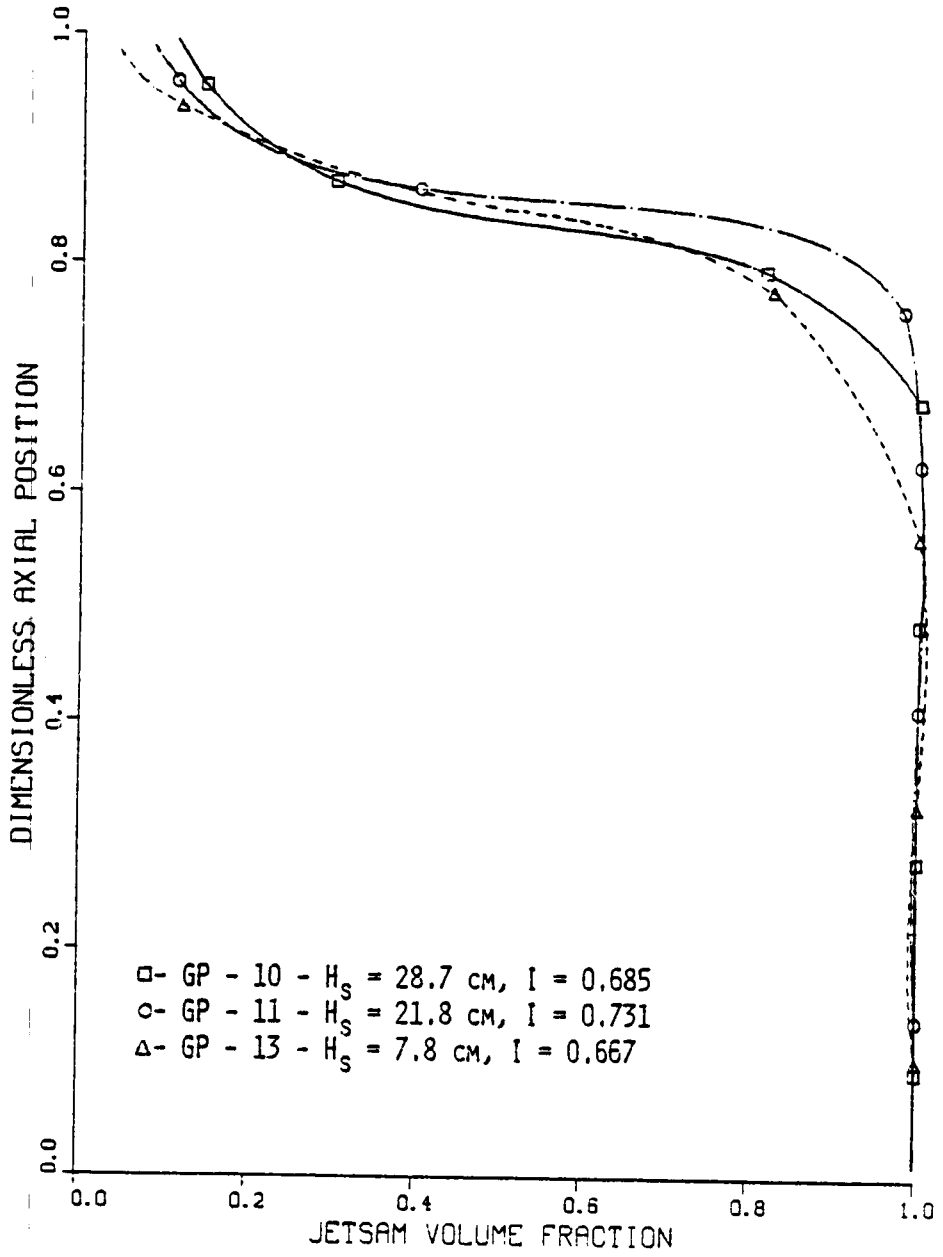

Figure 4.27. Effect of variations in bed height on the Region 2 glass-polypropylene segregation profile.

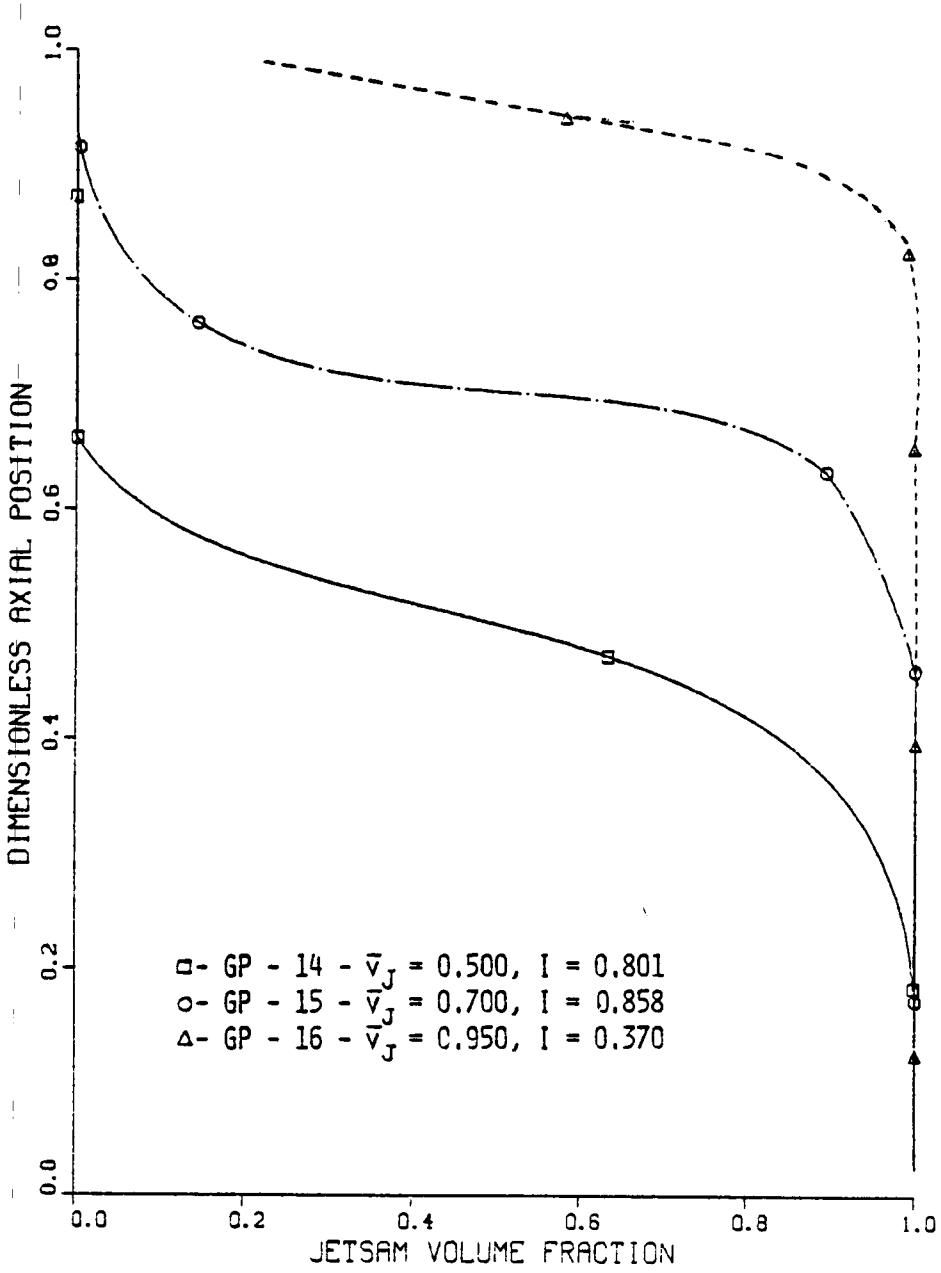

Figure 4.28. Effect of variations in the overall jetsam fraction on the Region 2 glass-polypropylene segregation profile.

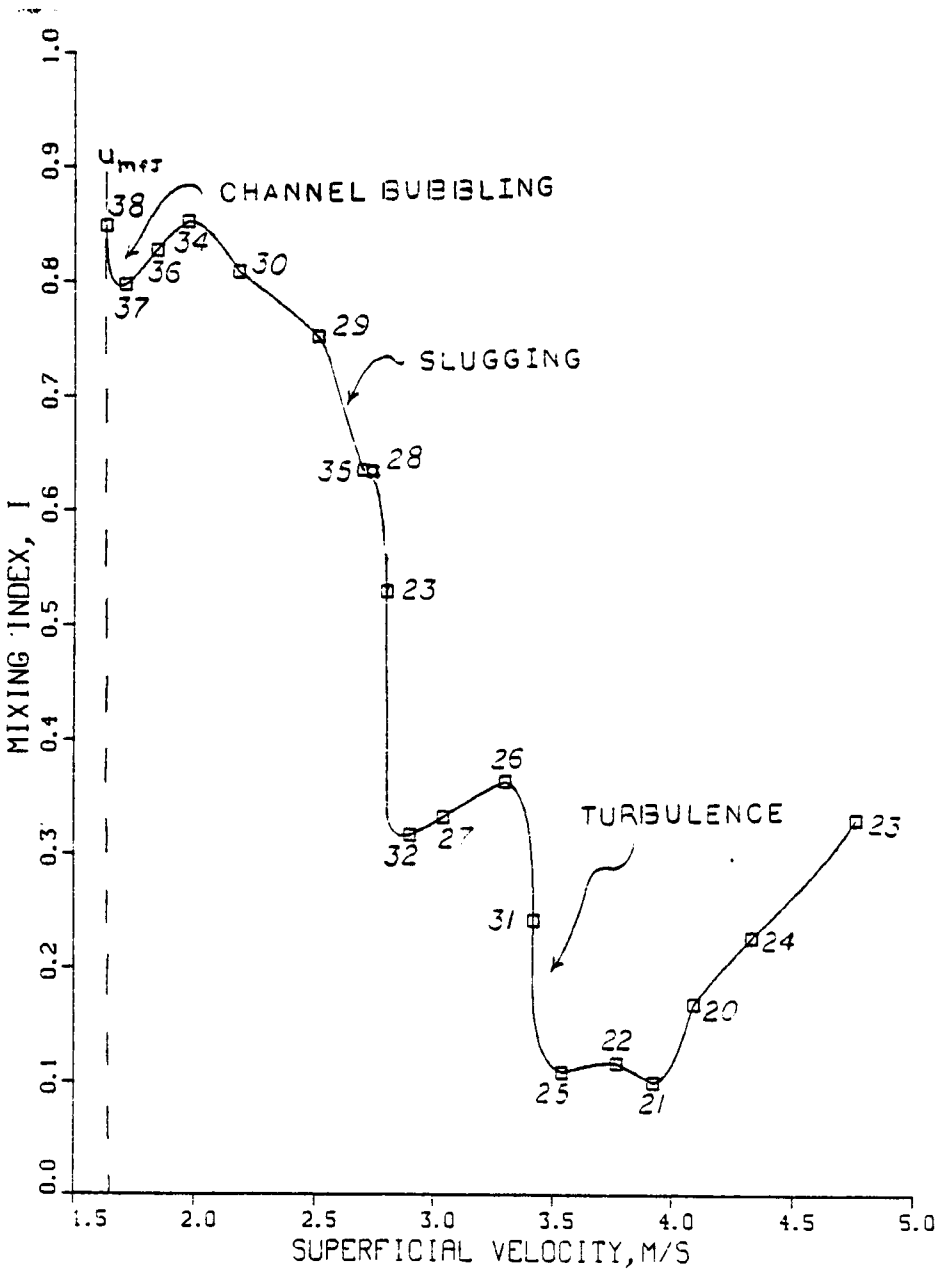

Figure 4.29. Variation of the Region 2 acrylic-polypropylene mixing index with air velocity (horizontal tube internals present).

well developed. The transition from channel bubbling to slugging was well-defined, but the slugging region appeared to encompass a mixture of slugging-bumping-swirling motions which were somewhat indistinct and hard to separate. Maximum mixing occurred in the turbulent regime. Beyond this region, the polypropylene began to appear as a low density "cloud" above the acrylic, and mixing decreased with increasing air velocity.

Figures 4.30 and 4.31 illustrate typical segregation profiles as a function of air velocity. Profiles produced near u_{mfJ} were of the sigmoid type. At higher velocities, the profiles tended to develop two or three distinctive zones. Occasionally, as in AP-23 and 26, the profile appeared to return to a more sigmoid shape.

The effect of bed internals on the segregation profile at $u_o \simeq 3.4$ m/s are shown in Figure 4.32. Very little, if any, change resulted when the PVC tube walls were lined with wire mesh. Addition of horizontal bed tubes increased segregation slightly, producing a three-zone type profile. The bed height effects shown in Figure 4.33 were more pronounced. The profiles shown appear to indicate that the mixing first decreased and then increased as the bed height was increased. Both of the lower bed height profiles were similar, and it is difficult to tell whether the slight change was real or due to experimental uncertainty. The high bed height clearly produced increased separation with a steep gradient between the jetsam-rich and flotsam-rich zones.

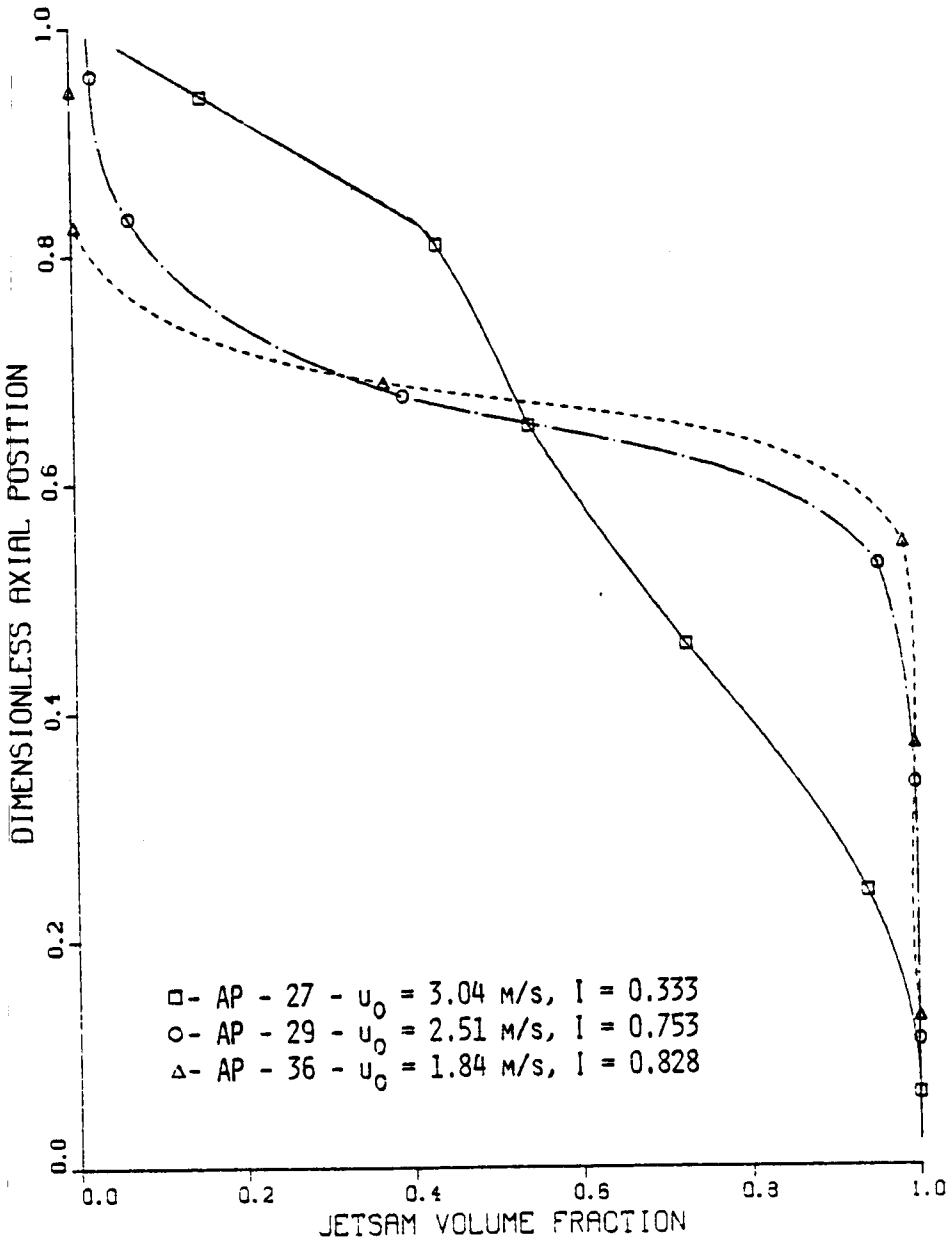

Figure 4.30. Effect of air velocity on the Region 2 acrylic-polypropylene segregation profile.

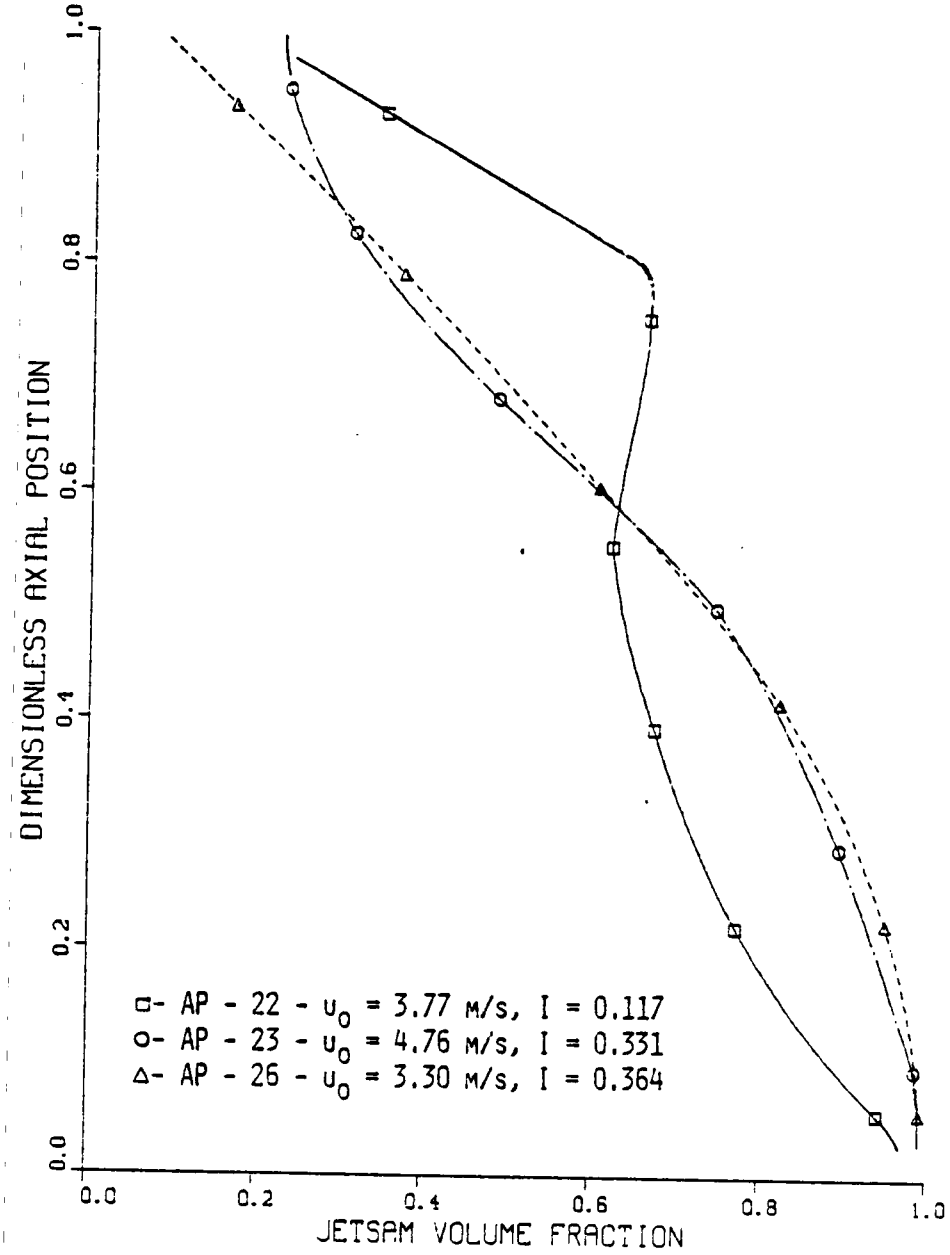

Figure 4.31. Effect of air velocity on the Region 2 acrylic-polypropylene segregation profile.

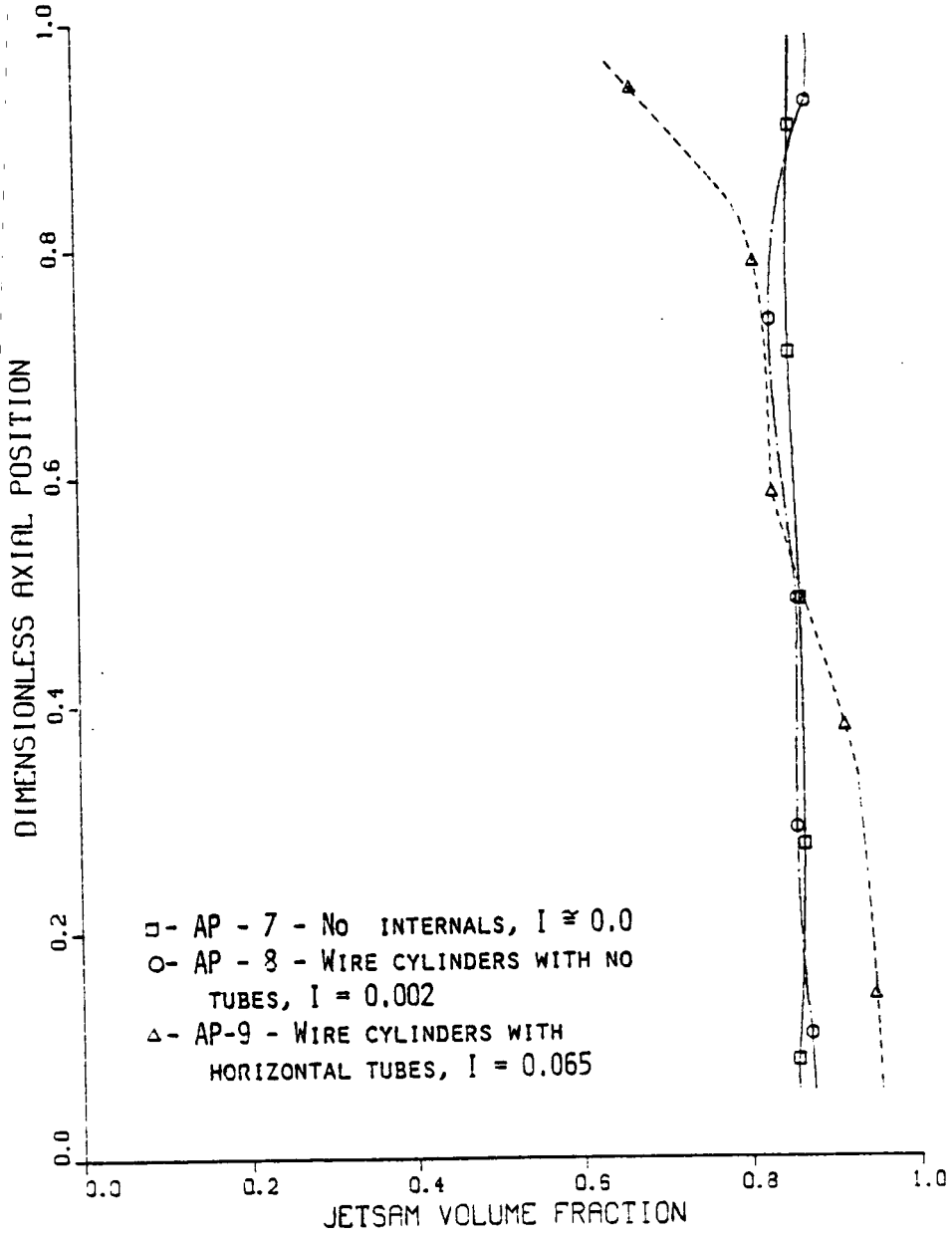

Figure 4.32. Effect of bed internals on the Region 2 acrylic-polypropylene segregation profile.

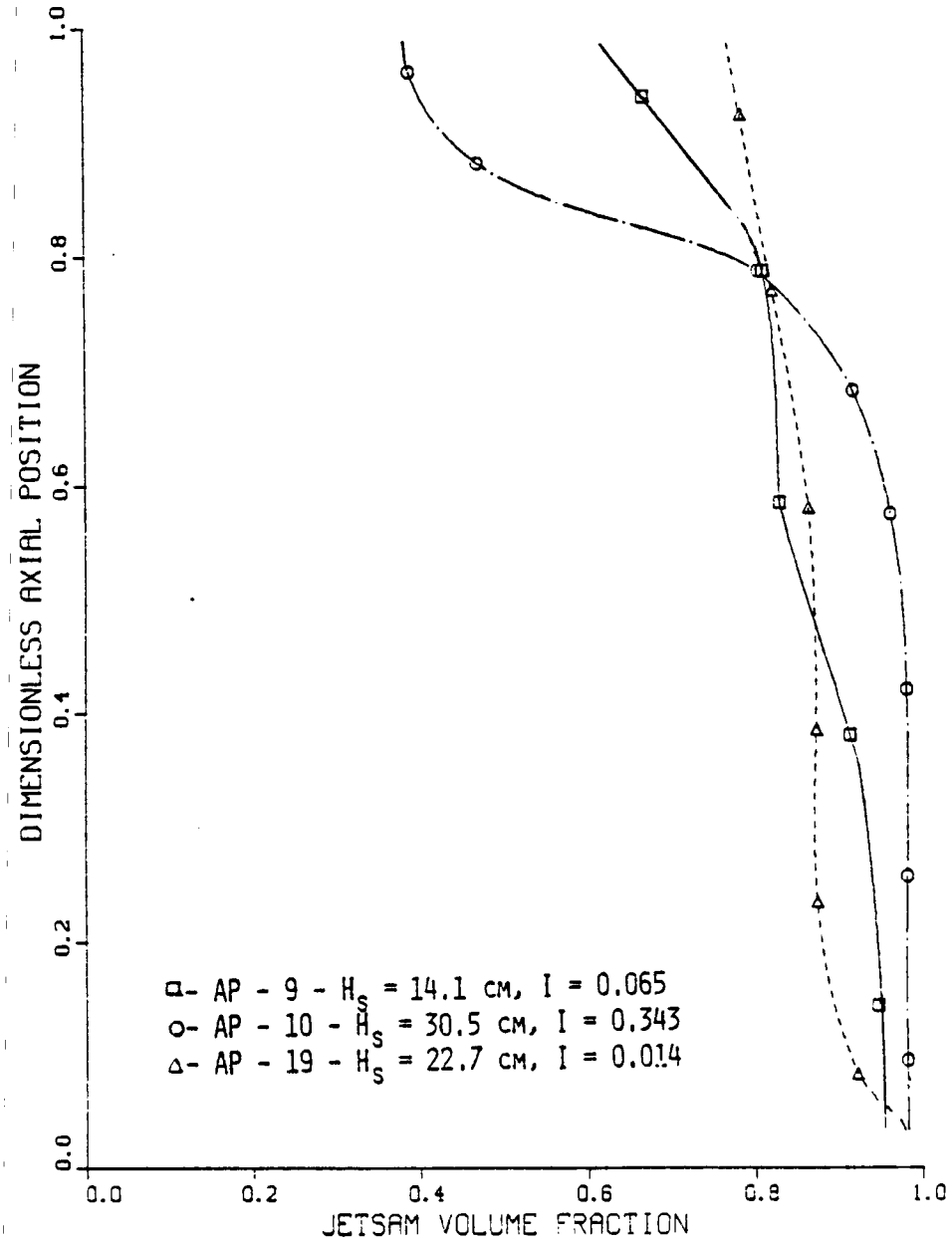

Figure 4.33. Effect of bed height on the Region 2 acrylic-polypropylene segregation profile.

4.1.8 Comparisons of different solid systems

One way to evaluate the effects of differences in the size and density of the components is to compare the segregation profiles for different systems at common conditions; i.e., at essentially the same air velocity, bed height, jetsam volume fraction, and type of internals. Figure 4.34 illustrates such a comparison for the clear acrylic-glass, clear acrylic-polypropylene, #2 glass-polypropylene, and #1 glass-#2 glass systems at $u_o \approx 2.8$ m/s. Note that the glass-polypropylene and acrylic-polypropylene systems exhibited sigmoid-type profiles while the acrylic-glass and glass-glass systems exhibited the typical steep-gradient upper and lower zones with the well-mixed middle zone.

Because of the variation in fluidization/bubbling modes among the various systems, it is probably more correct to compare them at the same "reduced" velocity; i.e., at the same velocity relative to u_{mfJ}. Figures 4.35 and 4.36 illustrate such a comparison at $u_o/u_{mfJ} = 1.0$ and 1.7, respectively. Note that at $u_o = u_{mfJ}$ differences between the systems became much less clear-cut than at the higher ratio. The profiles at u_o/u_{mfJ} appeared very similar to those produced at $u_o = 2.8$ m/s.

Although there were insufficient data produced in these experiments to develop correlations for the effects of particle properties on mixing, an interesting trend was found. Table 4.1 illustrates the trend for the conditions depicted in Figures 4.34, 4.35, and 4.36. Note that the mixing index correlates best with the product of the density ratio and the size ratio. It appears that general correlations should probably include both of these parameters with unequal weighting. The need for unequal weighting is most clearly indicated by the observation that

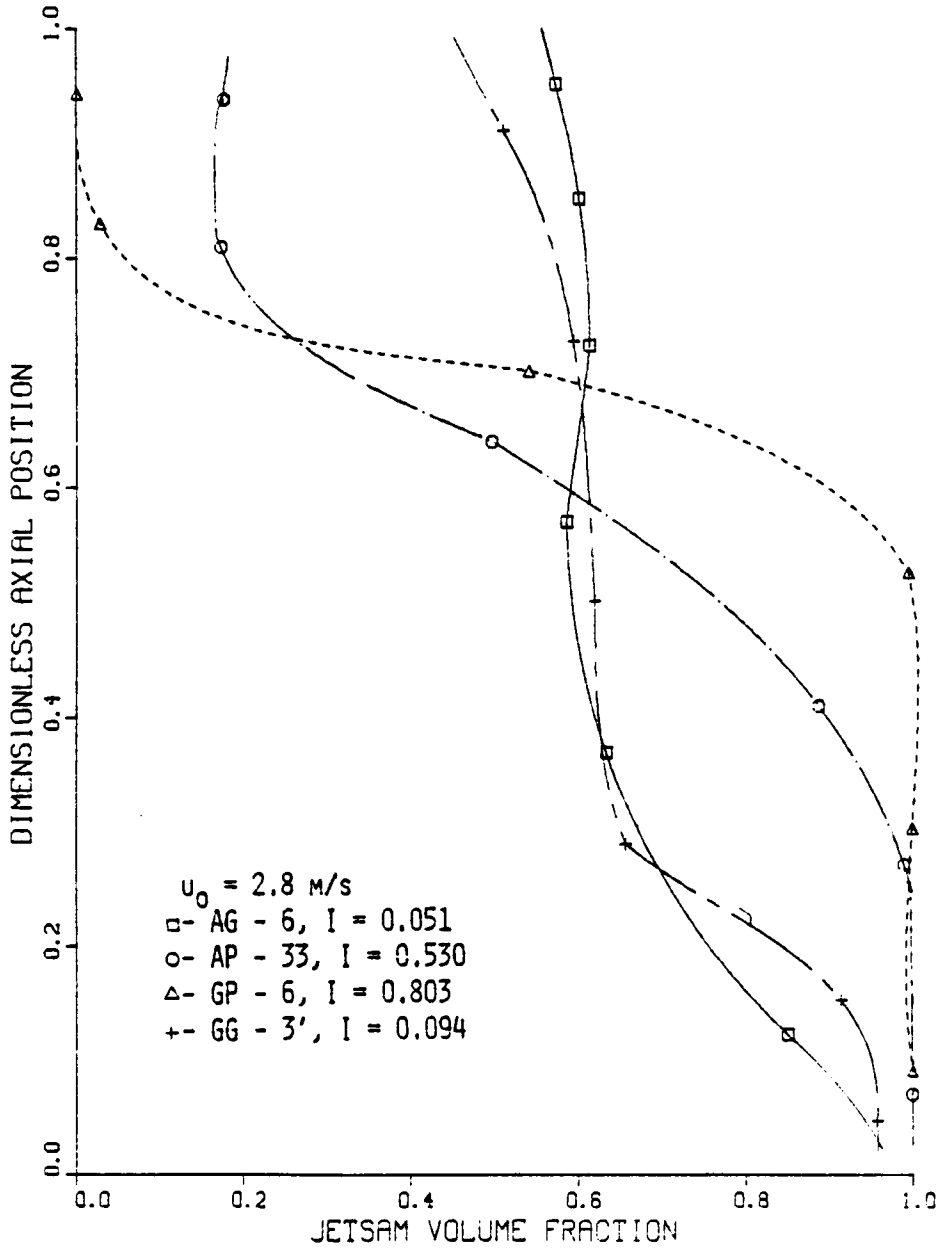

Figure 4.34. Comparison of the segregation profiles for the acrylic-glass, acrylic-polypropylene, glass-polypropylene, and glass-glass systems at a superficial air velocity of 2.8 m/s.

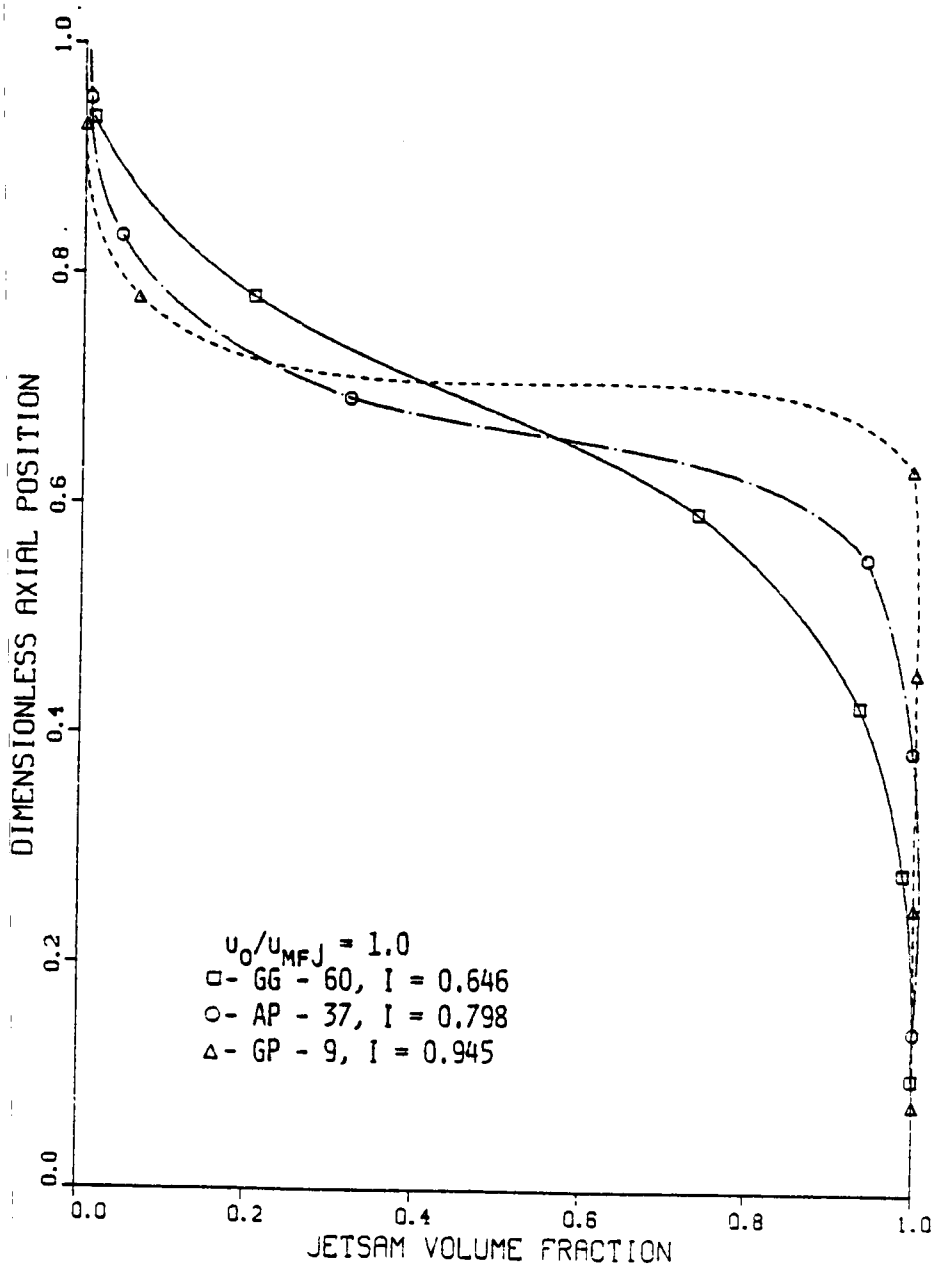

Figure 4.35. Comparison of the segregation profiles for the glass-glass, acrylic-polypropylene, and glass-polypropylene systems at a reduced air velocity of 1.0.

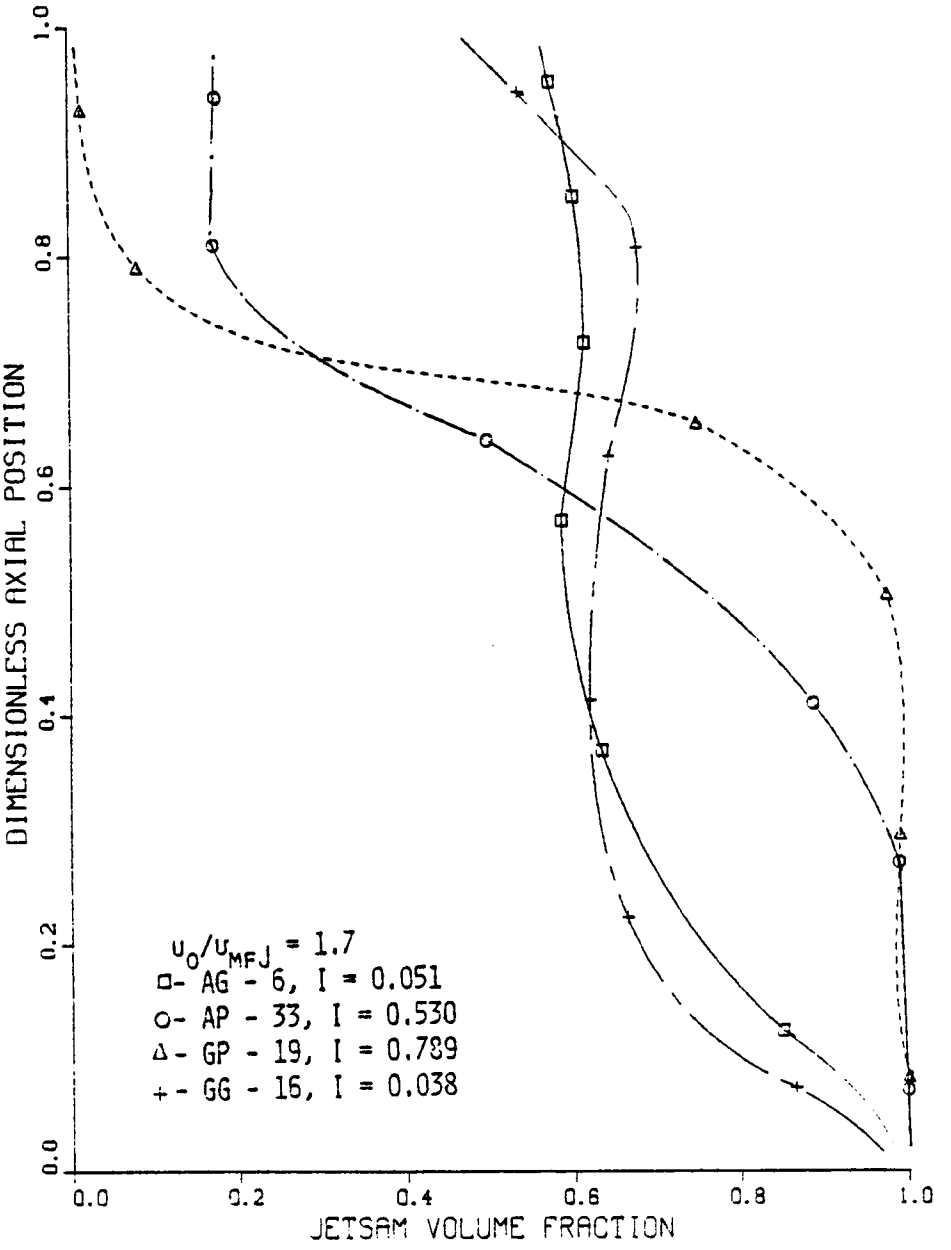

Figure 4.36. Comparison of the segregation profiles for the acrylic-glass, glass-glass, acrylic-polypropylene, and glass-polypropylene systems at a reduced air velocity of 1.7.

Table 4.1. Correlation between particle properties and segregation*

Velocity condition	Run no.	I	$\bar{d}_J/\bar{d}_F$	ρ_J/ρ_F	u_{mfJ}/u_{mfF}	$\left(\frac{\rho_J}{\rho_F}\right)\left(\frac{\bar{d}_J}{\bar{d}_F}\right)$
u_o = 2.8 m/s	AG-6	0.051	0.50	1.91	0.91	0.96
	GG-3'	0.094	1.50	1.00	1.27	1.50
	AP-3	0.530	1.92	1.30	1.71	2.50
	GP-6	0.803	1.43	2.49	1.55	3.56
u_o/u_{mfJ} = 1.0	GG-60	0.646	1.50	1.00	1.27	1.50
	AP-37	0.798	1.92	1.30	1.71	2.50
	GP-9	0.945	1.43	2.49	1.55	3.56
u_o/u_{mfJ} = 1.7	GG-16	0.038	1.50	1.00	1.27	1.50
	AG-6	0.051	0.50	1.91	0.91	0.96
	AP-33	0.530	1.92	1.30	1.71	2.50
	GP-19	0.789	1.73	2.49	1.55	3.56

*Unlisted common bed conditions were: $\bar{v}_J$ = 0.7, horizontal tube internals, H_s = 14 cm.

the product of the ratios for the acrylic-#1 glass system is less than 1, and yet the glass still tended to act as jetsam. Thus, the density ratio appears to override the effects of the size ratio.

4.1.9 Summary of the steady-state results

In general, it appeared that all of the segregation profiles produced in these experiments fell within the basic patterns reported by earlier investigators. The consistency between these results and those of Rowe et al. (1972 b, 1978 a and b) for small particles and Fan and Chang (1979) for large particles is especially evident.

In most cases, the composition profile could be roughly depicted as consisting of combinations of up to three zones: (1) a lower, high-jetsam zone, (2) a well-mixed region, and (3) an upper, high-flotsam zone. One or two of the zones could be absent in any particular experiment. The two extreme limits of this pattern occurred when the bed was completely segregated and when the bed was completely mixed. Beds near the former limit typically exhibited sigmoid-type profiles. Beds near the latter limit typically exhibited enlarged mid-zones with steep gradients in one or both of the other zones. The upper zone appeared to be composed of the splash or bubble ejected solids which were suspended above the bulk of the bed during fluidization.

Air velocity was the most important variable affecting the mixing of a given particle system. It was convenient to separate segregation into two principle categories based on velocity; Region 1 segregation where $u_{mfF} < u_o < u_{mfJ}$ and Region 2 segregation where $u_{mfJ} < u_o < u_{tF}$. Region 1 segregation exhibited hysteresis in the lower, unfluidized zone, where flotsam could be trapped by jetsam. Some initial conditions

produced inverted profiles or "humps" in the unfluidized zone. The upper, fluidized zone appeared to exhibit behavior similar to the entire bed when it operated in Region 2. Above some critical velocity less than u_{mfJ}, hysteresis vanished. Segregation above this velocity always produced the same final composition profile, regardless of the initial conditions. The approach to the steady-state condition was much faster in Region 2 than in Region 1.

Increasing air velocity in Region 1 tended to reduce the size of the unfluidized zone and increase mixing. Near u_{mfJ}, increasing air velocity in Region 2 also tended to enhance mixing, but above a certain velocity the trend reversed. Both regions exhibited localized maxima and minima in the mixing index which appeared to be associated with changes in the fluidization or bubbling mode. In most cases, mixing seemed to improve abruptly near the boundary of a change in the hydrodynamic mode. The hydrodynamic modes observed were: (1) expanded bed with no bubbling, (2) channel bubbling, (3) slugging/pseudo-slugging, and (4) turbulence.

Bed internals tended to enhance segregation, with horizontal tubes producing the largest effect. In hydrodynamic terms, internals inhibited large-scale particle motion and reduced the tendency to slug. Transitions in the fluidization/bubbling mode were made less distinct. As might be expected, this also appeared to influence the size of the localized maxima and minima in the mixing index.

The overall bed composition strongly affected the shape of the steady-state segregation profiles. In jetsam-lean beds, the upper zone

tended to be much less distinct, and the lower and middle zones predominated. In beds of roughly equal jetsam and flotsam proportions, all three zones tended to be visible. Jetsam-rich beds exhibited a predominant upper zone with a gradually decreasing flotsam concentration with depth.

Bed height definitely affected segregation, but there were variations in the trends between solid systems. It appeared that at least a portion of the bed height's influence was brought about by its impact on the associated large-scale solids motion. Shallow beds tended to be more particulate in behavior and more readily exhibited channel bubbling. The non-ideality associated with treating the jetsam and flotsam as continuous phases was also more pronounced in shallow beds. Even when a shallow bed was completely segregated, the interface became less distinct because of the "bumpy" character of the solids.

4.2 Transient Results

Transient segregation experiments were carried out on only three solids systems, clear acrylic — black acrylic, clear acrylic polypropylene, and #1 glass-#2 glass. Details are given in Table A-3 in the Appendix. Two types of initial conditions were studied, segregated and inverted. In the segregated condition, the jetsam was placed in the bed first and then flotsam was carefully poured on top. In runs AA-6T and GG-36T, the air flow was started after the flotsam addition. The air flow was started before the flotsam addition in the other segregated runs. The inverted condition represents the inverse of the segregated condition; i.e., the flotsam was on bottom and the jetsam on top. In

this case, the air flow was always started after both components were added.

For the acrylic-acrylic system, the static bed height ranged from approximately 25 to 28 cm, runs were made with and without internals, the superficial air velocity was held at 2.02 m/s (Region 2), and the overall jetsam volume fraction was fixed at 0.024. A single acrylic-polypropylene transient run was made at a static bed height of approximately 31 cm, a superficial air velocity of approximately 3.4 m/s (Region 2), an overall jetsam volume fraction of 0.856, and with horizontal tube internals. Glass-glass transient runs were made with 13.7 cm static bed height, a superficial air velocity from approximately 1.8 to 2.1 m/s (Regions 1 and 2), an overall jetsam volume fraction of 0.667, and no bed internals.

Figure 4.37 depicts the segregation profiles for three of the transient acrylic-acrylic runs and the corresponding steady-state run, AA-1. The transient runs were initiated with the inverted segregation condition. Note that the jetsam appeared to move down through the bed as a "pulse" until it reached the steady-state condition. The mixing index decreased rapidly from 1, approached 0, and then increased and stabilized at the final steady-state value of approximately 0.05.

Figures 4.38 and 4.39 depict the behavior of the glass-glass system in Regions 1 and 2, respectively, starting from the segregated condition. Note that in the Region 2 case, the transient condition is less well-mixed than the steady-state condition. This would be expected as the system "relaxes" from the segregated condition. The Region 1 transient, however, is better mixed than the steady-state condition. This

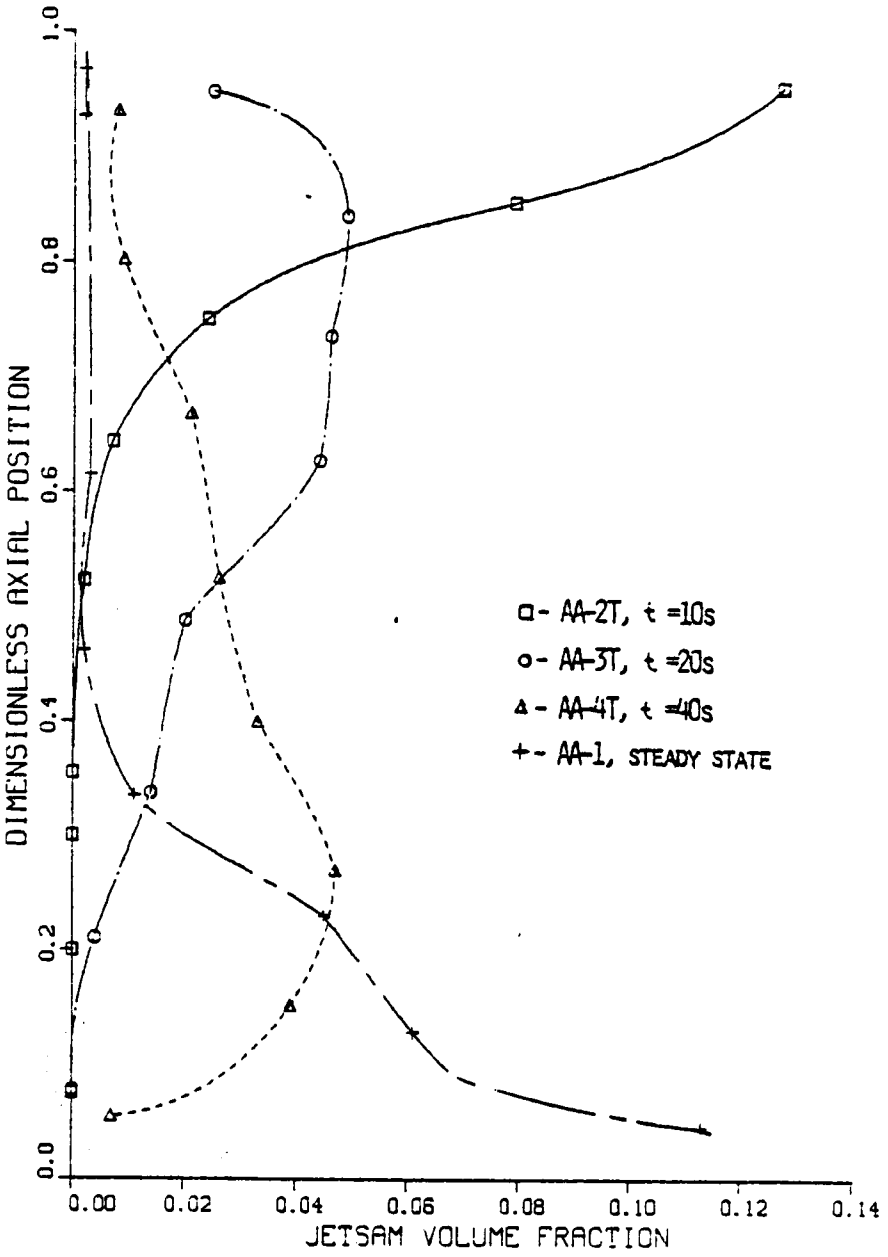

Figure 4.37. Transient segregation profiles for the acrylic-acrylic system starting with the inverted initial condition at a superficial air velocity of 2.02 m/s (no internals).

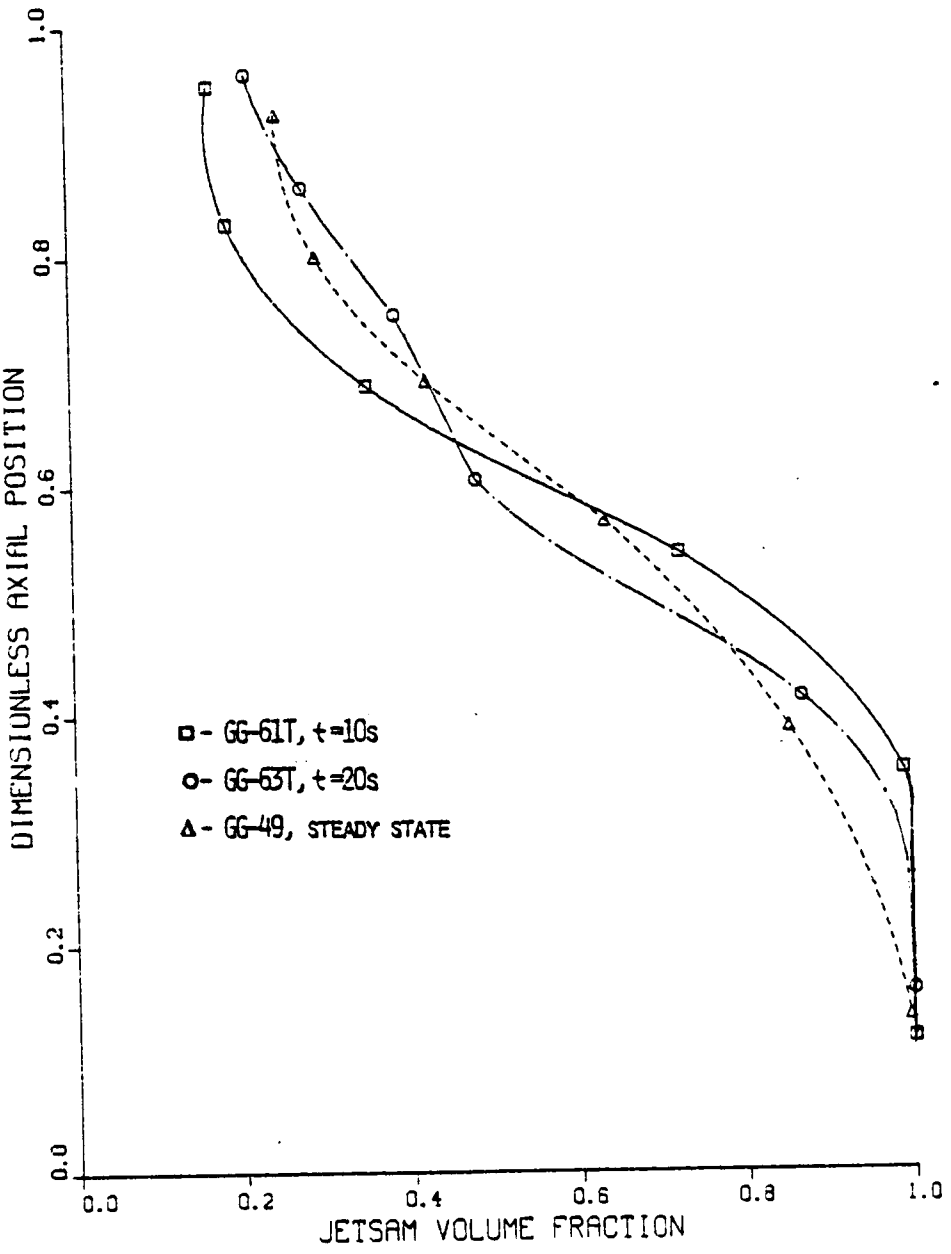

Figure 4.38. Transient segregation profiles for the initially segregated glass-glass system, Region 2, at a superficial air velocity of 2.08 m/s.

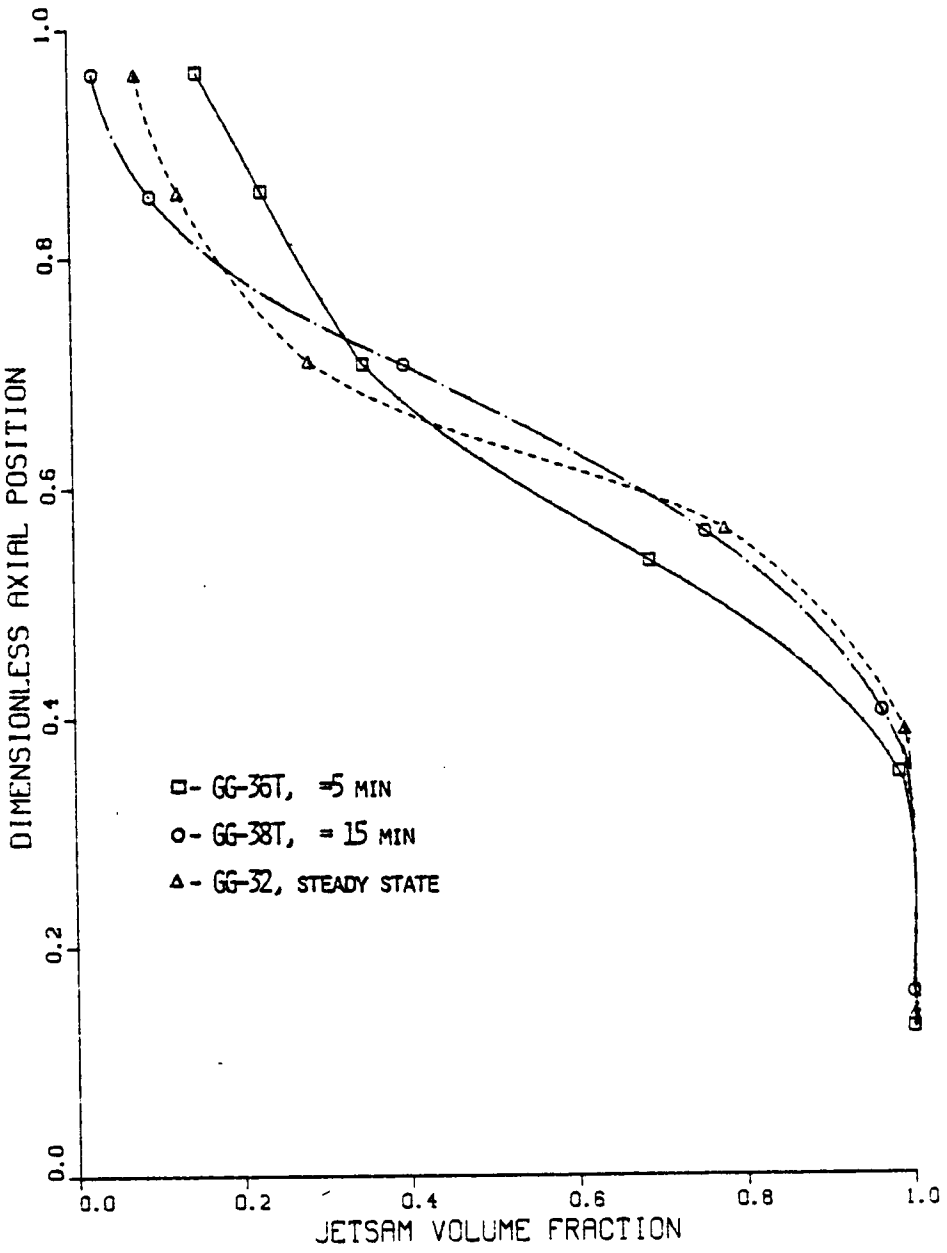

Figure 4.39. Transient segregation profiles for the initially segregated glass-glass system, Region 1, at a superficial air velocity of 1.83 m/s.

appeared to occur because of a reduction in the degree of solids circulation as the system approached steady-state. Such a reduction appeared to be associated with channel-bubbling and with development of the fluidized/unfluidized interface.

The general patterns observed for Region 2 conditions appeared to be consistent with the transient results of Burgess et al (1977) and Fan and Chang (1979). The Region 1 results appeared to indicate a different pattern than those reported by Yoshida et al (1980).

4.3 Measurements of Bed Pressure Profiles

Bed pressure profiles were measured as described in Section 3.6. Detailed results are given in Table A-4 in the Appendix. The experiments were done with three systems of particles: clear acrylic, #2 coal-#3 limestone, and clear acrylic-polypropylene. For the clear acrylic runs, the superficial air velocity varied from approximately 1.7 to 3.4 m/s, and the static bed height ranged from approximately 12.7 to 27.7 cm. Runs were made with and without bed internals. The ranges for the limestone-coal conditions were: superficial air velocity, approximately 0.7 to 2.5 m/s; static bed height, constant at approximately 27 cm; and overall bed composition constant with a jetsam volume fraction of approximately 0.68. No bed internals were used. The acrylic-polypropylene ranges were: superficial air velocity, approximately 1.5 to 3.4 m/s; static bed height, approximately 14 to 30 cm; and overall bed composition constant with a jetsam volume fraction of approximately 0.86. Runs were made with and without bed internals.

Typical pressure profiles for all of these solid systems are illustrated in Figures 4.40 through 4.44. The horizontal axis represents $z = y/H_{mf}$, and the vertical axis is the gauge pressure at z divided by the overall bed pressure drop.* All of the measured profiles had the same basic pattern; i.e., a steep, constant slope near the bottom of the bed which gradually merged into a shallow-slope "tail." The relative size of the tail increased with increasing gas velocity and was particularly pronounced when there was slugging. The tail also increased when internals were removed and when the bed height was increased. Physically, the tail appeared to represent the splash zone of particles which are thrown up by the eruption of bubbles.

Assuming that the two-phase theory holds, the pressure drop over a section of expanded bed should be approximately proportional to the weight of solids in that section. This assumption makes it possible to transform the pressure profiles into voidage profiles as illustrated in Figure 4.45. The "wiggles" in the curves of Figure 4.45 may be due to experimental uncertainty, rather than actual fluctuations in the profile slope. The transformation is fairly simple to do for single component systems, since the slope of the pressure profile is directly proportional to the solids void fraction, $1-\varepsilon$. For binary or multicomponent systems, segregation data are needed to correct for changes in the average solids density with height.

*In binary beds, H_{mf} refers here to the bed height at the minimum fluidizing velocity of the lightest component.

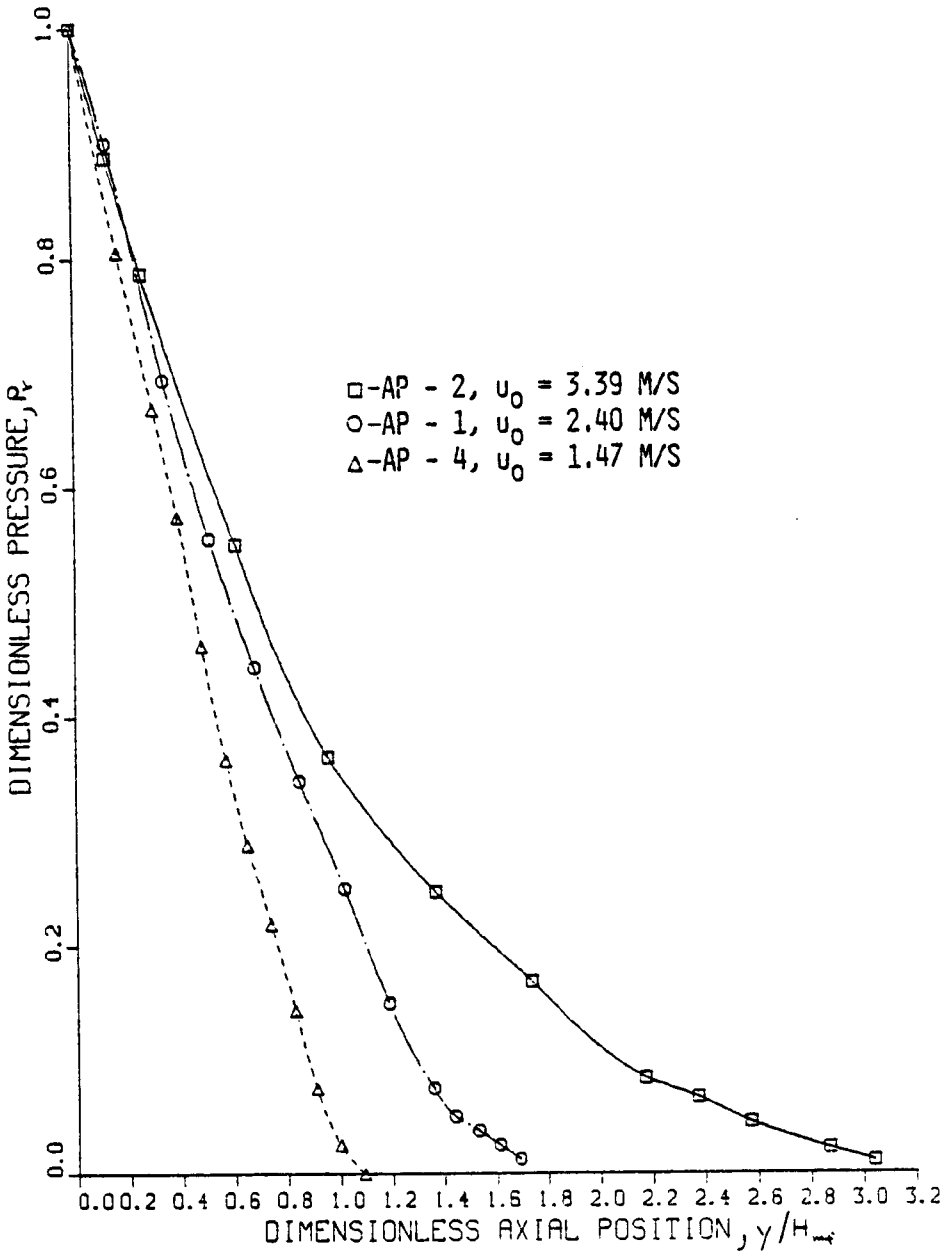

Figure 4.40. Effect of air velocity on the pressure profile in the pure acrylic system.

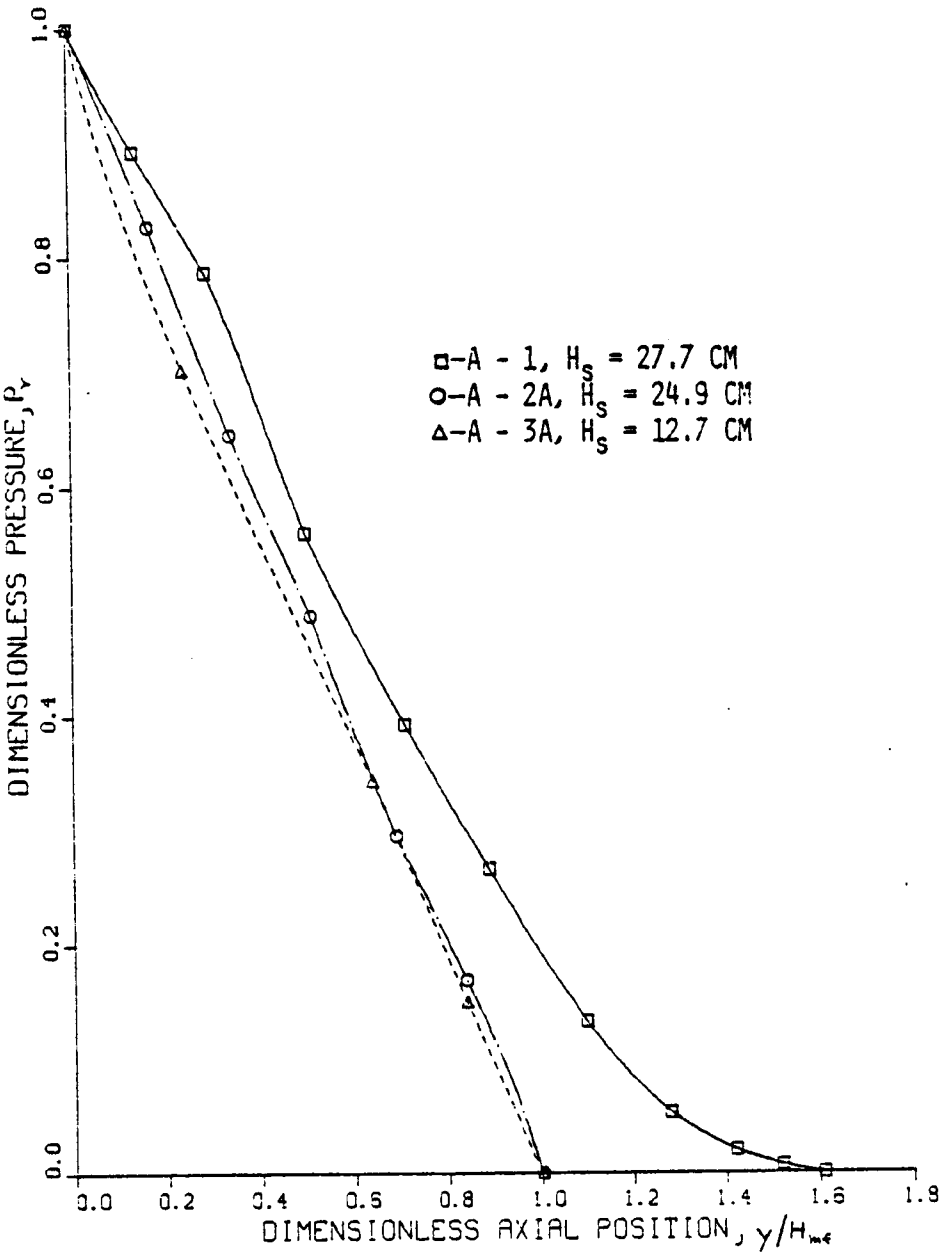

Figure 4.41. Effect of static bed height on the pure acrylic pressure profile.

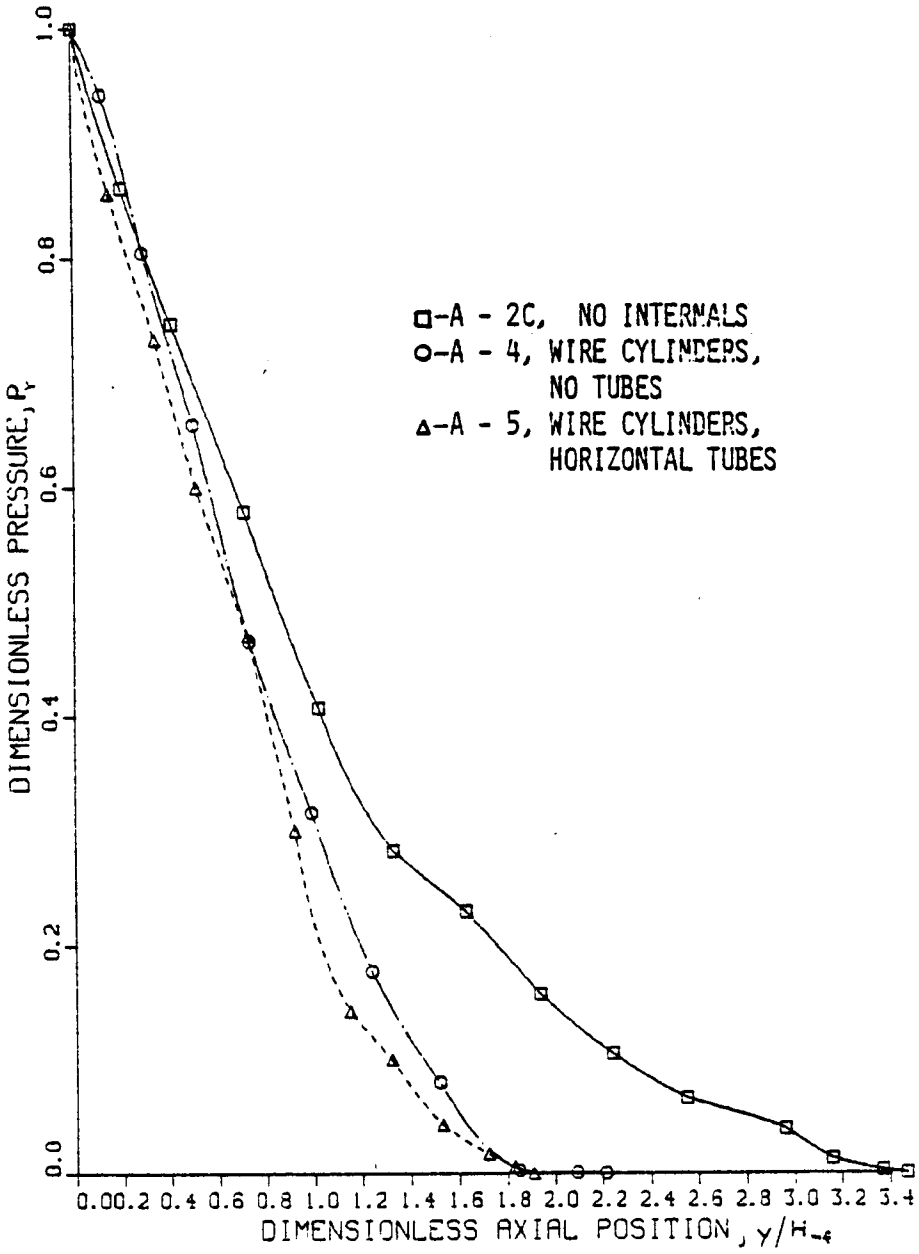

Figure 4.42. Effect of bed internals on the pressure profile in the pure acrylic system.

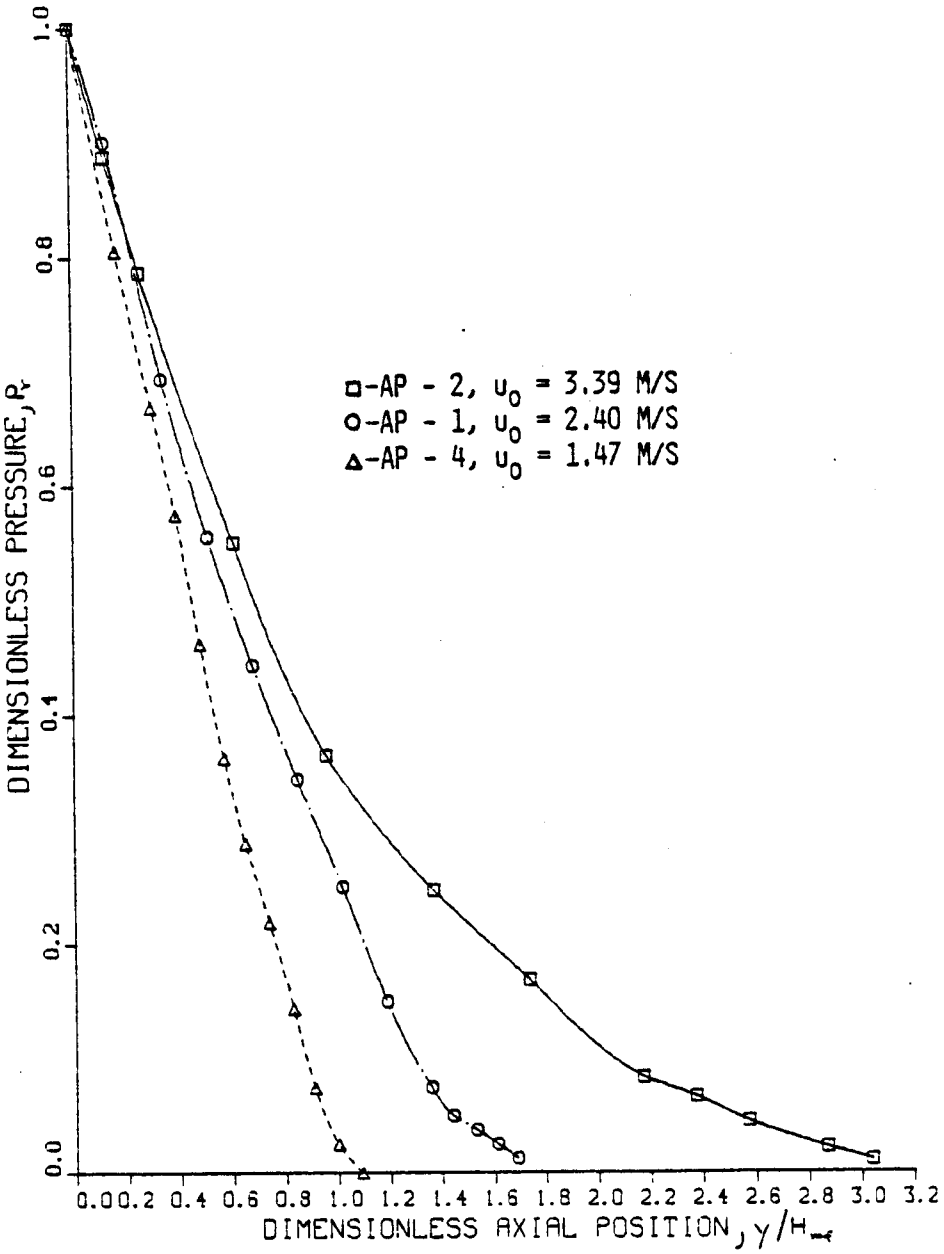

Figure 4.43. Effect of air velocity on the pressure profile in the acrylic-polypropylene system.

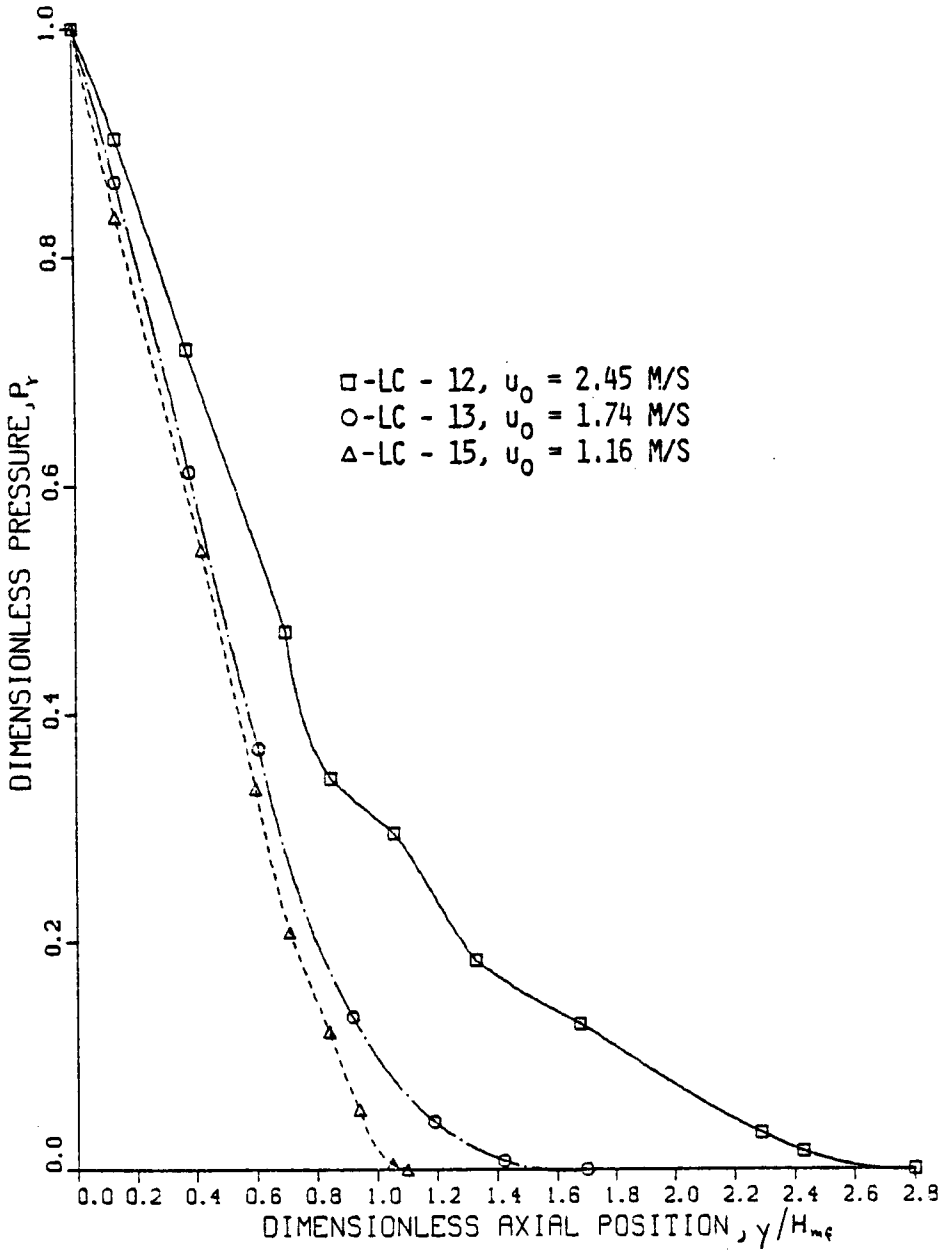

Figure 4.44. Effect of air velocity on the pressure profile in the limestone-coal system.

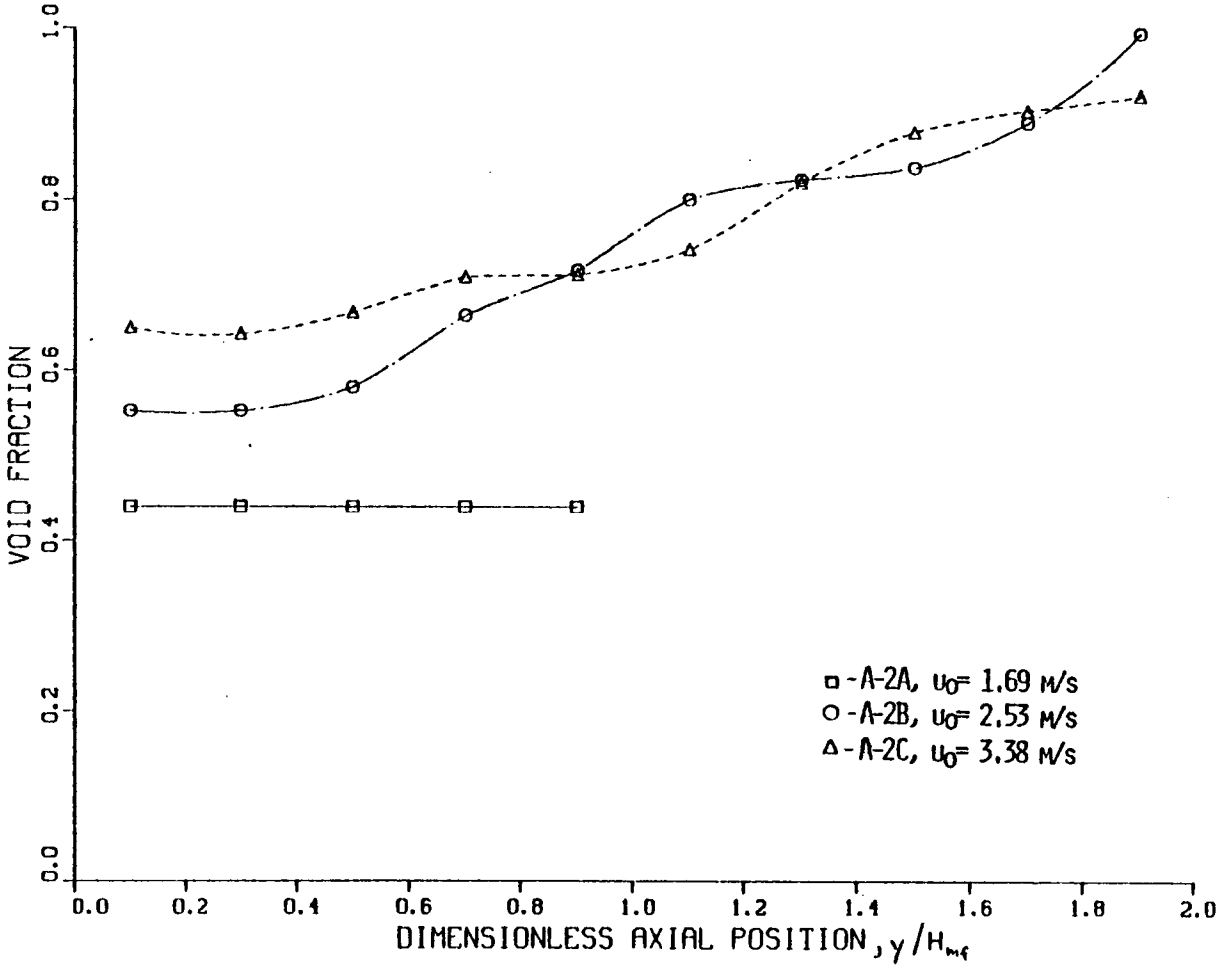

Figure 4.45. Examples of void fraction profiles calculated from pressure profiles.

Perhaps more useful for multi-component systems is a transformation of the segregation profile to expanded coordinates. This is illustrated for run AP-1 in Figure 4.46. The procedure for making this transformation is to: (1) measure the expanded-bed pressure profile, (2) sample the static bed to determine the static segregation profile, and (3) use the weight of each sample (starting at the top) to locate the bottom of each sample on the pressure versus expanded coordinate curve. All of this, of course, depends on the validity of the assumption that the time average pressure gradient is proportional to the time average mass gradient in the expanded bed.

4.4 Estimates of Experimental Error

In addition to the estimates of sampling bias discussed in Section 3.4, I estimated the maximum error due to all other possible causes by replicating experimental runs. Replicates were usually designated by a prime next to the run number, although a few were given unique numbers. Interpretation of these replicates was complicated by the unusual sensitivity of the segregation behavior to slight changes in gas velocity near the transition points described previously. Slight errors in reproducing the air flow sometimes produced significant changes which were actually due to changes in the fluidization mode rather than experimental error.

Rather than attempting to separate the effects of flow transitions from pure error, the replicates were analyzed "as is" to produce an upper limit for experimental error. The results are detailed in Table A-5 in the Appendix. The final results are given in terms of estimates

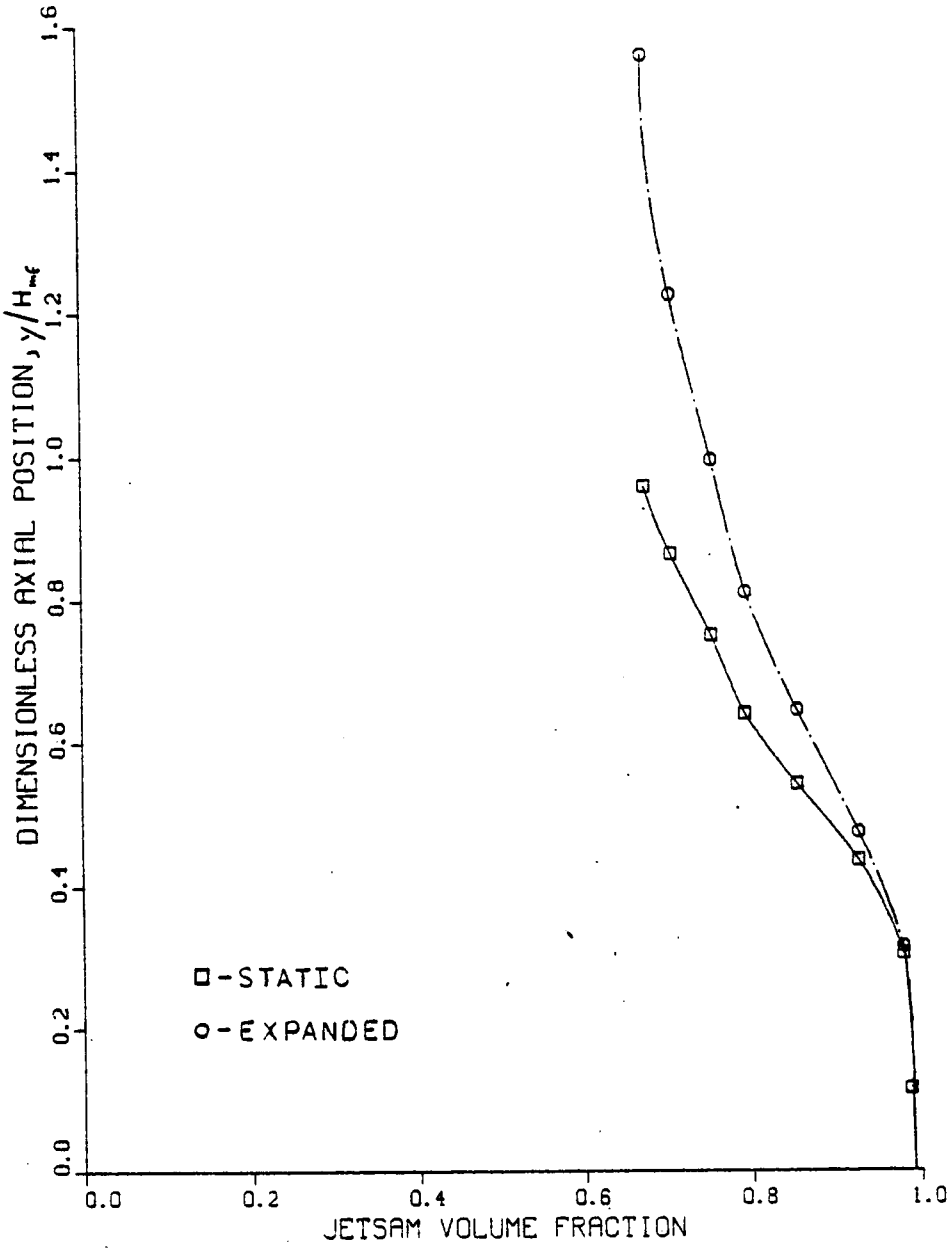

Figure 4.46. Comparison of the segregation profile for run AP-1 in static and expanded coordinates.

of the standard deviation of the error, σ_e. Individual σ_e's were estimated for the mixing index and for the interpolated compositions located at normalized axial positions of z = 0.9, 0.5, and 0.1. These were found to be 0.031, 0.030, 0.023, and 0.014, respectively. Note that the largest composition error occurred in the upper portion of the bed. A good estimate of the maximum error limits for each of these measurements would be $\pm 2\sigma_e$.

5. DATA INTERPRETATION AND MODEL DEVELOPMENT

5.1 Transformation of the Gibilaro-Rowe Equation to Static Coordinates

The strong similarity of my experimental results to those reported by Rowe et al. (1972a and b, 1978, and 1979) prompted me to choose the Gibilaro-Rowe model as a starting point for analyzing large-particle segregation profiles. One of the primary shortcomings of this model, as it was originally proposed, is the assumption of constant void fraction over the length of the bed. As my observations clearly demonstrated, the void fraction in my experiments was far from constant. Yet, in spite of this, my results still seemed to follow the segregation described by the Gibilaro-Rowe model, even when the beds were violently slugging. I found a possible explanation for this by redeveloping the segregation model in terms of static bed coordinates. Note that in the following discussion, all bed characteristics are still considered to be time-average values.

To begin with, the expressions for the dispersion and segregation rates should include the effect of local void fraction.* I propose that the dispersion flux of jetsam at any location y should be given by

$$J_J = D\ (1-\varepsilon)\ \frac{\partial v_J^B}{\partial y}\ . \qquad (5.1)$$

*Compare the following expressions with those used by Gibilaro and Rowe in Figure 2.7.

Note that the effect of the voidage gradient has been specifically excluded, i.e., if the dispersion rate is proportional to the solids volume concentration gradient, then

$$\frac{\partial C_J^B}{\partial_y} = (1 - \varepsilon) \frac{\partial v_J^B}{\partial y} + v_J^B \frac{\partial (1 - \varepsilon)}{\partial y} ,$$

but the second term has been dropped. This has been done because it is assumed that the steady-state voidage distribution is reached more quickly than the steady-state segregation profiles and the solids dispersion due to the voidage gradient is balanced by a reverse settling tendency.* Thus I have considered only the relative motion of the jetsam and flotsam with no net translation of the bed as a whole.

Similar reasoning leads to a revised expression for the relative rate of jetsam segregation

$$S_J = k' (1 - \varepsilon) v_J^B\Big|_y (1 - v_J^B)\Big|_{y+\Delta y} . \qquad (5.2)$$

In this case, it seems reasonable that the segregation rate should be proportional to the local solids volume concentration.

With these modifications, the incremental mass balance for jetsam in finite-difference form is

*The implications of this model for the voidage distribution are discussed further in Sect. 5.5.

Bulk Phase:

$$- DA_b (1 - \varepsilon) \frac{\partial v_J^B}{\partial y}\bigg|_{y,t} + DA_b (1 - \varepsilon) \frac{\partial v_J^B}{\partial y}\bigg|_{y + \Delta y,t}$$

$$+ k' A_b (1-\varepsilon) v_J^B\Big|_{y+\Delta y,t} (1-v_J^B)\Big|_{y,t} - k'A_b (1-\varepsilon) v_J^B\Big|_{y,t} (1-v_J^B)\Big|_{y-\Delta y,t}$$

$$+ w v_J^B\Big|_{y+\Delta y,t} - w v_J^B\Big|_{y,t} + q v_J^w\Big|_{\overline{y},t} \Delta y$$

$$- q v_J^B\Big|_{\overline{y},t} \Delta y = \Delta [A_b v_J^B (1-\varepsilon)]/\Delta t\Big|_{\overline{y}} \Delta y \qquad (5.3a)$$

Wake Phase:

$$w v_J^w\Big|_y - w v_J^w\Big|_{y+\Delta y} + q v_J^B\Big|_{\overline{y}} \Delta y - q v_J^w\Big|_{\overline{y}} \Delta y = \Delta[A_w v_J^w (1-\varepsilon)]/\Delta t\Big|_{\overline{y}} \Delta y$$

(5.3b)

where

D = axial dispersion coefficient, $[L^2/T]$,

k' = axial segregation coefficient, $[L/T]$,

w = solids circulation rate, $[L^3/T]$,

q = solids exchange rate between the bulk and wake phases per unit height, $[L^3/LT] = [L^2/T]$,

A_b = cross-sectional area of bulk phase, $[L^2]$, and

A_w = cross-sectional area of wake phase, $[L^2]$.

Equation 5.3a and b can be further simplified for steady-state conditions when phase exchange is negligible and the phase cross-sectional areas are constant (i.e., Gibilaro-Rowe Case 3):

Bulk Phase:

$$- D(1-\varepsilon) \left.\frac{dv_J^B}{dy}\right|_y + D\,(1-\varepsilon) \left.\frac{dv_J^B}{dy}\right|_{y+\Delta y}$$

$$+ k'\,(1-\varepsilon)\, v_J^B\Big|_{y+\Delta y}\,(1-v_J^B)\Big|_y - k'\,(1-\varepsilon)\, v_J^B\Big|_y\,(1-v_J^B)\Big|_{y-\Delta y}$$

$$+ \frac{w}{A_b}\, v_J^B\Big|_{y+\Delta y} - \frac{w}{A_b}\, v_J^B\Big|_y = 0 \qquad (5.4a)$$

Wake Phase:

$$\frac{w}{A_w}\, v_J^w\Big|_y - \frac{w}{A_w}\, v_J^w\Big|_{y+\Delta y} = 0\ . \qquad (5.4b)$$

The axial position coordinate in Eqs. (5.4a and b) is the position as it occurs in the expanded bed. The location of any point, y, also corresponds to a different location, y_s, in the collapsed (static) bed. Equations 5.4a and b can be rewritten in terms of the static coordinate by determining the transformation relationship between y and y_s. Assuming no relative solids motion when the bed is slumped, conservation of mass within corresponding increments of the expanded and static bed require that

$$\Delta y\,(1-\varepsilon) = \Delta y_s\,(1-\varepsilon_s)$$

or

$$\Delta y = \frac{(1-\varepsilon_s)}{(1-\varepsilon)} \Delta y_s \ . \tag{5.5}$$

Thus each increment of length in the expanded bed transforms into an increment of length in the static bed by the ratio of the solids volume concentrations. Since the transport coefficients D, k', and w also incorporate characteristic axial lengths, these might be expected to transform as well. Such transformations would be made as follows:

D α (mean free axial path length) (mean axial velocity)

D α L_1 L_2

$$\frac{D}{D_s} = \frac{L_1 L_2}{L_{1s} L_{2s}} = \frac{(1-\varepsilon_s)^2}{(1-\varepsilon)^2} \ , \tag{5.6}$$

k α (mean axial segregation velocity)

k α L_3

$$\frac{k}{k_s} = \frac{L_3}{L_{3s}} = \frac{(1-\varepsilon_s)}{(1-\varepsilon)} \ , \tag{5.7}$$

w α (mean solids volumetric circulation rate)

$= A_w (1-\varepsilon)$ (mean axial velocity)

w α $L_4 (1-\varepsilon)$

$$\frac{w}{w_s} = \frac{L_4 (1-\varepsilon)}{L_{4s}(1-\varepsilon_s)} = 1 \ ,$$

where D_s, k_s, and w_s are the transformed transport coefficients and L_i are characteristic axial lengths incorporated in these coefficients.

Substituting Eqs. 5.5 through 5.8 into 5.4a and b gives the following result

Bulk Phase:

$$- D_s\,(1-\varepsilon_s)\,\frac{dv_J^B}{dy_s}\bigg|_{y_s} + D_s\,(1-\varepsilon_s)\,\frac{dv_J^B}{dy_s}\bigg|_{y_s+\Delta y_s}$$

$$+ k_s\,(1-\varepsilon_s)v_J^B\Big|_{y_s+\Delta y_s}\,(1-v_J^B)\Big|_{y_s} - k_s\,(1-\varepsilon_s)\,v_J^B\Big|_{y_s}\,(1-v_J^B)\Big|_{y_s-\Delta y_s}$$

$$+ \frac{w_s}{A_b}\,v_J^B\Big|_{y_s+\Delta y_s} - \frac{w_s}{A_b}\,v_J^B\Big|_{y_s} = 0 \qquad (5.9a)$$

Wake Phase:

$$w_s\,v_J^w\Big|_{y_s} - w_s\,v_J^w\Big|_{y_s+\Delta y_s} - \frac{w_s}{A_b}\,v_J^B\Big|_{y_s} = 0\ . \qquad (5.9b)$$

Dividing by Δy_s and taking the limit as $\Delta y_s \to 0$ gives the differential form

Bulk Phase:

$$D_s\,(1-\varepsilon_s)\,\frac{d^2v_J^B}{dy_s^2} + \left[\left(\frac{w_s}{A_b}\right) + k_s\,(1-\varepsilon_s) - 2\,k_s(1-\varepsilon_s)v_J^B\right]\frac{dv_J^B}{dy_s} = 0 \qquad (5.10a)$$

Wake Phase:

$$\frac{dv_J^w}{d\,y_s} = 0\ . \qquad (5.10b)$$

Equations 5.10a and b can be expressed in dimensionless form as

Bulk Phase:

$$\lambda_{Ds} \frac{d^2 v_J^B}{d\, z^2} + (\lambda_{ws} + 1 - 2v_J^B) \frac{dv_J^B}{dz} = 0 \qquad (5.11a)$$

Wake Phase:

$$\frac{dv_J^w}{dz} = 0 \qquad (5.11b)$$

where

$$z = y_s/H_s \ ,$$

$$\lambda_{Ds} = \frac{D_s}{H_s\ k_s} \ , \text{ and}$$

$$\lambda_{ws} = \frac{w_s}{A_b\ k_s(1-\varepsilon_s)} \ ,$$

The boundary conditions likewise transform to give

$$\text{at } z = 0,\ v_{J_o}^B (1 - v_{J_o}^B + \lambda_{Ds}) \left.\frac{dv_J^B}{dz}\right|_{z=0} = 0 \qquad (5.12a)$$

$$v_{Jo}^B = v_{Jo}^w \qquad (5.12b)$$

$$\int_0^1 v_J dz = \overline{v}_J \ . \qquad (5.12c)$$

Equations 5.11 and 5.12 are functionally the same as the original Gibilaro-Rowe Case 3 result, the only difference being that λ_D and

λ_w have been replaced by λ_{Ds} and λ_{ws}.* Thus the similarity between the static composition profiles and those predicted by the Gibilaro-Rowe model is no longer surprising. Also, this result implies that steady-state segregation profiles can be treated independently of bed expansion, as long as the basic assumptions in the foregoing discussion remain valid.

5.2 Further Discussion and Development of the Gibilaro-Rowe Model

As discussed in Section 2.4.6, Gibilaro and Rowe (1974) developed analytical expressions for three special cases of their general segregation equation: (1) when axial dispersion and phase exchange were negligible, (2) when phase exchange is allowed but axial dispersion is still negligible, and (3) when axial dispersion is allowed but phase exchange is negligible. Gibilaro and Rowe point out that their data appear to follow Cases 1 and 3 while the phase exchange allowed in Case 2 did not appear to be very important. With some exceptions which are covered later, my data also appeared to follow Cases 1 and 3. It should be noted that Case 1 is really a limit of Case 3, when the axial dispersion parameter, λ_D, is allowed to go to 0.

Another important limit of Case 3 which was not covered by Gibilaro and Rowe is the condition when circulation is negligible and particle mixing occurs only by axial dispersion (i.e., when λ_w is allowed to go to 0). The analytical solution for this limit is

---

*Three parameters are still needed to determine a segregation profile, λ_{Ds}, λ_{ws}, and v_w. As is discussed later, v_w can be set approximately equal to 0 in many cases.

$$v_J = \frac{1}{1 + Ae^{z/\lambda_{Ds}}} \tag{5.13}$$

where

$$A = (1-v_{Jo})/v_{Jo} = [e^{(\bar{v}_J-1)/\lambda_{Ds}} - 1]/[1 - e^{\bar{v}_J/\lambda_{Ds}}] \ .$$

Note that the absence of circulation implies the absence of a wake phase, and the problem is reduced to describing segregation in a single phase where $v_J^B = v_J$. Figures 5.1 through 5.3 illustrate the profiles produced by Eq. 5.13 for varying λ_{Ds} and $\bar{v}_J$. Note the typical sigmoid shapes.

The limit represented by Eq. 5.13 is particularly interesting because it illustrates the relationship between fluidized bed segregation and the much more general problem of particle distributions in gravitational fields. Two examples help clarify this; the distribution of atoms in a binary mixture of ideal gases and the distribution of particles undergoing Brownian motion in a fluid. Any component of a mixture of ideal gases follows the well-known barometric equation

$$p_i = p_{io} e^{-B_i y} \tag{5.14}$$

where

p_i = the partial pressure of component i, $[F/L^2]$

p_{io} = the partial pressure of i at the datum elevation, $[F/L^2]$,

$B_i = g\ M_i/(g_c\ R\ T)$, $[L^{-1}]$,

g = acceleration due to gravity, $[L^2/T]$,

M_i = molecular weight of component i,

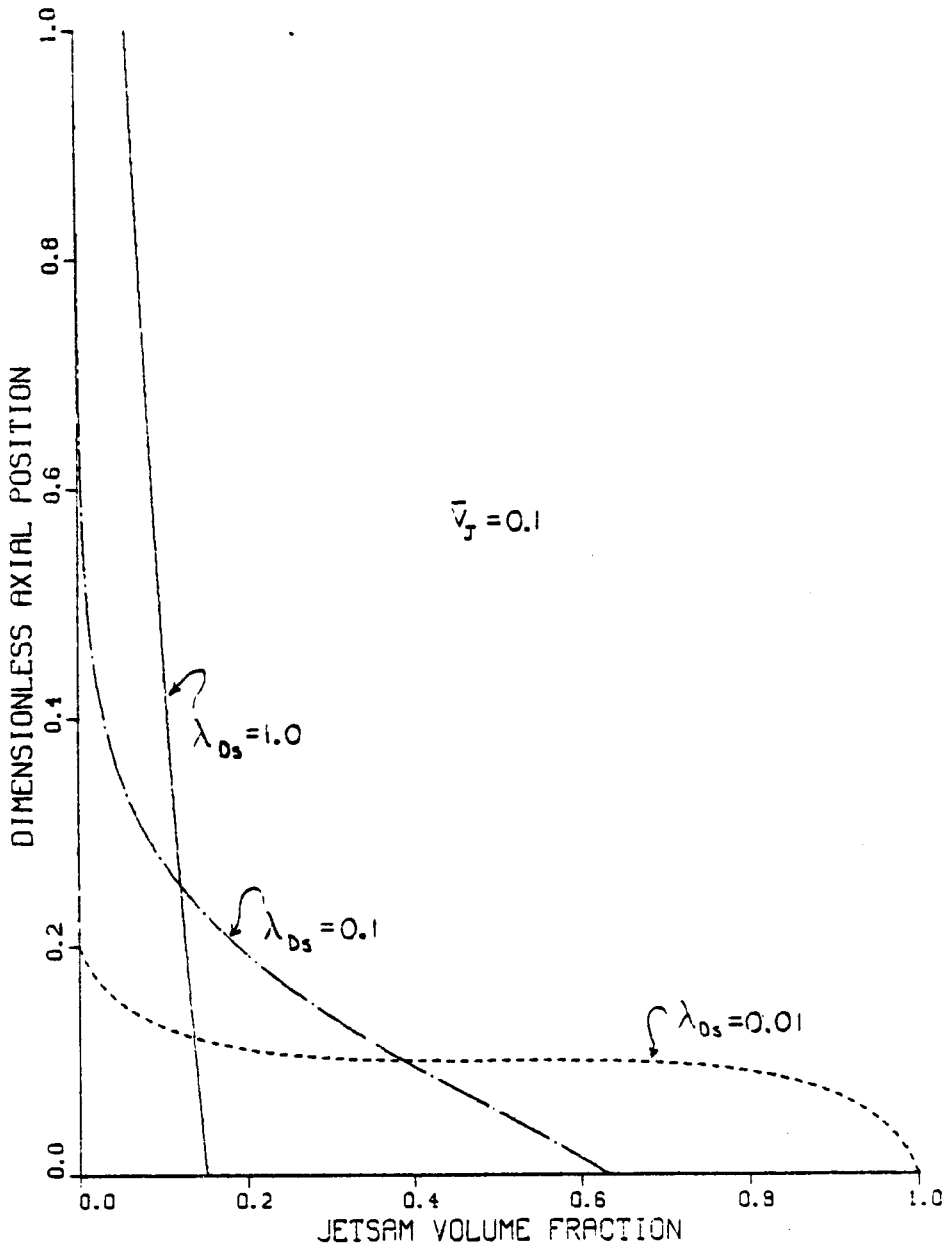

Figure 5.1. Segregation patterns predicted by Eq. 5.13 for varying dispersion parameter at low overall jetsam content.

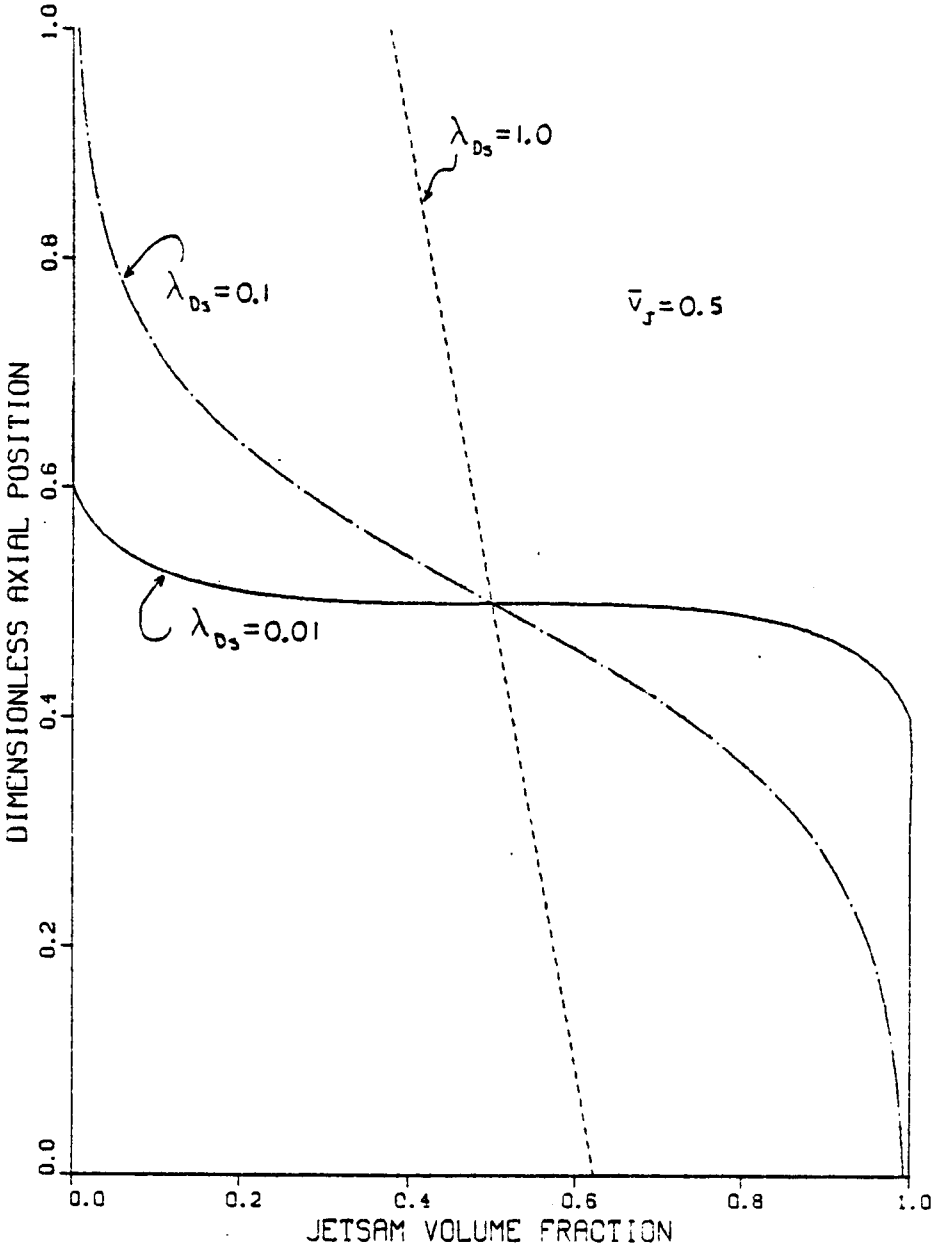

Figure 5.2. Segregation patterns predicted by Eq. 5.13 for varying dispersion parameter at moderate jetsam content.

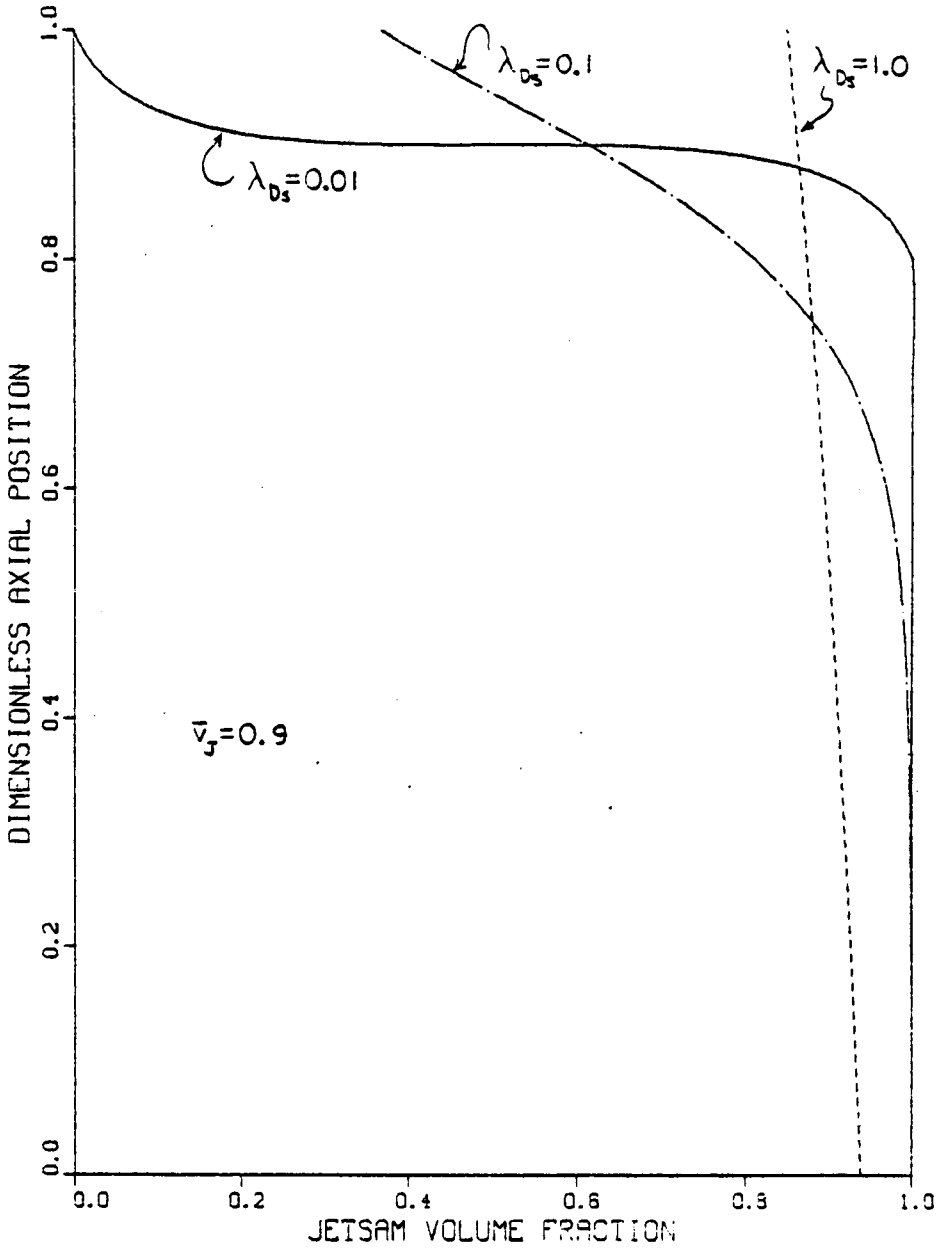

Figure 5.3. Segregation patterns predicted by Eq. 5.13 for varying dispersion parameter at high overall jetsam content.

g_c = Newton's second law proportionality constant,

R = ideal gas constant, [F L/mole K] and

T = temperature, [K].

Considering a two-component mixture (components labeled 1 and 2), the mole fraction of component 1 at any level y is given by

$$\mu_1 = p_1/(p_1 + p_2) = \frac{1}{1 + C\, e^{(B_1 - B_2)y}} \tag{5.15}$$

where

$C = (1 - \mu_{10})/\mu_{10}$, and

μ_{10} = mole fraction of component 1 at datum, [-].

If the gas is confined in a container of finite height H, Eq. (5.15) can be written

$$\mu_1 = \frac{1}{1 + C\, e^{z/\lambda_G}} \tag{5.16}$$

where

$z = y/H$, [-],

$\lambda_G = H/(B_1 - B_2)$, [-], and

$C = [e^{(\bar{\mu}_1 - 1)/\lambda_G} - 1]/[1 - e^{\bar{\mu}_1/\lambda_G}]$.

Thus it is clear that Eqs. 5.13 and 5.16 are analogous, with μ_1 and v_J interchanged and λ_{Ds} and λ_G reflecting the segregation tendencies of the components.

A similar analogy can be made between fluidized bed segregation and particles undergoing Brownian motion in a fluid. Einstein (1922) showed that for particles of mass m_p and density ρ_p suspended in a medium of

density ρ_f at absolute temperature T, the particle concentration at distance y above some datum is given by

$$c_p = c_{po}\, e^{-\Omega_p y} \tag{5.17}$$

where

$\Omega_p = m_p g\ (\rho_p - \rho_f) N_o / (\rho_p R\ T)$, $[L^{-1}]$, and

N_o = Avogadro's number.

As in the case of the ideal gas, this leads to the following result for number fraction of particles (relative to the total number of particles and molecules) at location y in a container of height H,

$$n_p = \frac{1}{1 + E\, e^{z/\lambda_B}} \tag{5.18}$$

where

$E = (1-n_{po})/n_{po}$, and

n_{po} = number fraction of particles at the datum, [-],

$\lambda_B = H/(\Omega_p - \Omega_f)$, [-], and

$\Omega_f = m_f g(\rho_f - \rho_p)\ N_o/(\rho_f\ R\ T)$, $[L^{-1}]$.

The similarity of the ideal gas and suspended particle distributions to fluidized bed segregation suggests other possibilities. For instance, the statistical mechanics of gas and suspended particles has been thoroughly developed, and careful analogies with fluidized beds may lead to new insights into bed hydrodynamics. Also, fluid and/or suspended particle systems having large-scale circulation patterns may be amenable to analysis with Gibilaro and Rowe's Case 3 result.

One feature of my data which is clearly not represented by the Gibilaro-Rowe model is the steep-gradient zone which sometimes occurred in the upper region. Observations seemed to indicate that this zone was composed of particles which had been ejected from the main bed by collapsing bubbles. It is interesting that Rowe et al. (1972a and b) depicted a similar zone in their results, but they did not attempt to explain or model it. One possible way to model this behavior is to divide the bed into two parts, the main body of the bed and the upper splash zone. The Gibilaro-Rowe model for the lower portion can be represented as in Eqs. 2.13a-c, while the model for the upper zone must account for the different behavior of the ejected particles. Perhaps the simplest method (and the one which also appeared to me to most closely reflect reality) is to assume that the wake phase has completely disappeared in the upper region. This leads to consideration of Eq. 5.13 as a possible model for the upper-zone profile.

The overall profile for this "stacked-bed" model can then be represented as follows:

$$v_J = v_{J\ell} \langle z_c - z \rangle + v_{Ju} \langle z - z_c \rangle \tag{5.19}$$

where

$v_{J\ell}$ = the profile predicted by Eq. 2.13 with λ_{Ds} and λ_{ws} replacing λ_D and λ_w,

v_{Ju} = the profile predicted by Eq. 5.13,

z_c = the position of the interface between the upper and lower zones, and

$\langle\ \rangle$ = the singularity function which equals 0 when the argument is negative and 1 when the argument is 0 or positive.

The value of the dispersion parameter is likely to be different between the upper and lower zones due to differences in the mechanisms of particle motion. Of course the boundary conditions require that both $v_{J\ell}$ and v_{Ju} should approach the same value at $z=z_c$. Figure 5.4 depicts the change in the profile of the upper zone with variation in the upper dispersion parameter. The lower profile assumes $\lambda_{ws} = 0.5$, $\lambda_{Ds} = 0.1$, and $V_w \simeq 0$. The interface between the upper and lower zones is assumed to be at $z = 0.8$.

5.3 Estimation of the Model Parameters from the Steady-State Data

I tested the agreement between the modified Gibilaro-Rowe model and the steady-state data by adjusting the values of the model parameters to minimize the sum of the squared deviations between the model and the data. The non-linearity of the model significantly complicated parameter fitting, and it was necessary to use an iterative stepwise procedure based on a simplex evolutionary operation strategy per Spendley et al. (1962). Detailed results are given in Tables A-6 and A-7 in the Appendix. In all cases, it was found that the wake phase comprised a negligible portion of the bed, and thus the parameter v_w was approximately zero. This finding is supported by the observations of Gibilaro and Rowe (1974).

Table A-6 contains the results for all Region 1 runs, and Table A-7 contains the Region 2 results. In the former case, only those portions

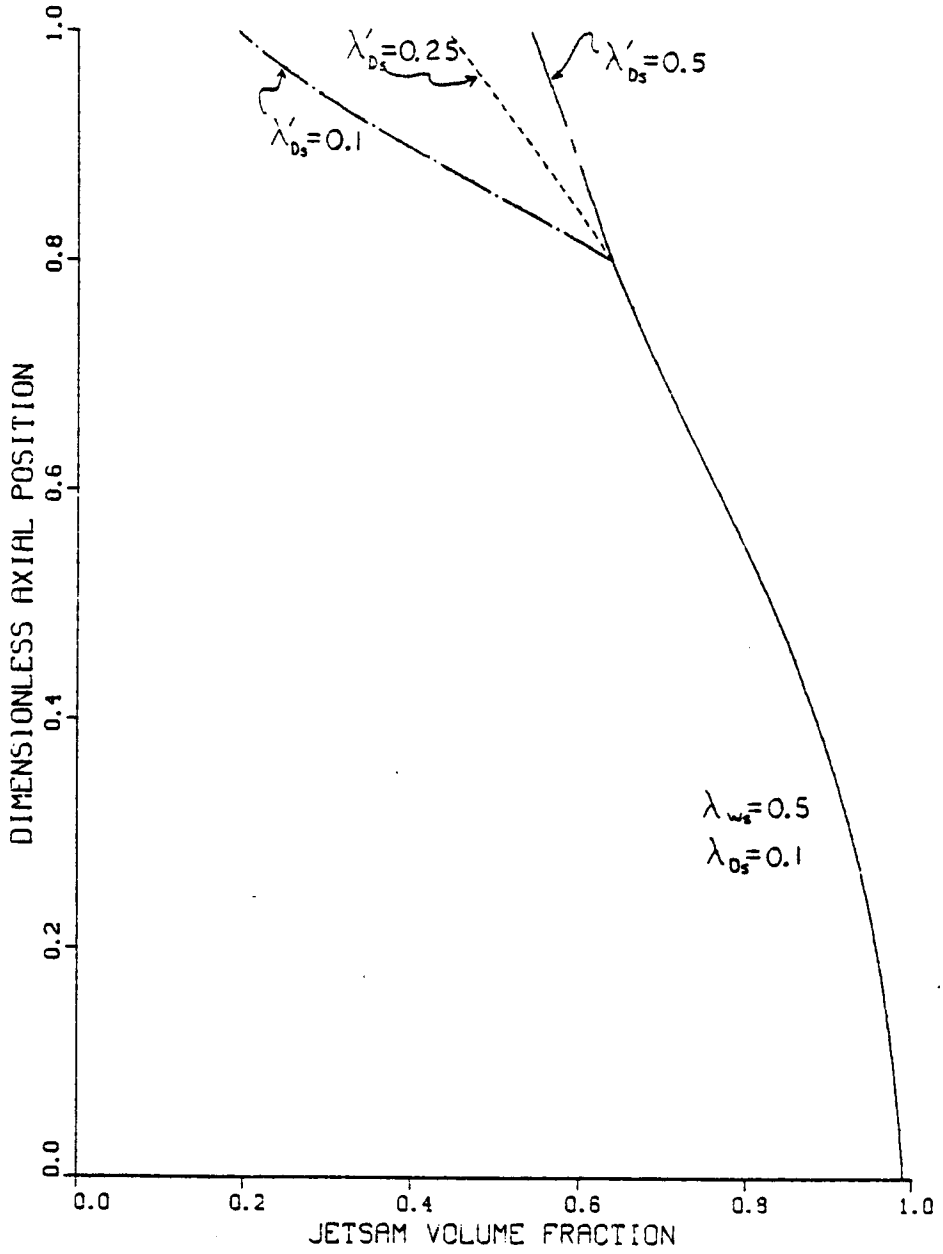

Figure 5.4. Segregation patterns predicted by Eq. 5.19 for varying upper dispersion parameter, λ_{Ds}'; with $\lambda_{Ds} = 0.1$ and $\lambda_{ws} = 0.5$.

of the bed above the fluidization interface were considered. The parameters listed are: The location of the fluidization interface, z_i; the composition at the interface v_{Ji}; the dimensionless dispersion and convection parameters in the bulk of the fluidized zone, λ_{Ds} and λ_{ws}; the location of the start of the splash zone, z_c; the dispersion parameter in the splash zone, λ_D'; and the sum of the squared deviations, SSD. The quantities z_i and z_c were visually observed during the course of the experiment. Values of 0.0 under z_i indicate that the entire bed was fluidized. At the low velocities typical of Region 1, the splash zone was rarely visible to any extent. Blanks under z_c and λ_D' indicate that the splash zone was not visible. The parameters λ_{Ds}, λ_{ws}, and λ_D' were determined with the iterative procedure to minimize SSD, which was calculated from the following equation:

$$SSD = \sum_{i=1}^{n} v_{si} \, (v_{Jmod.} - v_{Jexp.})^2 \qquad (5.20),$$

where

$v_{Jmod.}$ = the composition of sample i predicted by the modified Gibilaro-Rowe model and

$v_{Jexp.}$ = the measured composition of sample i.

Note that SSD is equivalent to a mean squared error, and the square root of SSD represents a mean error (a measure of lack of fit) between the model and the data. The maximum SSD found for the Region 1 data was 3.8×10^{-4}, representing a mean composition error of 0.019. This compares favorably with the estimates of the maximum experimental error

discussed in Section 4.4, which ranged from 0.028 to 0.060 for compositions at different bed levels. It is important to remember, however, that because only the fluidized portions of the bed were fit with the model, the number of experimental points considered in each case were less than in the Region 2 runs. Typically there were three or four points which were fit with the model for Region 1. It would be expected that the SSD would increase as the number of data points increased.

The parameters given in Table A-7 are: The dispersion and convection parameters in the major portion of the bed; λ_{Ds} and λ_{ws}; the location of the start of the splash zone, z_c; the dispersion parameter in the quantities which also reflect the "goodness of fit," SSD/SST_{max}, I_{exp}, and I_{mod}. The ratio SSD/SST_{max} is a kind of normalized measure of the lack of fit. It compares the SSD to the total possible sum of squared deviations about the mean, SST_{max}, which is equal to $\bar{v}_J(1-\bar{v}_J)$. The terms I_{exp} and I_{mod} are the mixing indices determined from the experimental data and from the model, respectively. A perfect fit would result in both of these terms being equal.

The maximum SSD found between the modified Gibilaro-Rowe model and the Region 2 data was approximately 1.9×10^{-3}, representing a maximum mean deviation of 0.044. This case is illustrated in Figure 5.5. Most of the mean deviations were typically less than 0.03. An example of a "typical" case is illustrated in Figure 5.6. Figure 5.7 is an example of one of the "best-fit" cases. Overall, the deviations observed compare favorably with the maximum error estimates given in Section 4.4. The maximum difference between the measured and predicted mixing indices

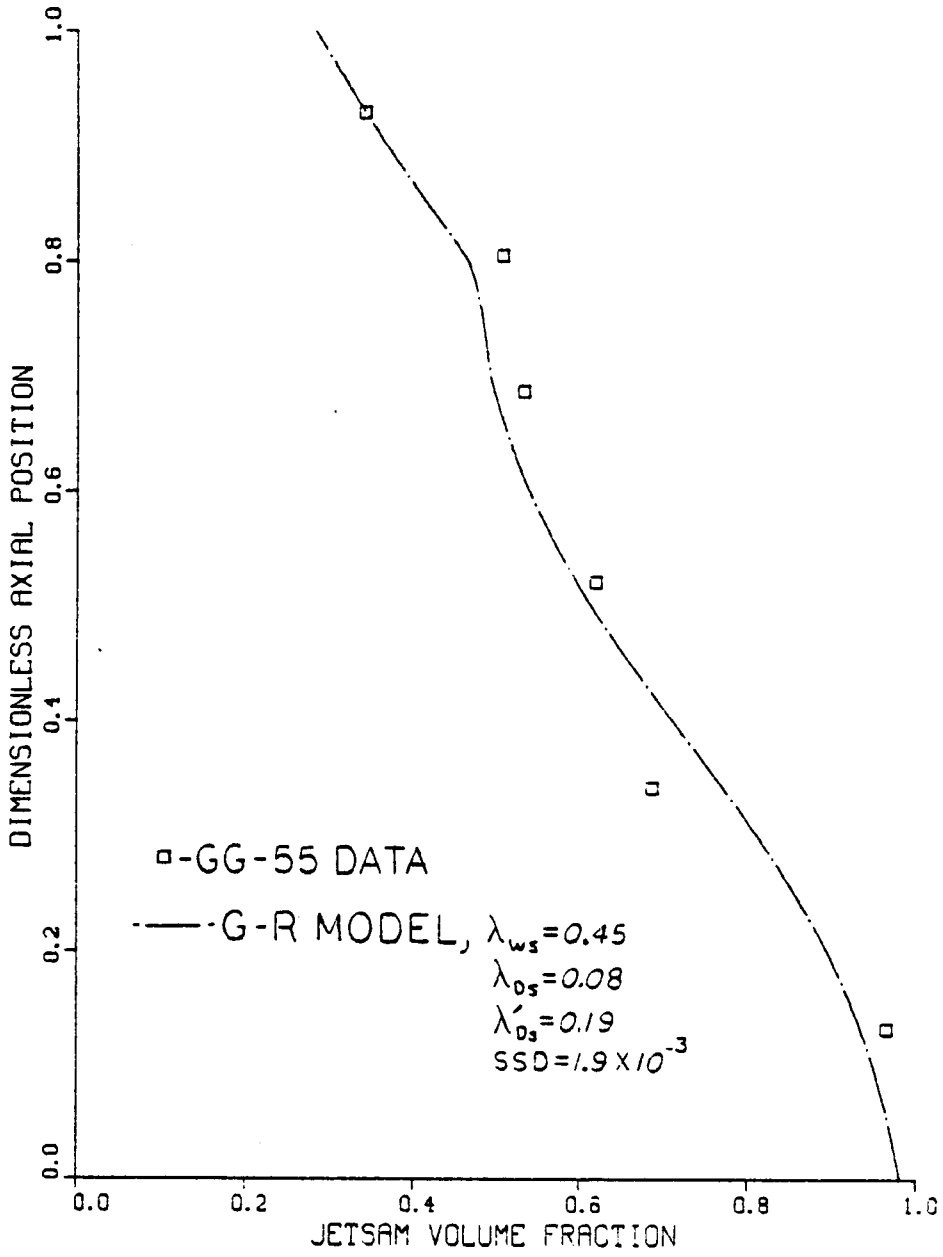

Figure 5.5. Comparison between experimental data and modified Gibilaro-Rowe model for "worst-fit" case.

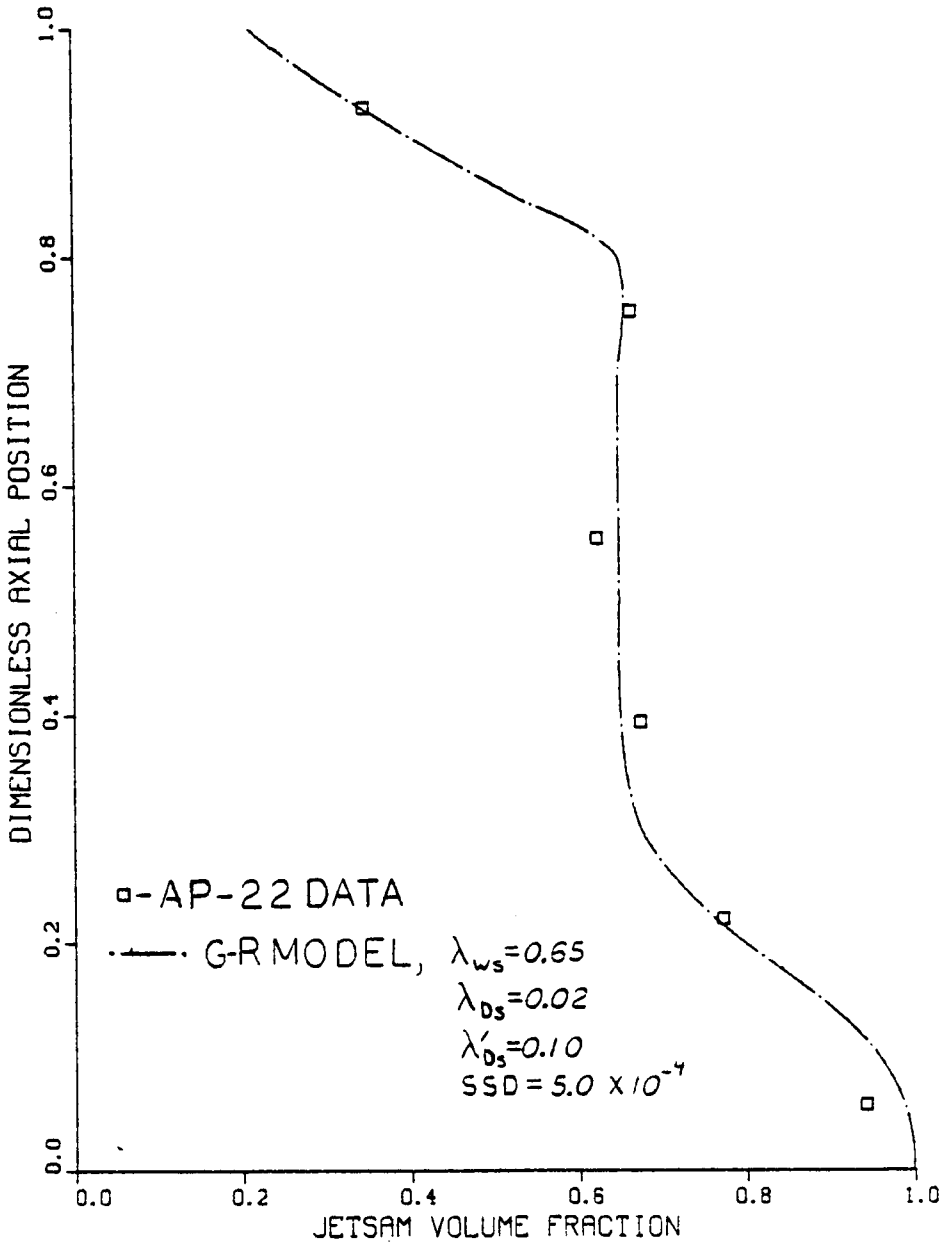

Figure 5.6. Comparison between experimental data and modified Gibilaro-Rowe model for case with typical degree of fit.

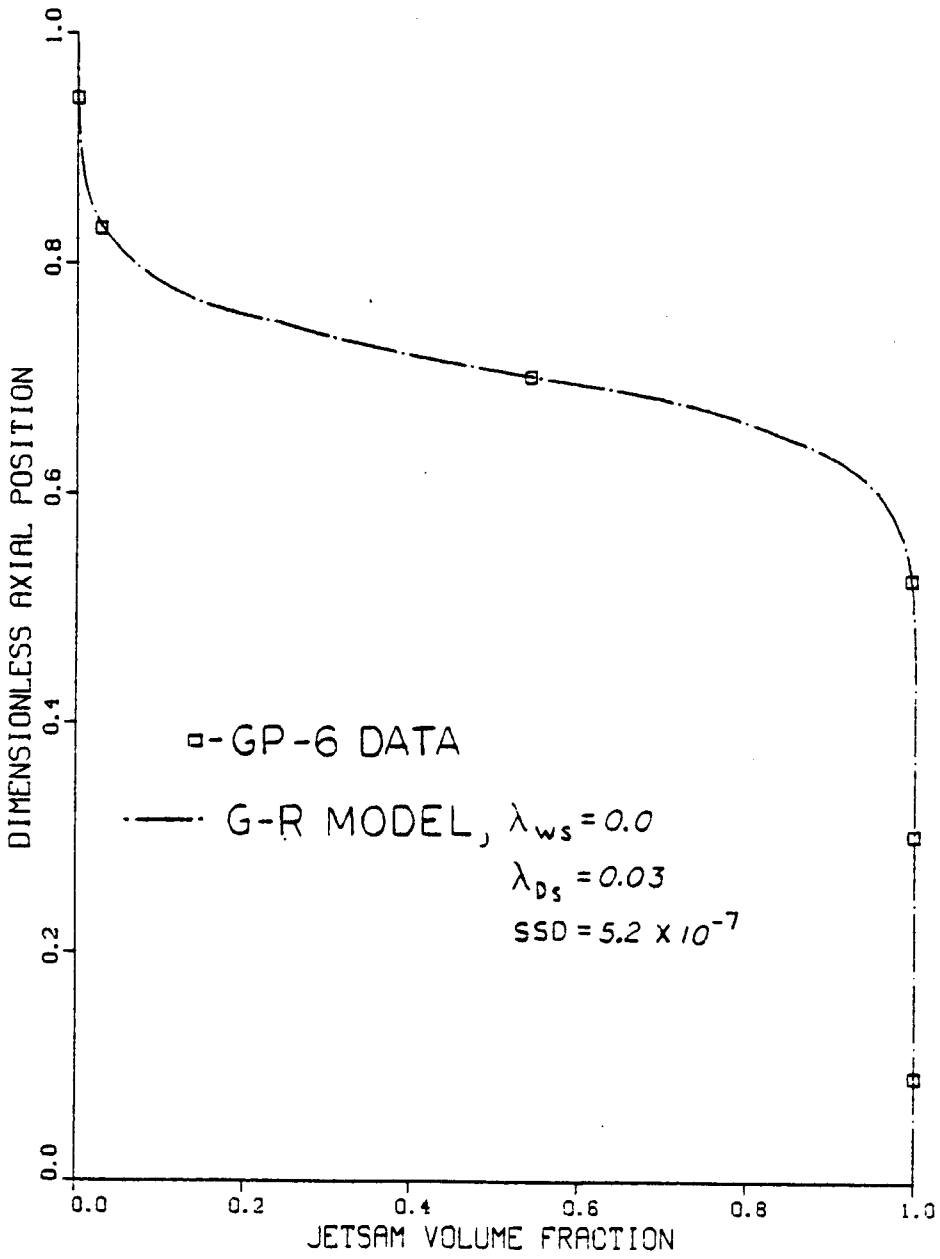

Figure 5.7. Comparison between experimental data and modified Gibilaro-Rowe model for a case with extremely good fit.

was 0.061, which also compares favorably with the maximum estimated error in I of 0.062. These statistics clearly indicate that the modified Gibilaro-Rowe model is a good representation of the steady-state data.

Further insights into usefulness of the model can be gained by observing the changes in the model parameters as bed conditions are changed. Tables 5.1 through 5.5 illustrate typical cases for changes in air velocity, bed height, overall bed composition, bed internals, and particle properties, respectively. As air velocity increased in the glass-glass system with tube internals, the wake parameter, λ_{Ds}, varied up and down similarly to the mixing index I (as the index I went down, λ_{ws} went up). The dispersion parameter, λ_{Ds}, gradually decreased with velocity, except for a "spike" at about 2.25 m/s. The upper bed zone was not visible until the superficial velocity exceeded about 2.6 m/s. Bed height increases in the same system appeared to enhance λ_{ws}, diminish λ_{Ds}, and cause varying behavior in the upper zone. The upper zone was not visible in this system when $H_s \lesssim 12$ cm.

The overall bed composition had a dramatic effect on the modified Gibilaro-Rowe parameters of the glass-glass system. As $\bar{v}_J$ increased from 0.133 to 0.80, λ_{ws} increased and λ_{Ds} generally decreased. Further increases in $\bar{v}_J$, however, produced a sudden change in the nature of the solids motion, with λ_{ws} virtually going to zero and λ_{Ds} increasing rapidly. The upper bed zone was discernable only at intermediate values of $\bar{v}_J$. Bed internals tended to reduce the convection parameter and had a varying effect on both the dispersion parameter and the upper bed zone.

Table 5.1. Illustration of the effect of air velocity on the modified Gibilaro-Rowe parameters

Run*	u_o (m/s)	λ_{ws}	λ_{Ds}	λ'_{Ds}	z_c
GG-60	1.95	0.0	0.080		
17	1.98	0.135	0.071		
18	2.08	0.230	0.050		
14	2.16	0.270	0.055		
14'	2.17	0.270	0.056		
19	2.25	0.178	0.117		
15	2.34	0.029	0.078		
1	2.44	0.0	0.068		
1'	2.46	0.054	0.066		
21'	2.45	0.109	0.083		
21	2.51	0.136	0.080		
4	2.61	0.358	0.052	1.57	0.80
3'	2.76	0.609	0.024	0.448	0.75
3	2.77	0.540	0.026	1.19	0.80
2	2.91	0.636	0.030	0.792	0.80
2'	2.91	0.604	0.024	0.607	0.80
20	3.14	0.640	0.025	0.474	0.80
16	3.24	0.685	0.022	0.335	0.80
16'	3.29	0.647	0.011	0.404	0.80
65	3.86	0.710	0.011	0.153	0.85
64	4.55	0.713	0.010	0.132	0.82
61	5.14	0.690	0.010	0.210	0.81
63	5.59	0.701	0.011	0.170	0.80
62	6.03	0.690	0.010	0.151	0.82

*All runs made with $\bar{v}_J = 0.667$, $H_s \approx 14.8$ cm, and with wire cylinders and horizontal tubes in the bed.

Table 5.2. Illustration of the effect of bed height on the modified Gibilaro-Rowe parameters

Run	H_s (cm)	λ_{ws}	λ_{Ds}	λ_{Ds}'	z_c
GG-12	7.4	0.0	0.105		
13	11.7	0.220	0.090		
28	13.2	0.560	0.030	0.688	0.75
3	14.7	0.540	0.026	1.19	0.80
3'	15.0	0.609	0.024	0.448	0.75
27	18.8	0.650	0.020	0.229	0.80
11	21.3	0.670	0.020	0.173	0.75

Table 5.3. Illustration of the effect of overall bed composition on the modified Gibilaro-Rowe parameters

Run	$\bar{v}_J$	λ_{ws}	λ_{Ds}	λ_{Ds}'	z_c
GG-10	0.133	0.050	0.048		
23	0.200	0.138	0.047		
22	0.350	0.264	0.037	0.684	0.80
24	0.500	0.420	0.039	0.451	0.80
3	0.667	0.540	0.026	1.19	0.80
3'	0.667	0.609	0.024	0.448	0.75
25	0.800	0.620	0.086		
5'	0.933	0.0	0.357		

Table 5.4. Illustration of the effect of bed internals on the modified Gibilaro-Rowe parameters

Run	Internals	λ_{ws}	λ_{Ds}	λ_{Ds}'	z_c
GG-30	None	0.800	0.050	0.259	0.80
30'	None	0.800	0.035	0.733	0.80
31	Cylinders w no tubes	0.647	0.013	0.228	0.80
31'	Cylinders w no tubes	0.665	0.029	0.263	0.85
3	Cylinders w single tube	0.540	0.026	1.19	0.80
3'	Cylinders w single tube	0.609	0.024	0.448	0.75
29	Cylinders w two tubes	0.642	0.036		
29'	Cylinders w two tubes	0.650	0.036		

Table 5.5. Illustration of the variation of the Gibilaro-Rowe parameters between particle systems

Velocity condition	Run No.	I	λ_{ws}	λ_{Ds}	λ'_{Ds}	z_c
u_o = 2.8 m/s	AG-6	0.051	0.612	0.017	0.864	0.85
	GG-3'	0.094	0.609	0.024	0.448	0.75
	AP-3	0.530	0.0	0.064		
	GP-6	0.803	0.0	0.035		
u_o/u_{mfJ} = 1.0	GG-60	0.646	0.0	0.080		
	AP-37	0.798	0.0	0.038		
	GP-9	0.945	0.0	0.023		
u_o/u_{mfJ} = 1.7	GG-16	0.038	0.685	0.022	0.335	0.80
	AG-6	0.051	0.612	0.017	0.864	0.85
	AP-33	0.530	0.0	0.069	-5.18	0.80
	GP-19	0.789	0.0	0.039		

Table 5.5 illustrates the variation of parameters between different solids systems at common velocity conditions. It appears from this that those systems having a strong tendency to segregate (AP and GP) exhibited relatively little convection behavior, and mixing was primarily by dispersion. The strong segregating systems also did not exhibit much tendency to form a well-defined upper zone. In one, Table 5.5, run AP-33, the negative value for λ'_{Ds} indicates a reversal of jetsam and flotsam roles. This may be just experimental error, but it could also be explained by the high momentum of the much larger acrylic particles, which might tend to carry them up above the propylene in the splash zone.

In general, it appears that λ_{ws} rarely exceeded 1.0 in my experiments. This appears to be the same range observed by Gibilaro and Rowe (1974). The parameter λ_{Ds} also was usually <1, but it occasionally was much greater in well-mixed conditions where λ_{ws} was small. Gibilaro and Rowe, on the other hand, reported that λ_{Ds} rarely exceeded 0.1. Thus the typical magnitudes of λ_{Ds} may be different betweem large- and small-particle systems.

5.4 Interpretation of the Transient Data

For transient segregation conditions, the assumptions of the modified Gibilaro-Rowe model yield the following partial differential equation for the bulk phase:

$$\lambda_{Ds} \frac{\partial^2 v_J^B}{\partial z^2} + (\lambda_{ws} + 1 - 2\, v_J^B) \frac{\partial v_J^B}{\partial z} = \frac{\partial v_J^B}{\partial \Theta} \qquad (5.21)$$

where $\Theta = k_s t/H_s$, representing a dimensionless time coordinate. It is assumed that the wake phase is relatively small, Eq. 5.21 should approximate the complete transient segregation behavior of a binary solids system when it is integrated with respect to the proper initial and boundary conditions. The latter can be expressed as

$$\text{at } z=0,\ v_{Jo}^B\ (1 - v_{Jo}^B) + \lambda_{Ds} \left.\frac{\partial v_J^B}{\partial z}\right|_{z=0} = \left.\frac{\partial v_J^B}{\partial \Theta}\right|_{z=0} \tag{5.22a}$$

and at $z=1$,

$$\lambda_{ws}\ (v_{Jo}^B - v_{J1}^B) - \lambda_{Ds} \left.\frac{\partial v_J^B}{\partial z}\right|_{z=1} + v_{J1}^B\ (1 - v_{J1}^B) = \left.\frac{\partial v_J^B}{\partial \Theta}\right|_{z=1} \tag{5.22b}$$

Three initial conditions which are convenient from an experimental viewpoint are the segregated bed, the inverted bed, and the well-mixed bed. These are represented, respectively, by

$$v_J = 0 \text{ for } z > \overline{v}_J \text{ and } v_J = 1 \text{ for } z \leq \overline{v}_J\ , \tag{5.23a}$$

$$v_J = 1 \text{ for } z > \overline{v}_J \text{ and } v_J = 0 \text{ for } z \leq \overline{v}_J\ , \tag{5.23b}$$

and

$$v_J = \overline{v}_J \text{ for all } z\ . \tag{5.23c}$$

To evaluate the transient experimental results, I integrated Eq. 5.21 assuming that the parameters λ_{Ds} and λ_{ws} were constant and that the height of the splash zone was negligible. The nonlinear, non-homogeneous form of Eq. 5.21 makes analytical solution extremely difficult, and I found it most convenient to develop a numerical solution based on the Crank-Nicholson method described by Lapidus (1960). In order to integrate each case of interest, the steady-state λ_{Ds} and λ_{ws} were used. Matching the experimentally observed behavior with the results of the numerical integration allowed me to make conclusions about the order of magnitudes of the parameters k_s, D_s, and w, as well as the suitability of Eq. 5.21 for simulating transient segregation behavior.

Figures 5.8 and 5.9 illustrate the integration results for the acrylic-acrylic and glass-glass systems, respectively. I found it convenient to plot the mixing index and the bed composition at two bed levels as function of the dimensionless time, Θ. The experimentally observed points at known times were located on these plots by their vertical coordinates as indicated by the symbols. The corresponding dimensionless times were then known, and k_s, D_s, and w_s estimated from $k_s = H_s\Theta/t$, $D_s\ k_s\ H_s$, and $w_s = \lambda_{ws}\ A_b\ k_s(1-\varepsilon_s)$. Table 5.6 summarizes the results of such analyses for some of the glass-glass,acrylic-acrylic, and acrylic-polypropylene experiments. The parameter estimates based on shorter times tended to be less than those based on longer times. This may be due to non-ideality in starting the experiment (i.e., the actual initial conditions may be somewhat different than those assumed) or due to variations in the state of fluidization and the parameters during the

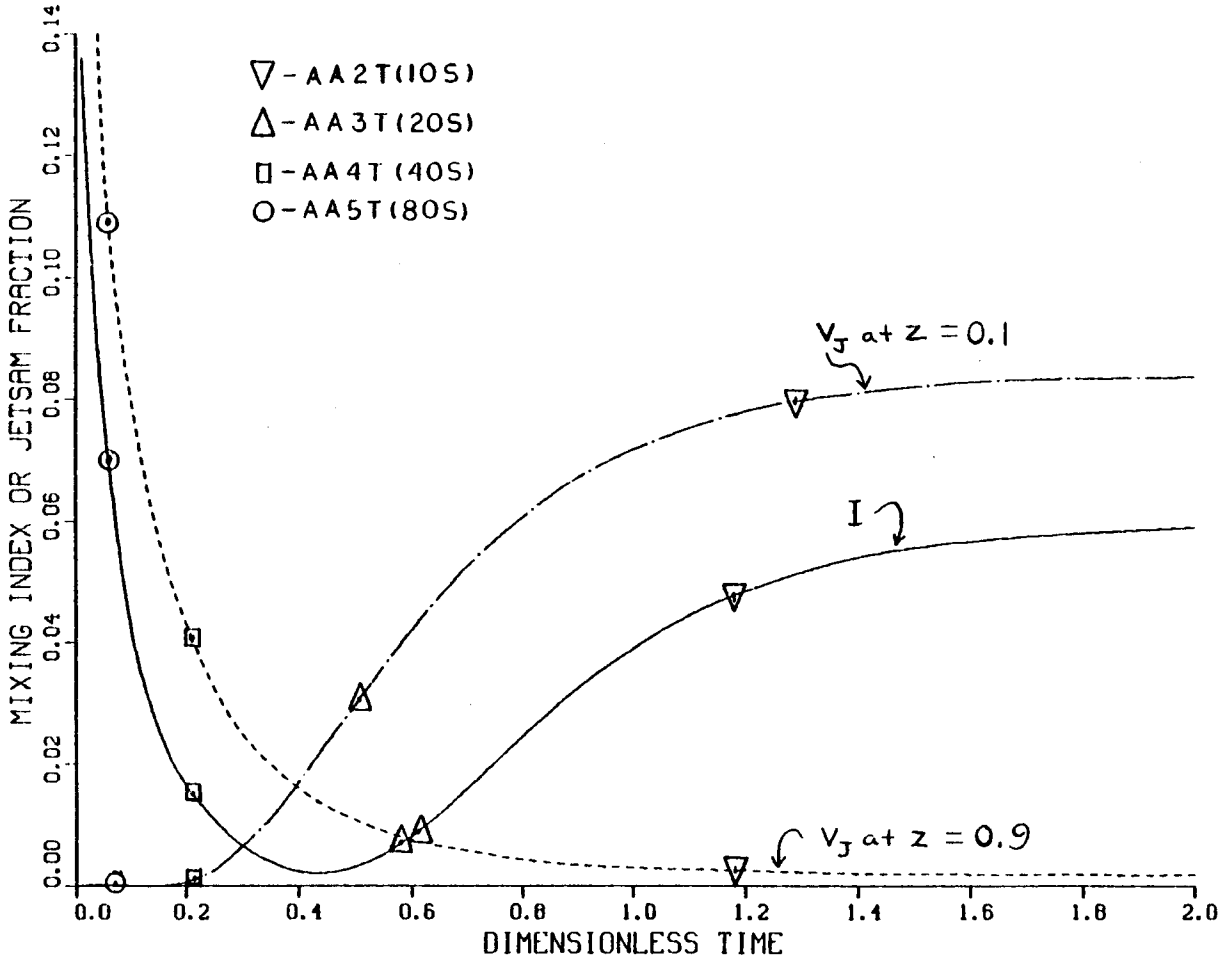

Figure 5.8. Comparison between the observed transient behavior and that predicted by the modified Gibilaro-Rowe model for the acrylic-acrylic system.

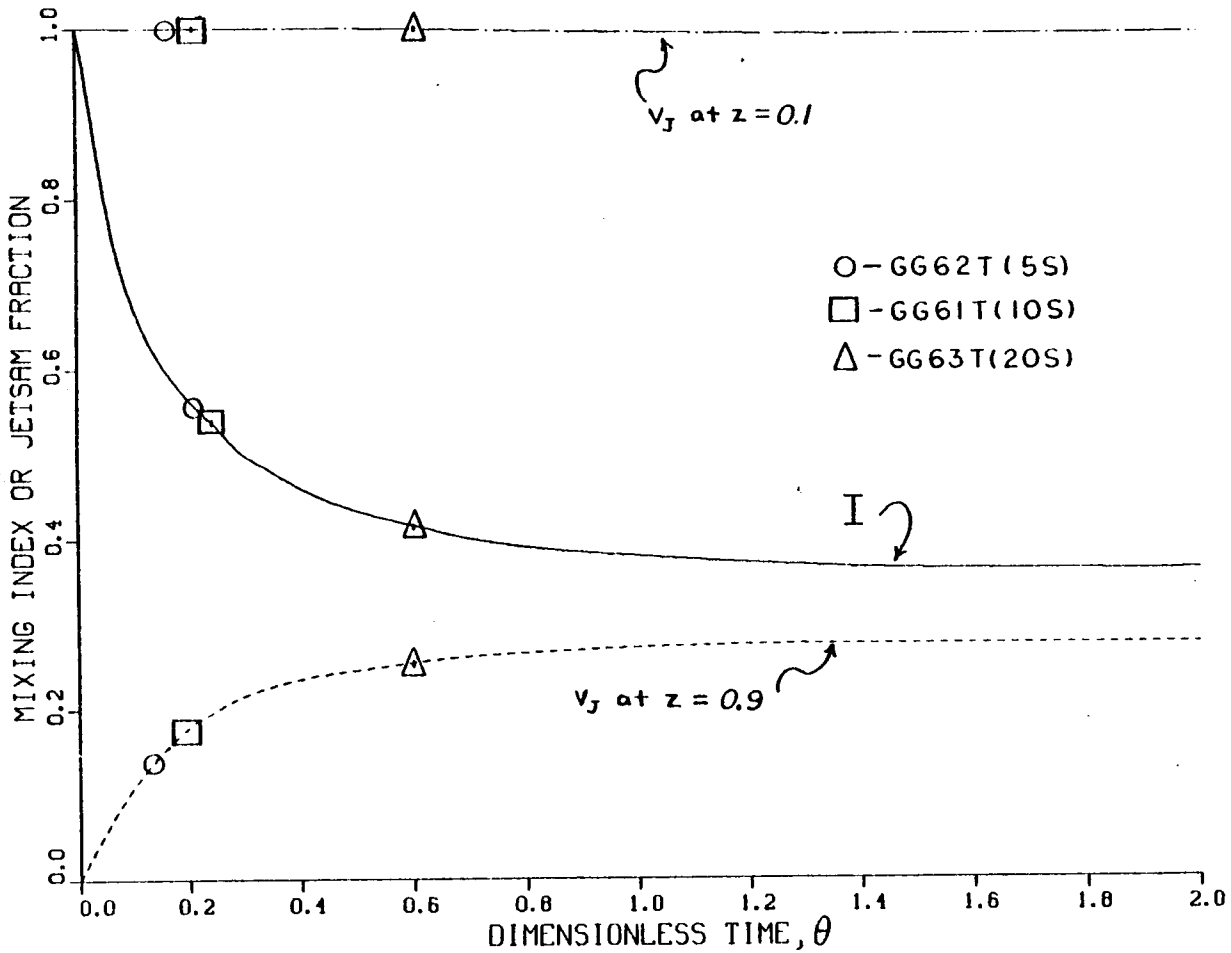

Figure 5.9. Comparison between the observed transient behavior and that predicted by the modified Gibilaro-Rowe model for the glass-glass system.

Table 5.6. Results of the comparison between the transient experiments and the numerical integration of Eq. 5.21

Run No.	λ_{Ds}	λ_{ws}	Time (s)	θ^*	k_s (cm/s)	D_s (cm^2/s)	w_s (cm^3/s)
AA-1	0.130	0.010					
AA-2T	0.130	0.010	10	0.057	0.15	0.50	0.068
AA-3T	0.130	0.010	20	0.215	0.27	0.89	0.12
AA-4T	0.130	0.010	40	0.568	0.36	1.2	0.16
AA-5T	0.130	0.010	80	1.19	0.38	1.3	0.17
GG-49	0.069	0.230					
GG-61T	0.069	0.230	10	0.215	0.29	0.27	3.0
GG-62T	0.069	0.230	5	0.175	0.48	0.45	5.0
GG-63T	0.069	0.230	20	0.600	0.41	0.39	4.3
AP-10	0.120	0.0					
AP-11T	0.120	0.0	10	0.656	2.0	7.3	0.0

*Estimated by averaging values for I, $v_J\big|_{z=0.10}$, and $v_J\big|_{z=0.90}$.

transient. Note also that significant variations in parameter magnitude occurred between systems. As might be expected, the strongly segregating system (AP) appeared to have a much larger segregation parameter.

Another important point illustrated by Figures 5.8 and 5.9 is that the initial conditions produced unique transient profiles in the mixing index. The segregated and well-mixed initial conditions produce mixing index profiles that asymptotically approach the final value, while the inverted initial condition has a profile that "overshoots" through a minimum and then approaches the final value. In practice, it appears that the inverted initial condition is easier to analyze with the procedure used in this study, because the higher slope over most of the profile makes it easier to precisely locate a specific Θ value from its vertical coordinate.

5.5. Interpretation of the Pressure Profiles

The success of the Gibilaro-Rowe approach in representing the relative separation of different types of particles makes it seem reasonable that a similar approach might be followed in representing the axial distribution of emulsion phase and voids (bubbles) in a single component bed. In fact, this method has already been applied to voidage distributions in fast fluidized beds by Youchou and Kwank (1980) with apparent success. In bubbling beds the voids do not generally participate in a large-scale circulation pattern, and it might also be reasonable to assume that the segregation of solids and voids might follow the behavior represented by Eq. 5.13. If these assumptions are indeed valid, then the steady-state distribution of emulsion phase would be given by

$$v_p = \frac{1}{1 + be^{z/\lambda_p}} , \qquad (5.24)$$

where

v_p = the volume fraction of emulsion phase,

λ_p = a dimensionless dispersion/separation parameter, and

b = a constant determined by the boundary conditions.

The two-phase model requires that the pressure drop over a slice of the bed be proportional to the mass of solids in that slice, and if there is only one component, then

$$\frac{dP}{dz} \alpha v_p \qquad (5.25)$$

Integrating Eq. 5.25 and "normalizing" the result by dividing by the overall bed pressure drop gives

$$P_r = \lambda_p \ln (1/b + e^{z/\lambda_p}) - z , \qquad (5.26)$$

where

P_r = gauge pressure/ΔP_{bed} and

$b = 1/(e^{1/\lambda_p} - 1)$.

Thus the solids distribution has been transformed into a normalized pressure profile.

Figure 5.10 illustrates Eq. 5.26 for varying values of λ_p. Qualitatively at least, these profiles look very similar to the experimental results. A more quantitative comparison was made by doing a "least-squares" fit for each experimental run. Two interesting facts emerged from these analyses: (1) in many cases the value of λ_p seemed to change abruptly at $z = 1$ ($y = H_{mf}$) and (2) the model seemed to fit binary beds as well as single-component beds. Table A-8 summarizes the "least-squares" results. Next to each run number is the optimum value

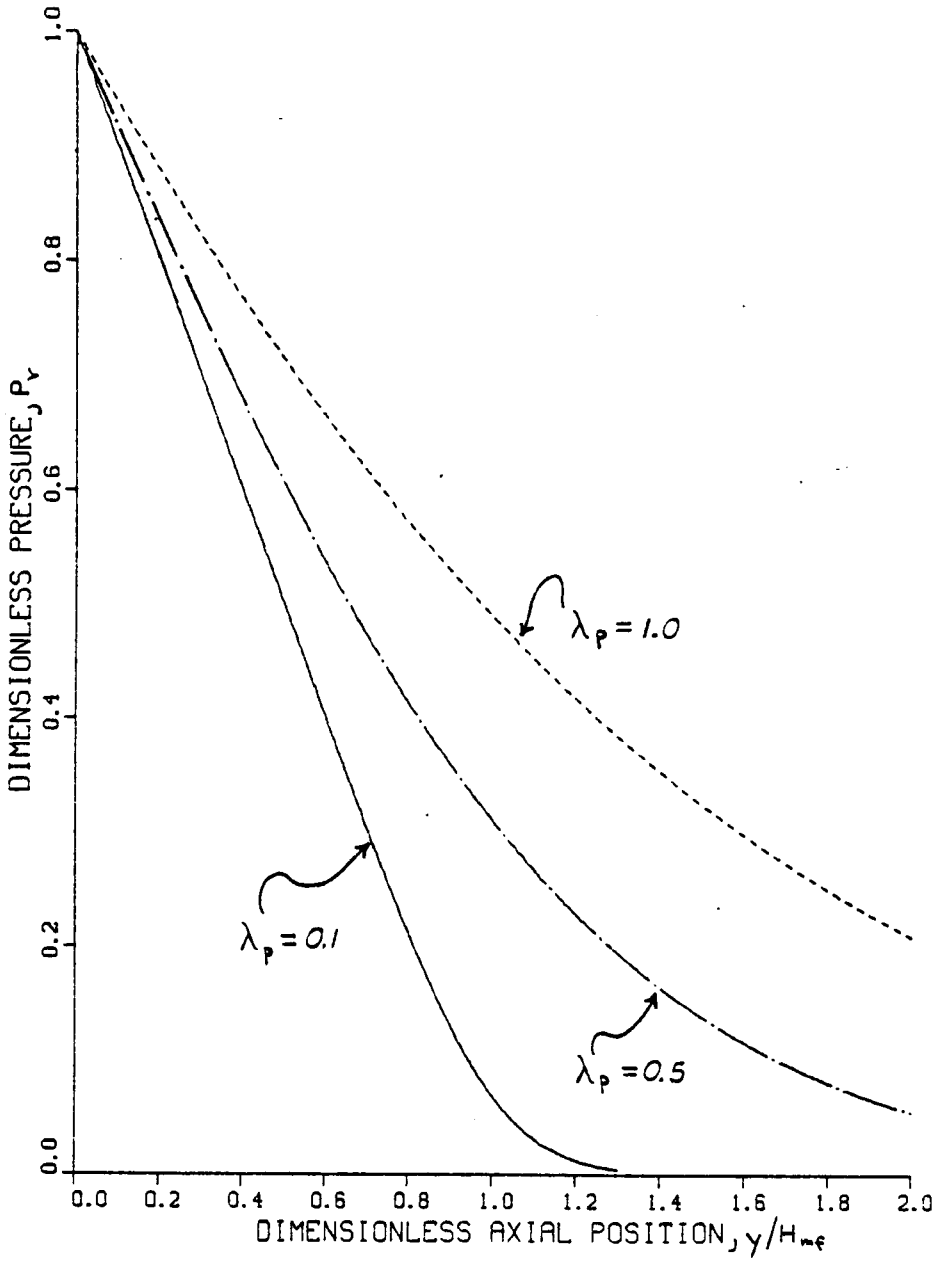

Figure 5.10. Pressure profiles predicted by Eq. 5.26 for varying dispersion parameter, λ_p.

of the dispersion/separation parameter below z=1, λ_p, and also the optimum value above z=1, λ_p'. The columns under the headings MSE, RMSE,and n are the mean squared error, root mean squared error (effectively an average error), and the number of measurement points, respectively, Figures 5.11 through 5.13 graphically illustrate fits for some typical cases.

Tables 5.7 through 5.9 summarize typical variations in λ_p and λ_p' as bed operating conditions are changed. As expected, both λ_p and λ_p' increased sharply with increasing air velocity. Increasing bed depth also appeared to increase the effective parameter values. The upper parameter, λ_p', appeared to increase consistently as bed internals were removed, but the effect on λ_p appeared to be more complicated.

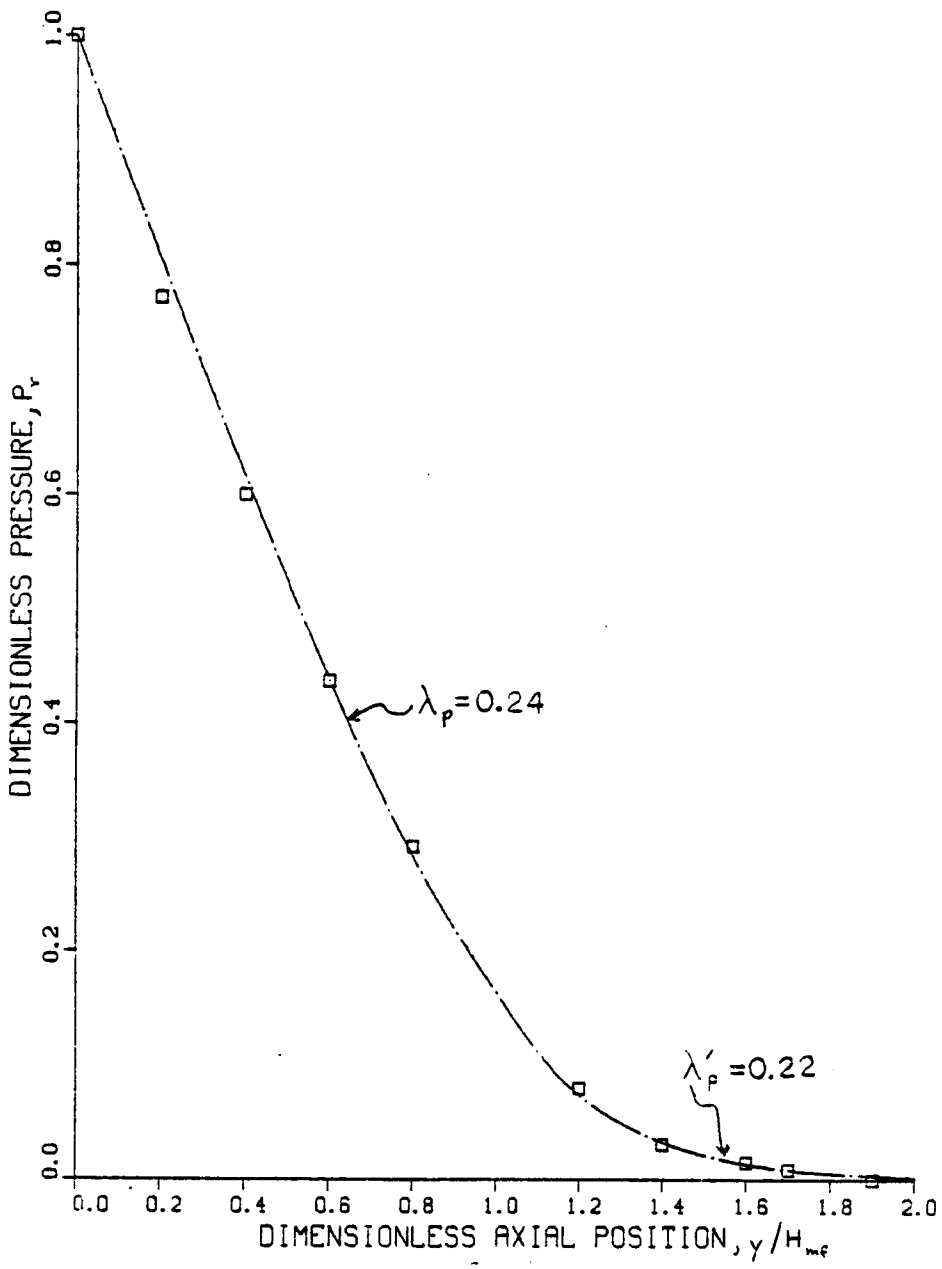

Figure 5.11. Comparison of measured pressure profile for run A-3B with "best-fit" prediction of the solid-void-distribution model.

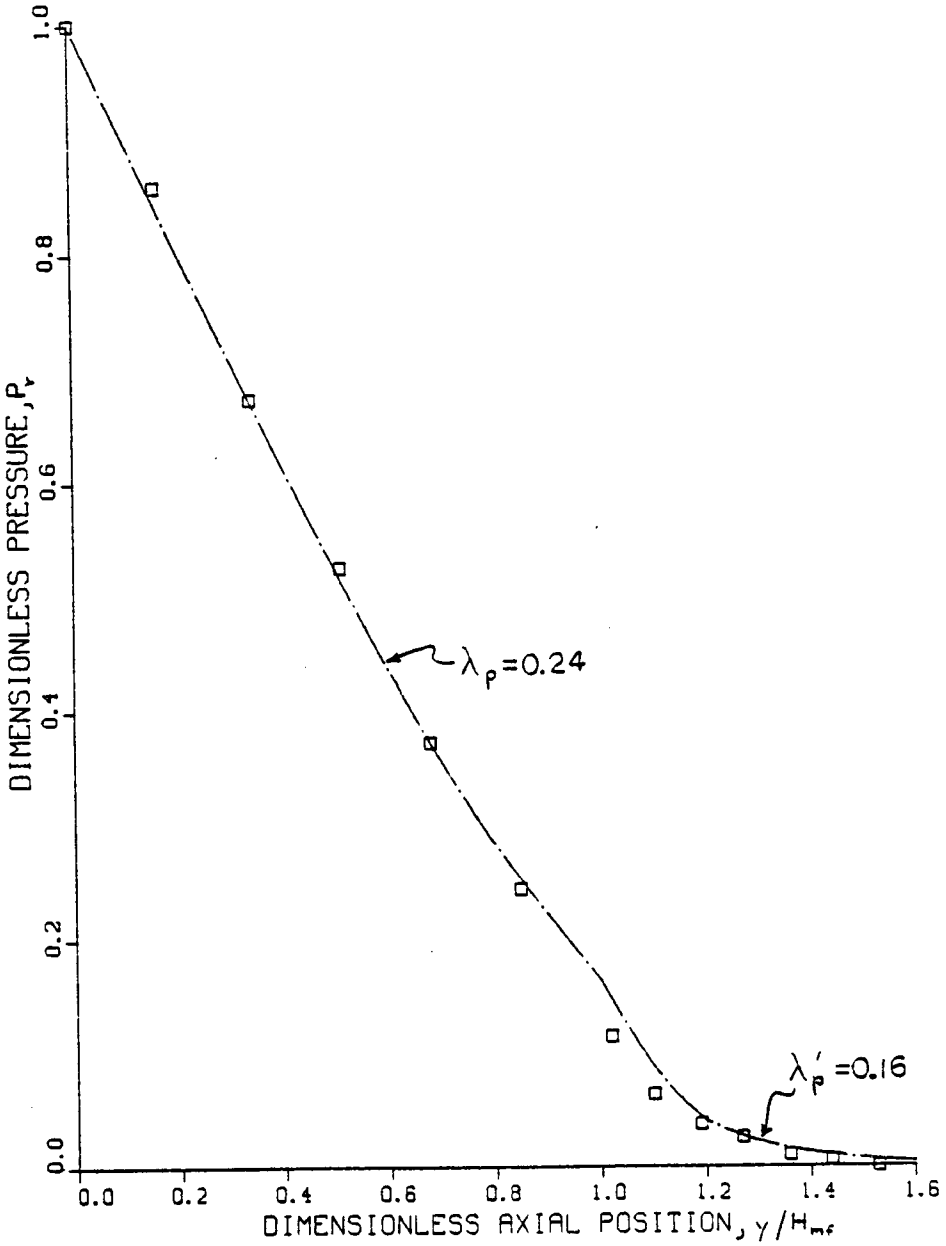

Figure 5.12. Comparison of measured pressure profile for run AP-3 with "best-fit" prediction of the solid-void distribution model.

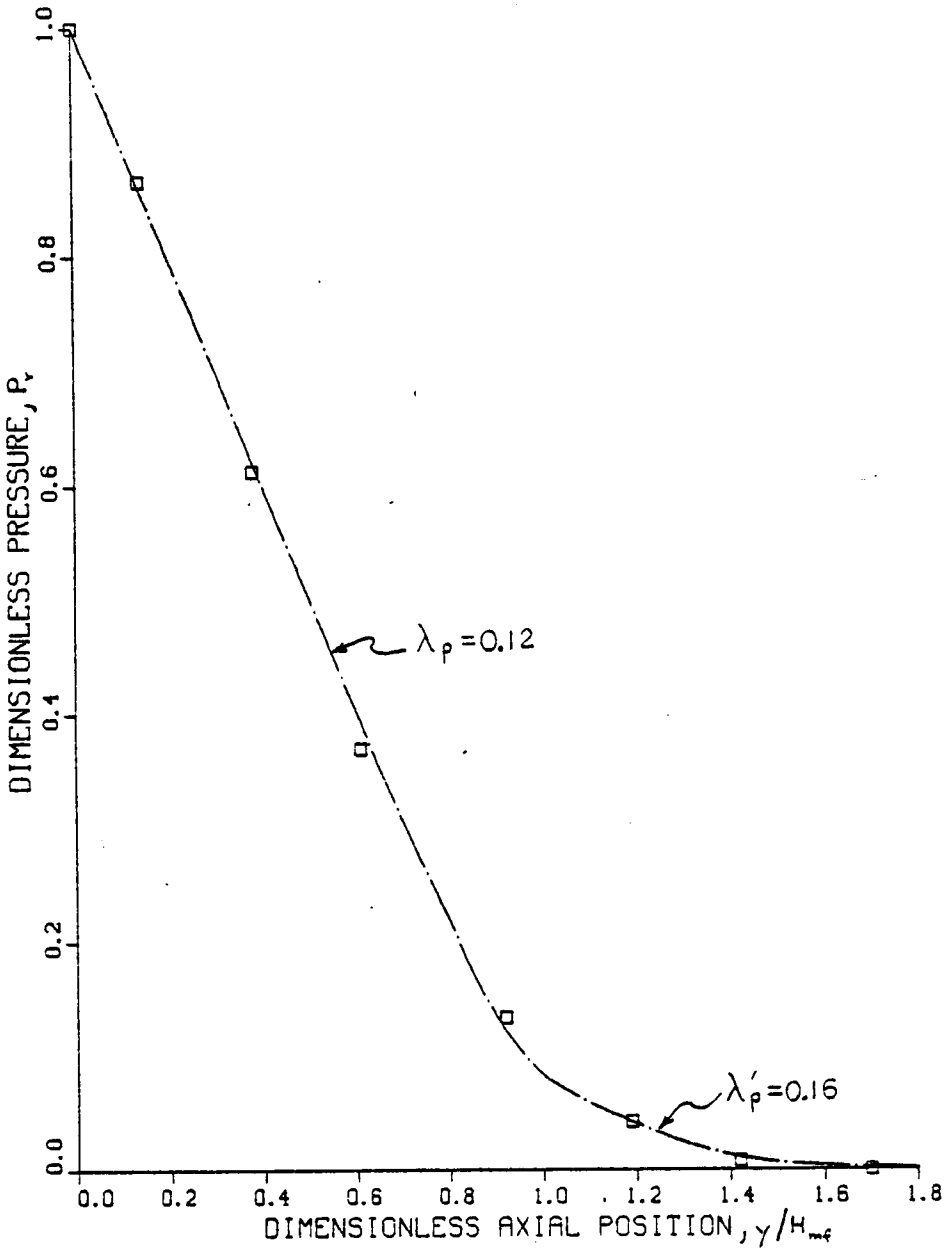

Figure 5.13. Comparison of measured pressure profile for run LC-13 with "best-fit" prediction of the solid-void distribution model.

Table 5.7. Effect of velocity on the parameters of the mass distribution model

Run No.	u_o (m/s)	λ_p	λ_p'
A-2A	1.69	0.0	
A-2B	2.53	0.49	0.46
A-2C	3.38	0.85	0.76
AP-3	2.00	0.24	0.16
AP-1	2.40	0.40	0.32
AP-2	3.39	0.57	0.67

Table 5.8. Effect of bed height on the parameters of the mass distribution model

Run No.	H_s (cm)	λ_p	λ_p'
AP-1	30.0	0.40	0.32
AP-6	15.2	0.30	0.25
A-2B	24.9	0.49	0.46
A-3B	12.7	0.24	0.22

Table 5.9. Effect of bed internals on the parameters of the mass distribution model

Run No.	Internals		λ_p	λ_p'
A-2C	None	0.85	0.76	
A-4	Wire cylinders w no tubes		0.56	0.38
A-11	Wire cylinders w tubes		0.69	0.29
AP-7	None	0.47	0.50	
AP-8	Wire cylinders w no tubes		0.54	0.39
AP-10	Wire cylinders w tubes		0.62	0.35

6. IMPLICATIONS OF SOLIDS SEGREGATION FOR REACTOR PERFORMANCE

Segregation in fluidized beds is of concern in chemical reactor design because of its effect on the overall conversion. The first five sections of this study have dealt with the general segregation phenomena which can occur and how these can be modeled. This section combines segregation with fluidized bed reactor principles to illustrate how segregation can affect reactor performance. My intent here has been to focus on developing and illustrating the method by which segregation is accounted for, not to recommend specific correlations for reactor designs. As I have already shown, general correlations will not be possible until more is known about the relationship of bed conditions to the segregation parameters λ_w and λ_D.

6.1 First Order Reaction with One Active Solid Component

One reacting system of widespread interest is a first order reaction between a gas-phase component and a solid. Such a reaction is not uncommon in fluidized beds, where the solid component may be a catalyst or reactive solid which is diluted with another, inert solid. Perhaps the most generally useful method for making a differential mass balance on the reactive gas component in a fluidized bed is that described by Davidson and Harrison (1963). With this method, two first order, ordinary differential equations result for steady-state,

$$(1 - \beta) \frac{dC_p}{dy} + \beta \frac{dC_b}{dy} + \tilde{k}_a C_p / H = 0 \ , \qquad (6.1a)$$

and

$$\frac{dC_b}{dy} + (X/H)(C_b - C_p) = 0 \ , \qquad (6.1b)$$

where

C_p = the emulsion-phase concentration of the reactive gas component, [moles/volume of emulsion gas],

C_b = the bubble-phase concentration of the reactive gas component, [moles/volume of emulsion gas],

$\beta = 1-u_{mf}/u_o$ = the fraction of the gas flowing through the bubble phase, [-],

$\tilde{k}_a = k_a H_{mf}/u_o$ = dimensionless reaction constant, [-],

k_a = first order reaction rate constant, [1/T]

H_{mf} = the bed height at minimum fluidization, [L],

H = the expanded bed height, [L],

$X = QH/(u_b V_b)$ = gas interchange coefficient between the bubble and emulsion phase, [-],

Q = effective gas flow through the bubbles, [volume/T],

u_b = bubble rise velocity, [L/T],

V_b = volume of individual bubble, [volume].

Equations 6.1a and b assume that the two-phase theory holds, that the gas in both phases is in plug flow, that the bed expansion is uniform, that there is no volume change through the bed, and that the reaction is first order and occurs only in the emulsion phase. Equation 6.1a represents the differential reactive species mass balance over a slice of the bed containing both emulsion and bubble phases. Equation 6.1b represents a differential balance for the bubble phase only.

The effect of solids segregation can be incorporated into the reaction rate term by making $\tilde{k}_1$ a function of the local solids composition. For example, if the system can be considered binary and if the jetsam is the active solid component, then $\tilde{k}_a$ might be rewritten as

$$\tilde{k}_a = k'_a \, v_J \ , \tag{6.2}$$

where $\tilde{k}'_a$ = the dimensionless reaction constant for pure jetsam, [-]. If the bed is well-mixed, $v_J = \bar{v}_J$ = constant, and Eqs. 6.1a and 6.1b can be integrated per Davidson and Harrison (1963) by eliminating C_p to get

$$\frac{C_H}{C_o} = \frac{1}{(m_1 - m_2)} \left\{ m_1 e^{-m_2} \, [1 + m_2(\beta - 1)/X] - m_2 e^{-m_1} \, [1 + m_1(\beta - 1)/X] \right\} \tag{6.3}$$

where

C_o = reactor inlet gas concentration, [moles/unit gas volume],

C_H = reactor outlet gas concentration, [moles/unit gas volume],

$$m_1 = \{(X + \tilde{k}'_a \bar{v}_J) + [(X + \tilde{k}'_a \bar{v}_J)^2 - 4 \, \tilde{k}'_a \bar{v}_J \, X \, (1 - \beta)]^{1/2}\}/[2(1-\beta)] \ ,$$

and

$$m_2 = \{(X + \tilde{k}'_a \bar{v}_J) - [(X + \tilde{k}'_a \bar{v}_J)^2 - 4 \, \tilde{k}'_a \bar{v}_J \, X(1 - \beta)]^{1/2}\}/[2(1-\beta)] \ .$$

A completely segregated bed can be treated in a similar fashion, except that the effective bed height should correspond only to the lower jetsam layer, and $\bar{v}_J$ there would be equal to 1.

Note that the derivation of Eq. 6.3 assumes that the bed properties such as β do not change with axial position. For a well-mixed bed, this is reasonable, but a segregated bed could have a significant change in bubbling and expansion characteristics over the length. A more accurate model would require knowledge of how local composition affects these. In spite of these limitations, it is instructive to compare the results for well-mixed and segregated beds to see the effect of particle distribution alone. Figure 6.1 illustrates the ratio C_H/C_o as a function of $\tilde{k}_a'$ for well-mixed and segregated beds having the fluidization parameters X=3 and β=0.8 with $\bar{v}_J$=0.5. Note that the difference between the well-mixed and segregated beds increases as the reaction rate parameter $\tilde{k}_a'$ increases.

In the general case, v_J will not be constant, and could vary with axial position according to the Gibilaro-Rowe model, i.e., $v_J = g(v_w, \lambda_w, \lambda_D, z)$ per Eq. 2.13. Ignoring the wake phase ($v_w = 0$) and ignoring non-uniform bed expansion, Eqs. 6.1a and 6.1b can be combined to give

$$(1-\beta)\frac{d^2C_b}{dz^2} + [X + \tilde{k}_a' v_J(\lambda_w,\lambda_D,z)]\frac{dC_b}{dz} + \tilde{k}_a' X v_J(\lambda_w,\lambda_D,z) C_b = 0 \qquad (6.4a)$$

and

$$C_p = \frac{1}{X}\frac{dC_b}{dz} + C_b \ , \qquad (6.4b)$$

where, in this case, z = y/H.

Equation 6.4a can be integrated numerically with the following boundary conditions:

$$\text{at } z = 0,\ C_b = C_o \qquad (6.5a)$$

and

$$\text{at } z = 0, \frac{dC_b}{dz} = 0 \ . \tag{6.5b}$$

Equation 6.4a can also be solved approximately by noting that the term $(1-\beta)$ is generally relatively small compared to the term $[X + \tilde{k}'_a v_J]$ (especially for large $\tilde{k}'_a$), and thus Eq. 6.4a can be approximated by

$$[X + \tilde{k}'_a v_J(\lambda_w,\lambda_D,z)] \frac{dC_b}{dz} + \tilde{k}'_a \ X \ v_J(\lambda_w,\lambda_D,z) \ C_b = 0 \ . \tag{6.6}$$

Equation 6.5 can be integrated directly using the Gibilaro-Rowe expression for v_J (assuming constant λ_w and λ_D) to get

$$\frac{C_b}{C_o} = e^{-\mu} \ \xi^{-\delta} \ , \tag{6.7}$$

where

$$\mu = \tilde{k}'_a \ X \ az/(2q),$$

$$a = \lambda_w + 1 + P,$$

$$q = X + \tilde{k}'_a a/2,$$

$$\xi = (q + re^{\alpha z})/(q + r),$$

$$r = B_2[\tilde{k}'_a(P - \lambda_w - 1)/2 - X],$$

$$\alpha = P/\lambda_D,$$

$$\delta = \tilde{k}'_a X \ (bq - ar)/(2 \ \alpha \ qr), \text{ and}$$

$$b = B_2 \ (P - \lambda_w - 1) \ .$$

Replacing z in the above equation with 1 gives C_{b_1}/C_o.

Equation 6.4b can be used with 6.6 to get an expression for the particulate phase concentration

$$\frac{C_p}{C_o} = \frac{C_b}{C_o}\left[\frac{-\tilde{k}'_a a}{2q} - \frac{\tilde{k}'_a}{2}\left(\frac{bq - ar}{q}\right)\left(\frac{e^{\alpha z}}{q + re^{\alpha z}}\right) + 1\right] . \qquad (6.8)$$

Combining the bubble and particulate-phase gas streams at the reactor exit gives the final effluent

$$C_H/C_o = \beta(C_{b1}/C_o) + (1 - \beta)(C_{p1}/C_o) . \qquad (6.9)$$

Example solutions for $\lambda_w = 0.10$, $\lambda_D = 0.091$, with $\bar{v}_J = 0.5$, $X = 3$, and $\beta = 0.8$ were obtained by means of Eqs. 6.7 through 6.9 and by numerical solution of Eq. 6.4a. These results are shown with the segregated and well-mixed limits in Figure 6.1. The values chosen for λ_w and λ_D are within the ranges observed in this study. Note that the effect of segregation is most pronounced at large values of $\tilde{k}'_a$. Above $\tilde{k}'_a > 10$, the reactor performance is largely independent of $\tilde{k}'_a$. The effect of segregation became insignificant for $\tilde{k}'_a < 1$.

6.2 First Order Reactions - Single Generating Solid, Single Reacting Solid

Some fluidized bed reactors, such as fluidized bed combustors, contain "generating" solids (e.g., high sulfur coal which releases sulfur dioxide) and "reacting" solids (e.g., limestone or dolomite sorbent). In this case, segregation affects both the rate of introduction and the rate of consumption of the active gaseous component. If it is assumed that the generation rate per unit volume of emulsion phase is proportional only to the flotsam volume fraction, Eqs. 6.1a and b can be rewritten as

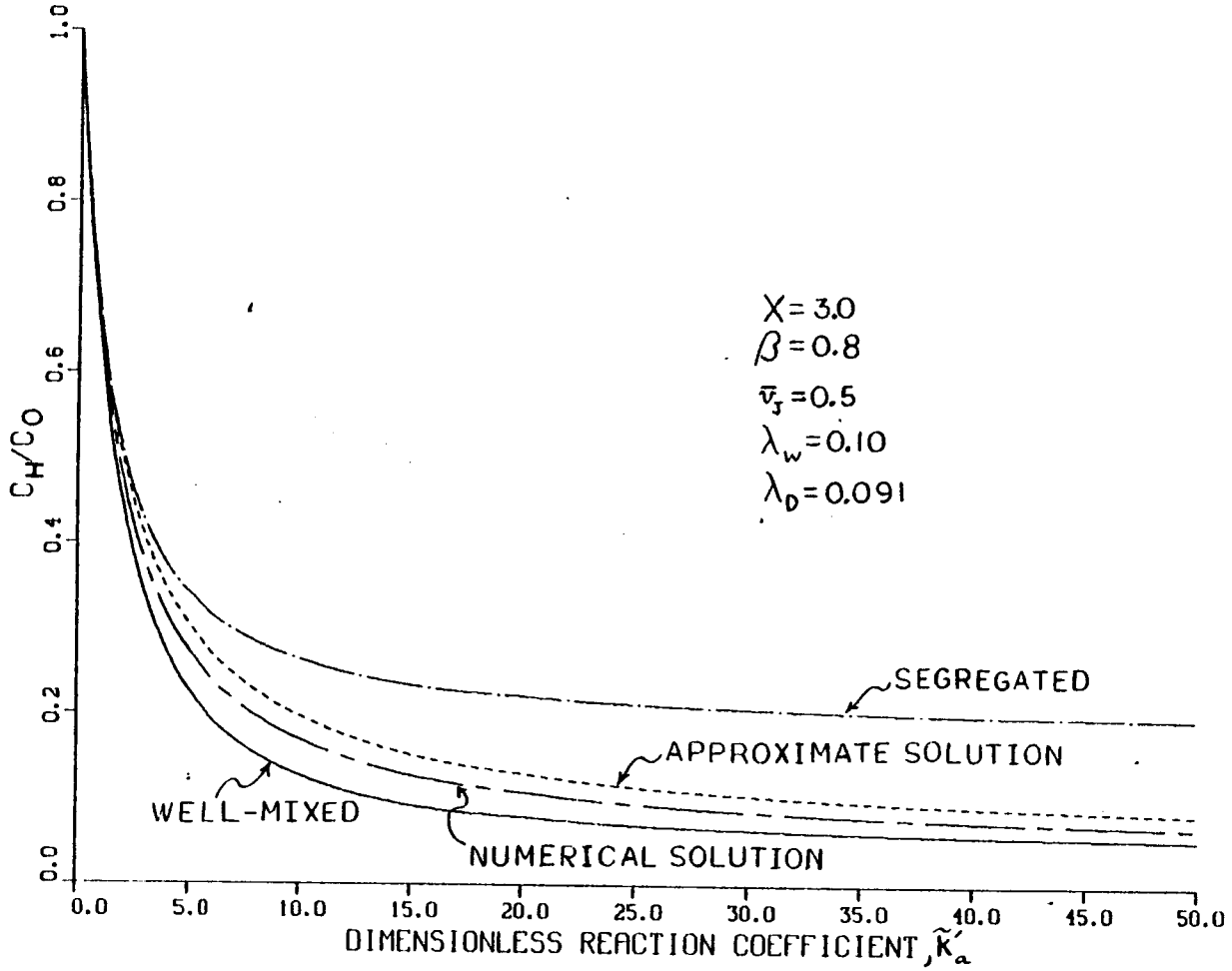

Figure 6.1. Effect of segregation and the dimensionless reaction coefficient on the performance of a fluidized bed reactor with a first-order reaction between the jetsam and an active gas species.

$$(1-\beta)\frac{dC_p}{dz} + \beta\frac{dC_b}{dz} + \tilde{k}'_a v_J C_p - \tilde{k}'_g (1-v_J) = 0 \qquad (6.10a)$$

and

$$\frac{dC_b}{dz} + X(C_b - C_p) = 0 \; . \qquad (6.10b)$$

where

$z = y/H$, [-],

$\tilde{k}'_g$ = generation rate factor = $\tilde{k}_g H_{mf}/u_o$, [moles/volume of gas],

and

$\tilde{k}_g$ = generation reaction rate constant, [moles/volume of emulsion phase/T].

The term $\tilde{k}'_g (1 - v_J)$ represents the rate of generation per unit volume of gas passing through the bed at level z, and, similarly, the quantity $\tilde{k}'_g(1 - \bar{v}_J)$ would be the overall generation of the active species in the bed. Dividing both Eqs. 6.10a and b by $\tilde{k}'_g(1 - \bar{v}_J)$ gives

$$(1-\beta)\frac{d\phi_p}{dz} + \beta\frac{d\phi_b}{dz} + \tilde{k}'_a v_J \phi_p - (1-v_J)/(1-\bar{v}_J) = 0 \qquad (6.11a)$$

and

$$\frac{d\phi_b}{dz} + X(\phi_b - \phi_p) = 0$$

where

ϕ_p = a dimensionless emulsion-phase composition = $C_p/[\tilde{k}'_g(1 - \bar{v}_J)]$, [-], and

ϕ_b = a dimensionless bubble-phase composition = $C_{b/}[\tilde{k}'_g(1 - \bar{v}_J)]$, [-].

Note that ϕ_p and ϕ_b represent the ratios of the actual emulsion- and bubble-phase concentrations to the average concentration which would be produced at the exit of the bed if there were no consumption reaction. The average of ϕ_b and ϕ_p at the reactor exit ($\phi_t = \phi_p(1 - \beta) + \phi_b\beta$) represent effective "performance" of the reactor in producing the active component, or, conversely, 1 minus the effective retention. Thus, reactor performance (retention) is seen to be a function of the fluidization parameters, β and X, the segregation profile, the absorption coefficient, $\tilde{k}'_a$, and the overall jetsam fraction.

If the jetsam profile is given by the Gibilaro-Rowe model, Eqs. 6.11a and b are extremely difficult to solve analytically. Numerical solution is relatively straightforward, however, and Figure 6.2 illustrates the calculated reactor performance for varying λ_D and $\tilde{k}'_a$ with $\lambda_w = 0$, X = 3.0, $\beta = 0.8$, and $\bar{v}_J = 0.95$. Note that in these simulations, λ_D is assumed to be constant over the entire bed length. As expected, higher values for λ_D produce lower ϕ_t (i.e., higher net retention of the reactive species. Most of the effect of λ_D on reactor performance is confined to the region $0 < \lambda_D < 1.0$. Above $\lambda_D = 1$, reactor performance is essentially that of a well-mixed bed. At $\lambda_D = 0$, the bed is completely segregated.

6.3 Additional Comments on Practical Application of Segregation Models to Reactor Performance Calculations

As has already been discussed, several key assumptions must be made to reach the solutions described in Sections 6.1 and 6.2. Of these

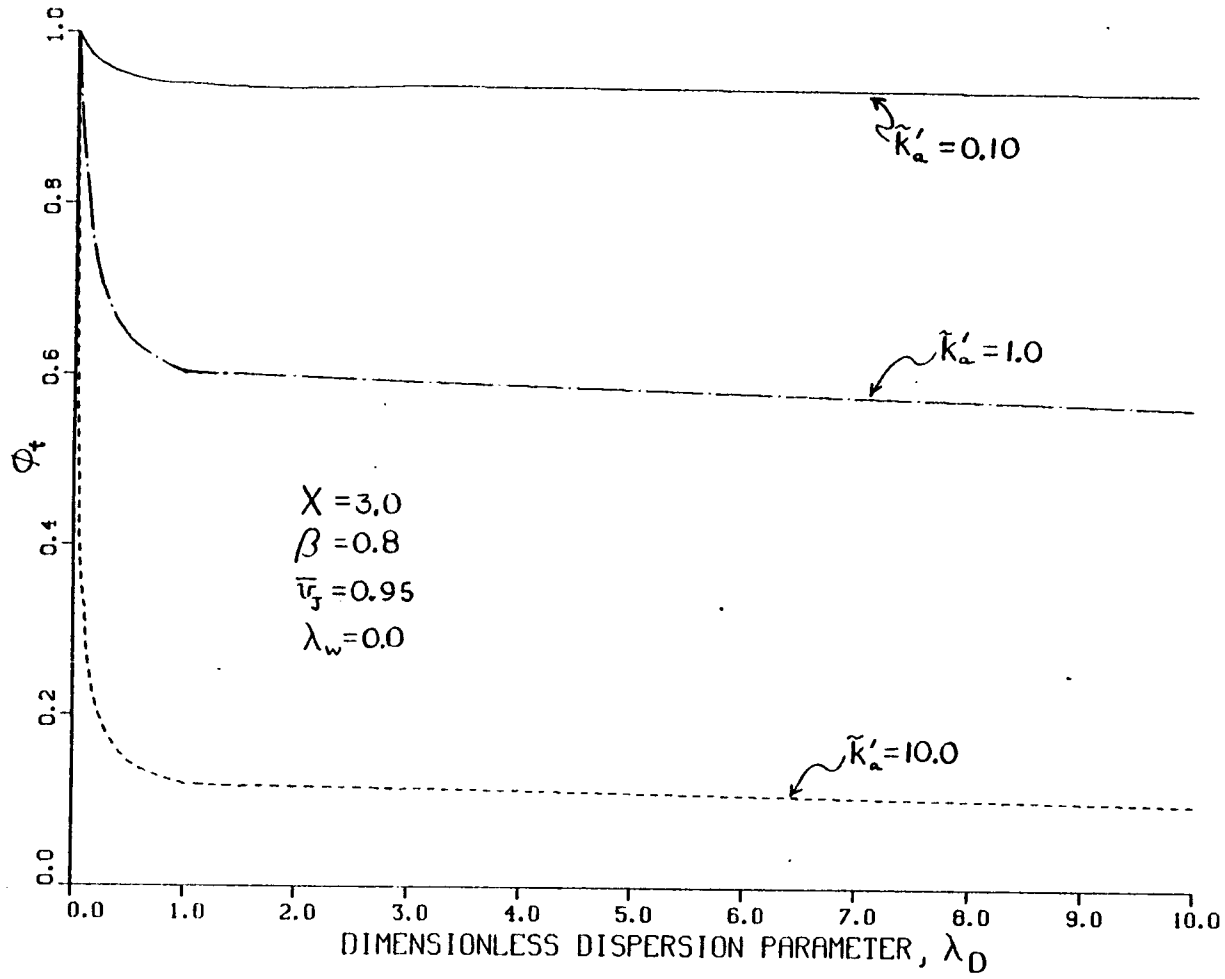

Figure 6.2. Effect of segregation and dimensionless reaction coefficient on the performance of a fluidized bed reactor with reactive species generation by the flotsam and first-order consumption reaction with the jetsam.

assumptions, probably the most inaccurate are that the bed expansion is uniform and that the segregation and fluidization parameters such as λ_w, λ_D, X and β do not vary with position. More accurate models would require development of axial profiles for voidage, X, and β. A basis for modeling voidage profiles is discussed in Section 5.5. The separation of the bed into bulk and splash zones is a start on dealing with variations in λ_w and λ_D. Models for variations in X and β will require fundamental measurements of interphase gas transfer and minimum fluidizing velocity as both position and solids composition varies.

One important case in which the variations in fluidization parameters are not very important is when the bed is primarily composed of one component (e.g. $\bar{v}_J < 0.1$ or $\bar{v}_J > 0.9$). Fluidized bed combustion of high-sulfur coal falls into this category. Typically, the coal/char volume fraction in the bed is less than 5%, and the bulk of the bed consists of limestone or dolomite sorbent. The fluidization behavior in this case is largely determined by the sorbent properties. Segregation in such a system appears to be described reasonably well by the dispersion-segregation model described in Section 5.2, although λ_D may vary between the bulk bed and the splash zone.

7. CONCLUSIONS AND RECOMMENDATIONS

7.1 Conclusions

While this study must be considered preliminary, the following important conclusions can be drawn from the results.

1. The extent of particle segregation can be appreciable in gas-fluidized beds of large particles. The same basic patterns appear to occur in large-particle beds as occur in small-particle beds. Differences between large and small particles appear to be in degree rather than in kind.

2. Two basic types of segregation occur in two-component beds. The first type, designated as Region 1 segregation, occurs when the superficial gas velocity is less than the jetsam minimum fluidizing velocity (u_{mfJ}) but greater than the flotsam minimum fluidizing velocity (u_{mfF}). The second type, designated as Region 2 segregation, occurs when the gas velocity is greater than the minimum fluidizing velocity of both components but less than the terminal velocity of the flotsam (u_{tF}).

3. In Region 1 segregation, the bed usually consists of a jetsam-rich unfluidized zone and a flotsam-rich fluidized zone. The relative sizes of the two zones and their compositions depend on the gas velocity, the particle densities and sizes, the overall bed composition (i.e., the relative amounts of jetsam and flotsam), and the initial condition. Hysteresis effects occur because of the "trapping" of flotsam particles in the defluidized zone.

4. In Region 2 segregation, a variety of axial composition profiles can occur, depending on the gas velocity, the particle densities and sizes, the type of bed internals, the bed height, and the overall bed composition. The final steady-state profile does not depend on the initial condition. Region 2 profiles can usually be considered as consisting of combinations of three zones: (1) a lower, high-jetsam zone, (2) a well-mixed region, and (3) an upper, high flotsam zone. In jetsam-lean beds, the upper zone tends to be much less distinct, and the lower and middle zones predominate. In beds of roughly equal jetsam and flotsam properties, all three zones are frequently visible. Jetsam-rich beds exhibit a predominant upper zone and a gradually decreasing flotsam concentration with depth. Approaching the perfectly segregated or well-mixed limits, the zones merge into two or one, respectively.

5. A mixing index $I = \sum_{i=1}^{n} v_{si} (v_{Ji} - \bar{v}_J)^2/[(\bar{v}_J)(1 - \bar{v}_J)]$ is a good indicator of the degree of segregation and provides a convenient means of quantifying the effect of parameter changes on segregation. This index represents the variance of the jetsam composition along the bed height and is more accurate than the mixing/segregation indices used previously for small particles. The index I trends generally downward with increasing gas velocity until it reaches a minimum at some velocity between u_{mfJ} and u_{tF}. However, prominent local maxima and minima appear to occur in the index at velocities where there are abrupt flow transitions; e.g., the velocity where there is a change from channeling to large-scale bubbling. These maxima and minima, which might be loosely described as mixing/segregation "resonances," have not been reported by others.

6. The basic shapes of the steady-state, large-particle segregation profiles appear to be analogous to those observed in small-particle experiments. The Region 2 profiles and the profiles in the fluidized portion of the beds in Region 1 were fit to within experimental error using a modified form of the segregation model originally proposed by Gibilaro and Rowe (1974). This model has two key dimensionless parameters, λ_D and λ_w, which represent, respectively, the importance of axial dispersion and large-scale circulation relative to segregation. A third parameter, v_w, which represents the fraction of the bed included in the wake phase, was found to be effectively zero. The profile resulting from this model (with $v_w \simeq 0$) is given by

$$v_J = \frac{1}{2}\left[\lambda_w + 1 + P\left(\frac{1 + B_2 e^{zP/\lambda_D}}{1 - B_2 e^{zP/\lambda_D}}\right)\right],$$

where

$$P = [(\lambda_w + 1)^2 - 4\,\lambda_w v_{Jo}]^{1/2} \text{ and}$$

$$B_2 = \frac{(\lambda_w + 1 - 2v_{Jo} + P)}{(\lambda_w + 1 - 2v_{Jo} - P)}.$$

7. The observed ranges for the two parameters λ_D and λ_w were 0 to 12.4 and 0 to 1.47, respectively. The variation in λ_w was similar to that reported by Gibilaro and Rowe (1874), but the larger values of λ_D were much greater than those reported by Gibilaro and Rowe. This implies that bulk phase dispersion is more important in large-particle beds than small-particle beds. The large values of λ_D appeared to occur primarily in beds where the overall fraction of flotsam was small in

comparison to the fraction of jetsam (e.g., an overall jetsam volume fraction of greater than 0.90).

8. The Gibilaro-Rowe model appears to be valid for profiles measured in a slumped bed, even though the bed expansion during fluidization is non-uniform. This observation appears to be consistent with the basic assumptions of the Gibilaro-Rowe model, and the governing differential equation can be expressed directly in terms of static-bed coordinates.

9. In some cases (e.g., when the overall flotsam fraction is small or when large-scale circulation is minimal), the convection parameter in the Gibilaro-Rowe model can be eliminated to yield a simplified expression for the profile,

$$v_J = \frac{1}{1 + A\, e^{z/\lambda_D}} ,$$

where

$$A = (1 - v_{Jo})/v_{Jo} = [e^{(\bar{v}_J - 1)/\lambda_D} - 1]/[1 - e^{\bar{v}_J/\lambda_D}] .$$

This same form occurs elsewhere in other natural phenomena such as Brownian motion in a gravitational field. The similarity suggests that useful analogies and generalizations may be possible.

10. In some profiles the upper zone is particularly pronounced, and the jetsam gradient is significantly steeper than below. This upper zone, which frequently comprises roughly 20% of the bed, appears to be composed of solids from the splash region. The upper-zone profile can be described with the simplified (no-convection) form of the Gibilaro-Rowe model. The modified model which is needed to describe the profile in such a bed can be written as

$$v_J = v_{J\ell} \langle z_c - z \rangle + v_{Ju} \langle z - z_c \rangle \ .$$

The terms $v_{J\ell}$ and v_{Ju} are the Gibilaro-Rowe profiles calculated with the appropriate parameters for the upper and lower zones, and $\langle\ \rangle$ represents the singularity function, which is 0 when its argument is <0 and 1 when its argument is ≥ 0. The value of the upper- and lower-zone dispersion parameters are usually different.

11. The overall solids and voidage distributions in the beds studied appear to follow an equation of the same basic form as the no-convection Gibilaro-Rowe model. Integration of this equation yields predicted pressure profiles which are remarkably similar to those observed. The best fits were obtained when two different values of the dispersion parameter were used, one value above $y = H_{mf}$ and one value below $y = H_{mf}$. Although this model was derived initially for a single-component bed, it appears to work for binary beds also.

12. The transient form of the Gibilaro-Rowe model seems to do a fairly good job of describing the transient segregation behavior observed, although the model parameters seem to change with time. Computer integrations can be used with transient profiles to estimate values for the dimensional Gibilaro-Rowe parameters, i.e., D, k, and w.

13. The Gibilaro-Rowe segregation model can be combined with a gas-species mass balance to predict fluidized-bed reactor performance. Sample results developed for simple cases appear to be reasonable. Jetsam-rich and jetsam-lean beds can probably be simulated fairly well, but, more fundamental information about the axial variation of

fluidization parameters such as β and X will probably be needed to adequately simulate highly segregated beds.

14. A long-range goal for future segregation studies should be the development of models or empirical correlations for predicting the dispersion parameter, λ_D, and the circulation parameter λ_W, in terms of particle properties such as relative sizes and densities and operational parameters such as the bed and particle Reynolds number. While such models cannot be derived solely from the present work, the present experimental data (comprised of 196 separate runs) should contribute significantly to the rather meager data base existing in the literature.

7.2 Recommendations for Future Work

Future gas-fluidized bed segregation studies should focus on five principle areas:

(1) Additional detailed mapping of the segregation behavior of a few specific solids systems of general interest; e.g., limestone and coal;

(2) Experiments aimed at developing the relative segregation behavior of a large number of different solids systems;

(3) Development of general correlations relating particle properties, gas velocity, bed internals, bed height, and bed composition to the segregation parameters;

(4) Experiments to measure the performance of actual reactors having well-defined segregation behavior; and

(5) Experiments to determine scale effects.

Item 1 should be carried out such that parameter interactions and beds having more than two component solids are included. Development of more rapid methods for measuring solids distributions is an important consideration, because of the highly time consuming nature of layer-by-layer, slumped-bed sampling. Radioactive tracer methods such as that used by Chen and Chao (1982) appear to have considerable promise.

Items 2 and 3 are closely related and are needed to provide a firm basis for general design methods. Perhaps the greatest difficulty here is to develop ways to account for the abrupt transitions between fluidization modes. Corresponding-states-type segregation maps, which would put all systems onto a common generalized coordinate system, should be pursued. Of course, fundamental understanding of the causes behind transitions in fluidization mode will be needed to develop truly predictive correlations. One approach, which I believe has considerable merit, is the application of the newly developed "chaos theory" [see Kadanoff (1983)]. This theory appears to be especially suitable for analyzing the development of hydrodynamic instabilities.

There appear to be some limiting cases of practical importance where models or correlations to predict λ_D and λ_w may be more easily derived. Three examples are: (1) at the boundary between Region 1 and Region 2 segregation (i.e., when $u_o = u_{mfJ}$); (2) at the gas velocity where the mixing index, I, is at its minimum value (i.e., at the point of best possible mixing); and (3) when the overall volume fraction of flotsam is very small. Limits 1 and 3 would be especially amenable to analysis because the parameter λ_w could probably be effectively

considered as being equal to 0. The "mixing resonances" would also not have to be considered in Limit 1. Limit 2 would probably represent a fundamental characteristic of a given solids system, although it may be related to the occurrence of "mixing resonances." Correlations involving λ_w would be the most difficult because of the many parameters (e.g., bed geometry, distributor plate design, tube bundle design) which could affect its value.

Item 4 is crucial for confirming the model predictions of reactor performance. Especially important is the need to evaluate axial variations in the fluidization parameters such as β and X and the effect of such variations on reactor performance. Perhaps the best way to accomplish this would be to begin with a binary bed having a simple first-order, catalytic reaction. A good candidate might be the decomposition of ozone in a bed of glass beads and alumina particles [see Chavarie and Grace (1975)]. Segregation could be characterized either separately or concurrently with the performance calculations. In-bed composition measurements should be especially useful in evaluating the combined segregation/reaction model. Further work with more complicated systems, e.g., coal and limestone, would be more appropriate after the simpler experiments.

Scale-up has traditionally been the most common and the most frustrating concern for designers of fluidized bed reactors. Segregation behavior is likely to be strongly influenced by the size of the fluidized bed, especially with regard to the large-scale convection parameter. For that reason, some large-scale experiments will be essential

in establishing the validity of laboratory and bench-scale data. Because of the difficulties in evaluating segregation in a large bed, only a few experiments will be practical, and these should be carried out only after careful planning based on the small-scale data. Development and application of radioactive tracers or similar techniques could result in tremendous savings of time and labor.

REFERENCES

REFERENCES

1. Avidan, A. A. and J. Yerushalmi, "Bed Expansion in High Velocity Fluidization," *Powder Tech.*, 32, 223 (1982).

2. Burgess, J. M., A. G. Fane, and C.J.D. Fell, "Measurement and Prediction of the Mixing and Segregation of Solids in Gas Fluidized Beds," Second Pachec Conference, Denver, 2, 1405 (1977).

3. Canada, G. S., M. H. McLaughlin, and F. W. Staub, "Flow Regimes and Void Fraction Distribution in Gas Fluidization of Large Particles with and without Tube Banks," in "Fluidization: Application to Coal Conversion Processes," *AIChE Symposium Series No. 176*, 74, 14 (1978).

4. Capes, C. E., "Basic Research in Particle Technology and Some Novel Applications," *Can. J. Chem. Eng.*, 54, 3 (1976).

5. Capes, C. E. and A. E. McIlhenney, "Expansion of Particulate Mixtures in Screen-Packed Gas-Fluidized Beds," *Trans. Instn. Chem. Eng.*, 50, 1 (1972).

6. Catapovic, N. M., N. G. Jovanovic, and T. J. Fitzgerald, "Regions of Fluidization for Large Particles," *AIChE J.*, 24, 3 (1978).

6a. Chavarie, C. and J. R. Grace, "Performance Analysis of a Fluidized Bed Reactor, II. Observed Reactor Behavior Compared with Simple Two-Phase Models," *Ind. Eng. Chem. Fund.*, 14, 79 (1975).

7. Chen, M. M. and B. T. Chao, "Measurement of Solids Motion in Gas Fluidized Beds," Department of Energy, Pittsburgh Energy Technology Center, Pittsburgh, Report No. DOE/PC/40804-T4 (August 1982).

8. Chen, J. L.-P. and D. L. Keairns, "Particle Segregation in a Fluidized Bed," *Can. J. Chem. Eng.*, 53, 395 (1975).

9. Chen, J.L.-P. and D. L. Keairns, "Particle Separation from a Fluidized Mixture. Simulation of the Westinghouse Coal Gasification Combustor/Gasifier Operation," *Ind. Eng. Chem.-Proc. Des. and Dev.*, 17, No. 2, 135 (1978).

10. Cooke, M. J., B. A. Napier, M. J. Parkinson, E. A. Rogers, "Segregation and Defluidization in Coal-Fired Fluidised Bed Combustors," Proceedings of the Seventh International Conference on Fluidized Bed Combustion, Philadelphia, Pennsylvania, 2, 792 (1982).

11. Cranfield, R. R., "Solids Mixing in Fluidized Beds of Large Particles," in "Fluidization: Application to Coal Conversion Process," *AIChE Symposium Series No. 176*, 74, 54 (1978).

12. Cranfield, R. R. and D. Geldert, "Large Particle Fluidization," *Chem. Eng. Sci.*, 29, 935 (1974).

13. Davidson, J. F. "Symposium on Fluidization Discussion," *Trans. Inst. Chem. Engrs.*, 39, 230 (1961).

14. Davidson, J. F. And D. Harrison, *Fluidized Particles*, Cambridge University Press, Cambridge (1963).

15. Einstein, A., "Untersuchungen uber die Theorie der Brownschen Bewegung," Akademische Verlagsgesellschaft M.B.H., Leipzig, Germany (1922).

16. Ergun, S., "Fluid Flow Through Packed Columns," *Chem. Eng. Progr.*, 48, 89 (1959).

17. Fan, L. T. and Y. Chang, "Mixing of Large Particles in Two-Dimensional Gas Fluidized Beds," *Can. J. Chem. Eng.*, 57, 88 (1979).

18. Fryer, C. and O. E. Potter, "Countercurrent Backmixing Model for Fluidized Bed Catalytic Reactions," *Ind. Eng. Chem. Fund.*, 11, 338 (1972).

19. Geldart, D., "Types of Gas Fluidization," *Powder Tech.*, 7, 285 (1973).

20. Geldart, D., "Behavior of Fine Particles in a Fluidized Bed of Coarse Solids," Electric Power Research Institute, Report No. CS-2094, Palo Alto, California (1981).

21. Geldart, D., J. Baeyens, D. J. Pope, and P. Van De Wijer, "Segregation in Beds of Large Particles at High Velocities," *Powder Tech.*, 30, 195 (1981).

22. Gelperin, N. I. and V. G. Einstein, "Analogy Between Fluidized Beds and Liquids," in *Fluidization*, J. F. Davidson and D. Harrison ed., Academic Press, London, 541 (1971).

23. Gibilaro, L. G. and P. N. Rowe, "A Model for a Segregating Gas Fluidised Bed," *Chem. Eng. Sci.*, 29, 1403 (1974).

24. Goossens, W.R.A., G. L. Dumont, and G. J. Spaepen, "Fluidization of Binary Mixtures in the Laminar Flow Region," in "Fluidization: Fundamental Studies, Solid-Fluid Reactions, and Applications," *AIChE Symposium Series 116*, 67, 38 (1971).

25. Harrison, D. and J. R. Grace, "Fluidized Beds with Internal Baffles," in *Fluidization*, J. F. Davidson and D. Harrison ed., Acadamic Press, London, 599 (1971).

26. High, M. D. and J. W. Bass III, "Utility Experience with FBC: A TVA Case History," Proceedings of the First National Conference on Evaluating the FBC Option, Washington D.C., Government Institute Publication No. ISPN-0-86587-117-5, Rockville, Maryland (1983).

27. Jovanovic, G. N. "Gas Flow in Fluidized Beds of Large Particles; Experiment and Theory," PhD. Thesis, Oregon State University, Corvvallis, Oregon (1979).

27a. Kadanoff, L. P., "Roads to Chaos," *Physics Today*, 8, 46 (1983).

28. Kato, K. and C. Y. Wen, "Bubble Assemblage Model for Fluidized Bed Catalytic Reactors," *Chem. Eng. Sci.*, 24, 1351 (1969).

29. Katz, H. M., "Studies of Particle Size Distribution in Fluidized Beds," Argonne National Laboratory Report No. ANL-5725 (1957).

30. Kondukov, N. B. and M. H. Sosna, *Teor. Osnovy Khim. Tekhnol.*, 1, 776 (1967).

31. Kunii, D. and O. Levenspiel, *Fluidization Engineering*, R. E. Kriegler Publishing Company, Huntington, New York (1969).

32. Lackey, M. E., personal communication (August 1984).

33. Lapidus, L., "Digital Computation for Chemical Engineers," McGraw-Hill, New York (1960).

34. Latham, R., C. Hamilton, and O. E. Potter, "Back-Mixing and Chemical Reaction in Fluidized Beds," *Brit. Chem. Eng.*, 13, 666 (1968).

35. McCabe, W. L. and J. C. Smith, *Unit Operations of Chemical Engineering*, Chapter 27, McGraw-Hill Book Company, New York (1967).

36. McGaw, D. R., "The Development of a Mechanism for Gas-Particle Heat Transfer in Shallow Fluidized Beds of Large Particles," *Chem. Eng. Sci.*, 32, 11 (1977).

37. McGrath, L. and R. E. Streatfield, "Bubbling in Shallow Gas-Fluidized Beds of Large Particles," *Trans. Instn. Chem. Eng.*, 49, T70 (1971).

38. McKendrick, "Incident Report: Tube Bank 'C' - Metal Wastage," IEA Grimethorpe Ltd., Fluidized Bed Combustion Project, Grimethorpe Experimental Facility, Report No. GEF/u/82/21, Grimethorpe, Great Britain (December 1982).

39. Miller, I. and J. E. Freund, *Probability and Statistics for Engineers*, Prentice-Hall, Englewood Cliffs, New Jersey (1977).

40. Mori, S. and C. Y. Wen, "Estimation of Bubble Diameter in Gaseous Fluidized Beds," *AIChE J.*, 21, 109 (1975).

41. Murray, J. D., "On the Mathematics of Fluidization: Part 2. Steady Motion of Fully Developed Bubbles," *J. Fluid Mech.*, 22, 57 (1965).

42. Nicklin, D. J., "Two-Phase Bubble Flow," *Chem. Eng. Sci.*, 17, 693 (1962).

43. Nienow, A. W. and D. J. Cheesman, "The Effect of Shape on the Mixing and Segregation of Large Particles in a Gas-Fluidized Bed of Small Ones," in *Fluidization*, J. R. Grace and J. M. Matsen ed., Plenum Press, New York, 373 (1980).

44. Nienow, A. W., P. N. Rowe, and L. Y.-L. Cheung, "A Quantitative Analysis of the Mixing of Two Segregating Powders of Different Density in a Gas-Fluidized Bed," *Powder Tech.*, 20,89 (1978a).

45. Nienow, A. W., P. N. Rowe, and T. Chiba, "Mixing and Segregation of a Small Proportion of Large Particles in Gas Fluidized Beds of Considerably Smaller Ones," in "Fluidization: Application to Coal Conversion Processes," *AIChE Symposium Series No. 176*, 74, 45 (1978b).

46. Partridge, B. A. and P. N. Rowe, "Chemical Reaction in a Bubbling Gas-Fluidized Bed," *Trans. Instn. Chem. Eng.*, 44, T335 (1966).

47. Piccinini, N., "Particle Segregation in Continuously Operating Spouted Beds," in *Fluidization*, J. R. Grace and J. M. Matson ed., Plenum Press, New York, 279 (1980).

48. Pyle, D. L. and P. L. Rose, "Chemical Reaction in Bubbling Fluidized Beds," *Chem. Eng. Sci.*, 20, 25 (1965).

49. Rios, G. M., J. L. Baxerres, and H. Gibert, "Potential Improvements in the Field of Large Particle Fluidization," in *Fluidization*, J. R. Grace and J. M. Matson ed., Plenum Press, New York, 529 (1980).

50. Rowe, P. N., "Gas-Solid Reaction in a Fluidized Bed," *Chem. Eng. Progr.*, 60(3), 75 (1964).

51. Rowe, P. N., personal communication (August 1984).

52. Rowe, P. N., A. W. Nienow, and A. J. Agbim, "The Mechanisms by Which Particles Segregate in Gas Fluidised Beds," *Trans. Instn. Chem. Eng.*, 50, 310 (1972a).

53. Rowe, P. N., A. W. Nienow, and A. J. Agbim, "A Preliminary Quantitative Study of Particle Segregation in Gas Fluidised Beds," *Trans. Instn. Chem Eng.*, 50, 324 (1972b).

54. Rowe, P. N., B. A. Partridge, A. G. Cheney, G. A. Henwood, and E. Lyall, "The Mechanisms of Solids Mixing in Fluidized Beds," *Trans. Inst. Chem. Eng.*, 43, T271 (1965).

55. Shannon, P. T., "Fluid Dynamics of Gas Fluidized Batch Systems," PhD. Thesis, Illinois Institute of Technology, Chicago, Illinois (1959).

56. Sitnai, O., "Solids Mixing in a Fluidized Bed with Horizontal Tubes," *Ind. Eng. Chem. Proc. Des. Dev.*, 20, No. 3, 533 (1981).

57. Spendley, W., G. R. Hext, and F. R. Himsworth, "Sequential Application of Simplex Designs in Optimization and Evolutionary Operation," *Technometrics*, 4, No. 4, 441 (1962).

58. Staub, F. W. and G. S. Canada, "Effect of Tube Bank and Gas Density on flow Behavior and Heat Transfer in Fluidized Beds," in *Fluidization*, Cambridge University Press, Cambridge, 339 (1978).

59. Sutherland, J. P. and K. Y. Wong, "Some Segregation Effects in Packed-Fluidized Beds," *Can. J. Chem. Eng.*, 42, 163 (1964).

60. Tanimoto, H., S. Chiba, T. Chiba, and H. Kobayashi, "Mechanism of Solid Segregation in Gas Fluidised Beds," in *Fluidization*, J. R. Grace and J. M. Matsen ed., Plenum Press, New York, 381 (1980).

61. Toomey, R. D. and H. F. Johnstone, "Gaseous Fluidization of Solid Particles," *Chem. Eng. Progr.*, 48, 221 (1952).

62. Van Deemter, J. J., "Mixing Patterns in Large-Scale Fluidized Beds," in *Fluidization*, J. R. Grace and J. M. Matsen ed., Plenum Press, New York, 69 (1980).

63. Wen, C. Y. and Y. H. Yu, "A Generalized Method of Predicting the Minimum Fluidization Velocity," *AIChEJ.*, 12, 610 (1966).

64. Yoshida, K., H. Kameyama, and F. Shimizu, "Mechanism of Particle Mixing and Segregation in Gas Fluidized Beds," in *Fluidization*, J. R. Grace and J. M. Matsen ed., Plenum Press, New York, 389 (1980).

APPENDIX

Table A-1. Summary of previous studies of solids segregation in gas-fluidized beds

Reference	Solids	Bed	Gas	Remarks
Katz (1957)	Glass beads — sized in intervals from 74 to 840 μm; no density given. Magnesium beads — no size or density given. Graphite — sized in intervals from 74 to 400 μm; no density given.	Lucite and copper cylinders, 5.08 cm (2 inch) inside diameter; no internals; static height 15.2 cm (6 in.).	Air, 0-0.17 m/s (0.55 ft/s).	Measured segregation due to particle size differences for steady-state conditions. The maximum size ratio was approximately 7.0. Observed that transition from fixed bed to fluidized state occurs over a range of gas flows for a mixture of particles. In the transition region, the bed appears to consist of two zones with a well-defined interface. As the flow increases, the upper region grows at the expense of the lower region. The process appears very similar to a phase transition.
Shannon (1959)	Glass beads — sized in intervals from 37 to 595 μm; density 2.45 g/cm^3. Sand-sized in intervals from 149 to 420 μm; density 2.66 g/cm^3. Fluid cracking catalyst — mean size 71 μm; density 2.0 g/cm^3. Hydroformer catalyst — mean size 61 μm; density 2.71 g/cm^3. Iron ore — two mean sizes — 129 μm and 69 μm; density 4.34 g/cm^3.	Cylindrical pyrex glass tube, 5.08 cm (2 inches) inside diameter; 58 cm (23 inches) tall; no internals.	Air, 0-.31 m/s (1 ft/s).	Conducted experiments in binary and ternary mixtures of different size particles. The maximum size ratio was approximately 4.0. Concluded that segregation is determined by minimum fluidizing velocity of each component and the the overall gas velocity; higher gas velocity and smaller differences in u_{mf} reduce segregation. Data indicate that segregation is not significant unless the ratio of the minimum fluidizing velocities is >2. Shannon provides a good review of the literature prior to 1959.

Table A-1. (continued)

Reference	Solids	Bed	Gas	Remarks
Sutherland and Wong (1964)	Ottawa sand — sized in intervals from 105 to 354 μm; density not reported.	Cylinder (material not specified) with 5.08 cm (2 inch) inside diameter; packed with 1.3 cm × 1.3 cm, 14 mesh stainless steel wire.	Air, 0-1.1 m/s (3.5 ft/s).	Ran steady-state and transient experiments with mixtures of different sand sizes in screen packed beds. The maximum size ratio was approximately 2.8. They concluded that segregation is a strong function of gas velocity and bed height. As gas velocity was increased from incipient fluidization, segregation decreased until reaching a minimum. Further increases in velocity resulted increasing segregation. Higher bed height increasee segregation. Proposed a model for the rate of segregation based on two well-mixed regions; a small one at the bottom and a large one at the top.
Goosens, Dumont, and Spaepen (1971)	Uranium dioxide particles -- two mean sizes, approximately 20 μm and 51 μm; density 10.43 g/cm^3. Aluminum oxide particles -- two mean sizes, 126 and 266 μm; density 3.98 g/cm^3.	Cylindrical Lucite column, 5.4 cm (2.1 in.) inside diameter; 63 cm (25 in.) tall; no internals.	Air, 0-1.07 m/s (3.5 ft/s).	Measured pressure drop and axial segregation with binary mixtures of uranium dioxide and aluminum oxide powder. The maximum size ratio and density ratio were approximately 18 and 1.6 respectively. Developed a correlation to predict u_{mf} of binary mixtures in the laminar flow region. Developed a de-mixing criterion for conditions above u_{mf}. This criterion is a function of the fraction of the component particle densities, and the ratio of the particle diameters.

Table A-1. (continued)

Reference	Solids	Bed	Gas	Remarks
Capes and McIlhinney (1972)	Glass beads--sized in intervals from 1000 to 1680 μm; density 2.73 g/cm^3. Polyvinylacetate beads--sized in intervals from 500 to 1680 μm; density 0.96 g/cm^3. Sand--sized in intervals from 149 to 841 μm; density 2.67 g/cm^3. Lead--sized in intervals from 841 to 1410 μm; density 11.34 g/cm^3. Nickel--sized in intervals from 125 to 841 μm; density 8.9 g/cm^3.	Cylindrical PMMA (Lucite), 5 cm inside diameter; 120 cm tall; packed with 1.3 cm × 1.3 cm 4 mesh wire cylinders (random); maximum static bed height 100 cm.	Air, 0-6.1 m/s (20 ft/s).	Measured expansion and segregation of mixtures with both size and density differences. Maximum size and density ratios tested were approximately 11.2 and 2.38, respectively. Did not quantify segregation, but did note a strong qualitative correlation between segregation and the differences between the fluidized bulk densities of the components; segregation increased with increased differences in bulk density. Also concluded that segregation decreased as the average particle density increased. Bed expansion appeared to be simply the sum of the expansions of the individual components.
Rowe, Nienow, and Agbim (1972 a)	Ballotini--sized in intervals from approximately 96 to 642 μm; density 2.94 g/cm^3. Polystyrene beads--mean size of 267 μm; density 1.05 g/cm^3. Steel shot--sized in intervals from 278 to 333 μm; density 7.5 g/cm^3. Copper shot--sized in intervals from 82 to 114 μm; density 8.86 g/cm^3.	2-D Perspex (Lucite) bed, 30.5 cm (12 in.) × 2.5 cm (1 in.) × 61 cm (24 in.) tall; 38.1 cm (15 in.) static bed height. Cylindrical Perspex bed, 14 cm (5.5 in.) inside diameter; 30 cm (11.8 in.) tall; no internals.	Air, 0-35.2 cm/s (1.15 ft/s).	Studies mixtures of particles differing in size only, density only, and in both size and density. Maximum size and density ratios were approximately 6.7 and 8.4, respectively. Concluded that particle density differences were most important cause of segregation. Segregation varied much more weakly with particle size differences. Also found that even at maximum segregation, it was usually not possible to produce a completely pure upper layer (i.e. some jetsam was invariably found more or less uniformly distributed in the flotsam). Relative particle movement occurred by three distinct mechanisms: (1) lifting in the wakes of rising bubbles, (2) falling through bubbles, and (3) inter-particle percolation. A fourth mechanism, the quasi-hydrostatic effect, was seen to preserve segregation but not to cause it initially.

Table A-1. (continued)

Reference	Solids	Bed	Gas	Remarks
Rowe, Nienow, and Agbim (1972 b)	Copper shot--mean size 277 μm; density 8.86 g/cm^3. Steel shot--mean size 2.78 μm; density 7.5 g/cm^3. Ballotini--mean size 271 μm; density 2.94 g/cm^3. Polystyrene beads--mean size 267 μm; density 1.05 g/cm^3. "Perail"--mean size 237 μm; density 1.02 g/cm^3. Sodium Perborate--mean size 261 μm; density 1.79 g/cm^3. Alumina catalyst--mean size 210 μm; density 2.1 g/cm^3. "Synclyst" catalyst--mean size 60.4 μm; density 2.2 g/cm^3.	Perspex (Lucite) cylinder 14.1 cm (5.6 in.) inside diameter; 45.5 cm (17.9 in.) tall; static bed depth 10 to 15 cm (2.9-5.9 in.), no internals.	Air, 0-60 cm/s (2.0 ft/s).	Continued studies begun by Rowe et al (1972 a). Observed that there was surprising uniformity of composition over a side middle region of the bed even when segregation was significant. Developed a segregation correlation $x_{J1} = f(u_0 - u_{mfF})\ (\rho_J/\rho_F)^{-5/2}\ \ (d_J/d_F)^{-1/5}$ where x is the jetsam concentration in the upper region. The proper form of the function $f(u_0 - u_{mfF})$ was not determined. Proposed a segregation index $M = x_{J1}/\overline{x}_J$ where $\overline{x}_J$ is the overall fraction of jetsam in the mixture.

Table A-1. (continued)

Reference	Solids	Bed	Gas	Remarks
Gibilaro and Rowe (1974)		Theoretical model. No data presented		Derived a differential equation model to describe steady-state segregation in binary system. The model was formulated to conform to the previous observations made by Rowe. Basic model components allow for axial particle motion by dispersion, convection, and segregation. Steady-state composition profiles were developed for certain limiting cases. General characteristics of these solutions appear to agree well with observed profiles.
Chen and Keairns (1975)	Dolomite--sized in intervals from 177 to 2830 μm; density 2.8 g/cm^3. Coal char--sized in intervals from 250 to 2000 μm; density 0.70 g/cm^3.	High pressure bed--1 to 6.5 atm, glass column; 10 cm (3.9 in.) inside diameter; 213.5 cm (84 in.) tall; no internals. Low pressure bed--1 to 1.41 atm, glass column; 11.4 cm (4.5 in.); 61.0 cm (24.0 in.) tall; no internals.	Air, 0-1 m/s (3.3 ft/s).	Collected steady-state segregation data for mixture of two and three components and wide-sized mixtures. Particle sizes in each bed ranged by a factor of about 7.2. Density ratio was maximum of 4.0. Concluded that segregation occurred for velocities near u_{bf} and u_{tf}, the beginning and complete fluidization velocities respectively. Constructed phase diagrams analogous to a solid-liquid system for binary mixtures. Also observed that segregation occurred for velocities near u_{tf} Study preliminary to work reported in Chen and Keairns (1978). Attainment of steady-state was rapid, usually <30 seconds. Wide-size mixtures of char and dolomite behaved as if they were a binary system of two densities having the average size of each component.

Table A-1. (continued)

Reference	Solids	Bed	Gas	Remarks
C. E. Capes (1976)	Chromite ore--125 to 108 μm; a mixture of Cr_2O_3 and SiO_2. Densities not given.	Cylindrical column, 3.0 cm (1.18 in.) inside diameter; 1 m (39.4 in.) tall; packed with screen cylinders. Materials of construction not given.	Air, 7.0 cm/s (0.23 ft/s).	Demonstrated beneficiation of chromite ore in a screen packed fluidized bed. Increased Cr_2O_3 from 15.8% to 28.5% and decreased SiO_2 from 23.9% to 6.7%. Very few details given.
Burgess, Pane, and Fell (1977)	Sand--mean sizes 143, 215, and 512 μm; density 2.7 g/cm^3. Ballotini--mean sizes 143 and 900 μm; density 2.9 g/cm^3. Iron powder--mean sizes 143 and 215 μm; density 6.3 g/cm^3. Steel shot--mean size 340 μm; density 7.5 g/cm^3.	Gas cylindrical column, 15.0 cm (5.9 in.) inside diameter; 60 cm (23.6 in.) tall; static bed depth 25.0 cm (9.8 in.); no internals.	Air, 0-0.45 m/s (1.48 ft/s).	Conducted both transient and steady-state segregation experiments with binary mixtures of small particles having both size and density differences. Maximum size and density ratios were 6.3 and 2.8, respectively. Observed that for initially segregated beds with mixtures of different sizes and density, mixing did began just above u_{mfF}. For initially segregated mixtures of different size and density, mixing did not begin until the gas velocity exceeded $u_{mf,J}$. Also observed that the denser component always behaved as jetsam, even when it had a similar or lower u_{mf} than the flotsam. Quantified overall mixing with Rowe et al's index, i.e., $M = x_J 1/\overline{x}$. Developed a transient numerical model based on relative solids movement by way of bubble wakes and by falling through bubble spaces.

Table A-1. (continued)

Reference	Solids	Bed	Gas	Remarks
Chen and Keairns (1978)	Char--sized in intervals from 420 to 841 μm; density 0.8-1.2 g/cm^3. Dolomite--sized in intervals from 420 to 1410 μm; density 2.88 g/cm^3.	Low velocity, high pressure cold model simulating the Westinghouse coal combustor/gasifier. Fluidized bed column made of 10.2 cm (4 in.) diameter glass and steel pipes. Combustor/separator composed of 5.1 cm (2 in.) diameter Plexiglass tube. High velocity, entrainment separation model; 11.4 cm (4.5 in.) diameter Plexiglass spouted bed with conical bottom.	Low velocity model--Air, 0-0.7 m/s (2.3 ft/s) High velocity model--Air, 0-7.0 m/s (23.0 ft/s)	Distinctive flow patterns in these models makes extrapolation to other fluidized beds difficult. Did demonstrate that separation can occur in two distinct velocity regimes; (1) velocities near u_{mf} and (2) velocities near terminal velocity of lighter component. Also demonstrated that practical gas separation in fluidized bed/entrained bed processes.

Table A-1. (continued)

Reference	Solids	Bed	Gas	Remarks
Nienow, Rowe, and Cheung (1978)	Copper shot--sized in intervals from 550 to 70 μm; density 8.86 g/cm^3. Copper powder--sized in intervals from 461 to 195 μm' density 8.86 g/cm^3. Bronze shot--sized in intervals from 388 to 114 μm; density 8.54 g/cm^3. Steel shot--sized in intervals from 388 to 138 μm; density 7.44 g/cm^3. Ballotini--sized in intervals from 550 to 165 μm; density 2.95 g/cm^3. Quartz--273 μm; density 2.65 g/cm^3. Glass--sized in intervals from 388 to 195 μm; density 2.25 g/cm^3. Sodium perborate--726 μm; density 2.13 g/cm^3. Carbon--sized in intervals from 388 to 195 μm; density 1.93 g/cm^3. Sugar--649 and 461 μm; density 1.59 g/cm^3. Sugar balls--928 μm; density 1.49 g/cm^3. Polystyrene--sized in intervals from 649 to 231 μm; density 1.05 g/cm^3.	Cylindrical beds, 14.1 and 22.2 cm (5.6 and 8.7 in.) diameter; 6-25 cm (2.4-9.8 in.) static bed height.	Air, 0-0.85 m/s (2.8 ft/s).	Measured axial composition profiles for binary systems with <50% volume of jetsam. Maximum size and density ratios were 2.38 and 8.44, respectively. Observed axial profiles typical of those reported earlier by Rowe et al. Determined that a mixing index can be correlated in the form $M = \frac{x_{J_1}}{\bar{x}_J} = \frac{1}{1 + e^{-Q}}$ where $Q = \frac{u_o - u_{to}}{u_o - u_{mfF}} \exp(u_o/u_{to})$ and u_{to} is the "takeover velocity." The takeover velocity was correlated by the empirical equation $\frac{u_{to}}{u_{mfF}} = \left(\frac{u_{mfJ}}{u_{mfF}}\right)^{1.2} + .9 \left(\frac{u_{mfJ}}{u_{mfF}}\right)^{1.1} \left(\frac{\phi_J d_J}{\phi_F d_F}\right)^{0.7} - 2.2(\bar{x})^{0.5} H^{*1.4}$ where $H^* = 1-\exp(-H/D)$.

Table A-1. (continued)

Reference	Solids	Bed	Gas	Remarks
Nienow, Rowe, and Chiba (1978)	Ballotini--461 and 243 μm; density 2.94 g/cm^3. Holochite--838 μm; density not given Sand--880 and 460 μm; density 2.72 g/cm^3. Shale--3030 μm; density 2.50 g/cm^3. Spheres of unknown composition 0.5-1.63 cm; density 0.94-1.64 g/cm^3. Char--.64-1.39 cm; density 0.97 g/cm^3. Washed coal--.73-1.21 cm; density 1.27 g/cm^3. Ollerton coal--.79-1.26 cm; density 1.30 g/cm^3. Anthracite--.74-1.10 cm; density 1.42 g/cm^3.	Cylindrical Perspex (Lucite) column, 14 cm (5.5 in.) diameter; static bed depth 25 cm (9.8 in.), no internals. 2D Perspex bed, 35.8 cm × 1.1 cm × 17.5 cm deep (14.1 in. × .43 in. × 6.9 in.); no internals	Cylindrical bed--Air, 0-.55 m/s (1.8 ft/s) 2D bed--Air, 0-.68 m/s (2.2 ft/s).	Discuss results of previous investigations which show that segregation patterns are significantly different for jetsam rich and jetsam lean systems. Describe experiments with jetsam rich systems (e.g. sand) with large pieces of flotsam (e.g. coal). Maximum size and density ratios were approximately 6.7 and 2.7, respectively. Concluded that the rise velocities for large flotsam particles can be approximated with the relation $\bar{u}_R = 1.9\ (u_o - u_{mfJ})^{1/2}$ and the average penetration depth estimated from $\frac{d}{H} = 0.12\ (u_o - u_{mfJ})^{1/2}$ Also determined that it is the absolute density of the large flotsam particle relative to the bulk density of the jetsam which determines whether it will float or sink. As long as it floats, the size and density of the flotsam does not appear to have much effect on the flotsam concentration profile.

Table A-1. (continued)

Reference	Solids	Bed	Gas	Remarks
Fan and Chang (1979)	Table tennis balls--3.65 cm diameter, single ball mass varied from 2.42 to 2.50 g/cm^3 by sealing sand inside.	2D Lucite bed, 330 cm high × 4.45 cm (130 in. × 15 in. × 1.75 in.); no internals.	Air, 0-3.4 m/s (11.2 ft/s).	First study of beds composed entirely of large (class D) particles. Observed that bubble or slug induced drift and gross circulation were the predominant mixing mechanisms. The contribution of wake mixing was concluded to be minor. Concluded like others that the bed divided itself into two zones; an upper, well-mixed zone and a lower, high gradient zone. Developed a non-stationary numerical random walk model to represent the axial composition profile as a function of time. Three parameters, representing a rate-of-mixing index, a segregation index, and a bed partition index are required by the model. The rate-of-mixing index and segregation parameters appeared to correlate with excess gas velocity.
N. Piccinini (1980)	Glass beads--1.24, 1.05, .78, and 0.65 mm diameter; density 2.67 g/cm^3.	2 plexiglass, spouted beds #1--8.0 cm (3.2 in.) 40° conical base 0.6 cm (0.24 in.) gas orifice #2--14.0 cm (5.5 in.) 40° conical base 0.9 cm (0.35 in.) gas orifice Continuous feed and overflow withdrawal system	Air, 0-0.44 m/s (1.44 ft/s).	Investigated beds containing different particles. Maximum size ratio was 1.9. Spouted bed behavior appeared considerably different from uniformly fluidized beds. Unusual flow patterns probably account for the observation that particle size differences had more effect on segregation than particle density differences. Accurate composition profiles could not be obtained due to biasing by the sampling method. In general, the material surrounding the "fountain" was richer in fines.

Table A-1. (continued)

Reference	Solids	Bed	Gas	Remarks
Nienow and Cheesman (1980)	Alumina--265 μm diameter, density 1.45 g/cm^3; primary bed solids. Foam rubber--pieces sized 2.8 × 25.4 × 25.4 mm; density 0.37 g/cm^3. Aluminum foil--15 mm and 9.8 mm spheres; density 0.370 and 0.809 g/cm^3, respectively. Cardboard--0.85 × 25.4 × 25.4 mm pieces; density 0.809 g/cm^3.	Cylindrical Perspex (Lucite) column, 14.0 (5.5 in.) diameter; 10.0 cm (3.94 in.) static bed height; no internals.	Air, 0-0.33 m/s (1.08 ft/s).	Made x-ray motion pictures of large spherical and flat-shaped particles in beds of alumina. Concluded that large, flat particles having a sphericity >0.5 behave similarly to spheres. Particles with sphericity <0.5 behave much differently, even to the point of becoming jetsam when more spheridal shapes would behave as flotsam.
Tanimoto, Chiba, Chiba, and Kobayashi (1980)	Glass beads--163 and 775 μm diameter; density 2.52 g/cm^3. Copper shot--194, 324, and 716 μm diameter; density 8.9 g/cm^3. Lead shot--385 and 555 μm diameter; density 11.3 g/cm^3.	PMMA (Lucite) 2-D bed, 1 cm (0.39 in.) thick × 30 cm (11.8 in.) wide × 1.0 m (39.4 in.) tall; no internals.	Air, 0-slightly above 0.025 m/s (0.082 ft/s).	Made motion pictures of jetsam segregation induced by the passage of a single bubble. Covered size and density ratios up to 4.8 and 4.5, respectively. Obtained the net descending distance and average descending velocity. These were related to the bubble diameter and density difference between jetsam and flotsam.
Yoshida, Kameyama, and Shimizu (1980).	Glass beads--2610, 1840, 650, 320, and 210 μm diameter; density 2.51 g/cm^3.	Segmented acrylic resin tube, 10 cm (3.94 in.) diameter; 38.5 cm (15.2 in.) tall; no inernals.	Air, 0-1.24 m/s (4.1 ft/s).	Measured segregation due to size in binary mixtures of glass beads. Covered size ratios up to 12.4. All experiments were made in the region between u_{mfp} and u_{mfj}. Developed a numerical model of Burgess, Fane, and Fell (1977). A significant difference is that there is no explicit allowance for drift dispersion. A variable segregation parameter is required to fit the model predictions with observed behavior.

Table A-1. (continued)

Reference	Solids	Bed	Gas	Remarks
Geldart, Baeyens, Pope, and Van De Wijer (1981)	Onyx sand--mean size 1000 μm; density not given. Grit--mean size 2500 μm; density not given. Southpart sand--500 to 45 μm, mean size 200 μm; density not given. Limestone—2000 to 6000 μm; density not given. Southpart sand--600 to 1400 μm; density not given. Polyvinyl chloride cubes--3350 μm on a side; density 1.49 g/cm^3. Polyethylene cubes--3350 μm on a side; density 1.04 g/cm^3.	Glass and aluminum column, 29 cm (11.4 in.) diameter; 5 m (16.4 ft) tall; with and without internal tubes.	Air, 0-5 m/s (16.4 ft/s).	Measured segregation in systems composed wholly or partly of large particles. Studied size segregation with the sand, grit, and limestone systems at size ratios up to about 12.5. Studied density segregation with PVC, polyethylene, and limestone systems at density ratios up to about 2.6. Concluded that the variation of the mixing index $M = x_j/\bar{x}_j$ is described well by the correlations developed by Nienow, Rowe, and Cheung (1978). Segregation by size difference appeared to increase with decreasing fines size, increasing bed mean size, and closer approach of gas velocity to u_{mff}. For beds with a wide size distribution of particles of similar density, an equation of the following form was found to be useful $$\frac{x_{fines}}{\bar{x}_{fines}} \propto \left[\frac{\bar{d}_p}{d_{fines}}\right]^m \left[\frac{u_o}{u_o - u_{mffines}}\right]^n$$ Effect of in-bed tubes appeared to be insignificant when fines were injected below the tubes.

Table A-1. (continued)

Reference	Solids	Bed	Gas	Remarks
Masson, Tran, and Rios (1981)	Sand--0-.250 μm range with mean about 140 μm; density 2.65 g/cm^3. Anthracite--0-2400 μm range with mean about 1020 μm; density 1.4 g/cm^3.	18 cm (7 in.) square Perspex bed, 1 m (3.3 ft) high, 50 cm (20 in.) static bed height, no internals.	Air, 0-9 cm/s (0.3 ft/s).	Studied the mixing and segregation of anthracite particles in a sand fluidized bed at ambient temperature. Used a radioactive tracer particle to follow anthracite motion. Concluded "good mixing" was achieved at 3 u_{mf}. The anthracite (flotsam) moved upwards twice as fast as downwards. The bed appeared to be divided into two characteristic regions, upper and lower.
Geldart (1981)	Large Bed Sand--45-500 μm, and coarse sizes nominally 200 μm, 1 mm, and 2.5 mm, density 2.65 g/cm^3. Alumina--60 μm mean, 1.83, density 1.83 g/cm^3. Small Bed Sand--106-255 μm, mean size =219 μm; density 2.65 g/cm^3. Alumina--38-125 μm, mean size =62 μm; density 1.83 g/cm^3. Metal shot--63-212 μm, mean size =114 μm; density 5.0 g/cm^3.	Large Bed Aluminum and glass cylinder, 29 cm (11.4 in.) diameter × 5 m (16.4 ft) high with and without internals. Static bed depth 0.15 m (0.49 ft)-0.60 m (2.0 ft). Operated with continuous feed and recycle. Small Bed Glass cylinder, 7.6 cm (3.0 in.) diameter × 7.3 m (24 ft) high, no tubes, batchwise operation. 2-D Bed 2-D Perspex bed, 1 cm (0.4 in.) × 30 cm (11.8 in.) wide × 1.5 m (4.9 ft) high, with and without internals, batch operation.	Large Bed Air, 0-5.2 m/s (17.1 ft/s). Small Bed Air, 0-3 m/s (9.8 ft/s). 2-D Bed Air, 0-5.2 m/s (17.1 ft/s).	Studied elutriation and segregation of fines relative to the large particles. Observed that segregation of fines within the bed and interaction between the fines and coarse particles in the freeboard play an important role. Used two mixing indices $C_s = 100\left(\frac{x_{Fl} - x_{Fo}}{x_{Fl} + x_{Fo}}\right)$ and $M = x_{fz}/\bar{x}_f$ to show that segregation is an inherent feature of large-particle beds containing fines. Segregation increased with increasing size difference.

Table A-1. (continued)

Reference	Solids	Bed	Gas	Remarks
Cooke, Napier, Parkinson, and Rogers (1982)	Cold tests--crushed coal washery discard which had been roasted in an electric furnace; size range 1.7 to 25 mm, mean size about 2 mm; density of 10% of total was 1.0 g/cm^3 and other 90% was 2.4 g/cm^3. Hot tests--washery discard sized 0 × 3 mm and 0 × 6 mm and run-of-mine coal 0 × 13 mm.	Cold tests--mild steel bed with Perspex (Lucite) panels, 1 m (3.28 ft) × 0.25 m (0.82 ft) × 3.4 m (11.2 ft) tall; with and without horizontal tubes. Hot tests--fluidized bed test combustor, 0.6 m (2 ft) × 0.6 m (2 ft) × 2.25 m (7.4 ft) deep (solids static height); in-bed cooling tubes.	Air, 0-5 m/s (16.4 ft/s).	Observed segregation patterns due to size differences in both cold and hot (combusting) beds of large bench-scale size. Concluded segregation is likely to be an inherent feat when fluidizing solids of a large size range, especially when $u_0 < u_{mf}$ of largest fraction. The degree of segregation decreased with increasing u_0, but never disappeared completely, even at $u_0 = 5$ m/s. Tubes significantly increased segregation. Bottom bed discharge, fines recycle, and a high velocity air spout decreased segregation.

Table A-2. Data from steady-state segregation experiments

Solids	Run no.	H_s Static bed height (cm)	u_o Superficial gas velocity (m/s)	Overall bed composition	Bed internals	Sample size (g)	z Average dimensionless axial position	v_J Sample jetsam volume fraction	Remarks
#1 coal, #1 limestone. Limestone acts as jetsam.	LC-1	23.4	1.44	$\bar{v}_J$ = 0.832, 200 g coal, 1976 g limestone.	None	309.1	0.929	0.520	H_s 27 cm. Region 2 segregation. Gradual transition between jetsam-rich and flotsam-rich zones. I = 0.178.
						429.3	0.755	0.741	
						354.0	0.571	0.877	
						354.0	0.408	0.964	
						680.5	0.163	0.967	
	LC-2	23.4	1.45	$\bar{v}_J$ = 0.832, 200 g coal, 1976 g limestone.	None	280.9	0.935	0.570	H_s 27 cm. Region 2 segregation. Gradual transition between jetsam-rich and flotsam-rich zones. I = 0.126.
						458.0	0.766	0.771	
						374.2	0.571	0.835	
						308.2	0.402	0.873	
						710.7	0.163	0.985	
#2 coal, #2 limestone. Limestone acts as jetsam.	LC-4	27.9	1.73	$\bar{v}_J$ = 0.939, 86 g coal, 2573 g limestone.	None	246.7	0.950	0.753	Region 2 segregation. Gradual decrease in flotsam concentration with depth. I = 0.081.
						267.8	0.846	0.900	
						452.3	0.710	0.930	
						528.9	0.526	0.972	
						574.6	0.323	0.979	
						588.4	0.108	0.982	
	LC-5	27.9	3.22	$\bar{v}_J$ = 0.936, 92 g coal, 2630 g limestone.	None	324.0	0.946	0.912	Region 2 segregation. H_s 51-76 cm. Bed essentially well-mixed. I = 0.002.
						351.0	0.832	0.940	
						438.8	0.686	0.933	
						560.0	0.496	0.931	
						633.6	0.264	0.946	
						414.8	0.068	0.947	
	LC-6	28.2	2.45	$\bar{v}_J$ = 0.939 88 g coal, 2647 g limestone.	None	357.6	0.932	0.906	Region 2 segregation. H_s 53 cm. Bed essentially well-mixed. I = 0.003.
						363.8	0.797	0.942	
						496.3	0.640	0.942	
						498.7	0.464	0.944	
						611.7	0.257	0.946	
						406.7	0.068	0.945	
	LC-7	26.9	2.45	$\bar{v}_J$ = 0.685, 438 g coal, 1854 g limestone.	None	280.4	0.939	0.649	Region 2 segregation. H_s 55 cm. Bed essentially well-mixed. I = 0.002.
						313.7	0.816	0.657	
						423.7	0.670	0.666	
						430.7	0.486	0.690	
						452.7	0.288	0.696	
						450.7	0.094	0.699	

Table A-2. (continued)

Solids	Run no.	H_s Static bed height (cm)	u_o Superficial gas velocity (m/s)	Overall bed composition	Bed internals	Sample size (g)	ξ Average dimensionless axial position	v_J Sample jetsam volume fraction	Remarks
#2 coal, #2 limestone. Limestone acts as jetsam.	LC-8	27.9	1.74	$\bar{v}_J$ = 0.642, 536 g coal, 1872 g limestone.	None	184.7	0.955	0.269	Region 2 segregation. H_o = 41 cm. Steep composition gradient. I = 0.269.
						176.6	0.864	0.273	
						208.8	0.764	0.374	
						461.8	0.591	0.571	
						575.2	0.373	0.816	
						391.9	0.223	0.912	
						408.0	0.068	0.894	
	LC-9	27.7	1.49	$\bar{v}_J$ = 0.658, 506 g coal, 1898 g limestone.	None	150.3	0.954	0.084	Initial condition was well-mixed. Air flow increased to final value. Fluidization interface located at z^* = 0.65. Region 1 segregation H_o = 31 cm. I = 0.469.
						191.7	0.853	0.125	
						190.9	0.748	0.334	
						292.8	0.647	0.815	
						457.3	0.509	0.862	
						550.5	0.321	0.887	
						572.4	0.110	0.888	
	LC-10	27.2	1.16	$\bar{v}_J$ = 0.665, 492 g coal, 1910 g limestone.	None	129.0	0.963	0.036	Air flow was increased to full fluidization, then reduced to final value. Fluidization interface at z^* = 0.70. H_o = 30 cm. Region 1 segregation. I = 0.617.
						129.3	0.879	0.052	
						146.9	0.785	0.061	
						259.9	0.692	0.761	
						273.1	0.598	0.945	
						427.3	0.472	0.929	
						1036.2	0.196	0.886	
	LC-16	26.9	0.72	$\bar{v}_J$ = 0.691, 448 g coal, 1950 g limestone.	None	132.5	0.961	0.0	Air flow was increased to full fluidization and then reduced to final value and held. Fluidization interface located at z^* = 0.75. Region 1 segregation. I = 0.835.
						147.2	0.869	0.0	
						116.4	0.786	0.007	
						224.3	0.718	0.940	
						574.2	0.578	0.952	
						431.6	0.381	0.959	
						313.8	0.243	0.962	
						457.2	0.097	0.934	

Table A-2. (continued)

Solids	Run no.	H_s Static bed height (cm)	u_o Superficial gas velocity (m/s)	Overall bed composition	Bed intervals	Sample size (g)	z Average dimensionless axial position	v_J Sample jetsam volume fraction	Remarks
#1 glass, steel shot. Steel acts as jetsam.	SG-1	22.9	2.61	$\bar{v}_J$ = 0.026, 200 g shot, 2215 g glass.	None	497.9	0.900	0.006	Initial condition inverted segregation (i.e., jetsam on top). Air flow was increased to final value and held. Amount of jetsam was insufficient to form a distinct lower layer. Region 1 segregation. I = 0.049.
						349.1	0.722	0.012	
						429.6	0.550	0.012	
						320.4	0.389	0.012	
						327.8	0.244	0.008	
						491.2	0.083	0.103	
	SG-2	23.1	2.94	$\bar{v}_J$ = 0.026, 200 g shot, 2215 g glass.	None	347.8	0.923	0.013	Initial condition inverted segregation. Air flow was increased to final value and held. Amount of jetsam was insufficient to form a distinct lower layer. Region 1 segregation. I = 0.040.
						525.7	0.747	0.009	
						347.2	0.560	0.013	
						382.7	0.408	0.010	
						339.1	0.247	0.011	
						472.0	0.082	0.098	
	SG-3	22.9	3.26	$\bar{v}_J$ = 0.026, 200 g shot, 2215 g glass.	None	384.3	0.922	0.004	Initial condition was well-mixed. Air flow was increased slowly to final value and held. Amount of jetsam was insufficient to form a distinct lower layer. Region 1 segregation. I = 0.031.
						545.7	0.733	0.018	
						405.5	0.533	0.015	
						300.9	0.383	0.015	
						296.2	0.244	0.015	
						482.7	0.083	0.086	
	SG-4	30.7	4.29	$\bar{v}_J$ = 0.026, 200 g shot, 2215 g glass.	None	657.8	0.901	0.002	Region 2 segregation. Distince separation. I = 0.736.
						550.9	0.715	0.011	
						495.8	0.558	0.043	
						705.4	0.401	0.125	
						747.7	0.269	0.626	
						821.4	0.174	0.944	
						1376.6	0.062	0.992	
	SG-5	30.5	2.26	$\bar{v}_J$ = 0.291, 3143 g shot, 2215 g glass.	None	573.7	0.910	0.0	Initial condition was segregated. Air flow was increased to final value and held. Region 1 segregation. I = 1.0.
						493.6	0.744	0.0	
						547.0	0.581	0.0	
						600.3	0.402	0.0	
						3142.8	0.154	1.0	

Table A-2. (continued)

Solids	Run no.	H_s Static bed height (cm)	u_o Superficial gas velocity (m/s)	Overall bed composition	Bed internals	Sample size (g)	z Average dimensionless axial position	v_j Sample jetsam volume fraction	Remarks
#1 glass, steel shot. Steel acts as jetsam.	SG-6	30.5	2.90	$\bar{v}_j$ = 0.291, 3143 g shot, 2215 g glass.	None	533.6	0.917	0.0	Initial condition was segregated. Air flow was increased to final value and held. Region 1 segregation. I = 1.0.
						533.6	0.750	0.0	
						587.0	0.575	0.0	
						560.3	0.396	0.0	
						849.4	0.267	1.0	
						2293.4	0.113	1.0	
	SG-7	30.5	3.53	$\bar{v}_j$ = 0.291, 3143 g shot, 2215 g glass.	None	533.5	0.917	0.0	H_s = 72 cm. Region 2 segregation. Bed totally segregated. I = 1.0.
						400.1	0.771	0.0	
						666.9	0.604	0.0	
						613.5	0.404	0.0	
						2200.0	0.200	1.0	
						942.8	0.046	1.0	
	SG-8	30.5	3.86	$\bar{v}_j$ = 0.291, 3143 g shot, 2215 g glass.	None	532.0	0.917	0.0	Violent turbulence/slugging. Region 2 segregation. Bed totally segregated. I = 1.0.
						614.5	0.738	0.0	
						480.1	0.567	0.0	
						253.4	0.452	0.0	
						333.4	0.360	0.0	
						849.4	0.267	1.0	
						2293.4	0.113	1.0	
	SG-9	30.5	4.65	$\bar{v}_j$ = 0.291, 3143 g shot, 2215 g glass.	None	576.1	0.917	0.001	Violent turbulence/slugging. Fairly clear interface at z = 0.3. Region 2 segregation. I = 0.788.
						559.5	0.750	0.021	
						599.6	0.575	0.020	
						375.4	0.425	0.048	
						816.2	0.308	0.427	
						2429.6	0.125	0.988	
	SG-10	30.5	5.20	$\bar{v}_j$ = 0.291, 3143 g shot, 2215 g glass.	None	591.9	0.917	0.003	Violent turbulence/slugging. Fairly clear interface at z = 0.3. In fluidized condition glass beads appear to be forming a highly dispersed cloud above the shot. Region 2 segregation. I = 0.837.
						649.6	0.750	0.028	
						605.3	0.575	0.028	
						437.2	0.408	0.023	
						793.5	0.292	0.737	
						895.2	0.188	0.976	
						1383.3	0.063	0.996	

Table A-2. (continued)

Solids	Run no.	H_s Static bed height (cm)	u_o Superficial gas velocity (m/s)	Overall bed composition	Bed internals	Sample size (g)	z Average dimensionless axial position	v_J Sample jetsam volume fraction	Remarks
Glass #1 and #2. Large glass acts as jetsam.	GG-1	14.7	2.44	$\bar{v}_J$ = 0.667, 500 g #1, 1000 g #2.	Wire cylinders with single horizontal tube in each. Tubes parallel.	149.4	0.948	0.031	H_e = 18 cm. Region 2 segregation.
						262.9	0.810	0.094	Clear separation. I = 0.709.
						271.4	0.629	0.586	
						242.9	0.457	0.986	
						317.3	0.276	0.997	
						254.9	0.086	1.0	
	GG-1'	15.2	2.46	$\bar{v}_J$ = 0.667, 500 g #1, 1000 g #2.	Wire cylinders with single horizontal tube in each. Tubes parallel.	175.9	0.941	0.078	Clear separation. H_e = 18 cm.
						153.5	0.832	0.126	Region 2 segregation. I = 0.657.
						313.3	0.676	0.384	
						287.3	0.476	0.964	
						569.7	0.190	0.998	
	GG-2	14.5	2.91	$\bar{v}_J$ = 0.667, 500 g #1, 1000 g #2.	Wire cylinders with single horizontal tube in each. Tubes parallel.	192.0	0.947	0.562	Bed appeared well-mixed except near
						454.6	0.728	0.614	bottom. H_e = 21 cm. Region 2
						283.2	0.474	0.613	segregation. I = 0.643.
						295.7	0.290	0.661	
						274.1	0.097	0.887	
	GG-2'	14.7	2.91	$\bar{v}_J$ = 0.667, 500 g #1, 1000 g #2.	Wire cylinders with single horizontal tube in each. Tubes parallel.	258.4	0.914	0.543	H_e = 21 cm. Region 2 segregation.
						323.6	0.724	0.647	Bed appeared well-mixed except near
						264.7	0.526	0.603	bottom. I = 0.060.
						242.9	0.353	0.588	
						409.3	0.138	0.848	
	GG-3	14.7	2.77	$\bar{v}_J$ = 0.667, 500 g #1, 1000 g #2.	Wire cylinders with single horizontal tube in each. Tubes parallel.	290.1	0.922	0.504	H_e = 20 cm. Region 2 segregation.
						292.8	0.733	0.531	Bed appeared well-mixed except near
						265.0	0.526	0.572	bottom. I = 0.136.
						369.3	0.319	0.728	
						281.1	0.103	0.985	

Table A-2. (continued)

Solids	Run no.	H_s Static bed height (cm)	u_o Superficial gas velocity (m/s)	Overall bed composition	Bed internals	Sample size (g)	z Average dimensionless axial position	v_J Sample jetsam volume fraction	Remarks
Glass #1 and #2. Large glass acts as jetsam.	GG-4	14.7	2.61	$\bar{v}_J$ = 0.667, 500 g #1, 1000 g #2.	Wire cylinders with single horizontal tube in each. Tubes parallel.	289.0	0.905	0.358	H_e = 18 cm. Region 2 segregation. Bed appeared to consist of two zones. I = 0.322.
						315.9	0.716	0.415	
						226.6	0.535	0.551	
						382.9	0.328	0.934	
						284.8	0.103	0.988	
	GG-5	15.2	2.71	$\bar{v}_J$ = 0.667, 100 g #1, 1400 g #2.	Wire cylinders with single horizontal tube in each. Tubes parallel.	191.4	0.925	0.651	H_e = 18 cm. Region 2 segregation. Flotsam concentrated near top. I = 0.192.
						253.3	0.775	0.938	
						300.6	0.596	0.980	
						271.4	0.396	0.980	
						483.0	0.150	0.988	
	GG-6	15.1	2.47	$\bar{v}_J$ = 0.933, 100 g #1, 1400 g #2.	Wire cylinders with single horizontal tube in each. Tubes parallel.	132.4	0.954	0.418	H_e = 17 cm. Region 2 segregation. Flotsam concentrated near top. I = 0.435.
						188.4	0.849	0.886	
						281.5	0.697	0.996	
						266.4	0.513	1.0	
						346.9	0.319	1.0	
						284.4	0.109	1.0	
	GG-7	15.5	3.11	$\bar{v}_J$ = 0.933, 100 g #1, 1400 g #2.	Wire cylinders with single horizontal tube in each. Tubes parallel.	208.4	0.926	0.854	H_e = 20 cm. Region 2 segregation. Bed approaching well-mixed conditions. I = 0.021.
						251.9	0.771	0.921	
						357.9	0.582	0.946	
						292.8	0.377	0.934	
						389.5	0.139	0.973	
	GG-8	14.2	4.60	$\bar{v}_J$ = 0.933, 100 g #1, 1400 g #2.	Wire cylinders with single horizontal tube in each. Tubes parallel.	286.5	0.905	0.873	H_e = 27 cm. Region 2 segregation. Bed approaching well-mixed conditions. I = 0.015.
						247.4	0.727	0.929	
						303.6	0.543	0.950	
						238.9	0.363	0.954	
						424.8	0.142	0.951	

Table A-2. (continued)

Solids	Run no.	H_s Static bed height (cm)	u_o Superficial gas velocity (m/s)	Overall bed composition	Bed internals	Sample size (g)	z Average dimensionless axial position	v_J Sample jetsam volume fraction	Remarks
Glass #1 and #2. Large glass acts as jetsam.	GG-9	15.5	2.48	$\bar{v}_J$ = 0.133, 1300 g #1, 200 g #2.	Wire cylinders with single horizontal tube in each. Tubes parallel.	220.6	0.918	0.034	H_e = 21 cm. Region 2 segregation. Bed appeared to consist of two layers. I = 0.417.
						273.0	0.754	0.035	
						283.4	0.582	0.041	
						470.1	0.336	0.031	
						252.4	0.090	0.621	
	GG-10	15.5	2.77	$\bar{v}_J$ = 0.133, 1300 g #1, 200 g #2.	Wire cylinders with single horizontal tube in each. Tubes parallel.	327.0	0.893	0.048	H_e = 22 cm. Region 2 segregation. Bed appeared to consist of two layers. I = 0.373.
						341.8	0.672	0.050	
						344.9	0.443	0.039	
						281.9	0.246	0.071	
						204.8	0.082	0.655	
	GG-11	21.3	2.70	$\bar{v}_J$ = 0.667, 750 g #1, 1500 g #2.	Wire cylinders with single horizontal tube in each. Tubes parallel.	286.0	0.937	0.381	H_e = 30 cm. Region 2 segregation. Bed appeared to consist of bottom and top layers with well-mixed middle layer. I = 0.107.
						342.5	0.797	0.579	
						412.2	0.629	0.627	
						484.7	0.430	0.686	
						373.7	0.240	0.735	
						351.0	0.078	0.932	
	GG-12	7.4	2.78	$\bar{v}_J$ = 0.667, 250 g #1, 500 g #2.	Wire cylinders with single horizontal tube in each. Tubes parallel.	150.0	0.897	0.103	H_e = 10 cm. Region 2 segregation. Steep composition gradient between upper and lower layers. I = 0.515.
						219.6	0.647	0.534	
						150.8	0.400	0.939	
						229.3	0.150	0.984	
	GG-13	11.7	2.79	$\bar{v}_J$ = 0.667, 375 g #1, 750 g #2.	Wire cylinders with single horizontal tube in each. Tubes parallel.	134.8	0.940	0.236	H_e = 16 cm. Region 2 segregation. Steep composition gradient between upper and lower layers. I = 0.399.
						279.1	0.756	0.362	
						198.1	0.545	0.600	
						302.0	0.323	0.953	
						212.8	0.095	0.996	

Table A-2. (continued)

Solids	Run no.	H_s Static bed height (cm)	u_o Superficial gas velocity (m/s)	Overall bed composition	Bed internals	Sample size (g)	z Average dimensionless axial position	v_J Sample jetsam volume fraction	Remarks
Glass #1 and #2. Large glass acts as jetsam.	GG-14	14.9	2.16	$\bar{v}_J$ = 0.667, 500 g #1, 1000 g #2.	Wire cylinders with single horizontal tube in each. Tubes parallel.	269.9	0.910	0.283	H_s = 16 cm. Region 2 segregation. Bed appears to consist of upper well-mixed zone, steep middle gradient, and lower jetsam zone. I = 0.418.
						337.8	0.707	0.342	
						329.0	0.485	0.749	
						295.0	0.277	0.994	
						267.5	0.089	1.000	
	GG-14'	15.2	2.17	$\bar{v}_J$ = 0.667, 500 g #1, 1000 g #2.	Wire cylinders with single horizontal tube in each. Tubes parallel.	136.7	0.955	0.274	H_s = 16 cm. I = 0.417. Region 2 segregation. Appearance same as GG-14.
						224.6	0.834	0.267	
						280.4	0.666	0.417	
						240.6	0.492	0.732	
						247.4	0.329	0.977	
						370.1	0.123	0.994	
	GG-15	15.0	2.34	$\bar{v}_J$ = 0.667, 500 g #1, 1000 g #2.	Wire cylinders with single horizontal tube in each. Tubes parallel.	220.3	0.926	0.079	H_s = 17 cm. Region 2 segregation. Steep composition gradient between upper and lower layers. I = 0.622.
						250.9	0.769	0.210	
						213.6	0.614	0.639	
						268.8	0.453	0.925	
						269.1	0.273	0.999	
						273.3	0.091	1.000	
	GG-16	15.0	3.24	$\bar{v}_J$ = 0.667, 500 g #1, 1000 g #2.	Wire cylinders with single horizontal tube in each. Tubes parallel.	167.3	0.944	0.536	H_s = 23 cm. Region 2 segregation. Bed approaching well-mixed condition. I = 0.038.
						241.8	0.808	0.677	
						300.8	0.627	0.642	
						338.8	0.414	0.619	
						229.7	0.224	0.663	
						221.9	0.074	0.865	
	GG-16'	15.2	3.29	$\bar{v}_J$ = 0.667, 500 g #1, 1000 g #2.	Wire cylinders with single horizontal tube in each. Tubes parallel.	244.1	0.919	0.558	H_s = 23 cm. Region 2 segregation. Bed approaching well-mixed condition. I = 0.023.
						363.7	0.716	0.761	
						166.2	0.539	0.673	
						246.2	0.401	0.647	
						238.9	0.239	0.614	
						239.4	0.080	0.792	
	GG-17	14.7	1.98	$\bar{v}_J$ = 0.667, 500 g #1, 1000 g #2.	Wire cylinders with single horizontal tube in each. Tubes parallel.	131.8	0.956	0.114	H_s = 15 cm. Region 2 segregation. Steep composition gradient between upper and lower layers. I = 0.554.
						225.9	0.837	0.221	
						286.5	0.665	0.388	
						297.1	0.471	0.906	
						274.4	0.280	0.990	
						281.7	0.094	0.999	

Table A-2. (continued)

Solids	Run no.	H_s Static bed height (cm)	u_o Superficial gas velocity (m/s)	Overall bed composition	Bed internals	Sample size (g)	z Average dimensionless axial position	v_j Sample jetsam volume fraction	Remarks
Glass #1 and #2, large glass acts as jetsam.	GG-18	15.0	2.08	$\bar{v}_j$ = 0.667, 500 g #1, 1000 g #2.	Wire cylinders with single horizontal tube in each. Tubes parallel.	221.7	0.926	0.230	H_s = 16 cm. Region 2 segregation. Steep composition gradient between upper and lower layers. I = 0.489.
						258.2	0.766	0.269	
						168.7	0.623	0.437	
						245.2	0.485	0.843	
						327.5	0.296	0.982	
						276.7	0.092	0.998	
	GG-19	15.0	2.25	$\bar{v}_j$ = 0.667, 500 g #1, 1000 g #2.	Wire cylinders with single horizontal tube in each. Tubes parallel.	267.3	0.904	0.253	H_s = 17 cm. Region 2 segregation. Steady composition gradient through most of the bed. I = 0.371.
						248.4	0.726	0.439	
						260.5	0.564	0.563	
						206.2	0.415	0.827	
						307.1	0.244	0.983	
						213.2	0.071	0.998	
	GG-20	15.0	3.14	$\bar{v}_j$ = 0.667, 500 g #1, 1000 g #2.	Wire cylinders with single horizontal tube in each. Tubes parallel.	209.2	0.930	0.548	H_s = 22 cm. Region 2 segregation. Bed nearly well-mixed except for steep gradient near bottom I = 0.055.
						282.4	0.767	0.635	
						303.8	0.572	0.637	
						230.1	0.396	0.596	
						196.5	0.252	0.653	
						280.8	0.094	0.887	
	GG-21	15.0	2.51	$\bar{v}_j$ = 0.667, 500 g #1, 100 g #2.	Wire cylinders with single horizontal tube in each. Tubes parallel.	249.5	0.917	0.160	H_s = 19 cm. Region 2 segregation. Steep composition gradient between upper and lower layers. I = 0.498.
						197.4	0.768	0.297	
						230.9	0.625	0.517	
						242.2	0.468	0.854	
						176.1	0.328	0.981	
						404.7	0.135	0.996	
	GG-22	14.7	2.79	$\bar{v}_j$ = 0.350, 975 g #1, 525 g #2.	Wire cylinders with single horizontal tube in each. Tubes parallel.	217.4	0.928	0.217	H_s = 23 cm. Region 2 segregation. Bed nearly well-mixed except for steep near bottom. I = 0.172.
						291.3	0.758	0.285	
						294.0	0.563	0.268	
						198.7	0.398	0.222	
						231.9	0.255	0.285	
						265.6	0.089	0.773	

Table A-2. (continued)

Solids	Run no.	H_s Static bed height (cm)	u_o Superficial gas velocity (m/s)	Overall bed composition	Bed internals	Sample size (g)	z Average dimensionless axial position	v_J Sample jetsam volume fraction	Remarks
Glass #1 and #2. Large glass acts as jetsam.	GG-23	15.0	2.80	$\bar{v}_J$ = 0.200, 1200 g #1, 300 g #2.	Wire cylinders with single horizontal tube in each. Tubes parallel.	283.3	0.905	0.102	H_e = 23 cm. Region 2 segregation. Bed nearly well-mixed except for steep gradient near bottom. I = 0.269.
						287.1	0.715	0.114	
						224.3	0.544	0.133	
						205.8	0.401	0.125	
						317.1	0.226	0.142	
						180.2	0.060	0.759	
	GG-24	15.0	2.80	$\bar{v}_J$ = 0.500, 750 g #1, 750 g #2.	Wire cylinders with single horizontal tube in each. Tubes parallel.	222.9	0.926	0.335	H_e = 22 cm. Region 2 segregation. Bed nearly well-mixed except for steep gradient near bottom. I = 0.120.
						266.1	0.763	0.426	
						231.9	0.597	0.463	
						224.0	0.444	0.387	
						269.4	0.280	0.468	
						284.9	0.095	0.846	
	GG-25	15.2	2.80	$\bar{v}_J$ = 0.800, 300 g #1, 1200 g #2.	Wire cylinders with single horizontal tube in each. Tubes parallel.	219.5	0.927	0.636	H_e = 20 cm. Region 2 segregation. Steady composition gradient through most of the bed. I = 0.092.
						232.1	0.776	0.673	
						237.0	0.620	0.748	
						214.7	0.469	0.811	
						287.2	0.302	0.867	
						308.9	0.103	0.984	
	GG-5'	15.2	2.79	$\bar{v}_J$ = 0.933, 100 g #1, 1400 g #2.	Wire cylinders with single horizontal tube in each. Tubes parallel.	197.5	0.934	0.845	H_e = 20 cm. Region 2 segregation. Steady composition gradient through most of the bed. I = 0.035.
						280.2	0.775	0.892	
						185.4	0.620	0.931	
						263.8	0.470	0.952	
						287.7	0.287	0.963	
						286.0	0.095	0.990	
	GG-26	13.7	1.64	$\bar{v}_J$ = 0.667, 500 g #1, 1000 g #2.	None	129.2	0.957	0.066	Initial condition segregated. Air flow was increased to final value and held. Fluidization interface located at z = 0.62. Region 1 segregation. H_e = 14 cm. I = 0.700.
						122.2	0.873	0.112	
						167.1	0.777	0.148	
						155.0	0.669	0.354	
						146.7	0.569	0.821	
						150.0	0.470	0.988	
						629.0	0.210	1.000	

Table A-2. (continued)

Solids	Run no.	H_s Static bed height (cm)	u_o Superficial gas velocity (m/s)	Overall bed composition	Bed internals	Sample size (g)	z Average dimensionless axial position	v_J Sample jetsam volume fraction	Remarks
Glass #1 and #2. Large glass acts as jetsam.	GG-27	18.8	2.77	$\bar{v}_J$ = 0.667, 620 g #1, 1240 g #2.	Wire cylinders with single horizontal tube in each. Tubes parallel.	306.0	0.918	0.507	H_e = 25 cm. Region 2 segregation
						371.8	0.735	0.630	Bed nearly well-mixed except for steep
						369.3	0.536	0.657	gradient near bottom.
						274.6	0.363	0.658	I = 0.061.
						272.8	0.216	0.673	
						264.7	0.071	0.920	
	GG-28	13.2	2.76	$\bar{v}_J$ = 0.667, 433 g #1, 867 g #2.	Wire cylinders with single horizontal tube in each. Tubes parallel.	182.6	0.930	0.489	H_e = 18 cm. Region 2 segregation.
						312.5	0.740	0.564	Bed nearly well-mixed except for steep
						265.5	0.518	0.613	gradient near bottom.
						188.8	0.343	0.621	I = 0.114.
						206.9	0.191	0.869	
						145.2	0.056	0.980	
	GG-3'	15.0	2.76	$\bar{v}_J$ = 0.667, 500 g #1, 1000 g #2.	Wire cylinders with single horizontal tube in each. Tubes parallel.	263.5	0.912	0.511	H_e = 20 cm. Region 2 segregation.
						286.1	0.729	0.594	Bed nearly well-mixed except for steep
						393.0	0.502	0.619	gradient near bottom.
						242.3	0.290	0.656	I = 0.094.
						167.5	0.154	0.913	
						146.4	0.049	0.957	
	GG-21'	15.0	2.45	$\bar{v}_J$ = 0.667, 500 g #1, 1000 g #2.	Wire cylinders with single horizontal tube in each. Tubes parallel.	136.0	0.955	0.124	H_e = 18 cm. Region 2 segregation.
						165.0	0.854	0.200	Steep gradient between upper and lower
						249.9	0.716	0.350	layers.
						223.4	0.559	0.677	I = 0.518.
						255.4	0.399	0.944	
						470.9	0.157	0.999	
	GG-29	15.0	2.77	$\bar{v}_J$ = 0.667, 500 g #1, 1000 g #2.	Wire cylinders with two horizontal tubes in each. Tubes parallel.	231.7	0.923	0.609	H_e = 20 cm. Region 2 segregation.
						265.8	0.757	0.596	Bed nearly well-mixed except for steep
						268.0	0.579	0.640	gradient near bottom.
						247.2	0.408	0.613	I = 0.041.
						329.9	0.215	0.705	
						157.7	0.053	0.920	

Table A-2. (continued)

Solids	Run no.	H_s Static bed height (cm)	u_o Superficial gas velocity (m/s)	Overall bed composition	Bed internals	Sample size (g)	z Average dimensionless axial position	v_J Sample jetsam volume fraction	Remarks
Glass #1 and #2. Large glass acts as jetsam.	GG-30	14.0	2.75	$\bar{v}_J$ = 0.667, 500 g #1, 1000 g #2.	None	209.5	0.930	0.522	High degree of slugging turbulence.
						192.2	0.796	0.644	H_e = 19-44 cm. Region 2 segregation.
						159.2	0.679	0.633	Bed nearly well-mixed except for steep
						297.3	0.527	0.653	gradient near bottom.
						228.4	0.352	0.685	I = 0.026.
						414.2	0.138	0.763	
	GG-30'	13.7	2.73	$\bar{v}_J$ = 0.667, 500 g #1, 1000 g #2.	None	194.4	0.935	0.600	High degree of slugging/turbulence.
						185.0	0.809	0.634	H_e = 21-41 cm. Region 2 segregation.
						306.3	0.645	0.653	Bed nearly well-mixed except for steep
						218.7	0.470	0.656	gradient near bottom.
						277.7	0.305	0.648	I = 0.020.
						179.3	0.153	0.688	
						139.1	0.046	0.861	
	GG-31	14.5	2.78	$\bar{v}_J$ = 0.667, 500 g #1, 1000 g #2.	Wire cylinders with no tubes.	204.4	0.932	0.488	H_e = 22 cm. Region 2 segregation.
						331.7	0.753	0.675	Profile shape appears somewhat erratic.
						223.1	0.569	0.702	I = 0.043.
						273.7	0.403	0.616	
						215.0	0.240	0.658	
						253.1	0.084	0.830	
	GG-31'	14.5	2.78	$\bar{v}_J$ = 0.667, 500 g #1, 1000 g #2.	Wire cylinders with no tubes.	266.8	0.911	0.555	H_e = 22 cm. Region 2 segregation.
						237.3	0.743	0.669	Profile shape appears somewhat erratic.
						268.0	0.575	0.652	I = 0.037.
						263.4	0.398	0.626	
						213.8	0.239	0.654	
						251.3	0.084	0.852	
	GG-29'	15.0	2.72	$\bar{v}_J$ = 0.667, 500 g #1, 1000 g #2.	Wire cylinders with two tubes in each. Tubes parallel.	245.5	0.918	0.638	H_e = 20 cm. Region 2 segregation.
						224.9	0.762	0.638	Bed nearly well-mixed except for steep
						264.8	0.599	0.606	gradient near bottom.
						223.3	0.436	0.576	I = 0.039.
						208.8	0.292	0.636	
						333.7	0.111	0.835	

Table A-2. (continued)

Solids	Run no.	H_s Static bed height (cm)	u_o Superficial gas velocity (m/s)	Overall bed composition	Bed internals	Sample size (g)	z Average dimensionless axial position	v_j Sample jetsam volume fraction	Remarks
Glass #1 and #2. Large glass acts as jetsam.	GG-32	13.7	1.80	$\bar{v}_j$ = 0.667, 500 g #1, 1000 g #2.	None	118.6	0.961	0.080	Initial condition segregated. Increased flow slowly to final value and held. Fluidization interface at z = 0.537. H_s = 15 cm. Region 1 segregation. I = 0.649.
						193.7	0.857	0.130	
						247.2	0.710	0.284	
						194.5	0.563	0.778	
						334.3	0.387	0.992	
						413.2	0.138	1.000	
	GG-33	14.0	1.95	$\bar{v}_j$ = 0.667, 500 g #1, 1000 g #2.	None	128.3	0.957	0.106	Initial condition segregated. Increased flow slowly to final value and held. Fluidization interface at z = 0.0. H_s = 16 cm. At boundary between Region 1 and Region 2 segregation. I = 0.491.
						195.5	0.850	0.231	
						186.7	0.722	0.334	
						208.7	0.591	0.644	
						268.5	0.432	0.898	
						513.8	0.171	0.982	
	GG-34	14.0	1.79	$\bar{v}_j$ = 0.667, 500 g #1, 1000 g #2.	None	126.2	0.958	0.036	Initial condition segregated. Increased flow until bed fully fluidized and then reduced flow to final value and held. Fluidization interface at z = 0.51. H_s = 15 cm. Region 1 segregation. I = 0.640.
						186.5	0.854	0.106	
						284.6	0.697	0.374	
						217.6	0.530	0.895	
						254.7	0.373	0.966	
						431.8	0.144	0.993	
	GG-35	14.0	1.63	$\bar{v}_j$ = 0.667, 500 g #1, 1000 g #2.	None	126.1	0.958	0.016	Initial condition segregated. Increased flow until bed fully fluidized and then slowly reduced flow to final value. Fluidization interface at z = 0.69. H_s = 14 cm. Region 1 segregation. I = 0.556.
						189.1	0.853	0.124	
						167.3	0.734	0.380	
						232.8	0.601	0.733	
						386.9	0.395	0.899	
						398.6	0.133	0.986	
	GG-37	13.7	1.82	$\bar{v}_j$ = 0.667, 500 g #1, 1000 g #2.	None	141.7	0.953	0.058	Initial condition segregated. Brought up air flow slowly to final value and held. Fluidization interface at z = 0.54. H_s = 16 cm. Region 1 segregation. I = 0.626.
						221.9	0.832	0.116	
						175.9	0.699	0.406	
						246.5	0.558	0.759	
						300.1	0.376	0.978	
						413.9	0.138	1.000	

Table A-2. (continued)

Solids	Run no.	H_s Static bed height (cm)	u_0 Superficial gas velocity (m/s)	Overall bed composition	Bed internals	Sample size (g)	z Average dimensionless axial position	v_J Sample jetsam volume fraction	Remarks
Glass #1 and #2. Large glass acts as jetsam.	GG-39	13.7	1.82	$\bar{v}_J$ = 0.667, 500 g #1, 1000 g #2.	None	140.5	0.953	0.071	Initial condition well-mixed. Brought up air slowly to final value and held. Fluidization interface at z = 0.54. H_e = 16 cm. Region I segregation. I = 0.607.
						161.2	0.853	0.113	
						254.4	0.714	0.341	
						186.7	0.567	0.775	
						298.8	0.405	0.988	
						456.4	0.152	0.973	
	GG-40	13.7	1.65	$\bar{v}_J$ = 0.667, 500 g #1, 1000 g #2.	None	114.4	0.962	0.051	Initial condition well-mixed. Brought up air slowly to final value and held. Fluidization interface at z = 0.83. H_e = 14 cm. Region I segregation. I = 0.286.
						173.5	0.866	0.236	
						216.2	0.736	0.733	
						287.3	0.568	0.863	
						237.8	0.393	0.766	
						471.4	0.157	0.773	
	GG-26'	13.7	1.67	$\bar{v}_J$ = 0.667, 500 g #1, 1000 g #2.	None	135.6	0.955	0.052	Initial condition segregated. Increased air flow slowly to final value and held. Fluidization interface at z = 0.63. H_e = 14 cm. Region I segregation. I = 0.717
						161.9	0.856	0.077	
						223.4	0.727	0.223	
						199.8	0.586	0.763	
						279.1	0.427	0.995	
						500.6	0.167	1.000	
	GG-32'	13.7	1.83	$\bar{v}_J$ = 0.667, 500 g #1, 1000 g #2.	None	168.8	0.944	0.074	Initial condition segregated. Increased air flow slowly to final value and held. Fluidization interface at z = 0.52. H_e = 15 cm. Region I segregation. I = 0.595.
						152.5	0.837	0.155	
						178.8	0.727	0.276	
						226.2	0.592	0.727	
						253.1	0.432	0.928	
						522.1	0.174	0.988	

Table A-2. (continued)

Solids	Run no.	H_s Static bed height (cm)	u_o Superficial gas velocity (m/s)	Overall bed composition	Bed internals	Sample size (g)	z Average dimensionless axial position	v_J Sample jetsam volume fraction	Remarks
Glass #1 and #2. Large glass acts as jetsam.	GG-41	13.7	1.58	$\bar{v}_J$ = 0.667, 500 g #1, 1000 g #2.	None	131.6	0.956	0.060	Initial condition segregated. Increased air flow slowly to final value and held. Fluidization interface at z = 0.70. H_e = 14 cm. Region 1 segregation. I = 0.695.
						140.2	0.866	0.165	
						190.6	0.755	0.130	
						210.8	0.622	0.561	
						344.1	0.437	0.995	
						483.8	0.161	1.000	
	GG-42	13.7	1.73	$\bar{v}_J$ = 0.667, 500 g #1, 100 g #2.	None	170.0	0.943	0.105	Initial condition segregated. Increased air flow slowly to final value and held. Fluidization interface at z = 0.54. H_e = 14 cm. Region 1 segregation. I = 0.620.
						121.0	0.847	0.103	
						189.6	0.743	0.256	
						256.3	0.595	0.631	
						251.3	0.426	0.984	
						513.0	0.171	1.000	
	GG-43	13.7	1.70	$\bar{v}_J$ = 0.667, 500 g #1, 1000 g #2.	None	130.8	0.957	0.138	Initial condition segregated. Increased air flow slowly to final value and held. Fluidization interface at z = 0.54. H_e = 14 cm. Region 1 segregation. I = 0.543.
						157.6	0.860	0.147	
						142.9	0.760	0.183	
						240.5	0.633	0.517	
						240.5	0.473	0.914	
						589.2	0.196	1.000	
	GG-44	13.7	1.88	$\bar{v}_J$ = 0.667, 500 g #1, 1000 g #2.	None	167.4	0.944	0.115	Initial condition segregated. Increased air flow slowly to final value and held. Fluidization interface at z = 0.15. H_e = 16 cm. Region 1 segregation. I = 0.535.
						142.8	0.841	0.155	
						146.9	0.745	0.278	
						222.6	0.622	0.625	
						276.8	0.455	0.874	
						545.2	0.182	0.986	
	GG-45	13.7	1.76	$\bar{v}_J$ = 0.667, 500 g #1, 100 g #2.	None	163.1	0.946	0.093	Initial condition well-mixed. Increased air flow slowly to final value and held. Fluidization interface at z = 0.56. H_e = 15 cm. Region 1 segregation. I = 0.559.
						186.4	0.829	0.157	
						182.1	0.707	0.346	
						229.3	0.570	0.839	
						238.6	0.414	0.986	
						501.5	0.167	0.928	

Table A-2. (continued)

Solids	Run no.	H_s Static bed height (cm)	u_o Superficial gas velocity (m/s)	Overall bed composition	Bed internals	Sample size (g)	z Average dimensionless axial position	v_J Sample jetsam volume fraction	Remarks
Glass #1 and #2. Large glass acts as jetsam.	GG-46	13.7	1.72	$\bar{v}_J$ = 0.667, 500 g #1, 1000 g #2.	None	115.8	0.961	0.146	Initial condition well-mixed. Increased air flow slowly to final value and held. Fluidization interface at z = 0.61. H_e = 14 cm. Region 1 segregation. I = 0.413.
						148.5	0.873	0.199	
						216.8	0.752	0.319	
						206.2	0.611	0.725	
						355.5	0.423	0.946	
						457.0	0.152	0.872	
	GG-47	13.7	1.57	$\bar{v}_J$ = 0.667 500 g #1, 1000 g #2.	None	160.3	0.947	0.099	Initial condition well-mixed. Increased air flow slowly to final value and held. Fluidization interface at z = 0.84. H_e = 14 cm. Region 1 segregation. I = 0.180.
						164.8	0.838	0.809	
						187.3	0.721	0.807	
						260.4	0.572	0.668	
						321.2	0.378	0.746	
						406.2	0.135	0.704	
	GG-33'	13.7	1.96	$\bar{v}_J$ = 0.667, 500 g #1, 1000 g #2.	None	219.1	0.927	0.172	Initial condition segregated. Increased air flow slowly to final value and held. Fluidization interface at z = 0.0. H_e = 16 cm. At boundary between Region 1 and Region 2 segregation. I = 0.432.
						204.4	0.786	0.302	
						312.3	0.614	0.585	
						251.1	0.426	0.830	
						250.9	0.259	0.985	
						262.8	0.088	1.000	
	GG-33"	13.7	1.94	$\bar{v}_J$ = 0.667, 500 g #1, 1000 g #2.	None	133.9	0.955	0.124	Initial condition well-mixed. Increased air flow slowly to final value and held. Fluidization interface at z = 0.0. H_e = 15 cm. At boundary between Region 1 and Region 2 segregation. I = 0.570
						164.1	0.856	0.156	
						231.5	0.724	0.273	
						209.4	0.577	0.736	
						261.3	0.421	0.978	
						500.5	0.167	0.969	
	GG-48	13.7	2.05	$\bar{v}_J$ = 0.667, 500 g #1, 1000 g #2.	None	174.0	0.942	0.121	H_e = 17 cm. Region 2 segregation. Steep composition gradient between upper and lower layers. I = 0.565.
						189.0	0.821	0.212	
						165.0	0.703	0.284	
						199.8	0.582	0.698	
						331.2	0.405	0.951	
						442.1	0.147	0.991	

Table A-2. (continued)

Solids	Run no.	H_s Static bed height (cm)	u_o Superficial gas velocity (m/s)	Overall bed composition	Bed internals	Sample size (g)	z Average dimensionless axial position	v_J Sample jetsam volume fraction	Remarks
Glass #1 and #2. Large glass acts as jetsam.	GG-49	13.7	2.07	$\bar{v}_J$ = 0.667, 500 g #1, 1000 g #2.	None	228.9	0.924	0.250	H_e = 16 cm. Region 2 segregation. Steep composition gradient between upper and lower layers. I = 0.379.
						143.3	0.800	0.295	
						182.6	0.691	0.424	
						185.2	0.569	0.615	
						356.8	0.388	0.853	
						404.0	0.135	0.995	
	GG-50	13.7	2.17	$\bar{v}_J$ = 0.667, 500 g #1, 1000 g #2.	None	133.9	0.955	0.255	H_e = 16-23 cm. Region 2 segregation. Jetsam-rich bottom layer with steadily decreasing jetsam concentration above. I = 0.337.
						282.6	0.817	0.375	
						202.3	0.655	0.486	
						212.2	0.517	0.586	
						243.1	0.365	0.871	
						426.0	0.142	1.000	
	GG-51	13.7	2.24	$\bar{v}_J$ = 0.667, 500 g #1, 1000 g #2.	None	154.4	0.949	0.432	H_e = 16-21 cm. Region 2 segregation. Bed nearly well-mixed except for steep gradient near bottom. I = 0.166.
						231.0	0.820	0.538	
						199.8	0.677	0.515	
						187.5	0.548	0.543	
						238.5	0.406	0.619	
						490.0	0.163	0.934	
	GG-52	13.7	2.33	$\bar{v}_J$ = 0.667, 500 g #1, 1000 g #2.	None	138.6	0.954	0.307	H_e = 17-25 cm. Region 2 segregation. Jetsam-rich bottom layer with steadily decreasing jetsam concentration above. I = 0.296.
						179.8	0.848	0.363	
						230.1	0.711	0.464	
						236.8	0.556	0.547	
						307.1	0.375	0.810	
						408.7	0.136	0.999	
	GG-53	13.7	2.44	$\bar{v}_J$ = 0.667, 500 g #1, 1000 g #2.	None	134.8	0.955	0.284	H_e = 18-26 cm. Region 2 segregation. Jetsam-rich bottom layer with steadily decreasing jetsam concentration above. I = 0.302.
						181.0	0.850	0.408	
						199.0	0.723	0.459	
						235.2	0.579	0.506	
						248.3	0.418	0.721	
						502.2	0.167	0.993	

Table A-2. (continued)

Solids	Run no.	H_s Static bed height (cm)	u_o Superficial gas velocity (m/s)	Overall bed composition	Bed internals	Sample size (g)	z Average dimensionless axial position	v_j Sample jetsam volume fraction	Remarks
Glass #1 and #2. Large glass acts as jetsam.	GG-54	13.7	1.91	$\bar{v}_j$ = 0.667, 500 g #1, 1000 g #2.	None	195.3	0.935	0.173	Initial condition well-mixed. Increased air flow to final value and held. Fluidization interface at z = 0.61. H_s = 15 cm. Region 1 segregation. I = 0.530.
						173.7	0.812	0.247	
						185.3	0.692	0.308	
						224.9	0.556	0.685	
						272.5	0.390	0.980	
						449.1	0.150	0.993	
	GG-55	13.7	2.57	$\bar{v}_j$ = 0.667, 500 g #1, 1000 g #2.	None	209.7	0.930	0.342	H_s = 18-26 cm. Region 2 segregation. Bed nearly well-mixed except for steep gradient near bottom. I = 0.179.
						162.2	0.806	0.506	
						192.2	0.688	0.532	
						308.1	0.522	0.618	
						230.1	0.343	0.687	
						399.2	0.133	0.965	
	GG-56	13.7	2.67	$\bar{v}_j$ = 0.667, 500 g #1, 1000 g #2.	None	226.4	0.925	0.405	H_s = 18-29 cm. Region 2 segregation. Bed nearly well-mixed except for steep gradient near bottom. I = 0.189.
						220.8	0.776	0.535	
						229.1	0.626	0.561	
						272.1	0.459	0.612	
						267.4	0.279	0.865	
						284.6	0.095	0.991	
	GG-56'	13.7	2.69	$\bar{v}_j$ = 0.667, 500 g #1, 1000 g #2.	None	235.7	0.922	0.505	H_s = 18-29 cm. Region 2 segregation. Bed nearly well-mixed except for steep gradient near bottom. I = 0.112.
						219.1	0.770	0.550	
						239.9	0.617	0.569	
						253.2	0.453	0.614	
						198.1	0.302	0.698	
						354.9	0.118	0.931	
	GG-57	13.7	2.87	$\bar{v}_j$ = 0.667, 500 g #1, 1000 g #2.	None	258.5	0.914	0.543	H_s = 18-44 cm. Region 2 segregation Bed nearly well-mixed except for steep gradient near bottom. I = 0.073.
						216.0	0.756	0.600	
						228.4	0.608	0.615	
						255.2	0.447	0.617	
						294.8	0.264	0.680	
						248.1	0.083	0.936	

Table A-2. (continued)

Solids	Run no.	H_s Static bed height (cm)	u_o Superficial gas velocity (m/s)	Overall bed composition	Bed internals	Sample size (g)	z Average dimensionless axial position	v_j Sample jetsam volume fraction	Remarks
Glass #1 and #2, large glass acts as jetsam.	GG-58	13.7	3.07	$\bar{v}_j$ = 0.667, 500 g #1, 1000 g #2.	None	163.0	0.946	0.553	H_s = 18-44 cm. Region 2 segregation. Bed nearly well-mixed except for steep gradient near bottom. I = 0.047.
						264.9	0.803	0.631	
						280.3	0.622	0.594	
						245.5	0.446	0.618	
						285.0	0.270	0.689	
						262.2	0.087	0.872	
	GG-59	13.7	3.26	$\bar{v}_j$ = 0.667, 500 g #1, 100 g #2.	None	181.1	0.940	0.570	H_s = 25-54 cm. Region 2 segregation. Bed essentially well-mixed. I = 0.008.
						263.9	0.792	0.661	
						207.9	0.635	0.687	
						298.8	0.466	0.701	
						260.2	0.280	0.648	
						290.6	0.097	0.700	
	GG-60	14.5	1.95	$\bar{v}_j$ = 0.667, 500 g #1, 1000 g #2.	Wire cylinders with single horizontal tube in each. Tubes parallel.	196.4	0.935	0.011	Air flow increased until bed well-fluidized at 2.63 m/s. Air then reduced to final value and held. H_s = 15.7 cm. At boundary between Region 1 and Region 2. I = 0.646.
						226.0	0.781	0.203	
						292.3	0.595	0.737	
						207.4	0.428	0.933	
						229.2	0.283	0.987	
						309.3	0.103	0.998	
	GG-61	14.5	5.14	$\bar{v}_j$ = 0.667, 500 g #1, 1000 g #2.	Wire cylinders with single horizontal tube in each. Tubes parallel.	184.2	0.939	0.535	H_s = 29 cm. Region 2 segregation. Bed nearly well-mixed. Clearly turbulent flow in bed. I = 0.011.
						203.9	0.809	0.678	
						231.8	0.664	0.681	
						242.0	0.506	0.671	
						237.1	0.347	0.683	
						401.2	0.134	0.700	

Table A-2. (continued)

Solids	Run no.	H_s Static bed height (cm)	u_o Superficial gas velocity (m/s)	Overall bed composition	Bed internals	Sample size (g)	z Average dimensionless axial position	v_j Sample jetsam volume fraction	Remarks
Glass #1 and #2. Large glass acts as jetsam.	GG-62	14.6	6.03	$\bar{v}_j$ = 0.667, 500 g #1, 1000 g #2.	Wire cylinders with single horizontal tube in each. Tubes parallel.	156.4	0.948	0.443	H_o = 37 cm. Region 2 segregation. Bed nearly well-mixed. Clearly turbulent flow in bed. I = 0.030.
						218.3	0.823	0.643	
						197.5	0.684	0.654	
						241.2	0.538	0.704	
						258.9	0.371	0.696	
						427.5	0.143	0.728	
	GG-63	14.6	5.59	$\bar{v}_j$ = 0.667, 500 g #1, 1000 g #2.	Wire cylinders with single horizontal tube in each. Tubes parallel	142.9	0.952	0.477	H_o = 34 cm. Region 2 segregation. Bed nearly well-mixed. Clearly turbulent flow. I = 0.019.
						223.7	0.830	0.649	
						248.9	0.673	0.665	
						346.6	0.474	0.696	
						237.4	0.280	0.707	
						300.5	0.100	0.706	
	GG-64	14.7	4.55	$\bar{v}_j$ = 0.667, 500 g #1, 1000 g #2.	Wire cylinders with single horizontal tube in each. Tubes parallel.	149.9	0.950	0.454	H_o = 29 cm. Region 2 segregation. Bed nearly well-mixed. Clearly turbulent flow. I = 0.025.
						157.6	0.848	0.644	
						212.4	0.724	0.691	
						326.8	0.545	0.677	
						332.8	0.325	0.705	
						321.1	0.107	0.711	
	GG-65	14.6	3.86	$\bar{v}_j$ = 0.667, 500 g #1, 1000 g #2.	Wire cylinders with single horizontal tube in each. Tubes parallel.	143.4	0.952	0.515	H_o = 27 cm. Region 2 segregation. Nearly well-mixed. Turbulent flow. I = 0.014.
						184.0	0.843	0.666	
						256.3	0.696	0.662	
						349.4	0.494	0.661	
						271.1	0.287	0.687	
						295.3	0.099	0.734	

Table A-2. (continued)

Solids	Run no.	H_2 Static bed height (cm)	u_o Superficial gas velocity (m/s)	Overall bed composition	Bed internals	Sample size (g)	z Average dimensionless axial position	v_J Sample jetsam volume fraction	Remarks
Clear acrylic and polypropylene Acrylic acts as jetsam.	AP-1	30.0	2.40	$\bar{v}_J$ = 0.857, 1362 g acrylic, 176 g polypro-pylene.	None	124.0	0.958	0.672	H_e = 53 cm. Region 2 segregation. Jetsam concentration increasing steadily with depth. I = 0.110.
						160.1	0.864	0.703	
						200.1	0.750	0.752	
						140.9	0.640	0.792	
						172.6	0.542	0.853	
						186.8	0.436	0.926	
						225.7	0.305	0.978	
						327.6	0.114	0.987	
	AP-2	29.2	3.39	$\bar{v}_J$ = 0.857, 1362 g acrylic, 176 g polypro-pylene.	None	206.4	0.935	0.669	H_e = 94 cm. Region 2 segregation. Jetsam concentration increasing steadily with depth. I = 0.065.
						219.9	0.791	0.798	
						283.9	0.626	0.863	
						312.5	0.448	0.890	
						207.4	0.287	0.917	
						100.1	0.174	0.953	
						208.9	0.065	0.953	
	AP-3	30.0	2.00	$\bar{v}_J$ = 0.857, 1362 g acrylic, 176 g polypro-pylene.	None	126.6	0.953	0.230	H_e = 44 cm. Region 2 segregation. Steep composition gradient in the upper layer. I = 0.528.
						140.1	0.856	0.489	
						188.4	0.752	0.875	
						165.1	0.646	0.982	
						236.6	0.517	0.996	
						262.2	0.364	0.999	
						214.3	0.208	0.999	
						204.5	0.064	0.999	
	AP-4	29.2	1.47	$\bar{v}_J$ = 0.857, 1361 g acrylic, 175 g polypro-pylene.	None	74.7	0.974	0.054	Initial condition was inverted segregation. Air flow was increased to full fluidization and then reduced slowly to final value and held. Fluidization interface located at z = 0.75. Region 1 segregation. I = 0.718.
						104.6	0.904	0.206	
						143.1	0.817	0.797	
						156.2	0.730	0.978	
						265.0	0.604	0.996	
						279.4	0.435	0.999	
						266.8	0.261	1.000	
						245.9	0.087	1.000	

Table A-2. (continued)

Solids	Run no.	H_s Static bed height (cm)	u_o Superficial gas velocity (m/s)	Overall bed composition	Bed internals	Sample size (g)	z Average dimensionless axial position	v_J Sample jetsam volume fraction	Remarks
Clear acrylic and polypropylene. Acrylic acts as jetsam.	AP-5	29.2	1.02	$\bar{v}_J$ = 0.857, 1361 g acrylic, 175 g polypropylene.	None	76.0	0.974	0.005	Initial condition was inverted segregation. Air flow was increased to full fluidization and then reduced to final value and held. Fluidization interface located at z = 0.75. Region 1 segregation. I = 0.778.
						110.7	0.909	0.211	
						132.1	0.826	0.864	
						166.5	0.739	0.980	
						278.8	0.609	0.996	
						272.2	0.430	1.000	
						251.3	0.257	1.000	
						249.1	0.087	1.000	
	AP-6	15.2	2.44	$\bar{v}_J$ = 0.857, 680 g acrylic, 87.5 g polypropylene.	None	116.2	0.917	0.577	H_e = 26 cm. Region 2 segregation. Gradual composition change through most of the bed. I = 0.139.
						191.0	0.708	0.839	
						131.9	0.492	0.925	
						180.6	0.300	0.935	
						147.4	0.100	0.964	
	AP-7	14.7	3.43	$\bar{v}_J$ = 0.857, 680 g acrylic, 87.5 g polypropylene.	None	147.0	0.905	0.853	H_e = 48 cm. Region 2 segregation. Bed essentially well-mixed. I = 0.0.
						151.0	0.707	0.850	
						184.6	0.491	0.861	
						152.8	0.276	0.865	
						131.9	0.086	0.855	
	AP-1'	30.0	2.44	$\bar{v}_J$ = 0.857, 1358 g acrylic, 175 g polypropylene.	None	336.8	0.879	0.637	H_e = 53 cm. Region 2 segregation. Jetsam concentration increasing steadily with depth. I = 0.181.
						246.3	0.681	0.742	
						213.3	0.535	0.916	
						226.6	0.397	0.981	
						286.8	0.238	0.993	
						223.2	0.069	0.997	
	AP-8	14.0	3.39	$\bar{v}_J$ = 0.857, 680 g acrylic, 87.5 g polypropylene.	Wire cylinders with no horizontal tubes.	139.9	0.927	0.873	H_e = 33 cm. Region 2 segregation. Bed essentially well-mixed. I = 0.002.
						160.5	0.736	0.828	
						177.8	0.491	0.857	
						113.4	0.291	0.856	
						175.8	0.109	0.871	

Table A-2. (continued)

Solids	Run no.	H_s Static bed height (cm)	u_0 Superficial gas velocity (m/s)	Overall bed composition	Bed internals	Sample size (g)	z Average dimensionless axial position	v_j Sample jetsam volume fraction	Remarks
Clear acrylic and polypropylene. Acrylic acts as jetsam.	AP-9	15.0	3.38	$\bar{v}_j$ = 0.857, 680 g acrylic, 87.5 g polypropylene.	Wire cylinders with single horizontal tube in each. Tubes parallel.	89.7	0.941	0.667	Region 2 segregation. Jetsam concentration increasing steadily with depth. I = 0.065.
						138.3	0.788	0.809	
						157.0	0.585	0.829	
						156.4	0.381	0.913	
						226.5	0.144	0.947	
	AP-10	30.5	3.38	$\bar{v}_j$ = 0.856, 1358 g acrylic, 175 g polypropylene.	Wire cylinders with single horizontal tube in each. Tubes parallel.	122.9	0.963	0.389	H_s = 53 cm. Region 2 segregation. Steep composition gradient in the upper layer. I = 0.343.
						117.7	0.883	0.470	
						170.2	0.788	0.803	
						161.7	0.683	0.917	
						150.8	0.575	0.962	
						302.3	0.421	0.981	
						188.0	0.258	0.982	
						319.9	0.096	0.982	
	AP-12	30.2	2.42	$\bar{v}_j$ = 0.857, 1358 g acrylic, 175 g polypropylene.	Wire cylinders with single horizontal tube in each. Tubes parallel.	132.6	0.941	0.169	H_s = 42 cm. Region 2 segregation. Steep composition gradient in the upper layer. I = 0.567.
						177.1	0.828	0.616	
						173.5	0.714	0.929	
						188.1	0.600	0.986	
						122.1	0.500	0.997	
						174.1	0.408	0.997	
						234.6	0.277	1.000	
						330.6	0.101	1.000	
	AP-13	30.5	2.96	$\bar{v}_j$ = 0.858, 1357 g acrylic, 174 g polypropylene.	Wire cylinders with single horizontal tube in each. Tubes parallel.	122.2	0.958	0.301	H_s = 60 cm. Region 2 segregation. Steep composition gradient in the upper layer. I = 0.433.
						153.9	0.863	0.522	
						181.2	0.750	0.836	
						198.6	0.629	0.971	
						158.0	0.513	0.987	
						237.4	0.375	0.994	
						198.4	0.238	0.997	
						280.6	0.092	0.998	

Table A-2. (continued)

Solids	Run no.	H_s Static bed height (cm)	u_0 Superficial gas velocity (m/s)	Overall bed composition	Bed internals	Sample size (g)	z Average dimensionless axial position	v_J Sample jetsam volume fraction	Remarks
Clear acrylic and polypropylene. Acrylic acts as jetsam.	AP-19	22.7	3.57	$\bar{v}_J$ = 0.857, 1020 g acrylic, 131 g polypro-pylene.	Wire cylinders with single horizontal tube in each. Tubes parallel.	169.1	0.925	0.783	H_s = 41 cm. Region 2 segregation. Bed nearly well-mixed. I = 0.014.
						191.4	0.771	0.821	
						217.8	0.581	0.864	
						235.0	0.386	0.873	
						167.9	0.235	0.874	
						170.1	0.084	0.922	
	AP-20	13.0	4.09	$\bar{v}_J$ = 0.667, 435 g acrylic, 175 g polypro-pylene.	Wire cylinders with single horizontal tube in each. Tubes parallel.	58.2	0.950	0.296	H_s = 32 cm. Region 2 segregation. Steep gradient near bottom and top with well-mixed middle region. I = 0.169.
						107.3	0.808	0.560	
						118.6	0.614	0.578	
						119.8	0.409	0.654	
						89.7	0.228	0.862	
						88.0	0.076	0.974	
	AP-21	13.5	3.92	$\bar{v}_J$ = 0.667, 435 g acrylic, 175 g polypro-pylene.	Wire cylinders with single horizontal tube in each. Tubes parallel.	74.2	0.936	0.390	H_s = 31 cm. Region 2 segregation. Steep gradient near bottom and top with well-mixed middle region. I = 0.100.
						122.5	0.767	0.604	
						103.2	0.573	0.676	
						83.7	0.412	0.632	
						106.7	0.248	0.727	
						91.0	0.078	0.928	
	AP-22	13.2	3.77	$\bar{v}_J$ = 0.667, 435 g acrylic, 175 g polypro-pylene.	Wire cylinders with single horizontal tube in each. Tubes parallel.	82.0	0.930	0.347	H_s = 29 cm. Region 2 segregation. Steep gradient near top and bottom with well-mixed middle region. I = 0.117.
						123.6	0.753	0.662	
						107.3	0.554	0.621	
						78.8	0.394	0.673	
						122.4	0.221	0.772	
						67.7	0.058	0.942	
	AP-23	13.2	4.76	$\bar{v}_J$ = 0.667, 435 g acrylic 175 g polypro-pylene.	Wire cylinders with single horizontal tube in each. Tubes parallel.	57.9	0.950	0.231	H_s = 42 cm. Region 2 segregation. Steady gradient through most of the bed. I = 0.331.
						86.0	0.826	0.310	
						80.9	0.682	0.484	
						130.5	0.500	0.745	
						112.5	0.290	0.893	
						112.1	0.097	0.986	

Table A-2. (continued)

Solids	Run no.	H_s Static bed height (cm)	u_o Superficial gas velocity (m/s)	Overall bed composition	Bed internals	Sample size (g)	z Average dimensionless axial position	v_J Sample jetsam volume fraction	Remarks
Clear acrylic and polypropylene. Acrylic acts as jetsam.	AP-24	13.5	4.33	$\bar{v}_J$ = 0.667, 455 g acrylic, 175 g polypro-pylene.	Wire cylinders with single horizontal tube in each. Tubes parallel.	65.7	0.944	0.219	H_s = 35 cm. Region 2 segregation. Steady gradient through most of the bed. I = 0.227.
						86.1	0.813	0.431	
						121.7	0.635	0.629	
						102.9	0.442	0.748	
						107.5	0.261	0.847	
						98.1	0.084	0.936	
	AP-25	13.2	3.54	$\bar{v}_J$ = 0.667, 455 g acrylic, 175 g polypro-pylene.	Wire cylinders with single horizontal tube in each. Tubes parallel.	48.1	0.959	0.375	H_s = 27 cm. Region 2 segregation. Steep gradient near top and bottom with well-mixed middle region. I = 0.109.
						92.7	0.838	0.546	
						107.0	0.666	0.637	
						110.0	0.480	0.633	
						111.8	0.289	0.675	
						112.4	0.097	0.941	
	AP-26	13.7	3.30	$\bar{v}_J$ = 0.667, 455 g acrylic, 175 g polypro-pylene.	Wire cylinders with single horizontal tube in each. Tubes parallel.	74.3	0.936	0.167	H_s = 28 cm. Region 2 segregation. Steady gradient throughout most of the bed. I = 0.364.
						95.7	0.790	0.370	
						118.7	0.606	0.605	
						99.5	0.418	0.821	
						124.6	0.225	0.949	
						68.8	0.059	0.992	
	AP-27	13.7	3.04	$\bar{v}_J$ = 0.667, 455 g acrylic, 175 g polypro-pylene	Wire cylinders with single horizontal tube in each. Tubes parallel.	71.3	0.939	0.156	H_s = 25 cm. Region 2 segregation. Steady gradient throughout most of the bed. I = 0.313.
						80.1	0.809	0.435	
						103.5	0.651	0.542	
						119.9	0.459	0.726	
						131.9	0.242	0.939	
						75.1	0.065	0.999	
	AP-28	13.7	2.74	$\bar{v}_J$ = 0.667, 455 g acrylic, 175 g polypro-pylene.	Wire cylinders with single horizontal tube in each. Tubes parallel.	68.5	0.941	0.069	H_s = 24 cm. Region 2 segregation. Relatively sharp interface between upper and lower layers. I = 0.634.
						96.8	0.799	0.132	
						103.5	0.627	0.637	
						113.0	0.441	0.928	
						120.9	0.240	0.997	
						79.4	0.068	1.000	

Table A-2. (continued)

Solids	Run no.	H_s Static bed height (cm)	u_o Superficial gas velocity (m/s)	Overall bed composition	Bed internals	Sample size (g)	z Average dimensionless axial position	v_J Sample jetsam volume fraction	Remarks
Clear acrylic and polypropylene. Acrylic acts as jetsam.	AP-29	13.7	2.51	$\bar{v}_J$ = 0.667, 455 g acrylic, 175 g polypropylene.	Wire cylinders with single horizontal tube in each. Tubes parallel.	48.7	0.958	0.025	H_s = 22 cm. Region 2 segregation. Relatively sharp gradient between upper and lower layers. I = 0.753.
						97.3	0.833	0.068	
						84.3	0.677	0.393	
						89.5	0.528	0.954	
						132.2	0.337	0.997	
						130.1	0.112	0.999	
	AP-30	13.7	2.18	$\bar{v}_J$ = 0.667, 455 g acrylic, 175 g polypropylene.	Wire cylinders with single horizontal tube in each. Tubes parallel.	52.7	0.955	0.0	H_s = 18 cm. Region 2 segregation. Relatively sharp gradient between upper and lower layers. I = 0.809.
						84.6	0.837	0.001	
						94.5	0.683	0.420	
						123.0	0.496	0.989	
						124.0	0.284	1.000	
						103.3	0.089	1.000	
	AP-31	13.7	3.42	$\bar{v}_J$ = 0.667, 455 g acrylic, 175 g polypropylene.	Wire cylinders with single horizontal tube in each. Tubes parallel.	79.6	0.932	0.270	H_s = 28 cm. Region 2 segregation. Steady composition gradient through most of the bed. I = 0.242.
						87.2	0.789	0.464	
						112.8	0.617	0.573	
						122.9	0.414	0.761	
						116.8	0.209	0.904	
						62.9	0.054	0.990	
	AP-32	13.7	2.90	$\bar{v}_J$ = 0.667, 455 g acrylic, 175 g polypropylene.	Wire cylinders with single horizontal tube in each. Tubes parallel.	73.4	0.937	0.219	H_s = 25 cm. Region 2 segregation. Steady composition gradient through most of the bed. I = 0.317.
						81.4	0.804	0.437	
						126.7	0.625	0.524	
						73.9	0.452	0.733	
						118.8	0.287	0.916	
						107.4	0.092	0.997	
	AP-33	13.7	2.80	$\bar{v}_J$ = 0.667, 455 g acrylic, 175 g polypropylene.	Wire cylinders with single horizontal tube in each. Tubes parallel.	70.6	0.939	0.177	H_s = 24 cm. Region 2 segregation. Relatively sharp gradient between upper and lower layers. I = 0.530.
						79.7	0.810	0.173	
						116.7	0.641	0.497	
						81.4	0.411	0.887	
						150.2	0.272	0.989	
						83.1	0.072	0.999	

Table A-2. (continued)

Solids	Run no.	H_s Static bed height (cm)	u_0 Superficial gas velocity (m/s)	Overall bed composition	Bed internals	Sample size (g)	z Average dimensionless axial position	v_j Sample jetsam volume fraction	Remarks
Clear acrylic and polypropylene. Acrylic acts as jetsam.	AP-34	13.7	1.97	$\bar{v}_j$ = 0.667, 455 g, acrylic, 175 g polypro-pylene.	Wire cylinders with single horizontal tube in each. Tubes parallel.	64.2	0.945	0.0	H_s = 16 cm. Region 2 segregation. Sharp interface between upper and lower layers. I = 0.853.
						87.3	0.815	0.003	
						69.8	0.680	0.418	
						112.0	0.523	0.986	
						114.7	0.303	0.999	
						103.4	0.089	1.000	
	AP-35	13.5	2.70	$\bar{v}_j$ = 0.667, 455 g, acrylic, 175 g polypro-pylene.	Wire cylinders with single horizontal tube in each. Tubes parallel.	54.3	0.953	0.028	H_s = 23 cm. Region 2 segregation. Relatively sharp gradient between upper and lower layers. I = 0.636.
						78.3	0.839	0.110	
						89.1	0.695	0.413	
						71.6	0.557	0.818	
						132.0	0.382	0.955	
						156.2	0.134	1.000	
	AP-36	13.5	1.84	$\bar{v}_j$ = 0.667, 455 g acrylic, 175 g polypro-pylene.	Wire cylinders with single horizontal tube in each. Tubes parallel.	64.5	0.945	0.0	H_s = 16 cm. Region 2 segregation. Sharp interface between upper and lower layers. I = 0.838.
						72.9	0.826	0.003	
						86.6	0.689	0.371	
						78.9	0.547	0.984	
						123.8	0.372	0.997	
						154.4	0.133	1.000	
	AP-37	13.5	1.71	$\bar{v}_j$ = 0.667 455 g acrylic, 175 g polypro-pylene.	Wire cylinders with single horizontal tube in each. Tubes parallel.	55.7	0.952	0.007	H_s = 15 cm. Region 2 segregation. Sharp interface between upper and lower layers. I = 0.798.
						82.7	0.833	0.045	
						79.9	0.693	0.318	
						78.5	0.557	0.940	
						117.4	0.389	0.997	
						167.7	0.144	1.000	
	AP-38	13.5	1.63	$\bar{v}_j$ = 0.667, 455 g acrylic, 175 g polypro-pylene.	Wire cylinders with single horizontal tube in each. Tubes parallel.	42.0	0.964	0.002	H_s = 14 cm. Boundary between Region 1 Region 2. Sharp interface between upper and lower layers. I = 0.849
						75.3	0.863	0.012	
						90.2	0.720	0.197	
						62.5	0.589	0.938	
						104.5	0.445	0.995	
						206.1	0.178	1.000	

Table A-2. (continued)

Solids	Run no.	H_s Static bed height (cm)	u_o Superficial gas velocity (m/s)	Overall bed composition	Bed internals	Sample size (g)	z Average dimensionless axial position	v_J Sample jetsam volume fraction	Remarks
#2 glass and polypropylene. Glass acts as jetsam.	GP-1	15.2	4.66	$\bar{v}_J$ = 0.709, 1065 g #2 glass, 176 g polypropylene.	Wire cylinders with single horizontal tube in each. Tubes parallel.	113.7 124.7 224.5 274.3 258.9 225.6	0.914 0.759 0.595 0.414 0.250 0.086	0.143 0.276 0.825 0.922 0.966 0.996	H_s = 61 cm. Region 2 segregation. Relatively sharp interface between upper and lower layers. I = 0.543.
	GP-1a	13.5	0.99	$\bar{v}_J$ = 0.696, 1000 g #2 glass, 176 g polypropylene.	None.	-	z > 0.696 z < 0.696	0.0 1.0	Initial condition segregated. Flotsam just starting to fluidize. I = 1.0.
	GP-2	15.0	3.94	$\bar{v}_J$ = 0.709, 1065 g #2 glass, 176 g polypropylene.	Wire cylinders with single horizontal tube in each. Tubes parallel.	84.9 167.9 272.0 240.0 290.3 188.8	0.939 0.794 0.606 0.417 0.228 0.063	0.102 0.432 0.791 0.868 0.911 0.991	H_s = 46 cm. Region 2 segregation. Diffuse interface between jetsam-rich and flotsam-rich zones. Convection appears unusually enhanced. I = 0.397.
	GP-2a, 2b, 2c, 2d	13.5	0.99, 1.11, 1.26, 1.40 respectively	$\bar{v}_J$ = 0.696, 1000 g #2 glass, 176 g polypropylene.	None	-	all z	0.696	Initial condition well-mixed. Bed completely unfluidized. I = 0.0.
	GP-3	15.2	3.67	$\bar{v}_J$ = 0.709, 1065 g #2 glass, 176 g polypropylene.	Wire cylinders with single horizontal tube in each. Tubes parallel.	99.9 112.5 300.5 260.8 239.2 228.7	0.923 0.778 0.603 0.405 0.234 0.076	0.044 0.255 0.886 0.953 0.958 0.998	H_s = 34 cm. Region 2 segregation. Relatively sharp interface between upper and lower layers. I = 0.661.
	GP-4	14.6	5.36	$\bar{v}_J$ = 0.709, 1065 g #2 glass, 176 g polypropylene.	Wire cylinders with single horizontal tube in each. Tubes parallel.	65.7 139.8 198.8 225.2 196.5 198.0	0.939 0.793 0.634 0.481 0.336 0.135	0.104 0.253 0.802 0.924 0.952 0.973	H_s = 64 cm. Region 2 segregation. Relatively sharp interface between upper and lower layers. I = 0.558.

Table A-2. (continued)

Solids	Run no.	H_s Static bed height (cm)	v_0 Superficial gas velocity (m/s)	Overall bed composition	Bed internals	Sample size (g)	z Average dimensionless axial position	v_j Sample jetsam volume fraction	Remarks
#2 glass and polypropylene. Glass acts as jetsam.	GP-5	15.0	3.12	$\bar{v}_j$ = 0.709, 1065 g #2 glass, 176 g polypropylene.	Wire cylinders with single horizontal tube in each. Tubes parallel.	65.5	0.946	0.004	H_s = 28 cm. Region 2 segregation. Sharp interface between upper and lower layers. I = 0.790.
						90.4	0.824	0.066	
						150.5	0.690	0.597	
						294.1	0.526	0.993	
						321.7	0.320	0.998	
						319.4	0.106	0.999	
	GP-6	14.7	2.77	$\bar{v}_j$ = 0.709, 1065 g #2 glass, 176 g polypropylene.	Wire cylinders with single horizontal tube in each. Tubes parallel.	67.5	0.944	0.001	H_s = 25 cm. Region 2 segregation. Sharp interface between upper and lower layers. I = 0.803.
						72.2	0.831	0.028	
						153.9	0.703	0.541	
						309.0	0.527	0.994	
						359.9	0.304	0.999	
						276.0	0.092	1.000	
	GP-7	14.7	2.28	$\bar{v}_j$ = 0.709, 1065 g #2 glass, 176 g polypropylene.	Wire cylinders with single horizontal tube in each. Tubes parallel.	71.3	0.941	0.00	H_s = 19 cm. Region 2 segregation. Sharp interface between upper and lower layers. I = 0.885.
						72.0	0.823	0.00	
						91.2	0.717	0.434	
						262.2	0.582	0.998	
						455.8	0.342	1.0	
						286.5	0.095	1.0	
	GP-2'	15.5	3.94	$\bar{v}_j$ = 0.709, 1065 g #2 glass, 176 g polypropylene.	Wire cylinders with single horizontal tube in each. Tubes parallel.	78.8	0.934	0.125	H_s = 40 cm. Region 2 segregation. Diffuse interface between jetsam-rich and flotsam-rich zones. Convection appears unusually enhanced. I = 0.424.
						158.6	0.787	0.378	
						244.0	0.615	0.679	
						228.1	0.441	0.900	
						158.7	0.304	0.956	
						372.0	0.126	0.984	
	GP-2"	14.9	3.90	$\bar{v}_j$ = 0.709, 1065 g #2 glass, 176 g polypropylene.	Wire cylinders with single horizontal tube in each. Tubes parallel.	100.7	0.930	0.131	H_s = 40 cm. Region 2 segregation. Diffuse interface between jetsam-rich and flotsam-rich zones. Convection appears unusually enhanced. I = 0.434.
						137.9	0.792	0.449	
						241.5	0.621	0.650	
						187.0	0.453	0.894	
						198.2	0.319	0.970	
						374.1	0.126	0.985	
	GP-8	15.2	4.26	$\bar{v}_j$ = 0.709, 1065 g #2 glass, 176 g polypropylene.	Wire cylinders with single horizontal tube in each. Tubes parallel.	97.5	0.930	0.107	H_s = 43 cm. Region 2 segregation. Diffuse interface between upper and lower layers. I = 0.562.
						104.8	0.796	0.239	
						252.9	0.633	0.764	
						252.2	0.447	0.938	
						182.9	0.297	0.961	
						347.0	0.117	0.982	

Table A-2. (continued)

Solids	Run no.	H_s Static bed height (cm)	u_o Superficial gas velocity (m/s)	Overall bed composition	Bed internals	Sample size (g)	z Average dimensionless axial position	v_J Sample jetsam volume fraction	Remarks
#2 glass and polypropylene. Glass acts as jetsam.	GP-9	14.5	1.98	$\bar{v}_J$ = 0.709, 1065 g #2 glass, 176 g polypro-pylene.	Wire cylinders with single horizontal tube in each. Tubes parallel.	85.3	0.929	0.001	H_s = 18 cm. Region 2 segregation. Sharp interface between upper and lower layers. I = 0.945.
						105.5	0.779	0.067	
						193.3	0.635	0.993	
						336.6	0.458	1.000	
						277.3	0.253	1.000	
						240.7	0.080	1.000	
	GP-10	28.7	2.93	$\bar{v}_J$ = 0.854, 2362 g #2 glass, 176 g polypro-pylene.	Wire cylinders with single horizontal tube in each. Tubes parallel.	129.2	0.956	0.145	H_s = 44 cm. Region 2 segregation. Sharp interface between upper and lower layers. I = 0.685.
						140.7	0.872	0.300	
						189.4	0.796	0.815	
						470.4	0.682	0.999	
						694.7	0.487	1.000	
						544.3	0.281	1.000	
						569.5	0.095	1.000	
	GP-11	21.8	2.95	$\bar{v}_J$ = 0.854, 1924 g #2 glass, 132 g polypro-pylene.	Wire cylinders with single horizontal tube in each. Tubes parallel.	107.6	0.959	0.111	H_s = 34 cm. Region 2 segregation. Steep gradient in upper layer. I = 0.731.
						127.1	0.866	0.400	
						225.2	0.762	0.978	
						392.4	0.628	1.000	
						592.7	0.413	1.000	
						611.6	0.140	1.000	
	GP-12	14.5	2.96	$\bar{v}_J$ = 0.854, 1283 g #2 glass, 88 g polypro-pylene.	Wire cylinders with single horizontal tube in each. Tubes parallel.	64.3	0.956	0.075	H_s = 23 cm. Region 2 segregation. Steep gradient in upper layer. I = 0.704.
						119.7	0.860	0.512	
						163.3	0.746	0.984	
						291.3	0.588	1.000	
						294.9	0.395	1.000	
						437.1	0.149	1.000	
	GP-13	7.8	2.99	$\bar{v}_J$ = 0.854, 642 g #2 glass, 44 g polypro-pylene.	Wire cylinders with single horizontal tube in each. Tubes parallel.	44.4	0.937	0.116	H_s = 10 cm. Region 2 segregation. Steep gradient in upper layer. I = 0.667.
						128.8	0.779	0.823	
						177.7	0.564	0.999	
						174.7	0.329	1.000	
						159.3	0.106	1.000	

Table A-2. (continued)

Solids	Run no.	H_s Static bed height (cm)	u_o Superficial gas velocity (m/s)	Overall bed composition	Bed internals	Sample size (g)	z Average dimensionless axial position	v_J Sample jetsam volume fraction	Remarks
#2 glass and polypropylene. Glass acts as jetsam.	GP-14	7.1	3.02	$\bar{v}_J$ = 0.500, 375 g #2 glass, 151 g polypro-pylene.	Wire cylinders with single horizontal tube in each. Tubes parallel.	76.8 51.1 123.1 276.0	0.873 0.662 0.473 0.184	0.0 0.002 0.633 0.998	H_s = 15 cm. Region 2 segregation. Steep gradient between upper and lower layers. I = 0.801.
	GP-15	6.6	2.97	$\bar{v}_J$ = 0.700, 526 g #2 glass, 91 g polypro-pylene.	Wire cylinders with single horizontal tube in each. Tubes parallel.	51.2 50.5 84.2 171.0 259.5	0.916 0.763 0.634 0.460 0.173	0.004 0.144 0.892 0.999 1.000	H_s = 13 cm. Region 2 segregation. Steep gradient between jetsam-rich and flotsam-rich zones. I = 0.858.
	GP-16	7.2	2.97	$\bar{v}_J$ = 0.950, 713 g #2 glass, 15 g polypro-pylene.	Wire cylinders with single horizontal tube in each. Tubes parallel.	64.7 88.9 166.2 221.0 187.4	0.943 0.826 0.655 0.397 0.125	0.582 0.988 0.997 1.000 1.000	H_s = 10 cm. Region 2 segregation. Steep gradient between jetsam-rich and flotsam rich zones. I = 0.370.
	GP-17	14.0	3.83	$\bar{v}_J$ = 0.696, 1000 g #2 glass, 176 g polypro-pylene.	Wire cylinders with single horizontal tube in each. Tubes parallel.	61.4 82.5 187.1 289.3 252.0 304.4	0.950 0.835 0.684 0.494 0.301 0.106	0.040 0.064 0.601 0.938 0.983 0.991	H_s = 38 cm. Region 2 segregation. Diffuse interface between jetsam-rich and flotsam-rich zones. I = 0.672.
	GP-18	14.2	4.05	$\bar{v}_J$ = 0.696, 1000 g #2 glass, 176 g polypro-pylene.	Wire cylinders with single horizontal tube in each. Tubes parallel.	88.4 77.8 181.5 246.1 274.8 306.2	0.931 0.805 0.665 0.494 0.310 0.107	0.067 0.133 0.593 0.961 0.993 0.998	H_s = 38 cm. Region 2 segregation. Diffuse interface between jetsam-rich and flotsam-rich zones. I = 0.667.

Table A-2. (continued)

Solids	Run no.	H_s Static bed height (cm)	u_o Superficial gas velocity (m/s)	Overall bed composition	Bed internals	Sample size (g)	z Average dimensionless axial position	v_J Sample jetsam volume fraction	Remarks
#2 glass and polypropylene. Glass acts as jetsam.	GP-19	14.2	3.37	$\bar{v}_J$ = 0.696, 1000 g #2 glass, 176 g polypropylene.	Wire cylinders with single horizontal tube in each. Tubes parallel.	84.2 85.9 168.0 228.9 367.4 240.9	0.929 0.791 0.656 0.506 0.297 0.084	0.015 0.082 0.748 0.975 0.991 1.000	H_e = 34 cm. Region 2 segregation. Diffuse interface between jetsam-rich and flotsam-rich zones. I = 0.789.
	GP-20	14.0	2.46	$\bar{v}_J$ = 0.696, 1000 g, #2 glass, 176 g polypropylene.	Wire cylinders with single horizontal tube in each. Tubes parallel.	38.4 90.1 171.3 247.5 231.8 396.5	0.967 0.856 0.694 0.524 0.357 0.138	0.0 0.0 0.518 0.999 1.000 1.000	H_e = 19 cm. Region 2 segregation. Sharp interface between jetsam-rich and flotsam-rich zones. I = 0.801.
	GP-21	13.5	1.05	$\bar{v}_J$ = 0.696, 1000 g #2 glass, 176 g polypropylene.	None	-	z > 0.696 z < 0.696	0.0 1.0	H_e = 14 cm. Sharp interface. Region 1 segregation. Initial condition segregated. Brought up air slowly to final value and held. Fluidization interface at z = 0.70. I = 1.0.
	GP-22	13.5	1.31	$\bar{v}_J$ = 0.696, 1000 g #2 glass, 176 g polypropylene.	None	-	z > 0.696 z < 0.696	0.0 1.0	H_e = 14 cm. Sharp interface. Region 1 segregation. Initial condition segregated. Brought up air slowly to final value and held. Fluidization interface at z = 0.65. I = 1.0.
	GP-23	13.5	1.57	$\bar{v}_J$ = 0.696, 1000 g #2 glass, 176 g polypropylene.	None	-	z > 0.696 z < 0.696	0.0 1.0	H_e = 15 cm. Sharp interface. Region 1 segregation. Initial condition segregated. Brought up air slowly to final value and held. Fluidization interface at z = 0.65. I = 1.0.

Table A-2. (continued)

Solids	Run no.	H_s Static bed height (cm)	u_o Superficial gas velocity (m/s)	Overall bed composition	Bed internals	Sample size (g)	z Average dimensionless axial position	v_j Sample jetsam volume fraction	Remarks
#2 glass and polypropylene. Glass acts as jetsam.	GP-24	13.5	1.83	$\bar{v}_j$ = 0.696, 1000 g #2 glass, 176 g polypro-pylene.	None	113.6	0.902	0.0	H_e = 16 cm. Sharp interface. Region I segregation. Initial condition segregated. Brought up air slowly to final value and held. Fluidization interface at z = 0.60. I = 0.938.
						53.1	0.758	0.0	
						137.8	0.659	0.855	
						408.7	0.464	1.000	
						202.2	0.251	1.000	
						259.8	0.091	1.000	
	GP-25	13.7	1.95	$\bar{v}_j$ = 0.696, 1000 g #2 glass, 176 g polypro-pylene.	None	73.6	0.936	0.0	H_e = 17 cm. Moderately diffuse interface. Region I segregation. Initial condition segregated. Brought up air slowly to final value and held. Bed totally fluidized. I = 0.905.
						86.6	0.798	0.0	
						135.2	0.668	0.760	
						267.1	0.520	1.000	
						306.6	0.320	1.000	
						306.6	0.107	1.000	
	GP-26	13.5	1.72	$\bar{v}_j$ = 0.696, 1000 g #2 glass, 176 g polypro-pylene.	None	82.7	0.929	0.0	H_e = 16 cm. Sharp interface. Region I segregation. Initial condition segregated. Brought up air slowly to final value and held. Fluidization interface at z = 0.60. I = 0.932.
						82.7	0.785	0.0	
						131.4	0.663	0.830	
						293.0	0.510	1.000	
						293.0	0.306	1.000	
						293.0	0.102	1.000	
	GP-27	13.5	1.45	$\bar{v}_j$ = 0.696, 1000 g #2 glass, 176 g polypro-pylene.	None	-	z > 0.696	0.0	H_e = 14 cm. Sharp interface. Region I segregation. Initial condition segregated. Brought up air slowly to final value and held. Fluidization interface at z = 0.68. I = 1.0.
							z < 0.696	1.0	
	GP-28	13.5	1.58	$\bar{v}_j$ = 0.696, 1000 g #2 glass, 176 g polypro-pylene.	None	56.0	0.952	0.0	H_e = 14 cm. Initial condition well-mixed. Brought up air slowly to final value and held. Fluidization interface at z = 0.85. I = 0.283.
						155.7	0.843	0.854	
						208.2	0.704	0.841	
						202.3	0.540	0.746	
						150.8	0.387	0.574	
						401.2	0.158	0.809	

Table A-2. (continued)

Solids	Run no.	H_s Static bed height (cm)	u_o Superficial gas velocity (m/s)	Overall bed composition	Bed internals	Sample size (g)	z Average dimensionless axial position	v_J Sample jetsam volume fraction	Remarks
#2 glass and polypropylene. Glass acts as jetsam.	GP-29	13.7	1.76	$\bar{v}_J$ = 0.696, 1000 g #2 glass, 176 g polypro-pylene.	None	51.7 104.9 243.1 196.3 255.2 322.7	0.955 0.823 0.650 0.496 0.334 0.120	0.0 0.027 0.998 0.987 0.923 0.892	H_e = 14 cm. Initial condition well-mixed. Brought up air slowly to final value and held. Fluidization interface at z = 0.74. I = 0.793.
	GP-30	13.5	1.83	$\bar{v}_J$ = 0.696, 1000 g #2 glass, 176 g polypro-pylene.	None	86.6 69.8 126.7 305.1 221.9 364.6	0.925 0.789 0.681 0.527 0.342 0.132	0.0 0.0 0.873 1.000 0.969 0.943	H_e = 16 cm. Initial condition well-mixed. Brought up air slowly to final value and held. Fluidization interface at z = 0.58. I = 0.859.
	GP-31	13.5	1.67	$\bar{v}_J$ = 0.696, 1000 g #2 glass, 176 g polypro-pylene.	None	79.6 42.0 133.0 288.1 252.9 379.5	0.931 0.826 0.743 0.591 0.388 0.145	0.0 0.0 0.978 0.927 0.837 0.850	H_e = 14 cm. Initial condition well-mixed. Brought up air slowly to final value and held. Fluidization interface at z = 0.75. I = 0.621.
	GP-32	14.2	3.87	$\bar{v}_J$ = 0.696, 1000 g #2 glass, 176 g polypro-pylene.	Wire cylinders with single horizontal tube in each. Tubes parallel.	65.1 87.9 92.8 158.2 358.1 413.3	0.949 0.830 0.712 0.603 0.416 0.144	0.066 0.091 0.390 0.890 0.963 0.995	H_e = 36 cm. Region 2 segregation. Diffuse interface between jetsam-rich and flotsam-rich zones. I = 0.699.
	GP-33	14.6	3.95	$\bar{v}_J$ = 0.696, 1000 g #2 glass, 176 g polypro-pylene.	Wire cylinders with single horizontal tube in each. Tubes parallel.	68.4 61.1 93.9 166.9 248.0 537.3	0.950 0.854 0.758 0.635 0.470 0.188	0.118 0.114 0.395 0.678 0.875 0.990	H_e = 37 cm. Region 2 segregation. Diffuse interface between jetsam-rich and flotsam-rich zones. I = 0.530.

Table A-2. (continued)

Solids	Run no.	H_s Static bed height (cm)	u_o Superficial gas velocity (m/s)	Overall bed composition	Bed internals	Sample size (g)	s Average dimensionless axial position	v_J Sample jetsam volume fraction	Remarks
#2 glass and polypropylene. Glass acts as jetsam.	GP-34	14.5	4.15	$\bar{v}_J$ = 0.696, 1000 g #2 glass, 176 g polypro-pylene.	Wire cylinders with single horizontal tube in each. Tubes parallel.	75.1	0.944	0.110	H_o = 38 cm. Region 2 segregation. Diffuse interface between jetsam-rich and flotsam-rich zones. I = 0.621.
						83.0	0.826	0.107	
						133.6	0.698	0.494	
						228.8	0.545	0.883	
						255.7	0.369	0.972	
						398.6	0.139	0.994	
	GP-35	14.4	3.49	$\bar{v}_J$ = 0.696, 1000 g #2 glass, 176 g polypro-pylene.	Wire cylinders with single horizontal tube in each. Tubes parallel.	78.9	0.937	0.055	H_o = 31 cm. Region 2 segregation. Diffuse interface between jetsam-rich and flotsam rich zones. I = 0.672.
						89.6	0.810	0.153	
						140.8	0.679	0.532	
						188.8	0.542	0.915	
						279.4	0.375	0.992	
						397.5	0.139	0.999	
	GP-36	14.2	5.92	$\bar{v}_J$ = 0.696, 1000 g #2 glass, 176 g polypro-pylene.	Wire cylinders with single horizontal tube in each. Tubes parallel.	48.2	0.963	0.079	H_o = 69 cm. Region 2 segregation. Polypropylene formed diffuse cloud above glass. I = 0.705.
						80.4	0.860	0.040	
						94.9	0.738	0.303	
						175.1	0.615	0.872	
						367.5	0.419	0.967	
						410.5	0.144	0.981	
	GP-37	14.2	3.93	$\bar{v}_J$ = 0.696 1000 g #2 glass, 176 g polypro-pylene.	Wire cylinders with single horizontal tube in each. Tubes parallel.	74.3	0.943	0.081	H_o = 36 cm. Region 2 segregation. Diffuse interface between jetsam-rich and flotsam-rich zones. Convection appears unusually enhanced. I = 0.426.
						97.0	0.830	0.348	
						132.2	0.711	0.541	
						193.3	0.568	0.751	
						207.4	0.414	0.921	
						470.7	0.169	0.951	

Table A-2. (continued)

Solids	Run no.	H_s Static bed height (cm)	u_0 Superficial gas velocity (m/s)	Overall bed composition	Bed internals	Sample size (g)	z Average dimensionless axial position	v_j Sample jetsam volume fraction	Remarks
Clear acrylic and black acrylic. Black acrylic acts as jetsam.	AA-1	25.4	2.01	$\bar{v}_j$ = 0.024, 1358 g clear acrylic, 33 g black acrylic.	None	203.6	0.927	0.002	Basis for transient experiments. Region 2 segregation. Upper portion of bed well-mixed, steep gradient in lower portion. Insufficient jetsam to completely form bottom layer. I = 0.052.
						237.1	0.768	0.002	
						167.6	0.615	0.003	
						237.9	0.462	0.002	
						114.1	0.335	0.011	
						169.7	0.230	0.045	
						96.3	0.129	0.061	
						113.8	0.046	0.113	

Table A-2. (continued)

Solids	Run no.	H_s Static bed height (cm)	u_o Superficial gas velocity (m/s)	Overall bed composition	Bed internals	Sample size (g)	z Average dimensionless axial position	v_J Sample jetsam volume fraction	Remarks
Acrylic and #1 glass. Glass acts as jetsam.	AG-1	14.0	1.97	$\bar{v}_J$ = 0.333, 450 g, #1 glass, 470 g clear acrylic.	Wire cylinders with single horizontal tube in each. Tubes parallel.	89.8	0.936	0.001	H_e = 15 cm. Region 2 segregation. Steep composition gradient in the lower part of the bed. I = 0.630.
						109.9	0.796	0.007	
						134.0	0.630	0.079	
						161.8	0.442	0.172	
						208.4	0.252	0.683	
						217.2	0.081	0.995	
	AG-2	13.5	2.79	$\bar{v}_J$ = 0.333, 450 g, #1 glass, 470 g clear acrylic.	Wire cylinders with single horizontal tube in each. Tubes parallel.	99.5	0.940	0.188	H_e = 21 cm. Region 2 segregation. Upper portion of the bed well-mixed. Steep gradient in lower portion. I = 0.228.
						143.4	0.794	0.202	
						181.6	0.601	0.215	
						164.5	0.399	0.259	
						162.6	0.218	0.369	
						169.1	0.066	0.890	
	AG-3	13.5	4.26	$\bar{v}_J$ = 0.333, 450 g, #1 glass, 470 g clear acrylic.	Wire cylinders with single horizontal tube in each. Tubes parallel.	92.1	0.951	0.376	H_e = 29 cm. Region 2 segregation. Slight inverse slope in upper portion of bed. Steep gradient in lower portion. Middle zone relatively well-mixed. I = 0.047.
						159.2	0.814	0.293	
						138.6	0.646	0.263	
						149.1	0.482	0.274	
						211.5	0.278	0.285	
						169.7	0.080	0.558	
	AG-4	13.2	4.92	$\bar{v}_J$ = 0.333, 450 g, #1 glass, 470 g clear acrylic.	Wire cylinders with single horizontal tube in each. Tubes parallel.	120.5	0.934	0.313	H_e = 36 cm. Region 2 segregation. Bed essentially well-mixed. I = 0.001.
						116.9	0.803	0.323	
						168.2	0.647	0.328	
						159.9	0.470	0.355	
						121.4	0.317	0.311	
						233.0	0.103	0.351	
	AG-5	12.4	1.55	$\bar{v}_J$ = 0.333, 450 g, #1 glass, 470 g clear acrylic.	None	76.4	0.946	0.002	H_e = 13.5 cm. Region 1 segregation. Initial condition segregated. Air flow brought up slowly to final value and held. Bottom layer clearly fluidized. Top layer agitated by bottom layer but not fluidized. I = 0.806.
						139.6	0.794	0.015	
						111.1	0.620	0.029	
						139.4	0.449	0.053	
						135.8	0.295	0.674	
						317.8	0.118	1.000	

Table A-2. (continued)

Solids	Run no.	H_s Static bed height (cm)	u_o Superficial gas velocity (m/s)	Overall bed composition	Bed internals	Sample size (g)	z Average dimensionless axial position	v_J Sample jetsam volume fraction	Remarks
Acrylic and #1 glass. Glass acts as jetsam.	AG-6	13.5	2.79	$\bar{v}_J$ = 0.667, 900 g #1 glass, 235 g clear acrylic.	Wire cylinders with single horizontal tube in each. Tubes parallel.	100.0	0.953	0.573	H_s = 22 cm. Region 2 segregation. Bed essentially well-mixed except for steep gradient near the bottom. I = 0.051.
						118.6	0.853	0.601	
						161.2	0.725	0.613	
						173.5	0.571	0.586	
						269.6	0.370	0.633	
						311.0	0.124	0.850	
	AG-7	13.5	2.79	$\bar{v}_J$ = 0.900, 1215 g #1 glass, 70.5 g clear acrylic.	Wire cylinders with single horizontal tube in each. Tubes parallel.	139.9	0.944	0.848	H_s = 22 cm. Region 2 segregation. Gradual decrease in flotsam concentration with depth. Almost pure jetsam layer on the bottom. I = 0.043.
						157.4	0.824	0.813	
						194.1	0.683	0.841	
						216.2	0.521	0.895	
						258.0	0.337	0.928	
						320.3	0.119	0.989.	

Table A-3. Data from transient segregation experiments

Solids	Run no.	H_s Static bed height (cm)	u_o Superficial gas velocity (m/s)	Overall bed composition	Bed internals	Sample size (g)	z Average dimensionless axial position	v_J Sample jetsam volume fraction	Remarks
Clear acrylic, black acrylic. Black acrylic acts jetsam.	AA-2T	25.4	2.02	$\bar{v}_J$ = 0.024, 1358 g clear acrylic, 33 g black acrylic.	None.	133.9	0.952	0.127	Time = 10 s. Corresponding steady-state run was AA-1. Run was started by dumping black acrylic on top of fluidized clear acrylic. Region 2.
						141.5	0.853	0.079	
						141.2	0.751	0.024	
						158.0	0.644	0.007	
						176.9	0.523	0.002	
						152.6	0.355	0.0	
						139.1	0.300	0.0	
						139.1	0.200	0.0	
						208.7	0.075	0.0	
	AA-3T	25.4	2.02	$\bar{v}_J$ = 0.024, 1358 g clear acrylic, 33 g black acrylic.	None.	144.2	0.948	0.025	Time = 20 s. See AA-2T.
						155.8	0.840	0.049	
						133.2	0.736	0.046	
						171.5	0.627	0.044	
						215.8	0.488	0.020	
						200.4	0.338	0.014	
						153.3	0.211	0.004	
						216.2	0.078	0.0	
	AA-4T	25.4	2.02	$\bar{v}_J$ = 0.024, 1358 g clear acrylic, 33 g black acrylic.	None.	189.9	0.932	0.008	Time = 40 s. See AA-2T.
						168.1	0.803	0.009	
						206.1	0.669	0.021	
						193.7	0.525	0.026	
						159.6	0.400	0.033	
						209.6	0.270	0.047	
						118.0	0.152	0.039	
						152.2	0.055	0.007	
	AA-5T	25.4	2.02	$\bar{v}_J$ = 0.024, 1358 g clear acrylic, 33 g black acrylic.	None.	292.0	0.895	0.001	Time = 80 s. See AA-2T.
						277.4	0.690	0.002	
						174.9	0.528	0.002	
						151.3	0.410	0.005	
						155.5	0.300	0.032	
						155.4	0.188	0.106	
						183.9	0.066	0.046	

Table A-3. (continued)

Solids	Run no.	H_s Static bed height (cm)	u_o Superficial gas velocity (m/s)	Overall bed composition	Bed internals	Sample size (g)	z Average dimensionless axial position	v_j Sample jetsam volume fraction	Remarks
Clear acrylic, black acrylic. Black acrylic acts as jetsam.	AA-6T	25.4	2.02	$\bar{v}_j$ = 0.024, 1358 g clear acrylic, 33 g black acrylic.	None.	278.2	0.900	0.0	Time = 40 s. Region 2. Corresponding steady-state run was AA-1. Run was started by setting up bed in inverted segregated condition and then turning up air flow rapidly to the final value.
						278.2	0.700	0.0	
						187.3	0.533	0.0	
						111.6	0.425	0.003	
						136.3	0.336	0.006	
						171.8	0.225	0.023	
						104.8	0.126	0.029	
						122.8	0.044	0.166	
	AA-7T	27.7	2.02	$\bar{v}_j$ = 0.024, 1358 g clear acrylic, 33 g black acrylic.	Wire cylinders with horizontal parallel tubes.	148.8	0.947	0.077	Time = 40 s. Region 2. Run was started by dropping black acrylic on top of fluidized clear acrylic.
						146.0	0.841	0.058	
						217.4	0.710	0.056	
						251.9	0.541	0.002	
						205.8	0.377	0.0	
						153.1	0.248	0.0	
						268.0	0.096	0.0	
Clear acrylic, polypropylene. Acrylic acts as jetsam.	AP-11T	30.7	3.38	$\bar{v}_j$ = 0.856, 1360 g acrylic, 175 g poly-propylene.	Wire cylinders with horizontal parallel tubes.	284.8	0.905	0.725	Time = 10 s. Region 2. Corresponding steady-state run was AP-10. Run was started by setting up bed in inverted segregated condition and then turning up air flow rapidly to the final value.
						183.2	0.748	0.826	
						164.7	0.628	0.847	
						172.1	0.517	0.865	
						192.3	0.401	0.865	
						135.3	0.298	0.933	
						173.1	0.207	0.914	
						230.8	0.079	0.950	
#1 glass, #2 glass. #2 glass acts as jetsam.	GG-36f	13.7	1.83	$\bar{v}_j$ = 0.667, 1000 g #2 glass, 500 g #1 glass.	None.	114.1	0.962	0.154	Time = 5 min. Region 1. Corresponding steady-state run was GG-32. Run was started by starting with the bed segregated and bringing up air flow to the final value.
						198.0	0.858	0.230	
						251.0	0.708	0.350	
						269.1	0.535	0.688	
						284.8	0.350	0.985	
						382.7	0.128	1.000	

Table A-3. (continued)

Solids	Run no.	H_s Static bed height (cm)	u_o Superficial gas velocity (m/s)	Overall bed composition	Bed internals	Sample size (g)	z Average dimensionless axial position	v_j Sample jetsam volume fraction	Remarks
#1 glass, #2 glass. #2 glass acts as jetsam.	CG-38T	13.7	1.83	$\bar{v}_j$ = 0.667, 1000 g #2 glass, 500 g #1 glass.	None.	116.6	0.961	0.029	Time = 15 min. See CG-36T.
						204.8	0.854	0.097	
						236.7	0.707	0.398	
						203.1	0.560	0.755	
						265.8	0.404	0.965	
						472.7	0.158	1.000	
	CG-61T	13.7	2.08	$\bar{v}_j$ = 0.667, 1000 g #2 glass, 500 g #1 glass.	None.	152.6	0.949	0.170	Time = 10 s. Region 2. Corresponding steady-state run was CG-49. Run was started by putting flotsam on top of fluidized jetsam.
						207.3	0.829	0.190	
						218.5	0.687	0.353	
						221.1	0.541	0.723	
						352.4	0.350	0.990	
						348.6	0.116	1.000	
	CG-62T	13.7	2.08	$\bar{v}_j$ = 0.067, 1000 g #2 glass, 500 g #1 glass.	None.	130.7	0.957	0.115	Time = 5 s. See CG-61T.
						175.2	0.855	0.235	
						255.3	0.711	0.290	
						255.5	0.541	0.730	
						192.5	0.392	0.998	
						492.1	0.164	1.000	
	CG-63T	13.7	2.08	$\bar{v}_j$ = 0.667, 1000 g. #2 glass, 500 g #1 glass.	None.	123.9	0.959	0.215	Time = 20 s. See CG-61T.
						158.2	0.749	0.388	
						173.4	0.860	0.280	
						276.3	0.605	0.482	
						295.9	0.414	0.869	
						473.3	0.158	1.000	

Table A-4. Bed pressure profiles

Solids	Run no.	Static bed height (cm)	Overall bed composition	Superficial gas velocity (m/s)	Bed internals	Height/static bed height	Gauge pressure/overall bed ΔP
Clear acrylic.	A-1	27.7	1460 g acrylic.	1.71	None.	1.61	0.0
						1.52	0.007
						1.42	0.020
						1.28	0.053
						1.10	0.133
						0.89	0.267
						0.71	0.393
						0.50	0.560
						0.29	0.787
						0.14	0.893
						0.0	1.0
	A-2A	24.9	1360 g acrylic.	1.69	None.	1.00	0.0
						0.84	0.169
						0.69	0.296
						0.51	0.488
						0.34	0.646
						0.17	0.827
						0.0	1.00
	A-2B	24.9	1360 g acrylic.	2.53	None.	2.65	0.0
						2.55	0.001
						2.45	0.007
						2.34	0.014
						2.24	0.021
						1.73	0.078
						1.43	0.149

Table A-4. (continued)

Solids	Run no.	Static bed height (cm)	Overall bed composition	Superficial gas velocity (m/s)	Bed internals	Height/static bed height	Gauge pressure/overall bed ΔP
Clear acrylic.	A-2B				•	1.12	0.248
						0.82	0.404
						0.51	0.575
						0.20	0.858
						0.0	1.00
	A-2C	24.9	1360 g acrylic.	3.38	None.	3.47	0.0
						3.37	0.003
						3.16	0.013
						2.96	0.039
						2.55	0.066
						2.24	0.105
						1.94	0.158
						1.63	0.230
						1.33	0.283
						1.02	0.408
						0.71	0.579
						0.41	0.743
						0.20	0.862
						0.0	1.00
	A-3A	12.7	680 g acrylic.	1.69	None.	1.00	0.0
						0.84	0.150
						0.64	0.344
						0.24	0.703
						0.0	1.00

Table A-4. (continued)

Solids	Run no.	Static bed height (cm)	Overall bed composition	Superficial gas velocity (m/s)	Bed internals	Height/static bed height	Gauge pressure/overall bed ΔP
Clear acrylic.	A-3B	12.7	680 g acrylic.	2.54	None.	1.90	0.0
						1.70	0.009
						1.60	0.015
						1.40	0.031
						1.20	0.080
						0.80	0.292
						0.60	0.437
						0.40	0.600
						0.20	0.772
						0.0	1.00
	A-3C	12.7	680 g acrylic.	3.38	None.	3.10	0.0
						3.00	0.002
						2.90	0.003
						2.80	0.004
						2.68	0.007
						2.38	0.013
						2.00	0.022
						1.64	0.037
						1.10	0.177
						0.82	0.294
						0.50	0.529
						0.20	0.824
						0.0	1.00

Table A-4. (continued)

Solids	Run no.	Static bed height (cm)	Overall bed composition	Superficial gas velocity (m/s)	Bed internals	Height/static bed height	Gauge pressure/overall bed ΔP
Clear acrylic.	A-4	26.4	1360 g acrylic.	3.44	Wire mesh cylinders (vertical next to walls) with no tubes.	2.21	0.0
						2.09	0.001
						1.85	0.003
						1.52	0.080
						1.24	0.178
						0.99	0.316
						0.73	0.466
						0.50	0.655
						0.29	0.805
						0.12	0.943
						0.0	1.00
	A-5	13.5	680 g acrylic.	3.39	Wire mesh cylinders (vertical next to walls) with no tubes.	1.91	0.0
						1.83	0.006
						1.72	0.017
						1.53	0.043
						1.32	0.100
						1.15	0.143
						0.92	0.300
						0.72	0.471
						0.51	0.600
						0.34	0.729
						0.15	0.857
						0.0	1.00

Table A-4. (continued)

Solids	Run no.	Static bed height (cm)	Overall bed composition	Superficial gas velocity (m/s)	Bed internals	Height/static bed height	Gauge pressure/overall bed ΔP
Clear acrylic.	A-11	27.2	1360 g acrylic.	3.41	Wire mesh cylinders with parallel horizontal tubes.	1.68	0.0
						1.59	0.006
						1.55	0.013
						1.49	0.025
						1.30	0.088
						1.08	0.220
						0.76	0.484
						0.40	0.742
						0.19	0.887
						0.0	1.0

Table A-4. (continued)

Solids	Run no.	Static bed height (cm)	Overall bed composition	Superficial gas velocity (m/s)	Bed internals	Height/static bed height	Gauge pressure/overall bed ΔP
Clear acrylic, polypropylene. Acrylic acts as jetsam.	AP-1	30.0	$\bar{v}_j$ = 0.857, 1360 g acrylic, 175 g polypropylene	2.40 (Region 2).	None.	1.69	0.013
						1.61	0.025
						1.53	0.038
						1.44	0.050
						1.36	0.075
						1.19	0.150
						1.02	0.250
						0.85	0.344
						0.68	0.444
						0.51	0.556
						0.34	0.694
						0.13	0.900
						0.0	1.00
	AP-2	29.2	$\bar{v}_j$ = 0.857, 1360 g acrylic, 175 g polypropylene	3.39 (Region 2).	None.	3.04	0.011
						2.87	0.022
						2.57	0.045
						2.37	0.067
						2.17	0.084
						1.74	0.169
						1.37	0.247
						0.96	0.365
						0.61	0.551
						0.26	0.787
						0.13	0.888
						0.0	1.00

Table A-4. (continued)

Solids	Run no.	Static bed height (cm)	Overall bed composition	Superficial gas velocity (m/s)	Bed internals	Height/static bed height	Gauge pressure/overall bed ΔP
Clear acrylic, polypropylene. Acrylic acts as jetsam.	AP-3	30.0	$\bar{v}_j$ = 0.857, 1360 g acrylic, 175 g polypropylene.	2.00 (Region 2).	None.	1.53	0.0
						1.44	0.006
						1.36	0.010
						1.27	0.026
						1.19	0.038
						1.10	0.064
						1.02	0.115
						0.85	0.244
						0.68	0.372
						0.51	0.526
						0.34	0.673
						0.16	0.859
						0.0	1.0
	AP-4	29.2	$\bar{v}_j$ = 0.857, 1360 g acrylic, 175 g polypropylene	1.47 (Region 1). Air flow reduced from fully fluidized condition and held at final value.	None.	1.09	0.0
						1.00	0.025
						0.91	0.075
						0.83	0.144
						0.74	0.219
						0.65	0.288
						0.57	0.363
						0.48	0.463
						0.39	0.575
						0.30	0.669
						0.17	0.806
						0.0	1.0

Table A-4. (continued)

Solids	Run no.	Static bed height (cm)	Overall bed composition	Superficial gas velocity (m/s)	Bed internals	Height/static bed height	Gauge pressure/overall bed ΔP
Clear acrylic, polypropylene. Acrylic acts as jetsam.	AP-6	15.2	$\bar{v}_j$ = 0.857, 680 g acrylic, 88 g polypropylene.	2.44 (Region 2).	None.	1.90	0.0
						1.72	0.003
						1.62	0.011
						1.43	0.029
						1.22	0.085
						1.02	0.173
						0.72	0.360
						0.45	0.587
						0.23	0.816
						0.0	1.0
	AP-7	14.7	$\bar{v}_j$ = 0.857, 680 g acrylic, 88 g polypropylene.	3.43 (Region 2).	None.	3.79	0.0
						3.28	0.005
						2.55	0.021
						2.07	0.066
						1.55	0.132
						1.21	0.211
						0.69	0.461
						0.36	0.711
						0.0	1.0
	AP-8	15.0	$\bar{v}_j$ = 0.857, 680 g acrylic, 88 g polypropylene.	3.39 (Region 2).	Wire cylinders (vertical and next to walls) with no tubes.	2.42	0.0
						2.25	0.002
						2.19	0.005
						1.76	0.049
						1.39	0.122
						1.00	0.317
						0.58	0.585
						0.20	0.829
						0.0	1.0

Table A-4. (continued)

Solids	Run no.	Static bed height (cm)	Overall bed composition	Superficial gas velocity (m/s)	Bed internals	Height/static bed height	Gauge pressure/overall bed ΔP
Clear acrylic, polypropylene. Acrylic acts as jetsam.	AP-10	30.5	$\bar{v}_j$ = 0.856, 1360 g acrylic, 175 g polypropylene	3.38 (Region 2).	Vertical wire cylinders with parallel horizontal tubes.	1.88	0.0
						1.83	0.001
						1.68	0.012
						1.54	0.041
						1.41	0.088
						1.32	0.118
						1.16	0.212
						1.00	0.306
						0.83	0.441
						0.64	0.588
						0.50	0.676
						0.32	0.776
						0.19	0.882
						0.0	1.0
#2 coal, #2 limestone. Limestone acts as jetsam.	LC-12	27.2	$\bar{v}_j$ = 0.665, 500 g coal, 1000 g limestone.	2.45 (Region 2).	None.	2.80	0.0
						2.43	0.016
						2.29	0.032
						1.68	0.128
						1.33	0.184
						1.06	0.296
						0.85	0.344
						0.70	0.472
						0.37	0.720
						0.14	0.904
						0.0	1.0

Table A-4. (continued)

Solids	Run no.	Static bed height (cm)	Overall bed composition	Superficial gas velocity (m/s)	Bed internals	Height/static bed height	Gauge pressure/overall bed ΔP
#2 coal, #2 limestone. Limestone acts as jetsam.	LC-13	26.9	$\bar{v}_j$ = 0.665, 500 g coal, 1000 g limestone.	1.74 (Region 2).	None.	1.70 1.42 1.19 0.92 0.61 0.38 0.14 0.0	0.0 0.008 0.042 0.134 0.370 0.613 0.866 1.0
	LC-14	27.2	$\bar{v}_j$ = 0.665, 500 g coal, 1000 g limestone.	1.49 (Region 1). Brought up air flow slowly to final value and held.	None.	1.31 1.21 1.12 0.90 0.70 0.56 0.40 0.14 0.0	0.0 0.001 0.008 0.109 0.248 0.391 0.538 0.857 1.0
	LC-15	27.2	$\bar{v}_j$ = 0.665, 500 g coal, 1000 g limestone.	1.10 (Region 1). Air flow reduced from fully fluidized condition and held at final value.	None.	1.10 1.05 0.94 0.84 0.71 0.60 0.42 0.14 0.0	0.0 0.005 0.053 0.121 0.209 0.335 0.544 0.835 1.0

Table A-5. Estimate of maximum experimental error

Replicate runs	I	Deviation from mean	$v_J\|_{z=0.9}$	Deviation from mean	$v_J\|_{z=0.5}$	Deviation from mean	$v_J\|_{z=0.1}$	Deviation from mean
LC-1	0.178	+0.026	0.565	-0.028	0.910	+0.028	0.975	-0.008
LC-2	0.126	-0.026	0.620	+0.028	0.855	-0.028	0.990	+0.008
GG-1	0.709	+0.026	0.040	- .028	0.950	+0.005	0.999	0.0
GG-1'	0.657	-0.026	0.095	+ .028	0.940	-0.005	0.990	0.0
GG-2	0.043	-0.009	0.580	+0.010	0.625	+0.013	0.875	-0.015
GG-2'	0.060	+0.009	0.560	-0.010	0.600	-0.013	0.905	+0.015
GG-3	0.136	+0.021	0.510	-0.004	0.575	-0.021	0.985	+0.018
GG-3'	0.094	-0.021	0.518	+0.004	0.616	+0.021	0.949	-0.018
GG-5	0.192	+0.079	0.730	-0.063	0.980	+0.015	0.990	-0.002
GG-5'	0.035	-0.079	0.855	+0.063	0.950	-0.015	0.987	+0.002
GG-14	0.418	+0.001	0.282	+0.005	0.715	-0.003	0.999	+0.002
GG-14'	0.417	-0.001	0.272	-0.005	0.720	+0.003	0.995	-0.002
GG-16	0.038	+0.008	0.580	+0.003	0.632	-0.012	0.815	+0.043
GG-16'	0.023	-0.008	0.575	-0.003	0.655	+0.012	0.730	-0.043
GG-21	0.498	-0.010	0.173	+0.007	0.800	-0.005	0.997	-0.001
GG-21'	0.518	+0.010	0.160	-0.007	0.810	+0.005	0.999	+0.001
GG-26	0.700	-0.009	0.105	+0.020	0.960	+0.013	1.000	0.0
GG-26'	0.717	+0.009	0.065	-0.020	0.935	-0.013	1.000	0.0
GG-29	0.041	+0.001	0.605	-0.016	0.639	+0.025	0.858	+0.001
GG-29'	0.039	-0.001	0.636	+0.016	0.590	-0.025	0.859	-0.001

Table A-5. (continued)

Replicate runs	I	Deviation from mean	$v_J\|_{z=0.9}$	Deviation from mean	$v_J\|_{z=0.5}$	Deviation from mean	$v_J\|_{z=0.1}$	Deviation from mean
GG-30	0.026	+0.003	0.555	-0.028	0.660	+0.004	0.800	+0.013
GG-30'	0.020	-0.003	0.610	+0.028	0.653	-0.004	0.775	-0.013
GG-31	0.043	+0.003	0.525	-0.020	0.672	+0.014	0.800	-0.012
GG-31'	0.037	-0.003	0.565	+0.020	0.645	-0.014	0.823	+0.012
GG-32	0.649	+0.027	0.107	+0.004	0.885	+0.005	1.000	+0.003
GG-32'	0.595	-0.027	0.100	-0.004	0.875	-0.005	0.995	-0.003
GG-33	0.491	-0.007	0.171	+0.002	0.822	+0.005	0.990	0.0
GG-33'	0.432	-0.066	0.195	+0.026	0.740	-0.077	0.999	+0.009
GG-33"	0.571	+0.073	0.140	-0.028	0.888	+0.071	0.980	-0.009
GG-56	0.189	+0.039	0.432	-0.042	0.590	-0.003	0.990	+0.018
GG-56'	0.112	-0.039	0.515	+0.042	0.595	+0.003	0.955	-0.018
GP-2	0.397	-0.024	0.200	+0.006	0.850	0.0	0.977	0.0
GP-2'	0.424	+0.004	0.185	-0.009	0.851	+0.001	0.987	+0.010
GP-2"	0.434	+0.014	0.208	+0.014	0.859	+0.009	0.989	+0.012
GP-37	0.426	+0.006	0.182	-0.011	0.840	-0.010	0.955	-0.022
AP-1	0.110	-0.036	0.690	+0.030	0.879	-0.029	0.988	-0.004
AP-1'	0.181	+0.036	0.630	-0.030	0.936	+0.029	0.995	+0.004
Total SSD		0.03441		0.032816		0.018583		0.007158
σ_e		0.031		0.030		0.023		0.014

Table A-6. Evaluation of Region 1 steady-state data in terms of modified Gibilaro-Rowe model

Run No.	z_i	v_{Ji}	λ_{Ds}	λ_{ws}	z_c	λ_D'	SSD
LC-9	0.65	0.815	0.115	0.112			3.0×10^{-5}
LC-10	0.70	0.760	0.054	0.060			3.0×10^{-5}
LC-16	0.75	0.940	0.018	0.0			$<10^{-10}$
SG-1	0.0	0.200	0.098	0.017	0.80	0.13	5.9×10^{-5}
SG-2	0.0	0.200	0.093	0.040			3.0×10^{-5}
SG-3	0.0	0.200	0.078	0.066	0.80	0.078	1.3×10^{-5}
GG-26	0.62	0.500	0.180	0.180			2.1×10^{-4}
GG-26'	0.63	0.590	0.153	0.077			4.2×10^{-5}
GG-32	0.54	0.820	0.135	0.107			1.1×10^{-4}
GG-32'	0.52	0.850	0.156	0.066			7.6×10^{-4}
GG-34	0.51	0.920	0.122	0.054			1.5×10^{-4}
GG-35	0.69	0.500	0.265	0.001			1.8×10^{-4}
GG-37	0.54	0.780	0.201	0.006			2.7×10^{-4}
GG-39	0.54	0.830	0.159	0.061			5.8×10^{-6}
GG-40	0.83	0.360	0.342	0.001			1.3×10^{-5}
GG-41	0.70	0.300	0.015	0.800	0.91	0.137	2.1×10^{-4}
GG-42	0.54	0.770	0.169	0.097			1.8×10^{-4}
GG-43	0.54	0.750	0.166	0.145			6.6×10^{-4}
GG-44	0.15	0.990	0.130	0.004			5.9×10^{-4}
GG-45	0.56	0.860	0.120	0.120			1.2×10^{-4}
GG-46	0.61	0.725	0.170	0.218			6.9×10^{-5}
GG-47	0.84	0.810	0.179	0.001			9.9×10^{-6}
GG-54	0.61	0.450	0.335	0.474			2.8×10^{-4}
AP-4	0.75	0.970	0.123	0.027			2.0×10^{-5}
AP-5	0.75	0.986	0.115	0.001			5.4×10^{-4}
GP-1a	Flotsam just barely fluidized.						
GP-2a-2d	Bed completely defluidized.						
GP-21	0.70	Pure flotsam above interface.					
GP-22	0.70	Pure flotsam above interface.					
GP-23	0.70	Pure flowsam above interface.					
GP-24	0.60	0.990	0.050	0.0			3.8×10^{-4}
GP-25	0.0	~1.0	0.024	0.0			3.5×10^{-5}
GP-26	0.60	~1.0	0.020	0.0			1.5×10^{-6}
GP-27	0.68	Pure flotsam above interface.					
GP-28	0.85	Pure flotsam above interface.					
GP-29	0.74	~1.0	0.025	0.0			1.3×10^{-6}
GP-30	0.58	~1.0	0.033	0.0			2.7×10^{-6}
GP-31	0.75	Pure flotsam above interface.					
AG-5	0.0	~1.0	0.045	0.0			3.2×10^{-4}

Table A-7. Evaluation of Region 2 steady-state data in terms of modified Gibilaro-Rowe model

Run No.	λ_{Ds}	λ_{ws}	z_c	λ'_{Ds}	SSD	SSD/ SST_{max}	I_{exp}	I_{mod}
LC-1	0.196	0.0			2.5×10^{-4}	1.8×10^{-3}	0.178	0.188
LC-2	0.275	0.0			8.9×10^{-4}	6.4×10^{-3}	0.125	0.116
LC-4	0.333	0.0	0.85	0.095	1.8×10^{-4}	3.1×10^{-3}	0.081	0.082
LC-5	3.13	0.0	0.85	0.269	2.8×10^{-5}	4.7×10^{-4}	0.002	0.002
LC-6	5.00	0.0	0.80	0.257	1.7×10^{-5}	3.0×10^{-4}	0.003	0.003
LC-7	3.64	0.0			5.7×10^{-5}	2.6×10^{-4}	0.002	0.001
LC-8	0.209	0.0			1.2×10^{-3}	5.1×10^{-3}	0.269	0.279
SG-4	0.051	0.0			4.4×10^{-4}	2.1×10^{-3}	0.736	0.753
SG-7	0.0	0.0			0.0	0.0	1.00	1.00
SG-8	0.0	0.0			0.0	0.0	1.00	1.00
SG-9	0.045	0.020	0.80	0.037	3.4×10^{-4}	1.5×10^{-3}	0.788	0.736
SG-10	0.030	0.022	0.80	0.057	5.9×10^{-4}	2.9×10^{-3}	0.837	0.810
GG-1	0.068	0.0			6.7×10^{-4}	3.0×10^{-3}	0.709	0.686
GG-1'	0.066	0.054			5.8×10^{-4}	2.6×10^{-3}	0.657	0.646
GG-2	0.030	0.636	0.80	0.792	7.9×10^{-5}	3.5×10^{-4}	0.054	0.047
GG-2'	0.024	0.604	0.80	0.607	8.0×10^{-4}	3.6×10^{-3}	0.060	0.062
GG-3	0.026	0.540	0.80	1.19	1.1×10^{-4}	4.9×10^{-4}	0.136	0.141
GG-3'	0.024	0.609	0.75	0.448	2.9×10^{-4}	1.3×10^{-3}	0.094	0.095
GG-4	0.052	0.358	0.80	1.57	3.8×10^{-4}	1.7×10^{-3}	0.322	0.323
GG-5	0.037	0.0	0.80	0.074	5.2×10^{-5}	8.4×10^{-4}	0.192	0.193
GG-5'	0.357	0.0			2.3×10^{-5}	3.7×10^{-4}	0.035	0.034
GG-6	0.074	0.0	0.70	0.044	1.3×10^{-6}	2.1×10^{-5}	0.435	0.435
GG-7	0.064	1.05	0.85	0.169	7.4×10^{-5}	1.2×10^{-3}	0.021	0.020
GG-8	0.212	1.47	0.80	0.178	1.4×10^{-4}	2.2×10^{-3}	0.015	0.013
GG-9	0.045	0.035			3.8×10^{-5}	3.3×10^{-4}	0.417	0.394
GG-10	0.048	0.050			2.3×10^{-4}	2.0×10^{-3}	0.373	0.323
GG-11	0.020	0.670	0.75	0.173	4.2×10^{-4}	1.9×10^{-3}	0.107	0.104
GG-12	0.105	0.0			2.1×10^{-4}	9.3×10^{-3}	0.515	0.516
GG-13	0.090	0.220			8.8×10^{-4}	4.0×10^{-3}	0.399	0.380
GG-14	0.055	0.270			8.3×10^{-5}	3.7×10^{-4}	0.417	0.415
GG-14'	0.056	0.270			2.9×10^{-4}	1.3×10^{-3}	0.417	0.414
GG-15	0.078	0.029			7.1×10^{-5}	3.2×10^{-4}	0.622	0.627
GG-16	0.022	0.685	0.80	0.335	3.4×10^{-4}	1.5×10^{-3}	0.038	0.036
GG-16'	0.011	0.647	0.80	0.404	1.6×10^{-3}	7.0×10^{-3}	0.023	0.025
GG-17	0.071	0.135			8.8×10^{-4}	4.0×10^{-3}	0.554	0.530
GG-18	0.050	0.230			1.1×10^{-4}	4.8×10^{-4}	0.489	0.486
GG-19	0.117	0.178			1.4×10^{-3}	6.1×10^{-3}	0.371	0.343
GG-20	0.025	0.640	0.80	0.474	2.9×10^{-4}	1.3×10^{-3}	0.055	0.052
GG-21	0.080	0.136			2.1×10^{-4}	9.3×10^{-4}	0.498	0.494
GG-21'	0.083	0.109			2.2×10^{-4}	9.7×10^{-4}	0.518	0.517
GG-22	0.037	0.264	0.80	0.684	4.6×10^{-4}	2.1×10^{-3}	0.172	0.175
GG-23	0.047	0.138			9.7×10^{-4}	6.1×10^{-3}	0.269	0.208
GG-24	0.039	0.420	0.80	0.451	8.1×10^{-4}	3.2×10^{-3}	0.120	0.125

Table A-7. (continued)

Run No.	λ_{Ds}	λ_{ws}	z_c	λ'_{Ds}	SSD	SSD/ SST_{max}	I_{exp}	I_{mod}
GG-25	0.086	0.620			2.6×10^{-4}	1.6×10^{-3}	0.092	0.089
GG-27	0.020	0.650	0.80	0.229	2.8×10^{-4}	1.3×10^{-3}	0.061	0.066
GG-28	0.030	0.560	0.75	0.688	6.3×10^{-4}	2.8×10^{-3}	0.114	0.122
GG-29	0.036	0.642			3.8×10^{-4}	1.7×10^{-3}	0.041	0.046
GG-29'	0.036	0.650			6.4×10^{-4}	2.9×10^{-3}	0.039	0.043
GG-30	0.050	0.800	0.80	0.259	1.2×10^{-4}	5.4×10^{-4}	0.026	0.026
GG-30'	0.035	0.800	0.80	0.733	1.1×10^{-4}	5.2×10^{-4}	0.020	0.018
GG-31	0.013	0.647	0.80	0.228	1.4×10^{-3}	6.2×10^{-3}	0.043	0.043
GG-31'	0.029	0.665	0.85	0.263	8.3×10^{-4}	3.7×10^{-3}	0.037	0.043
GG-33	0.087	0.100			7.6×10^{-4}	3.4×10^{-3}	0.491	0.495
GG-33'	0.150	0.0			6.8×10^{-4}	3.1×10^{-3}	0.453	0.397
GG-33"	0.050	0.120			6.2×10^{-4}	2.8×10^{-3}	0.570	0.611
GG-48	0.054	0.205	0.85	0.139	8.5×10^{-4}	3.8×10^{-3}	0.565	0.541
GG-49	0.069	0.230			1.0×10^{-3}	4.7×10^{-3}	0.379	0.423
GG-50	0.050	0.380	0.80	0.233	4.9×10^{-4}	2.2×10^{-3}	0.337	0.333
GG-51	0.040	0.530	0.82	0.343	1.9×10^{-4}	8.5×10^{-4}	0.166	0.168
GG-52	0.080	0.340	0.80	0.430	6.7×10^{-4}	3.0×10^{-3}	0.296	0.281
GG-53	0.079	0.330	0.80	0.192	1.2×10^{-3}	5.5×10^{-3}	0.302	0.284
GG-55	0.081	0.450	0.80	0.255	1.9×10^{-3}	8.4×10^{-3}	0.179	0.201
GG-56	0.051	0.500	0.80	0.280	6.6×10^{-4}	3.0×10^{-3}	0.189	0.194
GG-56'	0.057	0.550	0.80	1.21	3.6×10^{-4}	1.6×10^{-3}	0.112	0.112
GG-57	0.037	0.620	0.80	0.611	2.6×10^{-4}	1.2×10^{-3}	0.073	0.069
GG-58	0.077	0.692	0.80	1.25	5.3×10^{-4}	2.4×10^{-3}	0.047	0.047
GG-59	0.026	1.00	0.80	0.320	3.3×10^{-4}	1.5×10^{-3}	0.008	0.006
GG-60	0.080	0.0			2.2×10^{-4}	9.9×10^{-4}	0.646	0.640
GG-61	0.010	0.690	0.81	0.210	5.5×10^{-4}	2.5×10^{-3}	0.011	0.010
GG-62	0.010	0.690	0.82	0.151	4.2×10^{-4}	1.9×10^{-3}	0.030	0.029
GG-63	0.011	0.701	0.80	0.170	5.5×10^{-4}	2.5×10^{-3}	0.019	0.019
GG-64	0.010	0.713	0.82	0.132	3.9×10^{-4}	1.8×10^{-3}	0.025	0.025
GG-65	0.011	0.710	0.85	0.153	1.1×10^{-4}	5.0×10^{-4}	0.014	0.014
AP-1	0.077	0.607			1.8×10^{-4}	1.5×10^{-3}	0.100	0.102
AP-1'	0.034	0.609			4.7×10^{-5}	3.8×10^{-4}	0.181	0.186
AP-2	0.364	0.0			3.4×10^{-4}	2.8×10^{-3}	0.065	0.065
AP-3	0.064	0.0			3.6×10^{-4}	2.9×10^{-3}	0.528	0.523
AP-6	0.200	0.0			7.3×10^{-4}	5.9×10^{-3}	0.139	0.159
AP-7	12.4	0.0			2.0×10^{-5}	1.6×10^{-4}	~0.0	~0.0
AP-8	4.42	0.0			5.9×10^{-6}	4.8×10^{-5}	~0.0	~0.0
AP-9	0.379	0.0			4.8×10^{-4}	3.9×10^{-3}	0.065	0.060
AP-10	0.120	0.0	0.80	0.090	1.3×10^{-3}	1.1×10^{-2}	0.343	0.359
AP-12	0.054	0.0			1.6×10^{-4}	1.3×10^{-3}	0.567	0.584
*AP-13	0.084	0.0			2.2×10^{-4}	1.8×10^{-3}	0.433	0.428
AP-19	0.857	0.0			1.4×10^{-4}	1.1×10^{-3}	0.014	0.013
AP-20	0.021	0.590	0.81	0.126	5.9×10^{-4}	2.7×10^{-3}	0.169	0.179

Table A-7. (continued)

Run No.	λ_{Ds}	λ_{ws}	z_c	λ'_{Ds}	SSD	SSD/ SST_{max}	I_{exp}	I_{mod}
AP-21	0.018	0.620	0.80	0.145	1.1×10^{-3}	5.0×10^{-3}	0.100	0.120
AP-22	0.016	0.651	0.80	0.104	5.0×10^{-4}	2.3×10^{-3}	0.117	0.126
AP-23	0.157	0.0	0.75	0.306	1.4×10^{-4}	6.3×10^{-4}	0.331	0.336
AP-24	0.251	0.0	0.73	0.131	3.3×10^{-4}	1.5×10^{-3}	0.227	0.241
AP-25	0.010	0.650	0.78	0.174	1.9×10^{-4}	8.6×10^{-4}	0.109	0.112
AP-26	0.168	0.0			2.1×10^{-4}	9.5×10^{-4}	0.364	0.352
AP-27	0.031	0.580	0.78	0.091	5.9×10^{-4}	2.7×10^{-3}	0.333	0.331
AP-28	0.078	0.0			3.9×10^{-4}	1.8×10^{-3}	0.634	0.639
AP-29	0.050	0.0			7.0×10^{-4}	3.2×10^{-3}	0.753	0.774
AP-30	0.042	0.0			8.5×10^{-5}	3.8×10^{-4}	0.809	0.798
AP-31	0.237	0.0			8.2×10^{-4}	3.7×10^{-3}	0.242	0.227
AP-32	0.030	0.450	0.80	0.131	9.1×10^{-4}	4.1×10^{-3}	0.317	0.361
AP-33	0.069	0.0	0.80	-5.18*	8.5×10^{-4}	3.8×10^{-3}	0.530	0.561
AP-34	0.035	0.0			3.1×10^{-5}	1.4×10^{-4}	0.853	0.846
AP-35	0.077	0.0			1.3×10^{-4}	5.9×10^{-4}	0.636	0.658
AP-36	0.037	0.0			1.2×10^{-4}	5.4×10^{-4}	0.828	0.821
AP-37	0.038	0.0			1.9×10^{-4}	8.6×10^{-4}	0.798	0.825
AP-38	0.034	0.0			2.0×10^{-4}	9.0×10^{-4}	0.849	0.865
GP-1	0.068	0.0	0.77	0.182	1.0×10^{-3}	4.8×10^{-3}	0.543	0.538
GP-2	0.070	0.131	0.80	0.079	1.8×10^{-3}	8.7×10^{-3}	0.397	0.430
GP-2'	0.070	0.120	0.80	0.093	3.2×10^{-5}	1.6×10^{-4}	0.424	0.440
GP-2"	0.072	0.130	0.80	0.077	5.0×10^{-4}	2.4×10^{-3}	0.434	0.431
GP-3	0.059	0.010			6.5×10^{-4}	3.1×10^{-3}	0.661	0.672
GP-4	0.071	0.0	0.80	0.135	1.2×10^{-3}	5.8×10^{-3}	0.558	0.567
GP-5	0.044	0.0			2.1×10^{-5}	1.0×10^{-4}	0.790	0.785
GP-6	0.035	0.0			5.2×10^{-7}	3.7×10^{-3}	0.803	0.803
GP-7	0.023	0.0			5.4×10^{-4}	2.6×10^{-3}	0.885	0.883
GP-8	0.071	0.0	0.80	0.144	5.5×10^{-4}	2.7×10^{-3}	0.562	0.558
GP-9	0.023	0.0			1.6×10^{-4}	7.8×10^{-4}	0.945	0.958
GP-10	0.040	0.0			1.3×10^{-3}	1.0×10^{-2}	0.685	0.687
GP-11	0.038	0.0			6.5×10^{-4}	5.2×10^{-3}	0.731	0.771
GP-12	0.036	0.0			3.4×10^{-4}	2.7×10^{-3}	0.704	0.751
GP-13	0.045	0.0			2.0×10^{-4}	1.6×10^{-3}	0.667	0.626
GP-14	0.045	0.0			1.5×10^{-4}	6.0×10^{-4}	0.801	0.789
GP-15	0.033	0.0			4.0×10^{-5}	1.9×10^{-4}	0.858	0.868
GP-16	0.026	0.0			9.0×10^{-5}	1.9×10^{-3}	0.370	0.326
GP-17	0.057	0.0			8.0×10^{-4}	3.8×10^{-3}	0.672	0.714
GP-18	0.064	0.0			2.1×10^{-4}	9.7×10^{-4}	0.667	0.673
GP-19	0.039	0.0			1.0×10^{-4}	4.9×10^{-4}	0.789	0.818
GP-20	0.028	0.0			5.5×10^{-6}	2.6×10^{-5}	0.801	0.795
GP-32	0.048	0.045			5.3×10^{-4}	2.4×10^{-3}	0.699	0.716
GP-33	0.097	0.0	0.83	-2.17	4.5×10^{-4}	2.1×10^{-3}	0.530	0.560
GP-34	0.090	0.0	0.80	-3.94	2.3×10^{-4}	1.1×10^{-3}	0.621	0.612
GP-35	0.069	0.0			2.5×10^{-4}	1.2×10^{-3}	0.672	0.676
GP-36	0.045	0.0	0.81	-0.142	4.1×10^{-4}	1.9×10^{-3}	0.705	0.746
GP-37	0.130	0.073	0.80	0.070	3.8×10^{-4}	1.8×10^{-3}	0.426	0.447

Table A-7. (continued)

Run No.	λ_{Ds}	λ_{ws}	z_c	λ'_{Ds}	SSD	SSD/ SST_{max}	I_{exp}	I_{mod}
AA-1	0.130	0.010			3.4×10^{-5}	1.5×10^{-3}	0.052	0.045
AG-1	0.083	0.0			1.3×10^{-3}	5.9×10^{-3}	0.630	0.630
AG-2	0.031	0.220	0.75	1.69	2.9×10^{-4}	1.3×10^{-3}	0.228	0.274
AG-3	0.027	0.300	0.75	-0.369	7.2×10^{-5}	3.2×10^{-4}	0.047	0.048
AG-4	0.024	0.411			3.9×10^{-4}	1.8×10^{-3}	0.001	0.003
AG-6	0.017	0.612	0.85	0.864	2.5×10^{-4}	1.1×10^{-3}	0.051	0.052
AG-7	0.019	0.830			2.1×10^{-4}	9.5×10^{-4}	0.043	0.048

*Negative sign indicates flotsam/jetsam roles reversed in upper layer.

Table A-8. Evaluation of pressure profile data in terms of mass distribution model

Run No.	λ_p	λ_p'	MSE	RMSE	n
A-1	0.34	0.23	4.44×10^{-4}	2.1×10^{-2}	11
A-2A	0.0		7.11×10^{-5}	8.4×10^{-3}	7
A-2B	0.49	0.46	1.52×10^{-4}	1.2×10^{-2}	12
A-2C	0.85	0.76	1.41×10^{-4}	1.2×10^{-2}	14
A-3A	0.0		7.23×10^{-4}	2.7×10^{-2}	5
A-3B	0.24	0.22	1.44×10^{-4}	1.2×10^{-2}	10
A-3C	0.28	0.33	3.84×10^{-5}	6.2×10^{-3}	13
A-4	0.56	0.38	6.56×10^{-4}	2.6×10^{-2}	11
A-5	0.46	0.30	2.40×10^{-4}	1.6×10^{-2}	12
A-11	0.69	0.29	8.30×10^{-4}	2.9×10^{-2}	10
AP-1	0.40	0.32	3.24×10^{-4}	1.8×10^{-2}	13
AP-2	0.57	0.67	5.35×10^{-5}	7.3×10^{-3}	12
AP-3	0.24	0.16	5.43×10^{-5}	7.4×10^{-3}	13
AP-4	Region 1 - Model does not apply				
AP-6	0.30	0.25	1.79×10^{-4}	1.3×10^{-2}	10
AP-7	0.47	0.50	7.71×10^{-5}	8.8×10^{-3}	9
AP-8	0.54	0.39	1.30×10^{-4}	1.1×10^{-2}	9
AP-10	0.62	0.35	9.26×10^{-4}	3.0×10^{-2}	14
LC-12	0.47	0.52	2.89×10^{-4}	1.7×10^{-2}	11
LC-13	0.12	0.16	9.11×10^{-5}	9.5×10^{-3}	8
LC-14	Region 1 - Model does not apply				
LC-15	Region 1 - Model does not apply				

VITA

Charles Stuart Daw was born in Pensacola, Florida on March 16, 1950 to Charles Edward and Mildred Harris Daw. He graduated from Amador Valley Joint Union High School in Pleasanton, California in 1968 and returned to Pensacola to attend Pensacola Junior College in that year. After receiving his Associate of Arts degree in 1970, Stuart enrolled in the College of Engineering at the University of Florida. He graduated with a Bachelor of Science in Chemical Engineering in March of 1973 and accepted employment with E. I. DuPont de Nemours and Company in New Johnsonville, Tennessee. While at New Johnsonville, Stuart completed his Master of Science in Chemical Engineering through the University of Tennessee Engineering Graduate Extension Program. In April 1979, he resigned from DuPont and accepted employment at the Oak Ridge National Laboratory. He has continued working full-time at the laboratory while pursuing his Ph.D. on a part-time basis.